The University of Reading

Auxilin, clathrin trafficking and Parkinson's disease

Dorien A. Roosen

Thesis submitted for the degree of Doctor of Philosophy

March 2019

Supervisors:

Dr. Patrick A. Lewis
Department of Pharmacology
School of Pharmacy
University of Reading

Dr. Mark R. Cookson
Laboratory of Neurogenetics
National Institute on Aging
National Instituts of Health

Declaration: I confirm that this is my own work and the use of all material from other sources has been properly and fully acknowledged. Contributions from colleagues and collaborators in the execution of experiments have explicitly been acknowledged in the manuscript. The interpretation and analysis of data resulting from the research conducted in this thesis are entirely my own work.

- Dorien Annette Roosen

"Beyond the stimulation of variety and interest, the supreme joy of the intellect lies in seeing the divine harmony of the universe, and in knowing the truth – as beautiful and virginal as the flower opening its calyx to the caresses of the early morning sun."

Santiago Ramón y Cajal — Advice for a Young Investigator
1897

Voor Bompa

Word count: 50000

ACKNOWLEDGEMENTS

The completion of this thesis would not have been possible without the help of many people and I would need a separate thesis to thank them all. In the interest of space, I would like to express my thanks to a subset of people to whom I am particularly grateful.

First, I'd like to thank my family for their endless and unconditional support. Thanks mum, you have taught me about integrity, dedication and work-ethic by example, showed me that daughters should have goals instead of dreams. Thanks dad, for showing me to always be curious, mindful and appreciative of detail, which has in many ways shaped my scientific interests. My sister Lore, you are the kindest, most understanding person I know, thank you for being there for me on every step along the way. Wim, Petra, Landrie, Kathleine, Joëlle, Mathisse, Dieke & Cis - you are all wonderful, thank you for creating the warmest of homes.

I'd like to thank my PhD supervisors, Dr. Patrick Lewis and Dr. Mark Cookson. Mark, thanks for giving me the opportunity to do my PhD in such a stimulating research environment and for always supporting my PhD research on all sides. Patrick, thank you for the constant scientific support, guidance and constructive feedback, which have been invaluable throughout my PhD studies. I'd also like to thank Dr. Andy Singleton, for creating such a nice collaborative lab environment that is LNG.

A very special thanks goes to the LNG-family. The past few years have been some of my favourite, and that is largely because of you. You are not only the best colleagues anyone could ask for, but also great friends. Kumaran and Cornelis - thanks for always helping out with my problems and questions. I couldn't have done this PhD without you, and it wouldn't have been half the fun without the teasing and the jokes. Sasha, you are a great role model, your scientific creativity, energy and resilience will never stop to inspire me. Natalie and Melissa, thank you for patiently teaching me all things in vivo, and for your friendship along the way. Luis, Sara, Adam, Ruth, Laura, Jillian, Rebekah, Xylena, Alice, Nate, Megan, George, you are all brilliant scientists, thank you for always engaging in scientific discussions and for creating such a great lab atmosphere. I am sure we will stay in touch wherever we are in the world.

I would also like to thank many people that have supported me during my free time. David and Chad, you are not only two of the most inspiring scientists I have met, you are also great friends and my favourite running buddies. Long runs are (almost) easy on a science high. Deanna and Jonny 'what are they saying in Europe about Trump' Steege-Noel. Thanks for keeping me sharp on politics, for organizing the best book clubs and house parties, for being the all-around best 'zoo house' roomies. My dear friends Sophia, Greg, Ian Bu, Marco, and my favourite cats Boxoon and Major Tom. You are the best cabin trip companions and I have collected very fond memories of our concert nights and brunch dates. Landrie, Lien, Geert, Michelle, Briana and Megan - it has been wonderful to have you over in DC and to travel around in the US, I look forward to many more trips and can't wait to spend more time together in Europe. Finally, my long-time friends Sofie, Elke and Camille, thanks for all the good times and the support over the years, you mean a lot to me.

DECLARATION OF CONTRIBUTIONS

The work in this thesis was funded in part by the Intramural Research Program at the National Institute on Aging, National Institutes of Health. Many colleagues at LNG have contributed directly to the work presented in this thesis. Dr. Natalie Landeck performed all immunohistochemistry experiments and Dr. Melissa Conti contributed to behavioural testing. Alice Kaganovich contributed to the RNAseq library preparation and performed deep-sequencing, Dr. Jinhui Ding subsequently performed read count analysis and Dr. Mark Cookson differential expression analysis. Dr. Sara Saez-Atienzar performed RNAscope experiments and Dr. Nate Smith modelled protein structures presented within this work.

In addition, collaborations across different institutes of the National Institutes of Health have also contributed to the research presented in this thesis. A transgenic mouse model was generated in collaboration with the Transgenic Core (National Heart, Lung and Blood Institute), led by Dr. Chengyu Liu. All behavioural studies were conducted at Rodent Behavioral Core (National Institute of Mental Health) and Dr. Johann du Hoffman contributed to writing R scripts for the analysis of some of the data. Mass spectometry experiments were performed by the Proteomics Core, led by Dr. Yan Li (National Institute of Neurological Disorders and Stroke). Finally, transmission electron microscopy imaging was performed in collaboration with the Electron Microscopy Core (National Heart, Lung and Blood Institute), led by Dr. Cristopher Bleck.

ABSTRACT

Clathrin trafficking is crucial for cellular function in all eukaryotes and plays a specialized role in synaptic transmission in higher organisms. Clathrin-coated vesicles (CCVs) mediate selective transport of cargo from the plasma membrane and trans-Golgi network (TGN) to intracellular destinations. Auxilin is the major neuronal CCV uncoating protein required for successful delivery of cargo to its destination compartments. Whereas its role in the uncoating of CCVs at the synapse has been well-documented, the role of Auxilin in the uncoating of TGN-derived CCVs is less established.

Parkinsons disease (PD) is a common neurodegenerative disorder, characterized in part by neuropathological lesions in the nigrostriatal pathway. Multiple loss of function mutations in the gene encoding Auxilin have been found to cause an aggressive form of young onset PD. However, the mechanism of action of the pathogenic Auxilin mutations remains to be elucidated.

In this thesis, the impact of pathogenic Auxilin mutations was investigated *in vivo* and in cellular and molecular settings. A novel mouse model carrying the pathogenic R857G Auxilin mutation was found to display neurological phenotypes that phenocopy clinical features seen in patients, including seizures and motor impairments. Mapping the interactome of Auxilin led to the identification of novel *bona fide* TGN-resident interactors. Impaired clathrin trafficking in R857G Auxilin mice, both at the synapse and the TGN, was found to result in neuropathological lesions in the nigrostriatal pathway. Taken together, the work presented in this thesis provides novel insights in the physiological role of Auxilin as well as PD pathogenesis in Auxilin mutation carriers. In addition, these data underscore an important role for clathrin trafficking in PD.

CONTENTS

LIST OF FIGURES

LIST OF TABLES

ABBREVIATIONS

AAO ..... *age at onset*

AP ..... *adaptor protein*

AP-MS ..... *affinity purification coupled with mass spectometry*

AP180 ..... *assembly protein 180*

ARF ..... *ADP ribosylation factor*

BAR ..... *Bin-Amphiphysin-Rvs*

BIG2 ..... *brefeldin A-inhibited GEF 2*

CALM ..... *clathrin assembly lymphoid myeloid leukemia*

CCV ..... *clathrin coated vesicle*

CDMPR ..... *cation-dependent M6P receptor*

CHC ..... *clathrin heavy chain*

CIMPR ..... *cation-independent M6P receptor*

CLC ..... *clathrin light chain*

CME ..... *clathrin-mediated endocytosis*

COP ..... *coat protein complex*

CRISPR ..... *clustered regularly interspaced short palindromic repeats*

DA ..... *dopaminergic*

DNAJC13 ..... *DNAJ heat shock protein family member C13*

DNAJC26 ..... *DNAJ heat shock protein family member C26*

DNAJC6 ..... *DNAJ heat shock protein family member C6*

EGFR ..... *epidermal growth factor receptor*

EM ..... *electron microscopy*

ER ..... *endoplasmatic reticulum*

ESCRT ..... *endosomal sorting complex required for transport*

FBS ..... *fetal bovine serum*

FCHO ..... *Fer/CIP4 homology domain only protein*

FDR ..... *false discovery rate*

GAE ..... *γ-adaptin ear*

GAK ..... *cyclin G-dependent kinase A*

GAP ..... *GTPase activating protein*

GAT ..... *GGA and TOM*

GBF1 ..... *Golgi-specific brefeldin A-resistant GEF 1*

GEF ..... *guanine nucleotide exchange factor*

GGA ..... *Golgi-localized, γ-ear containing, Arf-binding proteins*

GO ..... *gene ontology*

GWAS ..... *genome-wide association studies*

HSC70 ..... *heat shock cognate 71 kDa protein*

HSP70 ..... *heat shock protein 70*

KO ..... *knockout*

L-DOPA *L-3,4-dihydroxyphenylalanine*

LAMP ..... *lysosomal-associated membrane protein*

LB ..... *Lewy body*

LC-MS/MS ..... *liquid chromatograph with tandem mass spectometry*

LDLR ..... *low density lipoprotein receptor*

M6P *mannose-6-phosphate*

MPR ..... *M6P receptor*

MPTP *1-methyl-4-phenyl-1,2,3,6-tetrahydropyridine*

NEF ..... *nucleotide exchange factor*

P0 ..... *postnatal day 0*

P2 ..... *postnatal day 2*

PAM ..... *protospacer adjacent motif*

PBS ..... *phosphate-buffered saline*

PD ..... *Parkinson's disease*

PI(3,4)P2 ..... *phosphatidylinositol (4,5) biphosphate*

PI(4,5)P2 ..... *phosphatidylinositol (4,5) biphosphate*

PI3P ..... *phosphatidylinositol 3 phosphate*

PI4P ..... *phosphatidylinositol 4 phosphate*

PIPKIγ ..... *PI4P 5 kinase type I* γ

RIN ..... *RNA integrity number*

RME-8 ..... *receptor-mediated endocytosys protein 8*

RT ..... *room temperature*

Rlog ..... *regularized logarithm*

SD ..... *standard deviation*

SEM ..... *standard error of the mean*

SILAC ..... *stable isotope labeling with amino acids in cell culture*

SN ..... *substantia nigra*

SNP ..... *single nucleotide polymorphism*

SNX ..... *sorting nexin*

SorLA ..... *Sortilin-related receptor*

TBS ..... *Tris-buffered saline*

TFR ..... *Transferrin receptor*

TGN ..... *trans-Golgi network*

TMEM175 ..... *transmembrane protein 175*

TOM ..... *target of myb*

VAMP4 ..... *vesicle-associated membrane protein 4*

VHS ..... *Vps27, Hrs, Stam*

VPS ..... *vacuolar protein sorting*

VTA ..... *ventral tegmental area*

WASH ..... *Wiskott-Aldrich syndrome protein and Scar homologue*

WB ..... *Western blot*

cDNA ..... *complementary DNA*

co-IP ..... *co-immunoprecipitation*

eQTL ..... *expression quantitative trait locus*

qPCR ..... *quantitative polymerase chain reaction*

1 INTRODUCTION

1.1 PARKINSON'S DISEASE

1.1.1 History and overview

> "*Involuntary tremulous motion, with lessened muscular power, in parts not in action and even when supported; with a propensity to bend the trunk forward, and to pass from a walking to a running pace: the senses and intellects being uninjured.*"
>
> James Parkinson — Essay on the Shaking Palsy
> *1817*

It has been more than 200 years since the British clinician James Parkinson nosologically described 'paralyis agitans' as a novel neurological syndrome, recognizing gait disturbance and tremor to be the pathognomic characteristics (Parkinson, 1817). The term 'Parkinson's disease' was coined by William Rutherford Sanders in 1865 (Sanders, 1865). However, the eponymous term only went into general usage in 1872 through the influence of Jean Martin Charcot, who provided a refined clinical description of the disease (Charcot, 1872). A pathological understanding began to be unearthed in the 1912 when Friedrich Lewy described the description of proteinaceous intracellular inclusions in the brain of patients, now known as Lewy bodies (LBs) (Lewy, 1912). The degeneration of neurons in the substantia nigra (SN), another major pathological hallmark, was described 7 years later (Tretiakoff, 1919). Lesions in the SN and the presence of LB were subsequently considered the definitive criteria for *post mortem* diagnosis (Greenfield and Bosanquet, 1953). The first understandings of the underlying

biochemistry of the neuropathology and symptomatology was fuelled by the identification of the neurotransmitter dopamine in the late 1950s, as it was found to be highly concentrated in the nigral pathways and its decreasing levels positively correlated with nigral cell loss in patients (Bertler and Rosengren, 1959; Carlsson *et al.*, 1958; Ehringer and Hornykiewicz, 1960; Sano *et al.*, 1959).

Parkinson's disease (PD) is now recognized as a major neurodegenerative movement disorder. Age is an important risk factor for PD, as the worldwide prevalence steeply increases from 107 per 100 000 people between the ages of 50-59 to 1087 per 100 000 people at the ages of 70-79 (Pringsheim *et al.*, 2014). The global burden of PD has more than doubled over the past generation, with over 6 million people currently suffering from PD worldwide (GBD 2016 Parkinson's Disease Collaborators *et al.*, 2018). The number of individuals with PD is projected to double again by 2030, due to improved living conditions and increased life expectancy (Dorsey *et al.*, 2007; GBD 2016 Parkinson's Disease Collaborators *et al.*, 2018). Neurological disorders are currently considered the leading cause of disabilities in the world, of which PD is the fastest growing disorder (Feigin *et al.*, 2017). PD is present across all ethnicities and males have a 1.4 times higher chance for developing the disease compared to females (GBD 2016 Parkinson's Disease Collaborators *et al.*, 2018). Despite great advances in symptomatic treatments, there is no definite cure for PD, likely because of its largely unknown disease aetiology. Understanding underlying disease mechanisms and the development of therapeutics that prevent, halt or slow down disease progression is therefore imperative.

1.1.2 Symptomatology

PD is characterized by neurological symptoms that include both motor and non-motor symptoms. The onset of PD motor symptoms is typically asymmetric and progressive, with a mean age at onset (AAO) of 55.3 years old (Hoehn and Yahr, 1967). Disease course varies between patients, but the average life expectancy at diagnosis is 15 years. However, PD is not fatal and although the cause of death is difficult to identify in most cases, pneumonia is the most common certificated secondary cause of death (Hoehn and Yahr, 1967; Lees *et al.*, 2009).

PD has an insidious onset and the first symptoms of PD may include fatigue, loss of smell, decreased amplitude of speech or slower handwriting. These are relatively unspecific symptoms and may therefore go unnoticed or misinterpreted (Lees *et al.*, 2009).

Parkinsonism is the main clinical feature of PD and is characterized by four cardinal motor symptoms: tremor at rest, bradykinesia, muscle rigidity and postural imbalance. Additional motor impairments can include gait problems and the freezing phenomenon (Lees *et al.*, 2009). Non-motor symptoms of PD may occur during disease progression or precede the motor symptoms. These can include mood disorders, cognitive impairments, sleep disturbances, olfactory impairments and autonomic insufficiencies such as constipation (Fahn, 2003; Lees *et al.*, 2009).

PD is clinically diagnosed by the presence of at least two cardinal motor symptoms including bradykinesia. A careful neurological examination is needed, looking for supportive criteria such as secondary motor or non-motor symptoms as well as the absence of indications for other parkinsonisms than PD. Responsiveness to L-DOPA (L-3,4-dihydroxyphenylalanine), a dopamine precursor, is often included

in the examination to support a correct diagnosis (Gibb and Lees, 1988; Lees *et al.*, 2009).

Although parkinsonism is the main clinical feature of PD, they can also be found in other neurological diseases that are grouped as secondary parkinsonian syndromes (i.e. the presence of parkinsonism symptoms but through a different mechanism than neurodegeneration), or atypical parkinsonian syndromes, which present additional clinical features 'atypical' of PD, such as ataxia and seizures (Scholz *et al.*, 2015). Atypical parkinsonian syndromes include Lewy body dementia, multiple system atrophy and progressive supranuclear palsy. Given the heterogeneity of clinical features of PD and other parkinsonian syndromes, an accurate diagnosis can be challenging (Hughes *et al.*, 1992, 2001).

1.1.3 Neuropathology

A definite diagnosis of PD can only be made by *post mortem* findings of dopaminergic (DA) cell loss in the SN, more specifically the ventral pars compacta, and the presence of Lewy pathology in surviving neurons (Figure 1.1) (Lees *et al.*, 2009).

Progressive deterioration of DA neurons in the SN is the first neuropathological hallmark of PD. DA neurons in the SN release the neurotransmitter dopamine in the putamen, the dorsolateral part of the striatum. At the onset of PD symptoms, approximately 50% of nigrostriatal neurons are lost and striatal neurotransmitter dopamine has been depleted up to 80% (Fearnley and Lees, 1991). DA neurons contain neuromelanin, which accounts for the normal dark pigmentation of the SN (literally translated 'black substance'). The macroscopic observation of loss of

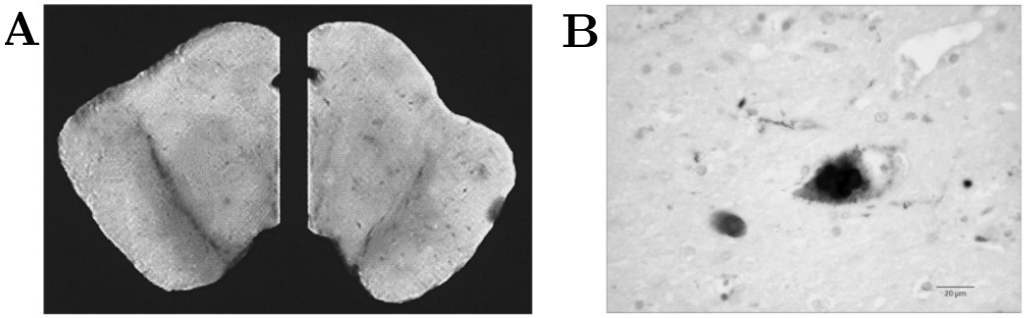

Figure 1.1: **Neuropathology in PD** A Healthy (left) midbrain showing normal dark pigmentation of the SN, midbrain of PD patient (right) showing loss of pigmentation due to degeneration of neurons in the SN. B Light microscopy image of LBs (positive for α-synuclein) in a surviving neuron in the SN. Images are reproduced from (Lees *et al.*, 2009; Mazzio *et al.*, 2011).

pigmentation therefore marks the progressive degeneration of DA neurons in the SN (Figure 1.1). DA neurons in the ventral tegmental area (VTA), a nucleus lateral to the SN, project to the ventromedial part of the striatum (caudate nucleus). Interestingly, neurons of the VTA are less susceptible to neurodegeneration in PD (Dauer and Przedborski, 2003).

Loss of DA neurons and the resulting depletion of DA in the striatum are thought to underlie at least some of the motor symptoms in PD through abnormalities in the basal ganglia signalling (Obeso *et al.*, 2000). The striatum is the main input nucleus of the basal ganglia and balances stimulatory and inhibitory signals on the output nuclei. In PD, the depletion of dopamine in the striatum results in net stimulatory effect on the output nuclei of the basal ganglia and the resulting hyperactivity of the motor thalamus confers the typical motor deficiencies of PD (Obeso *et al.*, 2000).

Next to neuronal loss, the presence of protein aggregates known as LBs in the surviving neurons is the second major neuropathological feature of PD. LBs are cytoplasmic spherical inclusions with a diameter between 8 and 30 μm. LBs

primarily constitute misfolded, aggregated α-synuclein, as well as lipids and other insoluble aggregated proteins including tau, tubulin and ubiquitin (Jellinger, 2012). It is important to note that LBs are not specific to PD, as they also occur in normal ageing and other diseases collectively called synucleinopathies, such as Lewy body dementia (Kotzbauer *et al.*, 2001).

The accumulation of LBs is not restricted to DA neurons in the SN during PD pathogenesis. Braak and colleagues have described a staging scheme where LB pathology appears to follow a stereotyped distribution throughout the brain during disease progression, starting from the brainstem, to the midbrain and eventually to the neocortex (Braak *et al.*, 2003, 2004). In line with Braak's proposed staging scheme, disturbances in non-dopaminergic systems have been suggested to underlie non-motor symptoms in PD (Goldman and Postuma, 2014). α-Synuclein pathology has been found to be present in the vagal nerve and enteric nervous system prior to accumulation in the central nervous system (Braak *et al.*, 2006). This apparent spreading of LB pathology in combination with the finding LB are present in neuronal grafts in the brains of PD patients (Kordower *et al.*, 2008; Li *et al.*, 2008), has given rise to the idea that α-synuclein aggregates may spread from one cell to another (Figure 1.2).

1.1.4 Aetiology

Historically, PD has been considered a purely sporadic disorder, until William Langston recognized in 1983 that 1-methyl-4-phenyl-1,2,3,6-tetrahydropyridine (MPTP), a toxic byproduct of heroin, caused advanced PD in 6 drug addicts through selective neurodegeneration in the SN (Langston *et al.*, 1983a). Ever since, a broad range of epidemiological studies assessing environmental risk factors as a

trigger for PD have been performed. Tobacco and caffeine have been associated with a protective effect for PD, whereas traumatic brain injury and certain pesticides and herbicides are thought to increase risk for PD (Lau and Breteler, 2006). However, it has been challenging to conclusively link environmental factors to disease pathogenesis, as acute exposures can be distant in time in place from the onset of symptoms and chronic low-dose exposures are hard to detect.

Over the past two decades, genetic studies have shown that PD has a substantial heritable compound and that polygenic factors underlie a heterogenic range of phenotypes (Singleton and Hardy, 2016). A total of 19 chromosomal loci have been associated with clinical PD or parkinsonism. Mutations in eleven genes within these *PARK* loci have a robust association with monogenic familial PD (Table 1.1). Whereas monogenic mutations with Mendelian inheritance only account for 5% of all PD cases, risk factors have been nominated by genome-wide association studies (GWAS) to increase the lifetime risk for developing sporadic PD (Nalls *et al.*, 2014, 2018). These risk factors only impart modest contributions to the lifetime risk of disease development and are oligogenic in nature. Sporadic cases of PD are thought to be the result of an interplay between genetic predisposition and both environmental and stochastic factors on the background of an aging brain.

The first gene to be linked to PD in 1996 was *SNCA*, encoding the protein α-synuclein (Polymeropoulos *et al.*, 1996; Polymeropoulos *et al.*, 1997). α-Synuclein is the major constituent of LBs and therefore links familial forms of PD with sporadic forms, as Lewy pathology is a hallmark of all PD cases (Spillantini *et al.*, 1997). Dominant mutations as well as locus triplication and duplication were found to cause hereditary PD (Chartier-Harlin *et al.*, 2004; Dick *et al.*, 2013; Ibáñez *et al.*, 2004; Kiely *et al.*, 2013; Krüger *et al.*, 1998;

Locus	Gene	Protein	Inheritance	Clinical presentation	Function	Reference
PARK1	*SNCA*	α-synuclein	AD	Early onset PD	Synaptic function, protein aggregation	(Krüger *et al.*, 1998; Polymeropoulos *et al.*, 1997; Zarranz *et al.*, 2004)
PARK2	*PRKN*	Parkin	AR	Early onset PD	Mitochondrial function, mitophagy	(Hattori *et al.*, 1998a,b; Leroy *et al.*, 1998; Lücking *et al.*, 1998)
PARK4	*SNCA*	α-synuclein	AD	Early onset PD	Synaptic function, protein aggregation	(Chartier-Harlin *et al.*, 2004; Ibáñez *et al.*, 2004; Singleton *et al.*, 2003)
PARK6	*PINK1*	PINK1	AR	Early onset PD	Mitochondrial function, mitophagy	(Valente *et al.*, 2004)
PARK7	*DJ-1*	DJ-1	AR	Early onset PD	Mitochondrial function	(Bonifati *et al.*, 2003)
PARK8	*LRRK2*	LRRK2	AD	Late onset classical PD	Endomembrane trafficking, autophagy, synaptic function	(Di Fonzo *et al.*, 2005; Kachergus *et al.*, 2005; Paisán-Ruíz *et al.*, 2004; Zimprich *et al.*, 2004)
PARK9	*ATP13A2*	ATP13A2	AR	Juvenile atypical PD	Lysosomal function	(Ramirez *et al.*, 2006)
PARK14	*PLA2G6*	PLA2G6	AR	Juvenile atypical PD	Mitochondrial function	(Lu *et al.*, 2012; Sina *et al.*, 2009)
PARK15	*FBXO7*	FBXO7	AR	Juvenile atypical PD	Mitochondrial function, mitophagy	(Di Fonzo *et al.*, 2009)
PARK17	*VPS35*	VPS35	AD	Late onset classical PD	Endomembrane trafficking	(Vilariño-Güell *et al.*, 2011; Zimprich *et al.*, 2011)
PARK19	*DNAJC6*	Auxilin	AR	Juvenile and early onset atypical PD	Clathrin trafficking	(Edvardson *et al.*, 2012; Elsayed *et al.*, 2016; Köroglu *et al.*, 2013; Olgiati *et al.*, 2016)
PARK20	*SYNJ1*	Synapotojanin 1	AR	Juvenile atypical PD	Clathrin trafficking	(Krebs *et al.*, 2013; Olgiati *et al.*, 2014; Quadri *et al.*, 2013)

Table 1.1: **Genes harbouring causal mutations for monogenic PD**
AD (autosomal dominant), AR (autosomal recessive).

Polymeropoulos *et al.*, 1997; Singleton *et al.*, 2003; Zarranz *et al.*, 2004). GWAS have also nominated single nucleotide polymorphisms (SNPs) in the *SNCA* locus as risk factors contributing to sporadic PD, again emphasizing the overlap both forms of disease (Nalls *et al.*, 2014, 2018).

1.1.5 Pathobiology

Even though familial PD constitutes only a small fraction of all PD cases, a genetic understanding of PD contributes greatly to defining pathways underlying PD pathogenesis. It is thought that there are functional relationships between PD genes, that converge on a handful of biological pathways (Hardy *et al.*, 2009; Kumaran and Cookson, 2015; Singleton and Hardy, 2016) (Figure 1.2).

First, since insoluble protein aggregates are found to be packed in LB, it is thought that protein aggregation may play a role in PD pathology (Jellinger, 2012; Taschenberger *et al.*, 2012; Winner *et al.*, 2011). The main constituent of LBs is α-synuclein and Mendelian mutations as well as GWAS-nominated SNPs in its gene *SNCA* have been associated with PD. Familial mutations in α-synuclein were shown to increase its propensity to aggregate and locus duplication and triplication increase expression of the protein, thereby promoting aggregation by mass action (Conway *et al.*, 1998; Giasson *et al.*, 1999; Greenbaum *et al.*, 2005; Ibáñez *et al.*, 2004; Singleton *et al.*, 2003). The locus harbouring *SNCA* has been suggested to be an expression quantitative trait locus (eQTL), with SNPs nominated by GWAS resulting in slight increases of *SNCA* expression that could contribute to the lifetime risk of developing PD (Pihlstrøm *et al.*, 2018; Soldner *et al.*, 2016).

Mitochondrial maintenance is a second convergence point of PD genes that have mostly been associated with autosomal recessive, early-onset/juvenile PD (*PINK1*, *PRKN*, *FBXO7*, *PLA2G6*, *DJ-1*) (Table 1.1) (Hauser *et al.*, 2017; Narendra *et al.*, 2010). Mitochondrial damage and the resulting oxidative stress have therefore been suggested to underlie DA neurodegeneration. Notably, MPTP, an agent causing PD, also induces neurodegeneration through mitochondrial damage (Langston *et al.*, 1983b).

Third, risk factors (*LRRK2*, *HLA*) have pointed to a role for the immune system in PD pathogenesis (Nalls *et al.*, 2014, 2018). Genes in the *HLA* region encode the major histocompatibility complex, supporting a role for the complement system in PD (Kumaran and Cookson, 2015). *LRRK2* is highly expressed in microglia and mutations in *LRRK2* have been found to sensitize microglia to a pro-inflammatory state (Russo *et al.*, 2014). Similarly, activated microglia and neuroinflammation have been found to accompany LB pathology in the brain of PD patients (Wilms *et al.*, 2003). However, it remains to be elucidated whether neuroinflammation is a cause or consequence of DA neurodegeneration (Tansey and Goldberg, 2011).

Finally, multiple familial PD genes and risk factors can be mapped to vesicular trafficking pathways. These pathways include endosomal protein sorting (*VPS35*, *LRRK2*, *RAB29*, *VPS13C*, *DNAJC6*, *GAK*) (Beilina *et al.*, 2014; Follett *et al.*, 2014; McGough *et al.*, 2014; Zavodszky *et al.*, 2014), synaptic function (*SNCA*, *SYNJ1*, *DNAJC6*, *GAK*) (Burré *et al.*, 2010; Cao *et al.*, 2017; Olgiati *et al.*, 2016) and the lysosomal-autophagy pathway (*GBA*, *ATP13A2*, *LRRK2*) (Fernandes *et al.*, 2016; Manzoni *et al.*, 2013, 2016; Schultheis *et al.*, 2013; Usenovic *et al.*, 2012). Although the exact mechanisms on the involvement of endomembrane trafficking in PD is unclear, it is a plausible hypothesis that deficient retrieval and clearance of lipids and proteins may be detrimental for neuronal survival

(Kumaran and Cookson, 2015). Remarkably, multiple genes with key functions in clathrin trafficking have been associated with PD (*DNAJC6*, *GAK*, *SYNJ1*). These will be discussed in more detail in a separate paragraph (Paragraph 1.5), given the relevance for the thesis subject.

It is important to note that the above-mentioned pathological pathways are not mutually exclusive hypothesis. There is a strong association between oxidative stress resulting from mitochondrial damage and the inflammatory pathway, and vesicular trafficking and mitochondrial maintenance are interconnected through mitophagy, a specialized form of autophagy. In addition, these pathways can function through both cell autonomous and non-autonomous mechanisms, as neuroinflammation involves both neurons and microglia, whereas mitochondrial maintenance and endomembrane trafficking are likely involved with more neuronal-restricted damage pathways (Figure 1.2) (Kumaran and Cookson, 2015).

How these pathways contribute to the observed neuropathology, i.e. accumulation of α-synuclein in LB and neurodegeneration in the SN, remains incompletely understood. Misfolding of α-synuclein is correlated with oxidative stress and the accumulation of intracellular and extracellular α-synuclein may well trigger neuroinflammatory pathways and the adaptive immune system, respectively. In addition, both the immune system and vesicular trafficking pathways are thought to be involved in the clearance of misfolded and aggregated α-synuclein (Figure 1.2) (Hardy *et al.*, 2009; Kumaran and Cookson, 2015; Tansey and Goldberg, 2011).

Collectively, genetic studies have accelerated our understanding of underlying mechanisms in PD pathogenesis. Given the the clinical, pathological and genetic overlap between familial and sporadic PD, defining disease pathways in genetic

cases may help understand sporadic disease as well. Further mechanistic dissection will be key for the development of therapies that intervene with disease progression.

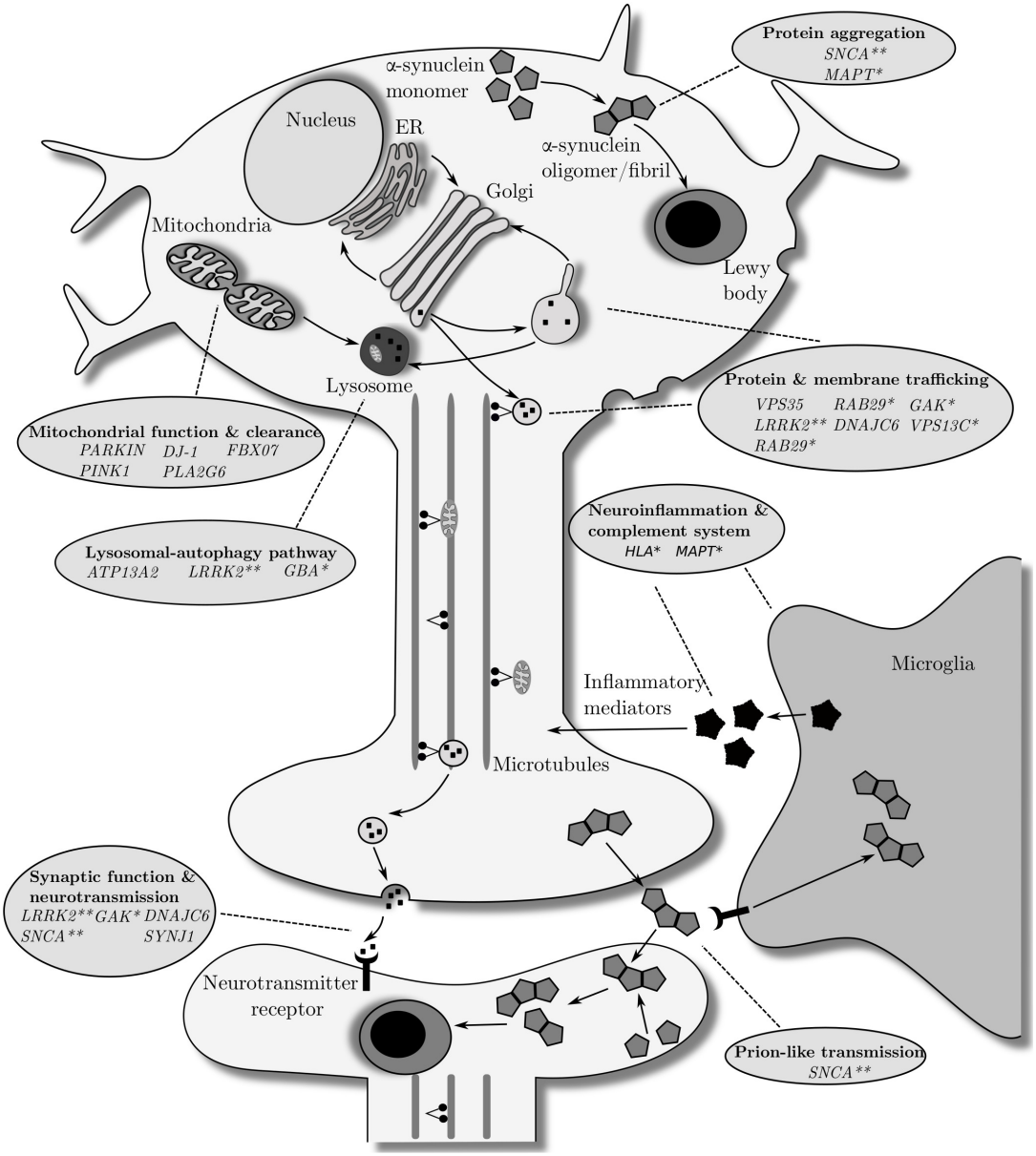

Figure 1.2: **Molecular processes involved in PD pathogenesis** Molecular processes underlying PD pathogenesis can be extrapolated from Mendelian genes and risk factors nominated through GWAS that are associated with PD. Pathobiological processes are circled in grey with indication of PD-associated genes. Asterisks (*) indicate risk factor candidates nominated by GWAS. Double asterisks (**) indicate genes that contain causative Mendelian mutations and are nominated to be a risk factor. Adapted from (Kumaran and Cookson, 2015).

1.2 CLATHRIN AND THE GENESIS OF COATED VESICLES

Vesicular transport is required to shuttle proteins and lipids between organelles whilst maintaining heterogeneity of compartments. Vesicles provide a mechanism to transport cargo, without having to cross membranes. The characterization of the coated vesicle has been a landmark discovery in the cell biology of vesicular trafficking. Vesicular coats not only serve a mechanical function but also allow for selective cargo loading into the vesicle. Coat protein complex I and II (COPI, COPII) and clathrin coats have been identified as the major classes of coated vesicles, depending on the molecular scaffolds that form the coat. COPI and COPII facilitate vesicular Golgi-to-endoplasmatic reticulum (ER) and ER-to-Golgi traffic, respectively. Clathrin facilitates vesicular transport from the plasma membrane (i.e. clathrin mediated endocytosis (CME)), as well as from the trans-Golgi network (TGN) along the axis of the secretory pathway (Figure 1.3).

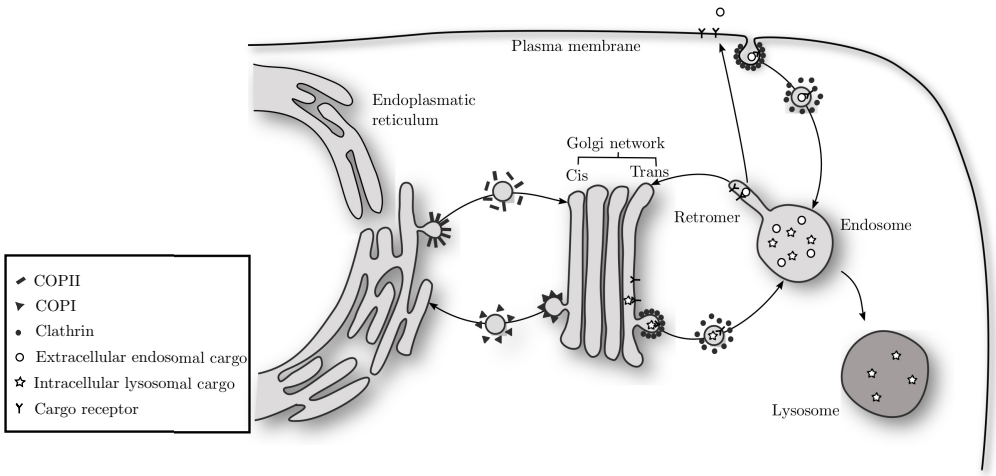

Figure 1.3: **Model of intracellular trafficking mediated by coated vesicles**

.

Clathrin mediated trafficking is defined by discrete steps, mediated by transient protein-protein interactions (Figure 1.4). The following paragraphs will give an overview of clathrin and the life of clathrin coated vesicles (CCVs). Special attention will be given to the role of clathrin adaptor proteins defining distinct cellular pathways and the uncoating of CCVs in separate paragraphs (Paragraph 1.3 and Paragraph 1.4 respectively), as these are important molecular events relevant for the subject of the thesis.

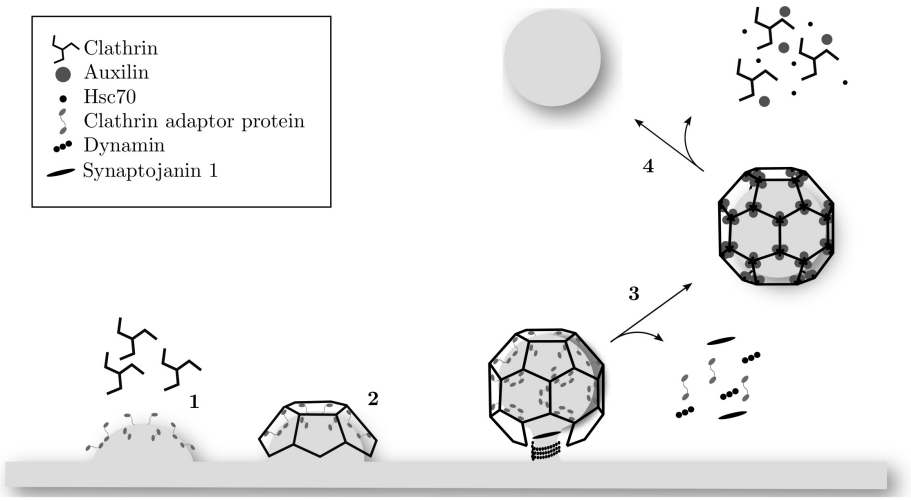

Figure 1.4: **Life of a clathrin coated vesicle** 1 Initiation. Clathrin adaptor proteins select and concentrate cargo and clathrin is recruited to form a clathrin coated pit. 2 Maturation. The clathrin coated pit commits to the formation of a CCV through membrane bending and the assembly of a clathrin coat. 3 Budding. The CCV is released from the membrane by fission. 4 Uncoating. The CCV is uncoated to allow the 'naked' vesicle to fuse with its destination compartment.

.

1.2.1 Overview and milestone discoveries

'Bristle coated pits and vesicles' were first observed by Thomas Roth and Keith Porter in 1964 by morphological electron microscopy studies on the uptake of yolk proteins by mosquito oocytes (Roth and Porter, 1964). They advanced a hypothesis where coated pits selectively 'adsorb' proteins and then become 'coated

vesicles' by pinching off from the cell membrane. The vesicles would then shed their coat for the 'naked vesicle' to fuse with intracellular compartments.

Five years later, Toku Kanaseki and Ken Kadota observed that these 'coated vesicles' were in fact 'vesicles in a basket', composed of pentagons and hexagons (Kanaseki and Kadota, 1969). Coated vesicles were shown to be involved with synaptic vesicle membrane recycling in another classic paper by John Heuser and Tom Reese (Heuser and Reese, 1973). Barbara Pearse was the first to biochemically characterize coated vesicles isolated from pig brain and identified a 180 kDa protein to be the main constituent of the coat. She proposed this protein to be named 'clathrin', derived from the Latin word 'clathratus' meaning 'like a lattice' (Pearse, 1975). Meanwhile, nobel laureates Mike Brown and Joe Goldstein were able to demonstrate that coated vesicles were able to selectively take up extracellular cargo via receptors and coined the term 'receptor mediated endocytosis' (Anderson *et al.*, 1977b; Brown and Goldstein, 1976). Thus, by the end of the 1970s, both roles for clathrin that were presciently proposed by Roth and Porter in 1964, were shown to be correct (Robinson, 2015). Although the precise mechanism is still under debate the present day, these studies implied a mechanical function for clathrin (Heuser and Reese, 1973; Kanaseki and Kadota, 1969). In addition, the finding that vesicles were able to pick and choose their cargo at sites of 'receptor mediated endocytosis' indicated a cargo selection function for clathrin (Anderson *et al.*, 1977b; Brown and Goldstein, 1976).

However, the mechanism through which the coat recognizes these receptor-rich regions wasn't discovered until years later. When purifying clathrin from coated vesicles, Barbara Pearse also noticed additional protein bands, which she proposed to be coat-associated proteins. James Keen later purified these proteins and named them 'assembly peptides' (AP) for their ability to promote the assembly of

the clathrin coat (Keen *et al.*, 1979). Margaret Robinson together with Barbara Pearse found that two distinct protein complexes were present in the clathrin assembly promoting fraction (Pearse and Robinson, 1984). James Keene purified the same complexes and proposed to call them AP1 and AP2 (Keen, 1987; Pearse and Robinson, 1984). Remarkably, AP1 and AP2 were shown to have distinct cellular colocalization at the Golgi membranes and the plasma membrane, respectively (Figure 1.8) (Ahle *et al.*, 1988; Robinson, 1987; Robinson and Pearse, 1986). Between 1996 and 2000, the laboratories of Margaret Robinson and Juan Bonifacino identified a multitude of additional clathrin adaptor proteins each with distinct intracellular distribution and involved with the selective uptake of different cargoes (Dell'Angelica *et al.*, 1997a,b, 1999, 2000; Hirst *et al.*, 1999, 2000; Simpson *et al.*, 1996, 1997), providing a mechanism by which CCVs could enrich certain cargo proteins at different places in the cell. Conveniently, the 'AP' acronym also stands for adaptor protein, which is the term used at the present day.

Much of the mechanisms of clathrin-mediated trafficking and the molecular machineries involved have now been studied in astonishing detail, as outlined in the paragraphs below. However, the dynamics and characterization of the molecular machinery required for clathrin trafficking has most extensively been studied in the context of CME. One of the major questions in the clathrin trafficking field therefore is to what extent the pathways in clathrin-mediated endocytosis can be extrapolated to clathrin trafficking from the TGN.

1.2.2 The clathrin coat

Genes and subunits of the clathrin coat

Clathrin exists as a triskelion, made up of a trimer of clathrin heavy chains (CHC), as well as three clathrin light chain (CLC) that are each associated with a CHC but not with each other (Figure 1.5) (Kirchhausen and Harrison, 1981; Ungewickell and Branton, 1981).

Two different isoforms of CHC, CHC17 and CHC22, have been described, encoded by *CLTC* and *CLTCL1* on chromosome 17 and 22 respectively (Kirchhausen *et al.*, 1987a; Long *et al.*, 1996). CHC17, hereafter simply referred to as CHC, is a ubiquitous 1675 amino acid protein and is the isoform that is involved with the formation of CCVs. CHC22 constitutes a 1640 residue protein restricted to muscular tissues. Despite 85% sequence identity, CHC22 is unable to associate with CLCs (Wakeham *et al.*, 2005) and has been suggested to play a role in specialized membrane organization rather than canonical CCV trafficking (Towler *et al.*, 2004). However, CHC22 was detected by proteomic analysis of purified CCVs, but not in CHC-depleted cells, suggesting that CHC22 is in fact a CCV component (Borner *et al.*, 2006).

There are also two human isoforms of CLC (named CLCa and CLCb), encoded by *CLTA* and *CLTB* on chromosome 9 and 5, respectively. CLCa and CLCb are much more divergent than CHC (60% amino acid identity) and in addition have multiple splicing variants, including neuronal specific variants (Jackson *et al.*, 1987). The association of CLCa and CLCb with CHCs is not fully understood, but has been suggested to occur in random fashion, depending on the relative expression levels in different cell types (Kirchhausen *et al.*, 1983; Winkler and Stanley, 1983). Without taking into account the splicing variants of LCa and

LCb, this gives rise to 4 possible clathrin triskelia depending on the incorporated CLCs: aaa, aab, bba or bbb.

Structure of clathrin triskelia

CHC exists as a kinked leg, with the carboxy terminals of three CHCs are joined in a tripod to form a triskelion (Figure 1.5 A). The leg of the CHC is ∼45 nm long and extends from the tripod to the N-terminal globular termnial domain (Kirchhausen *et al.*, 2014).

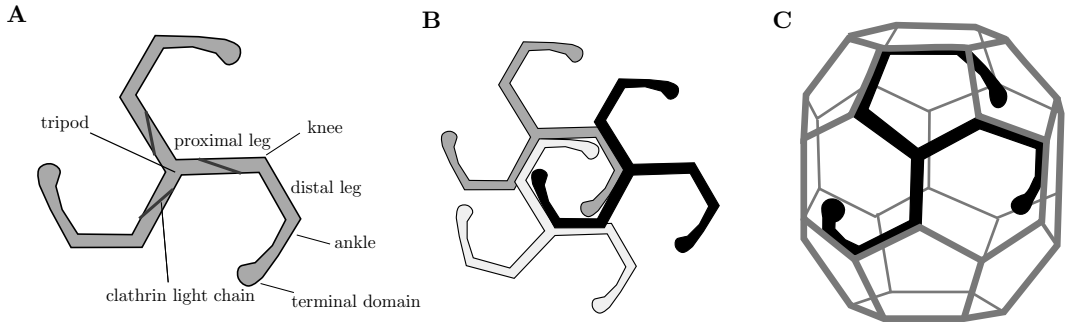

Figure 1.5: **Structure of clathrin triskelia and coat** A Molecular structure of a clathrin triskelion. B Assembly of clathrin triskelia to form hexagonal structures in the clathrin lattice, showing heavy chains only. C Structure of a hexagonal clathrin barrel of assembled clathrin triskelia. Single triskelion is represented in black.

The carboxy-terminus of clathrin contains an α-helix required for the CHC trimerization (Fotin *et al.*, 2004a). In addition, a small unstructured region extends from the tripod and contains a short hydrophobic motif ('QLMLT') that is required for the Auxilin/Hsc70-dependent uncoating (Böcking *et al.*, 2011; Rapoport *et al.*, 2008).

The leg makes up the largest part of the CHC chain and is characterized by a superhelix formation consisting of 42 α-helical zigzags of ∼30 amino acids each, creating a gently curved structure (Fotin *et al.*, 2004a). The leg consists of a proximal segment and a distal segment, separated by a flexible bend or the 'knee' (Kirchhausen *et al.*, 2014).

Finally, the amino-terminal domain consists of a β-propeller domain with 7 WD40 repeats (Fotin *et al.*, 2004a). The 'blades' of the propeller contain various binding sites for clathrin-interacting proteins, including Auxilin and clathrin APs (Haar *et al.*, 2000; Haar *et al.*, 1998; Smith *et al.*, 2004). The terminal domain is connected to the distal leg through α-helices, that appear to be more flexible than the leg itself, and forms the 'ankle' of the CHC leg (Fotin *et al.*, 2004a).

The CLCs have a disordered C- and N-terminus, but contain a long central α-helix, through which they interact with the three-fold proximal segment of the CHC leg (Chen *et al.*, 2002; Fotin *et al.*, 2004a; Kirchhausen and Toyoda, 1993; Kirchhausen *et al.*, 1987b).

Structure of the clathrin lattice and CCVs

The clathrin lattice is made up of clathrin triskelia forming hexagons, pentagons and occasionally heptagons (Figure 1.5 B, C). For example, a closed clathrin coat can be formed by exactly 12 pentagons and a variable number of hexagons (Crowther *et al.*, 1976). For every heptagonal opening, there must be a corresponding increase of pentagons to form a closed clathrin coat (Kirchhausen *et al.*, 2014). CCVs are heterogeneous in shape and size, depending on the number of pentagons, hexagons and heptagons that make up the coat, with observed diameters ranging between 66 and 134 nm (Cheng *et al.*, 2007; Heymann *et al.*, 2013).

The ability of clathrin to assemble under defined conditions *in vitro has* allowed for single-particle structural analysis by cryoelectron microscopy (cryoEM), with detailed reconstruction of a 3D coat up to ∼8 Å (Fotin *et al.*, 2004a; Musacchio *et al.*, 1999; Smith *et al.*, 1998; Vigers *et al.*, 1986). Each lattice point of the clathrin basket is made up of the centre of the tripod of a clathrin triskelion and

are connected by the interdigitating legs of the triskelia (Figure 1.5 B). A single leg of a triskelion is of such length, ∼45 nm, that it spans about three edges of the clathrin lattice. The proximal segment of the leg of a triskelion runs along one edge and forms contacts with the distal leg of the second neighbouring triskelion, with the knee in between the proximal and distal segment allowing for curvature on the first neighbouring lattice point. The ankle segment allows for curvature on the second neighbouring lattice point, in turn allowing for the terminal domain to be projected inward from the clathrin lattice in close proximity to the third neighbouring lattice point (Fotin *et al.*, 2004a; Kirchhausen *et al.*, 2014). The net result in an assembled lattice structure is the presence of 3 terminal domains underneath each lattice point or clathrin tripod, that allow for contacts with other membrane binding factors, including clathrin APs and Auxilin (Drake *et al.*, 2000; Fotin *et al.*, 2004b; Haar *et al.*, 1998; Miele *et al.*, 2004; Shih *et al.*, 1995).

1.2.3 Membrane bending

The formation of CCVs requires drastic remodelling of the membrane. The temporal and spatial regulation of this membrane plasticity remains much debated in the clathrin literature and multiple, often conflicting, models have aimed to answer the questions outlined below.

First, at what point is membrane curvature acquired during clathrin assembly? The observation of flat clathrin lattices in the proximity of curved structures and newly formed CCVs, has led to the hypothesis that flat structures rearrange to mature into curved structures (constant area model) (Avinoam *et al.*, 2015; Heuser, 1980, 1989; Heuser and Kirchhausen, 1985; Kanaseki and Kadota, 1969; Larkin *et al.*, 1986). However, this model would appear to be energetically unfavourable,

as flat lattices consisting of mostly hexagons would have to be disassembled and reassembled to include pentagons for curvature acquisition (Ehrlich *et al.*, 2004; Kirchhausen, 1993). In contrast, in the constant curvature model, the area of the clathrin lattice grows as the vesicle matures, with clathrin triskelia assembling into curved structures from the beginning of the process of membrane invagination (Cocucci *et al.*, 2012; Saffarian *et al.*, 2009). However, a number of recent studies using state-of-the-art microscopy techniques support the constant area model, showing a delay between the growth of clathrin lattices and the onset of curvature acquisition, with an average accumulation of about 70% of the final clathrin content at the onset of curvature acquisition (Figure 1.6 A-C) (Bucher *et al.*, 2018; Scott *et al.*, 2018; Yoshida *et al.*, 2018).

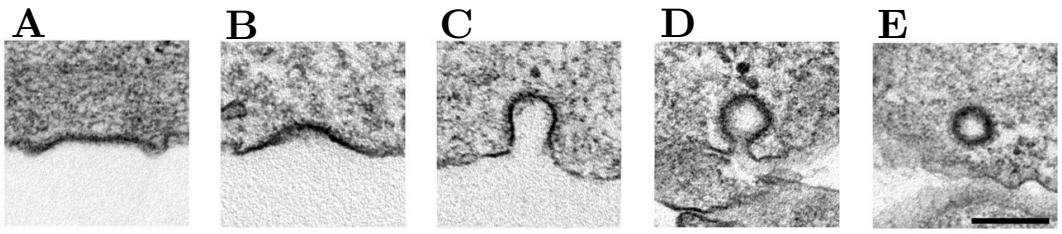

Figure 1.6: **Membrane bending and fission of CCVs** Reproduced from (Haucke and Kozlov, 2018).

.

Second, does clathrin bend membranes? Even though one of the first postulated functions of clathrin was membrane bending (Kirchhausen and Harrison, 1981; Pearse, 1975), clathrin assembly itself might not be strong enough to overcome membrane rigidity to drive curvature (Jin and Nossal, 2000; Otter and Briels, 2011; Saleem *et al.*, 2015). An apparent lack of strict temporal coupling of curvature acquisition and clathrin lattice area growth suggests that membrane reshaping is not a direct consequence of clathrin coat assembly (Haucke and Kozlov, 2018). Instead, curvature may be driven by membrane-protein interactions of CCV

machinery, through protein crowding or recruitment of curvature-inducing proteins (Haucke and Kozlov, 2018; Kirchhausen, 2012; Robinson, 2015). Protein crowding would create steric pressure, resulting in local membrane curvature (Busch *et al.*, 2015; Stachowiak *et al.*, 2012). Many proteins of the CME machinery contain intrinsic membrane shaping properties that may contribute to vesicle sculpting. BAR proteins, such as clathrin adaptors FCHo1/2 (Fer/CIP4 homology domain only protein 1/2) or dynamin, a GTPase involved in CCV fission, contain a crescent-shaped BAR (Bin-Amphiphysin-Rvs)-module that acts as a scaffold inducing curvature upon membrane binding (Faelber *et al.*, 2011; Ford *et al.*, 2011; Henne *et al.*, 2010; Sochacki *et al.*, 2017). Other clathrin adaptors such as AP180 (assembly protein 180), CALM (clathrin assembly lymphoid myeloid leukemia) and Epsin1/2 contribute to membrane bending through the insertion of an amphipatic helix into the membrane, resulting in local relaxation and thus bending of the membrane (Busch *et al.*, 2015; Ford *et al.*, 2002; Messa *et al.*, 2014; Miller *et al.*, 2011). Additional proteins involved with CCV constriction, including endophilin A and Amphiphysin, contain both a crescent-shaped BAR-domain for scaffolding and an amphipatic helix for wedge insertion (Gallop *et al.*, 2006; Peter *et al.*, 2004). Finally, actin remodelling may further counteract membrane tension to allow CCV curvature (Kaksonen and Roux, 2018).

It should be noted that even though the process of membrane bending has almost exclusively been studied in CME, it is thought that these models of membrane bending can be extrapolated to CCV formation at the TGN (Haucke and Kozlov, 2018).

1.2.4 Fission of clathrin coated vesicles

The final step in the genesis of a CCV is the separation of the initially continuous membrane of the CCV and the donor compartment (TGN or plasma membrane) into two distinct entities by constriction and fission (Figure 1.6 D-E). The budding step is regulated by the timely recruitment of BAR proteins that promote increasing membrane curvature for the constriction and scission of the CCV. Whereas the molecular machinery for fission in CME has been well-studied, it remains to be elucidated whether the same or equivalent machinery is involved with fission of CCVs at the TGN.

The fission pathway starts with the recruitment of BAR proteins with shallow BAR-domains (60-80 nm) SNX9, SNX15 and FBP17 to the neck of clathrin coated structure with low curvature (Frost *et al.*, 2008; Posor *et al.*, 2013; Shimada *et al.*, 2007). The BAR proteins Endophilin and Amphiphysin are subsequently recruited to the CCP and promote higher curvature through hydrophobic insertion of their highly curved BAR domains (∼10 nm) (Gallop *et al.*, 2006; Peter *et al.*, 2004). Endophilin and Amphiphysin finally recruit Dynamin to mediate the fission reaction (Meinecke *et al.*, 2013; Ringstad *et al.*, 1999; Shupliakov *et al.*, 1997).

Dynamin assembles as oligomers forming a helical collar (∼10 nm) around the neck of the clathrin structure (Figure 1.4) (Hinshaw and Schmid, 1995; Takei *et al.*, 1999). Hydrolysis of GTP by the large dynamin GTPase leads the oligomers to further constrict resulting in a spontaneous transition from hemi-fission to fission state (Chappie *et al.*, 2010; Chappie *et al.*, 2011; Faelber *et al.*, 2011; Ford *et al.*, 2011).

1.3 CLATHRIN ADAPTOR PROTEINS AND TRAFFICKING ROUTES

Even though clathrin plays a mechanical and cargo selection role, it does not bind the membrane nor cargo directly. In fact, there appears to be a relatively large space between the coat and the spheric vesicle, as clathrin coats of ∼70 nm in diameter have been observed to coat concentric vesicles that are ∼40 nm in diameter (Cheng *et al.*, 2007). This space allows for the presence of the rather bulky clathrin APs, bridging the gap between the vesicular membrane and its coat. Generally, transmembrane cargo and/or luminal cargo bound to transmembrane receptors bind to APs (Figure 1.7). The clathrin APs subsequently recruit clathrin to form the clathrin coat. Multiple clathrin APs have been identified displaying distinct binding preferences for transmembrane cargo receptors as well as distinct subcellular localizations. APs are therefore indeed responsible for much of the selective cargo loading in CCVs.

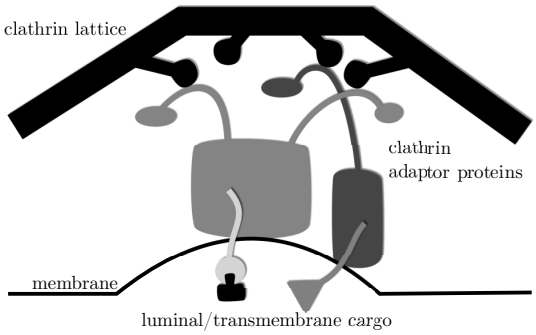

Figure 1.7: **Cargo selection by clathrin adaptor proteins**

.

1.3.1 Types of adaptor proteins

The APs are a family of heterotetrameric protein complexes (named AP1 to AP5) and function as coat proteins that are transiently recruited on to the membrane of vesicles for the selection of cargo (Dell'Angelica *et al.*, 1997a,b, 1999, 2000; Hirst *et al.*, 1999, 2000, 2011; Simpson *et al.*, 1996, 1997).

Since their discovery in 1984, AP1 and AP2 were long thought to be the only clathrin adaptor proteins (Keen, 1987; Pearse and Robinson, 1984). Both AP1 and AP2 play a role in the sorting of cargo in CCVs, however they localize to different intracellular compartments. Whereas AP1 can be found on the TGN and endosomes, AP2 is present at the plasma membrane (Figure 1.8) (Ahle *et al.*, 1988; Robinson, 1987; Seaman *et al.*, 1993).

Three additional adaptor proteins (AP3, AP4, AP5) were identified decades later by in silico analysis based on sequence homology search with AP1 and AP2 (Dell'Angelica *et al.*, 1997a,b, 1999; Hirst *et al.*, 1999, 2011; Simpson *et al.*, 1996, 1997). Like AP1, these APs localize to the endosomes and TGN, with AP3 being more abundantly present at endosomes, AP4 more at the TGN and AP5 at later endosomal compartments (Figure 1.8) (Hirst *et al.*, 2013). AP3, AP4 and AP5 are not enriched in purified clathrin coated vesicles and AP4 and AP5 were found to function independently of clathrin (Hirst *et al.*, 1999, 2011). The potential role for AP3 in clathrin trafficking is still under debate, since its interaction with clathrin has not been found consistently in mammalian cells and at least some of its functions appear to be clathrin independent (Bonifacino, 2004; Dell'Angelica *et al.*, 1998; Kirchhausen *et al.*, 2014; Peden *et al.*, 2002; Robinson, 2015). AP3 plays a role in trafficking to the lysosomes and AP4 is thought to mediate transport

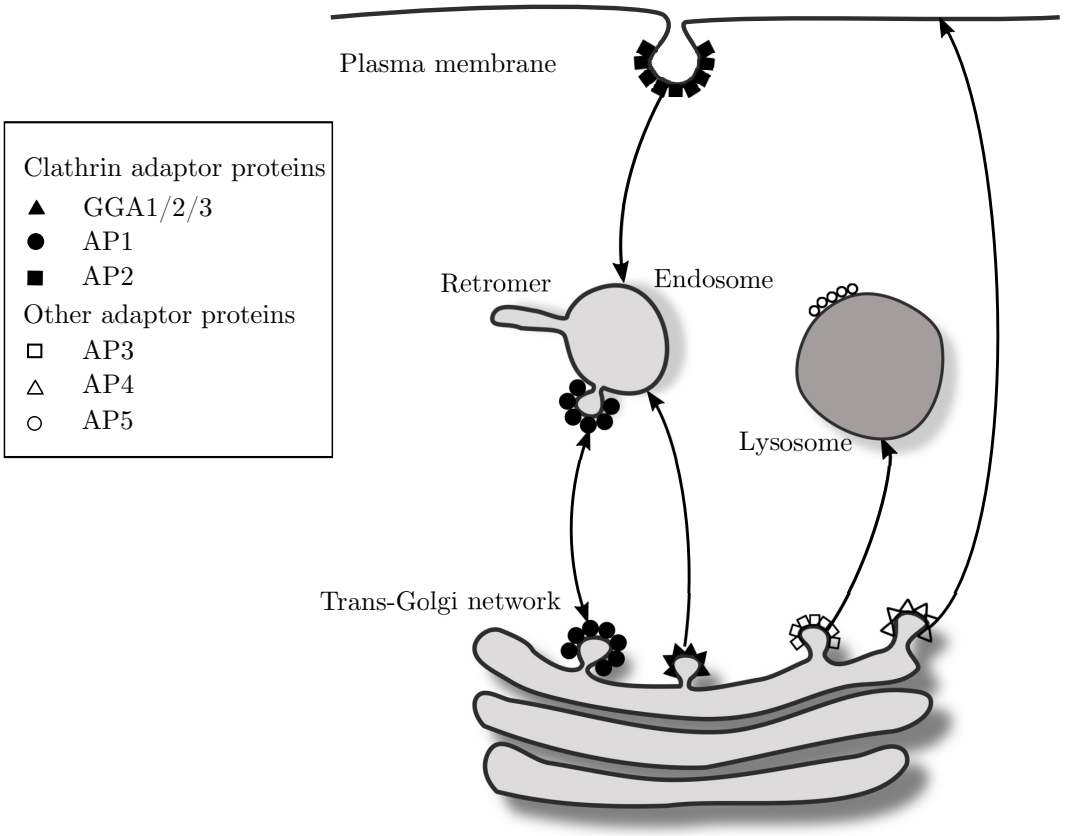

Figure 1.8: **Clathrin adaptor proteins and trafficking routes**

.

to the plasma membrane (Hirst *et al.*, 2013). The role of AP5 is currently still unclear (Hirst *et al.*, 2011, 2013).

A second family of adaptor proteins consists of monomeric proteins named the GGAs (Golgi-localized, γ-ear containing, Arf-binding proteins). GGAs were again identified by sequence homology searches of AP subunits and are localized to the TGN (Figure 1.8) (Boman *et al.*, 2000; Dell'Angelica *et al.*, 2000; Hirst *et al.*, 2000; Poussu *et al.*, 2000).

The remainder of the paragraph will be focused on the clathrin adaptor proteins, i.e. the adaptor proteins with an established role in clathrin trafficking (AP1, AP2, GGA1, GGA2 and GGA3), as those are relevant for the subject of the thesis.

1.3.2 Structure of clathrin adaptor proteins

AP1 and AP2 are heterotetrameric protein complexes, formed by subunits that are homologous across the APs: a small subunit (σ1/2, ~20 kDa), a medium subunit (μ1/2, ~50 kDa), a large subunit (β1/2, ~100 kDa) and an additional large subunit (γ, α) (figure 1.9) (Kirchhausen *et al.*, 2014; Owen *et al.*, 2004; Robinson, 2004). Several of those subunits exist in multiple isoforms, however the relative importance and potential functional diversity of the resulting assembly complexity is not understood (Hirst *et al.*, 2013).

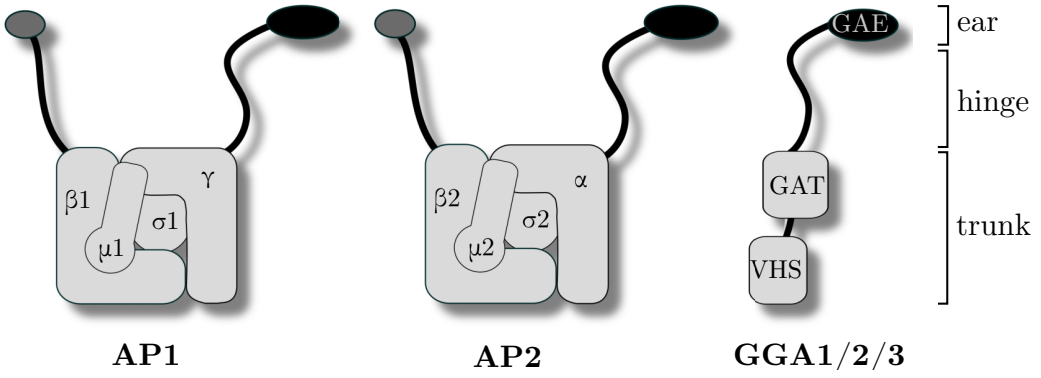

Figure 1.9: **Organisation of AP complexes and GGA proteins**

.

The large AP subunits are made up of an N-terminal trunk domain, connected through an unstructured hinge region to a C-terminal appendage or 'ear' domain. The core domain of the tetrameric complex is made up of the σ and μ subunits together with the trunk domains of β and either γ or α (Figure 1.9) (Collins *et al.*, 2002; Heuser and Keen, 1988). The core of the AP complex contains subdomains for phosphatidylinositol and/or ARF (ADP ribosylation factor) binding, required for recruitment of the AP to the membrane, as well as binding sites for the recognition of receptor sorting signals (Page and Robinson, 1995). The ear-domain of the β, α and γ domains interact with a wide range of clathrin adaptors and proteins that regulate the formation and disassembly of CCVs (Kent *et al.*, 2002;

Nogi *et al.*, 2002; Owen *et al.*, 1999; Owen *et al.*, 2000). Finally, the hinge domains of the large β-subunits contain clathrin binding motifs responsible for the interaction of the AP with the terminal domain of clathrin (Haar *et al.*, 2000; Shih *et al.*, 1995).

The GGA proteins (GGA1, GGA2 and GGA3) are monomeric proteins, and as their name implies ('Golgi-localized, γ-ear containing, ARF-binding proteins'), share strong homology with the γ-subunit of AP1 (Boman *et al.*, 2000; Dell'Angelica *et al.*, 2000; Hirst *et al.*, 2000; Poussu *et al.*, 2000). The GGAs share a conserved domain organization, comprising an N-terminal VHS (Vps27, Hrs, Stam) domain, followed by GAT (GGA and TOM (target of myb)) domain and a C-terminal GAE (γ-adaptin ear) domain, each separated by linker sequences (Figure 1.9) (Bonifacino, 2004).

The GGA proteins can be viewed as a condensed version of the AP tetrameric complex (Figure 1.9) (Bonifacino, 2004). Similarly to the trunk of the APs, the VHS domain interacts with receptor sorting signals (Misra *et al.*, 2002; Shiba *et al.*, 2002; Zhu *et al.*, 2003a) and the GAT domain interacts with ARF1-GTP (Collins *et al.*, 2003b; Shiba *et al.*, 2003; Suer *et al.*, 2003; Zhu *et al.*, 2003b), responsible for recruitment of GGA to the membrane. The hinge region between the GAT and GAE domain contains clathrin binding boxes (Costaguta *et al.*, 2001; Mullins and Bonifacino, 2001; Puertollano *et al.*, 2001b; Zhu *et al.*, 2001). Finally, the GAE domain, similarly to the γ-ear domain, binds with accessory clathrin proteins (Collins *et al.*, 2003a; Miller *et al.*, 2003).

1.3.3 Membrane recruitment of clathrin adaptor proteins

It was long thought that cargo proteins might be directly responsible for the recruitment of adaptor proteins for their incorporation into CCVs. However, cargo protein binding is not sufficient to explain specific recruitment of adaptor proteins, since cargo is present on both the donor and acceptor compartments as well as intermediary trafficking structures. Instead, in order to do their job efficiently, APs and GGAs require specific recruitment to intracellular donor compartments, which they acquire through additional interactions with ARF proteins and effectors, and/or with phosphatidylinositols (PIs).

Phosphatidylinositol composition is one of the major markers for intracellular membrane identity. Whereas phosphatidylinositol (4,5) biphosphate (PI(4,5)P2) is almost exclusively present at the plasma membrane, phosphatidylinositol 4 phosphate (PI4P) is the predominant Golgi membrane marker (D'Souza-Schorey and Chavrier, 2006). ARF proteins are small GTP-binding proteins that play a prominent role in membrane trafficking by modulating phosphatidylinositol composition of membranes (D'Souza-Schorey and Chavrier, 2006). The activity of ARFs is controlled by guanine nucleotide exchange factors (GEFs) that turn ARFs to their GTP-bound (active) state, and GTPase activating proteins (GAPs) that turn ARFs to their GDP-bound (inactive) state (Donaldson and Jackson, 2000). ARF proteins and effectors have a unique cellular localization, allowing for the recruitment of coat and adaptor proteins to distinct intracellular compartments through direct binding with the ARFs and effectors. In addition, ARFs activate lipid modifying enzymes, allowing for a local, compartment-specific concentration of phosphatidylinositols, which in turn play a role in the recruitment of coat and adaptor proteins (Bonifacino, 2004; Robinson, 2004).

ARF1 is localized to the Golgi apparatus and ARF1-GTP promotes the recruitment of AP1 and the GGAs from the cytosol to the TGN (Austin *et al.*, 2000; Dell'Angelica *et al.*, 2000; Stamnes and Rothman, 1993; Traub *et al.*, 1993). AP1 can directly bind ARF1-GTP through the β1- and γ1-trunk domains (Ren *et al.*, 2013), whereas the GGAs bind ARF1-GTP through their GAT domain (Puertollano *et al.*, 2001b; Shiba *et al.*, 2003). In addition, AP1 and the GGAs have also been found to bind PI4P directly (Ghosh and Kornfeld, 2003; Wang *et al.*, 2003). Some of the ARF1 GEFs have been suggested to further stabilize these interactions. BIG2 (Brefeldin A-inhibited GEF 2) is involved with the recruitment of AP1 and the GGAs to the TGN (Shin *et al.*, 2004; Shinotsuka *et al.*, 2002), whereas GBF1 (Golgi-specific brefeldin A-resistant GEF 1) has been suggested to specifically recruit GGAs but not AP1 to the TGN (Lefrançois and McCormick, 2007).

Interaction of AP2 with the plasma membrane marker PI(4,5)P2 through its μ2 and the trunk of its α subdomains, has been shown to be required and sufficient for for its recruitment to the plasma membrane (Gaidarov and Keen, 1999; Padrón *et al.*, 2003; Page and Robinson, 1995). ARF6, the only known plasma-membrane resident ARF protein, recruits PI4P 5 kinase type Iγ (PIPKIγ). Activated ARF6-GTP directly stimulates the activity of PIPKIγ, thereby stimulating local PI(4,5)P2 generation to facilitate further AP2 recruitment (Jackson *et al.*, 2010; Krauss *et al.*, 2003). Finally, direct interaction with ARF6-GTP has been suggested to contribute to the recruitment of AP2 to the plasma membrane as well (Paleotti *et al.*, 2005).

Taken together, these observations suggest that phosphatidylinositols and ARF-GTPs are essential components of a coincidence detection network, where

multiple low-affinity interactions are combined to recruit APs and GGAs to their respective membranes (He *et al.*, 2017; Robinson, 2015).

1.3.4 Cargo selection

Cargo is selectively concentrated to be included in CCVs. Soluble cargo relies on binding to transmembrane receptors for sorting. Upon synthesis in the ER, soluble proteins are translocated to the Golgi apparatus and acquire post-translational modifications upon migrating from the cis to trans Golgi network. Modified proteins are then bound by transmembrane receptors. In turn, transmembrane receptors as well as transmembrane cargo rely on the presence of sorting motifs in their cytoplasmic tails to be included into CCVs. Different sorting motifs have been defined and are recognized by distinct clathrin APs (Table 1.2).

Motif	Adaptor protein	Targeting	Examples of cargo
NPXY	AP2	Internalization	LDLR, APP, EGFR
YXXϕ	AP1, AP2	Internalization, targeting to intracellular compartments	TFR, CIMPR, CDMPR, LAMP1, LAMP2
[DE]XXXL[LI]	AP1, AP2	Internalization, targeting to intracellular compartments	CIMPR, CDMPR, VAMP4
DXXLL	GGA1, GGA2, GGA3	Targeting from TGN to endosomes	CIMPR, CDMPR, Sortilin, SorLA
Ubiquitin	GGA1, GGA3	Targeting to intracellular compartments	Ubiquitinated proteins

Table 1.2: **Sorting motifs for clathrin adaptor proteins**

The first cargo receptor sorting motif was discovered by nobel laureates Goldstein and Brown. Fibroblasts derived from familial hypercholesterolemia patients failed to internalize low density lipid protein bound to its receptor (LDLR), caused by a substitution of a cystein for a tyrosin in the cytoplasmic tail of LDLR (Anderson *et al.*, 1977a; Brown and Goldstein, 1976; Davis *et al.*, 1986; Goldstein *et al.*, 1977, 1979). This tyrosin residue was found to be part of a tetrameric motif, NPXY, known as a tyrosine-based motif (Chen *et al.*, 1990). In addition to LDLR, NPXY

motifs are also found in other cell surface proteins, including α-amyloid precursor protein (APP) and epidermal growth factor receptor (EGFR) (Bonifacino and Traub, 2003). The NPXY motif is recognized by the plasma-membrane localized AP2 adaptor, resulting in rapid internalization of the cargo (Boll *et al.*, 2002; Pearse, 1988).

An additional tyrosine-based sorting motif was discovered by studying recycling of the transferrin receptor (TFR). Recycling of the human TFR was studied by exogenous expression in cell lines derived from hamster and chicken, in which endogenous TFR fails to bind with human transferrin (Alvarez *et al.*, 1990b; Jing *et al.*, 1990; McGraw *et al.*, 1987). Deletional analysis narrowed down the sorting motif in the cytoplasmic tail to YXXϕ (Alvarez *et al.*, 1990a; Collawn *et al.*, 1990; Jing *et al.*, 1990). In addition to endocytic receptors such as TFR, the YXXϕ can also be found in lysosomal membrane proteins (e.g. lysosomal-associated membrane proteins (LAMP1, LAMP2)) and intracellular sorting receptors (e.g. cation-dependent and cation-independent mannose-6-phosphate receptors (CIMPR, CDMPR)) (Bonifacino and Traub, 2003; Harter and Mellman, 1992; Marks *et al.*, 1995; Williams and Fukuda, 1990). Even though these proteins have distinct cellular localizations, they all traffic to some extent via the plasma membrane (Bonifacino and Traub, 2003). Indeed, the YXXϕ motif, through AP2 binding, is key for rapid internalization at the plasma membrane (Boll *et al.*, 1996). The YXXϕ is also recognized by AP1 at intracellular compartments for correct sorting to endosomal/lysosomal structures (Höning *et al.*, 1996; Ohno *et al.*, 1995).

[DE]XXXL[LI] is a dileucine sorting motif, mostly found in proteins in the endosomal-lysosomal compartments, including CIMPR, CDMPR and VAMP4 (vesicle-associated membrane protein 4) (Bonifacino and Traub, 2003). Similar

to YXXϕ, the [DE]XXXL[LI] is critical for rapid internalization at the plasma membrane via AP2 binding. In addition, it is also recognized at intracellular compartments by AP1 for targeting to the endosomal-lysosomal structures (Fujita *et al.*, 1999; Heilker *et al.*, 1996; Hofmann *et al.*, 1999).

A second type of dileucine motif, the acidic cluster dileucine motif (DXXLL) is recognized by the GGA adaptor proteins. DXXLL motifs are present in the cytosolic tails of transmembrane proteins that travel between the TGN and endosomes/lysosomes, such as Sortilin, SorLA (Sortilin-related receptor), CIMPR and CDMPR (Bonifacino and Traub, 2003; Puertollano *et al.*, 2001a; Zhu *et al.*, 2001). Strikingly, GGA1 and GGA3, but not GGA2, also contain an internal DXXLL motif in their hinge region that interacts with their own VHS domain, which is thought to serve as an autoinhibitory role crucial for modulating their function (Doray *et al.*, 2002a).

Finally, GGA1 and GGA3, but not GGA2, have been found to function in ubiquitin-mediated sorting at the TGN and endosomes through direct interaction with ubiquitin (Prag *et al.*, 2005; Puertollano and Bonifacino, 2004; Scott *et al.*, 2004; Shiba *et al.*, 2004).

1.3.5 Cellular clathrin trafficking pathways

Clathrin trafficking has been most extensively studied in the context of CME, as CME is amenable to total internal reflection (TIRF) microscopy and can be visualized by applying extracellular probes (Robinson, 2015). Dissecting clathrin trafficking pathways at the TGN is further complicated by the presence of multiple adaptors with a more heterogeneous subcellular localization and the existence of multiple donor and acceptor compartments (Figure 1.8).

For CME, internalization of extracellular cargo and transmembrane receptors is mediated by the plasma membrane-localized AP2 complex. A classical example is the CME-mediated uptake of iron by Transferrin and TFR (Figure 1.3). Extracellular iron-bound Transferrin binds to the TFR, which in turn is recognized by AP2 through its YXXϕ motif to be internalized into a CCV (Jing *et al.*, 1990). Once the CCV delivers its contents to endosomes, the acidic pH causes Transferrin to release its iron ions. Transferrin and TFR are subsequently recycled back to the plasma membrane for another round of iron uptake (McMahon and Boucrot, 2011).

Sorting of lysosomal proteins by the CIMPR and CDMPR (M6P receptors (MPRs) in short) is the archetypical example of clathrin-mediated trafficking between the TGN and endosomes (Figure 1.3). MPRs bind to lysosomal hydrolases in the lumen of the TGN that have acquired M6P residues through post-translational modifications and are internalized into a CCV (Chen *et al.*, 1997; Johnson and Kornfeld, 1992; Kornfeld, 1992). The CCV delivers its content to endosomes after uncoating. Whereas the lysosomal hydrolases are retained in endosomes that mature to lysosomes, the MPRs are recycled back to the TGN via the retromer for additional rounds of sorting (Arighi *et al.*, 2004; Seaman, 2004, 2005; Seaman *et al.*, 1998).

CCV budding from the TGN can be mediated by multiple clathrin adaptor proteins, including AP1 and the GGAs (Figure 1.8). About $\sim$40% colocalization has been observed between AP1 and the GGAs (Daboussi *et al.*, 2012a; Hirst *et al.*, 2001; Mardones *et al.*, 2007; Puertollano *et al.*, 2003; Zhu *et al.*, 2001). In addition, some cargo, including the MPRs, contain cargo motifs for both AP1 and the GGAs (Table 1.2) (Bonifacino and Traub, 2003), raising the question to what extent the Golgi-localized clathrin adaptors are functionally redundant.

Whereas the functional relationship between AP1 and the GGAs remains incompletely understood, studies aiming to dissect their roles have given rise to three different, non-mutually exclusive models.

A first model suggests that AP1 and the GGAs function on parallel pathways in the same direction, to sort cargo from the TGN to endosomes. Indeed, studies in cells deficient of either AP1 or GGAs have been shown to be deficient in the sorting of the MPRs and lysosomal hydrolases (Hida *et al.*, 2007; Hirst *et al.*, 2009, 2012; Puertollano *et al.*, 2001a).

Second, AP1 and the GGAs may function in opposite pathways, with GGAs mediating anterograde transport and AP1 mediating retrograde transport between the TGN and endosomes. The DXXLL motif, recognized by GGAs but not AP1, appears to be the main determinant for anterograde MPR sorting from the TGN to endosomes (Lobel *et al.*, 1989; Puertollano *et al.*, 2001a; Takatsu *et al.*, 2001; Zhu *et al.*, 2001). Although AP1 knockout (KO) mice show embryonic lethality, cells derived from early embryos have shown an accumulation of the MPRs in endosomes (Meyer *et al.*, 2000).

A third model has been proposed by which the GGAs and AP1 function together on the same pathway, where cargo is bound to GGAs first and is then 'handed over' to AP1 (Doray *et al.*, 2002b). AP1 was also found to physically interact with the GGAs (Bai *et al.*, 2004; Doray *et al.*, 2002b). This model is further strengthened by the finding that AP1, but not GGAs, are detected in CCVs isolated from mammalian tissue (Hirst *et al.*, 2000).

The three GGA proteins have been shown to largely co-localize with each other (Dell'Angelica *et al.*, 2000; Ghosh *et al.*, 2003; Hirst *et al.*, 2000; Mardones *et al.*, 2007). Even though they share the same structural organization, they also differ

in a number of ways. GGA1 and GGA3, but not GGA2, contain an internal DXXLL motif important for auto-inhibitory regulation (Doray *et al.*, 2002a). In addition, GGA1 and GGA3 are able to bind ubiquitinated cargo (Prag *et al.*, 2005; Puertollano and Bonifacino, 2004; Scott *et al.*, 2004; Shiba *et al.*, 2004). GGA2 was found to be more strongly associated with membranes and has a longer half-life than GGA1 and GGA3 (Hirst *et al.*, 2007). At the organismal level, single knockout (KO) of GGA2, but not GGA1 or GGA3, is embryonically lethal, as well as double KO of GGA1 and GGA3 (Govero *et al.*, 2012). Taken together, these findings point to a non-redundant role of the GGAs, and in particular of GGA2 compared to GGA1 and GGA3. Further research is required to dissect the differences between the three GGAs and their functional relationship to each other to gain understanding how molecular differences reflect the observed physiological differences.

1.4 DNAJC PROTEINS AND CLATHRIN DYNAMICS

1.4.1 DNAJ proteins as co-chaperones of HSC70

HSC70 (heat shock cognate 71 kDa protein) is a member of the heat shock protein 70 (HSP70) family and is involved with a spectrum of cellular processes, including the ER stress response, synaptic transmission and vesicular trafficking. HSC70 is one of the most ubiquitously expressed chaperones and requires a DNAJ protein as co-chaperone for its precise recruitment to compartment-specific machineries, through interaction of HSC70 with the J-domain of the DNAJ protein. DNAJ proteins are often expressed in specific cell types or subcellular compartments and are responsible for much of the functional specificity of HSC70 (Kampinga and Craig, 2010; Stetler *et al.*, 2010).

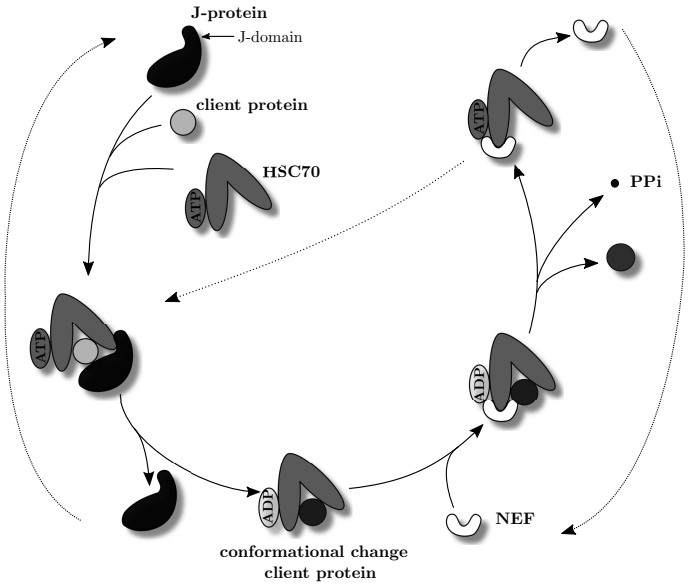

Figure 1.10: **Model of DNAJ-assisted conformational protein changes by HSC70** DNAJ is recruited to and transiently interacts with client proteins (unfolded protein to be folded or folded protein to undergo conformational change). HSC70 recruitment to the client protein is mediated by interaction of HSC70-ATP with the J-domain of DNAJ. DNAJ stimulates the ATPase activity of HSC70-ATP to induce the conformational change of the client protein and DNAJ is released from the complex. NEF protein is recruited to HSC70-ADP for nucleotide exchange of ADP to ATP and HSC70-ATP is released to undergo a new round of protein folding.

HSC70 contains an ATPase domain linked to a 'molecular clamp' domain (Figure 1.10). HSC70 and its client protein are brought together by a DNAJ protein, that interacts with both the substrate and HSC70 through its J-domain (Jiang *et al.*, 2003, 2005). ATP-bound HSC70 engages in an initial weak interaction with its client protein. Upon stimulation of the ATPase activity of HSC70 by the DNAJ protein, ATP hydrolysis tightens the molecular HSC70 clamp and results in a conformational change of the client protein (Hartl and Hayer-Hartl, 2002; Kampinga and Craig, 2010; Kelley, 1998). Replacement of ATP for ADP by nucleotide exchange factors (NEFs) opens the clamp and releases the client protein, enabling the recycling of HSC70 molecules (Figure 1.10) (Kampinga and Craig, 2010).

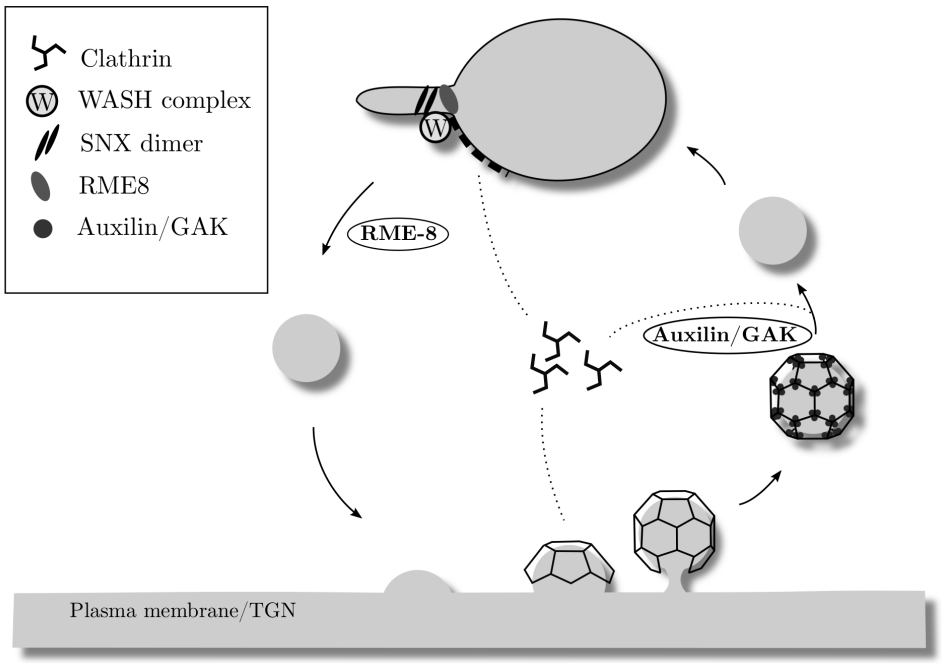

Figure 1.11: **Regulation of clathrin dynamics by Auxilin, GAK and RME-8**

DNAJ proteins can be further subdivided into DNAJA, DNAJB and DNAJC subclasses based on the presence and location of protein domains (Stetler *et al.*,

2010). Multiple members of the DNAJC subclass (Auxilin, GAK, RME-8) play important roles in the regulation of clathrin dynamics as co-chaperones of HSC70 (Figure 1.11) and are reviewed in the paragraph below. In addition, these DNAJC proteins have attracted recent attention for their involvement in PD, further outlined in Paragraph 1.5.

1.4.2 Auxilin and the uncoating of CCVs

Auxilin (short for Putative Tyrosine-Protein Phosphatase Auxilin) plays a prominent role in the uncoating of CCVs in neurons. The gene encoding Auxilin, *DNAJC6*, is located on the short arm of chromosome 1 (1p31.3) and has multiple different isoforms produced by alternative splicing (Figure 1.12). Two protein-coding isoforms (ENST00000371069, ENST00000395325) account for the majority of *DNAJC6* expression. Each is made up of 19 exons, with an alternative exon 1, and result in an Auxilin protein of 970 and 913 amino acids, respectively (Figure 1.12) (Lonsdale *et al.*, 2013). It is unclear whether these two isoforms exert physiological differences in function, but the known functional domains of Auxilin are unaffected by the alternative splicing of the first exon. *DNAJC6* expression is restricted to brain (Lonsdale *et al.*, 2013) and is most abundantly expressed in neurons (Zhang *et al.*, 2016a) (Figure 1.12).

At the molecular level, Auxilin contains an N-terminal Phosphatase and Tensin Homologue-like (PTEN-like) domain for lipid binding, followed by an unstructured hinge region, a clathrin binding domain and a C-terminal J-domain for HSC70 binding (Figure 1.14).

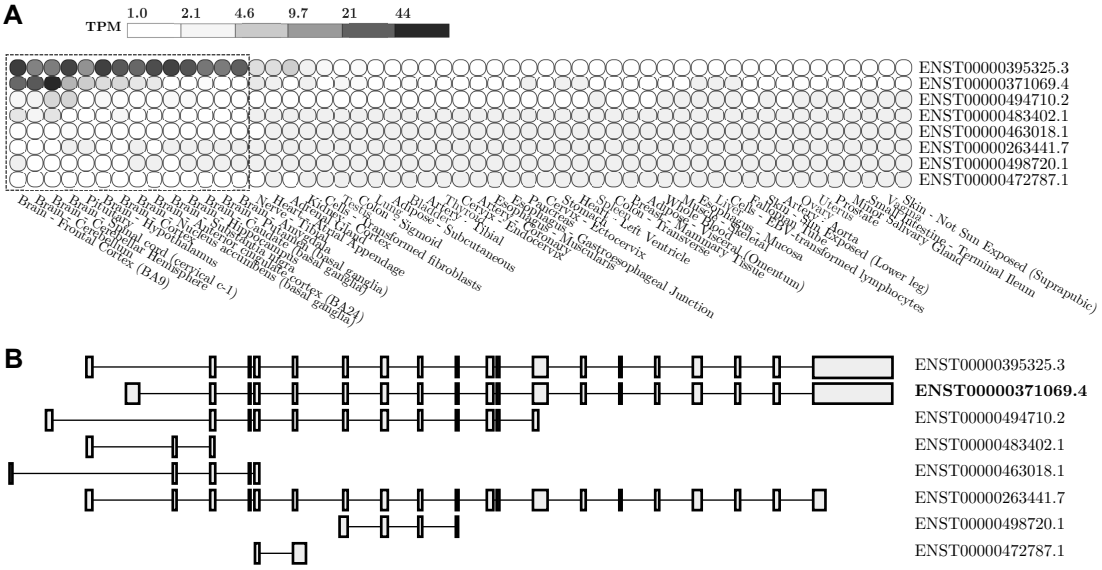

Figure 1.12: **Tissue expression profile of *DNAJC6* isoforms** A Tissue expression profile of *DNAJC6* isoforms. Dotted box indicates expression in brain. B Alternative splicing and exons making up the different *DNAJC6* isoforms. Adapted from GTEx Analysis release V7 (Lonsdale *et al.*, 2013).

Uncoating of CCVs very rapidly succeeds the pinching off of CCVs from the plasma membrane (Lee *et al.*, 2006; Massol *et al.*, 2006; Taylor *et al.*, 2011). Biochemical assays established that this uncoating reaction is dependent on the presence of both ATP and the ATPase HSC70 (Braell *et al.*, 1984; Schlossman *et al.*, 1984; Ungewickell, 1985). Auxilin was found to be required as a co-chaperone for the HSC70-mediated clathrin uncoating of CCVs in the brain (Ahle and Ungewickell, 1990). The onset of the uncoating reaction is marked by a burst of Auxilin to the CCVs after pinching off the membrane (Lee *et al.*, 2006; Massol *et al.*, 2006). The timing of these events is important, as early recruitment could lead to the disassembly of an unfinished clathrin coat.

The PTEN domain of Auxilin mediates binding to phosphatidylinositols, and is required for the timely recruitment of Auxilin to CCVs (Figure 1.14) (Guan *et al.*, 2010; Lee *et al.*, 2006; Massol *et al.*, 2006). The plasma membrane is chiefly composed of PI(4,5)P2, and smaller amounts of PI4P. A recent study by

the Kirchhausen lab has demonstrated that the budding of a CCV during CME results in a rapid burst of PI4P, PI3P (phosphatidylinositol 3 phosphate) and PI(3,4)P2 (phosphatidylinositol 3,4 biphosphate) on the CCV (He *et al.*, 2017). The fission of a CCV results in membrane discontinuity that inhibits free exchange and lateral diffusion of phosphatidylinositols along the membrane. The activity of multiple kinases and phosphatases present on CCVs, including Synaptojanin 1, can thus result in a rapid conversion of phosphatidylinositols on the membrane of CCVs (He *et al.*, 2017). Indeed, a burst of Synaptojanin 1 has been shown to precede the burst of Auxilin recruitment and the onset of CCV uncoating (Lee *et al.*, 2006). Remarkably, Auxilin has been shown to have a binding preference for PI4P, PI3P and PI(3,4)P2 over other phosphatidylinositol species (Massol *et al.*, 2006). Thus, the PTEN domain of Auxilin essentially serves as a coincidence detector of phosphatidylinositols, that senses the release of CCVs from the plasma membrane by its lipid content.

In addition to the PTEN domain, Auxilin also requires binding to clathrin for its correct localization to CCVs (Figure 1.14) (Fotin *et al.*, 2004b), as neither domain by itself is sufficient for timely recruitment to newly budded CCVs (He *et al.*, 2017; Lee *et al.*, 2006; Massol *et al.*, 2006). Auxilin contains multiple clathrin binding motifs that allow interaction with the terminal domain and distal leg of clathrin triskelia (Scheele *et al.*, 2001; Scheele *et al.*, 2003). The assembly of the clathrin coat is of such nature that three β-propeller domains are placed underneath the tripod of a clathrin triskelion (Figure 1.5), and each propeller domain interacts with a single Auxilin molecule (Fotin *et al.*, 2004b; Smith *et al.*, 2004; Xing *et al.*, 2010).

The precise placement of Auxilin molecules results in the recruitment of HSC70-ATP, through interaction with the J-domain of Auxilin, to the proximity

of the triskelion tripod (Fotin *et al.*, 2004b). The binding of Auxilin induces in a slight distortion of the clathrin coat, which allows HSC0-ATP to bind with hydrophobic motifs on the carboxy-termini of the clathrin heavy chains that protrude inward from the tripod (Rapoport *et al.*, 2008). The ATPase activity of HSC70 is stimulated by this peptide binding and Auxilin binding (Holstein *et al.*, 1996; Ungewickell *et al.*, 1997), and the resulting conversion of HSC70-ATP to HSC70-ADP tightens the HSC70 clamp with the hydrophobic clathrin motif, locking the local distortion of the clathrin coat into place (Böcking *et al.*, 2011; Fotin *et al.*, 2004b; Xing *et al.*, 2010). It is thought that a local distortion of a critical number of clathrin triskelia results in sufficient strain to destabilize the entire clathrin lattice for the subsequent uncoating of the CCV (Böcking *et al.*, 2011; Xing *et al.*, 2010).

Auxilin has also been found to interact with AP2 through a low affinity interaction of 'DPF' motifs within the clathrin binding domain (Kametaka *et al.*, 2007; Owen *et al.*, 1999; Scheele *et al.*, 2001; Scheele *et al.*, 2003). This interaction is not required for its recruitment to AP2 positive CCVs, but it is plausible that it helps stabilizing its interaction in a CCV and contributes to distinguish free and polymerized clathrin triskelia (Scheele *et al.*, 2003).

Altogether, the role for Auxilin in the uncoating of CCVs has been well established. However, the Auxilin-dependent dynamics of uncoating *in vivo* have nearly exclusively been studied in the context of CME. An important open question is therefore to what extent its function can be extrapolated to clathrin-mediated trafficking at the Golgi apparatus. CCVs derived from the TGN differ from those derived from the plasma membrane, as they contain different adaptor proteins and are derived from membranes with different lipid compositions. Remarkably, Auxilin has been found to interact with plasma membrane-resident adaptor protein

AP2, but not with Golgi-resident AP1 or the GGAs (Kametaka *et al.*, 2007). In addition, it is unclear whether the PTEN domain of Auxilin similarly senses the release of CCVs from the TGN by their lipid content as has been described for CME. Whereas the plasma membrane is chiefly composed of PI(4,5)P2, PI4P appears to be the principal phosphatidylinositol on the TGN (Daboussi *et al.*, 2012b). It remains to be determined whether CCV budding from the TGN is similarly accompanied by a rapid conversion of phosphatidylinositol contents as is the case for CME.

1.4.3 GAK, the ubiquitous homologue of Auxilin

GAK (cyclin G-dependent kinase A), encoded by *DNAJC26* (DNAJ HSP member C26), is the ubiquitously expressed paralogue of Auxilin (Figure 1.13) (Greener *et al.*, 2000). GAK and Auxilin serve a similar function as co-chaperones of HSC70 required for the uncoating of CCVs but there are a few important differences between both proteins.

At the molecular level, GAK has 44% sequence identity and 59% homology with Auxilin. GAK shares a similar domain structure to Auxilin, but has an additional N-terminal kinase domain. In contrast with Auxilin, GAK has been found to interact with both AP1 and AP2 (Greener *et al.*, 2000; Kametaka *et al.*, 2007) and the kinase domain of GAK was found to phosphorylate the μ-domains of AP1 and AP2 *in vitro* (Korolchuk and Banting, 2002; Umeda *et al.*, 2000). Whereas the exact physiological relevance of this phosphorylation *in vivo* remains to be elucidated, it has been suggested to modulate association of adaptor proteins with membranes and internalization signals of cargo (Fingerhut *et al.*, 2001; Olusanya *et al.*, 2001).

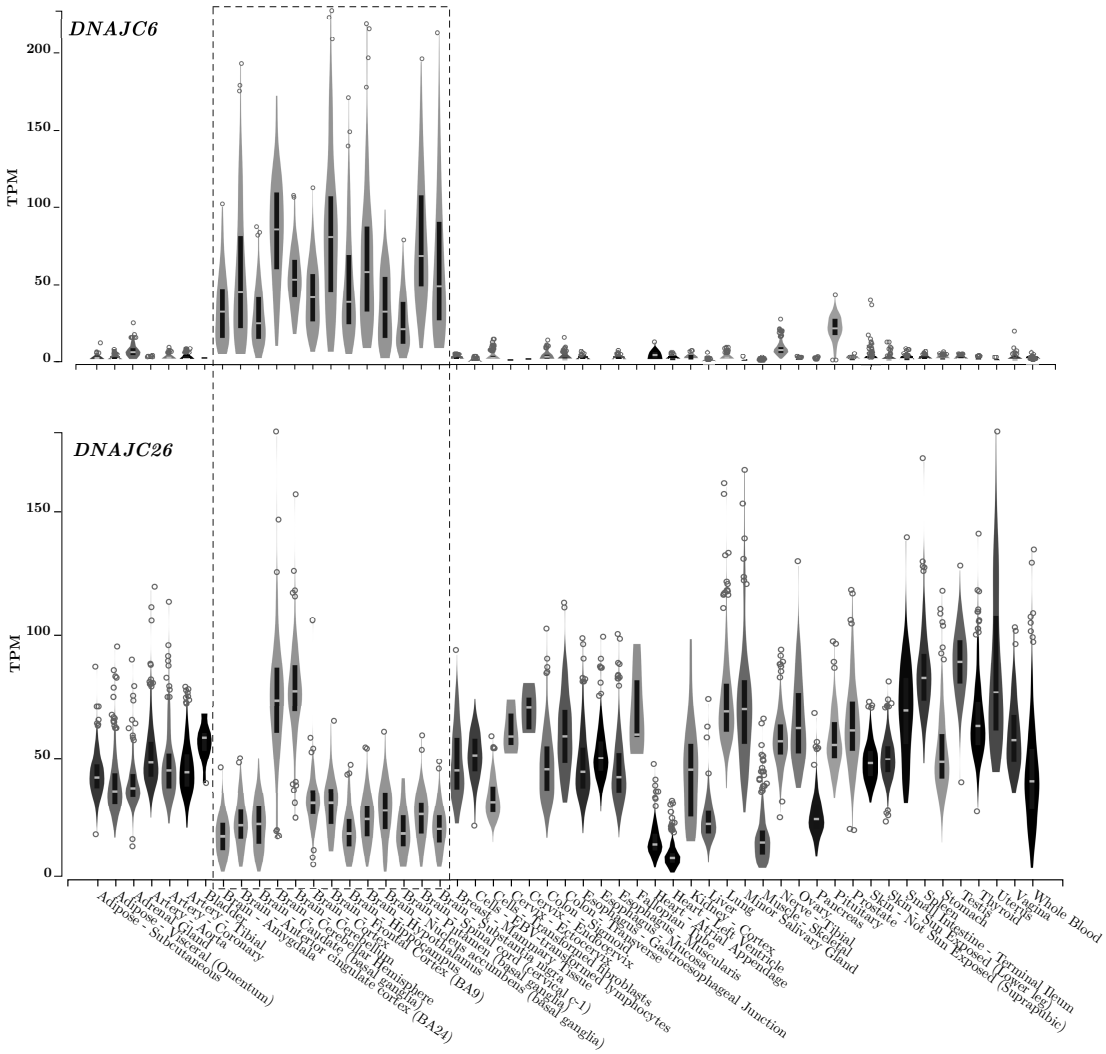

Figure 1.13: **Tissue expression *DNAJC6* (Auxilin) and *DNAJC26* (GAK) genes** Dotted box indicates expression in brain. Adapted from GTEx Analysis release V7. Gencode ID is ENSG00000116675.11 and ENSG00000178950.12 for *DNAJC6* and *DNAJC26*, respectively (Lonsdale *et al.*, 2013).

At the organismal level, GAK KO animals show embryonic mortality (Lee *et al.*, 2008), whereas Auxilin KO animals showed increased postnatal mortality, with surviving animals displaying decreased birth weight and delayed sexual maturity (Yim *et al.*, 2010). In addition, GAK was found to be upregulated in the brain of Auxilin KO animals, suggesting that GAK may partially compensate for the loss of Auxilin. However, conditional GAK KO animals with selective disruption

of GAK in the brain were lethal, indicating that Auxilin and GAK are not fully redundant in function (Lee *et al.*, 2008).

1.4.4 RME-8 and endosomal clathrin dynamics

The retromer is a pivotal complex for the selective sorting of proteins from endosomal tubules to the Golgi apparatus or plasma membrane (Seaman *et al.*, 1997; Seaman *et al.*, 1998). Cargoes that are delivered by CCVs to endosomes, including CIMPR, Sortilin and SorLA, are dependent on retromer for their retrieval and recycling to the TGN for another round of clathrin-mediated sorting (Arighi *et al.*, 2004; Fjorback *et al.*, 2012; Nielsen *et al.*, 2007; Seaman, 2004). The sorting nexin (SNX) dimer component of retromer enables the formation of tubules from the endosomes, whilst the vacuolar protein sorting (VPS) trimer component mediates protein selection and upconcentration on those tubules (Seaman and Williams, 2002; Seaman *et al.*, 1998). The WASH (Wiskott-Aldrich syndrome protein and Scar homologue) complex is a key accessory complex of retromer, facilitating the formation of an endosome-localized branched actin network required for cargo sorting (Derivery *et al.*, 2009; Gomez and Billadeau, 2009; Harbour *et al.*, 2010).

RME-8 (receptor mediated endocytosis 8) is encoded by *DNAJC13* (DNAJ HSP member C13) and is, like Auxilin and GAK, a J-protein that requires interaction with HSC70 for its function (Fujibayashi *et al.*, 2008; Girard *et al.*, 2005; Yoshida *et al.*, 2018; Zhang *et al.*, 2001). RME-8 plays a role in the regulation of endosomal tubule formation, through interaction with SNX1 and FAM21, components of the retromer SNX dimer and the WASH complex, respectively (Freeman *et al.*, 2014). Whereas RME-8 has not been found to interact with clathrin directly, loss of

RME-8 or HSC70 results in an accumulation of clathrin at early endosomes as well as the missorting of endosomal cargo (Fujibayashi *et al.*, 2008; Girard *et al.*, 2005; Norris *et al.*, 2017; Popoff *et al.*, 2009; Shi *et al.*, 2009). In addition to RME-8, the ESCRT (endosomal sorting complex required for transport) complex has also been found to interact with SNX1 (Popoff *et al.*, 2009). ESCRT-0 sorts endosomal cargo on clathrin-containing microdomains on the endosomes for degradation in the lysosomes (Chin *et al.*, 2001; Kurten *et al.*, 1996; Raiborg *et al.*, 2001).

Altogether, these findings have led to the hypothesis that SNX1 is placed at the interface of an endosomal degradative route and a retromer-dependent sorting route for retrieval and recycling of cargo. Interaction of SNX1 with the the ESCRT-complex on clathrin subdomains would lead to degradation of endosomal cargo. Alternatively, RME-8, through interaction with SNX1, has been proposed to regulate dynamics of endosomal clathrin domains to allow for the formation of functional retromer tubules. However, further research is required for the validation of this model (McGough and Cullen, 2011).

1.5 CLATHRIN TRAFFICKING AND PARKINSON'S DISEASE

Clathrin trafficking has attracted recent attention in the context of PD, as multiple genes with prominent roles in clathrin trafficking and dynamics harbour mutations associated with disease. Recessive loss of function mutations in proteins with key roles in the uncoating of CCVs, Auxilin and Synaptojanin 1, are causative for atypical, juvenile/early onset PD, with additional neurological phenotypes including seizures (Edvardson *et al.*, 2012; Elsayed *et al.*, 2016; Köroglu *et al.*, 2013; Krebs *et al.*, 2013; Olgiati *et al.*, 2014, 2016; Quadri *et al.*, 2013). GAK, the homologue of Auxilin, has been nominated by GWAS to be a risk factor candidate for PD (Nalls *et al.*, 2014, 2018). Dominant mutations in RME-8, a retromer-associated protein with a proposed role in the dynamics of flat clathrin microdomains on endosomes, are thought to cause typical, late onset PD (Gustavsson *et al.*, 2015; Vilariño-Güell *et al.*, 2011).

This paragraph will give an overview of genetics and functional involvement of clathrin genes in PD, with particular emphasis on Auxilin - the subject of the thesis.

1.5.1 Auxilin and Parkinson's disease

Multiple autosomal recessive mutations have been described in *DNAJC6* to cause juvenile and early-onset PD, with AAO ranging between 7-45 years old. For simplicity, amino acid positions of the mutations are based on the canonical *DNAJC6* transcript ENST00000371069 (Figure 1.12).

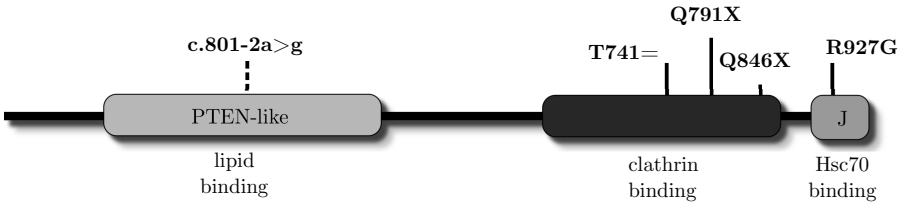

Figure 1.14: **Auxilin domain structure with indication of PD mutations**

Since 2012, 5 recessive homozygous recessive mutations have been described in *DNAJC6* and have been proposed to cause PD (Figure 1.14).

The intronic *DNAJC6* mutation c.801-2A>G was first discovered to cause juvenile onset PD in a consanguineous family of Palestinian origin (Edvardson *et al.*, 2012). The mutation lies within the intron-exon boundary at the start of exon 7 and has been suggested to result in mis-spliced mRNA and overall decreased mRNA levels (Edvardson *et al.*, 2012).

Similarly, the exonic synonymous *DNAJC6* mutation c.2223A>T is located 5 bases before the end of exon 15 in a splice-acceptor site. It is also predicted to result in mis-splicing and has been shown to result in decreased mRNA levels. The resulting recessive T741= Auxilin mutation was shown to cause early onset PD in a Brazilian family (Olgiati *et al.*, 2016).

In addition, two C-terminally truncating mutations that completely lack the J-domain as well as part of the domain containing clathrin-binding boxes, Q846X and Q791X, were described in consanguineous families from Turkish and Sudanese/Yeminis origin with juvenile PD, respectively (Elsayed *et al.*, 2016; Köroglu *et al.*, 2013).

Finally, R927G, a homozygous missense mutation in the highly conserved J-domain of *DNAJC6*, originates from a Dutch proband and was found to cause early onset PD (Olgiati *et al.*, 2016).

Interestingly, all of the homozygous recessive mutations described in *DNAJC6* show clear genotype-phenotype correlations (Table 1.3). Patients with missense mutations present with typical parkinsonism. Whereas the point mutation R927G results in early onset of disease, patients with splicing mutations (c.801-2A>G, T741=) present with both juvenile and early onset PD (Edvardson *et al.*, 2012; Olgiati *et al.*, 2016). In contrast, nonsense mutations (Q791X, Q846X) result in a very severe and rapidly progressing disease course with juvenile onset (Elsayed *et al.*, 2016; Köroglu *et al.*, 2013). These patients also presented additional atypical features including cognitive impairment, pyramidal signs and sometimes hallucinations and seizures. Remarkably, a homozygous 80kb deleterion encompassing the C-terminus of *DNAJC6* as well as the N-terminus of *LEPR* has previously been associated with epilepsies and developmental delay (Vauthier *et al.*, 2012). Although there was no report of parkinsonism, the very young presentation of phenotypes in this case at age 7 years, may mean that additional phenotypes may not have yet developed. Response to L-DOPA in patients with *DNAJC6* mutations is either absent or limited due to L-DOPA induced hallucinations and dyskinesias.

Apparently sporadic patients with early onset PD were found to carry compound heterozygous mutations (c.203813A>G and a c.1468183del) or heterozygous variants (p.L09P, p.R619C, p.M133L, p.F839LfsX22) in *DNAJC6*, of unknown pathogenicity (Olgiati *et al.*, 2016).

Whereas the role of Auxilin in the uncoating of CCVs is well recognized, the mechanism of action in disease pathogenesis remains to be studied. Genetics of *DNAJC6* point to a loss of function mechanism of Auxilin, which could lead to impairment of uncoating of CCVs at the Golgi or the synapse. Complete loss of Auxilin at the organismal level has previously been found to result in

neurodegeneration and locomotor deficits in drosophila and synaptic defects in mice (Song *et al.*, 2017; Yim *et al.*, 2010). Depletion of Auxilin in cells results in an accumulation of clathrin structures and impaired delivery of cargo (Gall *et al.*, 2000; Greener *et al.*, 2001; Hagedorn *et al.*, 2006; Hirst *et al.*, 2008; Morgan *et al.*, 2001; Pishvaee *et al.*, 2000). In addition, mass spectometry analysis has shown that double knockdown of Auxilin and its homologue GAK in cells results in depletion of cargo but accumulation of clathrin-binding proteins in purified CCVs (Borner *et al.*, 2006; Borner *et al.*, 2012).

Mutation	p.Q791X	p.Q846X	p.R927G	p.T741=	c.801-2a¿g
Age at onset	10-11	10	21/29	31/42	13/18
Assymmetric onset	+	+	+/-	+	+
Bradykinesia	+	+	+	+	+
Rest tremor	+	-	+/-	+	+
Rigidity	+	+	+	+	+
Postural instability	+	+	+	+	+
L-DOPA response	+	+	+	+	-
L-DOPA-induced dyskinesias	+	+	-	+	n/a
L-DOPA-induced hallucinations	+	-	+	+/-	n/a
Pyramidal signs	+	+	-	-	-
Cerebellar signs	+	-	-	-	-
Autonomic signs	-	-	-	-	-
Cognitive decline	+	+	-	+/-	-
Seizures	+/-	+	-	-	-

Table 1.3: **Clinical features of Auxilin mutation carriers**
+ = present, - = not reported, +/-: present in some but not all patients.

1.5.2 GAK as a risk factor candidate for PD

The locus containing *GAK* has been identified to be a risk factor candidate for PD (risk SNP rs17781378) (Nalls *et al.*, 2014, 2018). However, this region contains several other genes of interest including *TMEM175* (transmembrane protein 175) and it is currently unclear which is the causative gene on this locus. The locus is further complicated by the presence of two independent risk signals and because both genes share the same putative promoter (Nalls *et al.*, 2018).

From a functional perspective, both GAK and TMEM175 are plausible candidates as risk factors. GAK makes an interesting candidate because of its functional overlap with the Mendelian PD protein Auxilin. TMEM175 constitutes a lysosomal potassium channel and would also make a plausible candidate since multiple proteins that function in the endolysosomal pathway have been associated with PD (see Section 1.1.5). In addition, both GAK and TMEM175 have been found

to interact with other PD-associated proteins. TMEM175 has been shown to interact with α-synuclein, whereas GAK was found to form a co-complex with PD-associated proteins LRRK2 and Rab29 (Beilina *et al.*, 2014; Jinn *et al.*, 2017; Nagle *et al.*, 2016). Thus, more research is required to elucidate how this locus contributes to PD pathogenesis and whether either or both genes are risk factors for PD.

1.5.3 RME-8 and Parkinson's disease

An autosomal dominant mutation in the retromer-associated protein RME-8 (N855S) was originally described in a large, multi-incident pedigree of Dutch-German-Russian Mennonite ancestry to cause late-onset PD (Vilariño-Güell *et al.*, 2014). Five additional PD cases were described with this mutation, all carrying the same haplotype, indicating high evolutionary conservation and a common ancestor with the original Mennonite pedigree (Gustavsson *et al.*, 2015; Vilariño-Güell *et al.*, 2011). However, additional screening of Caucasian and Chinese cohorts did not identify additional mutation carriers, indicating it is not a common cause for disease (Foo *et al.*, 2014; Lorenzo-Betancor *et al.*, 2015; Ross *et al.*, 2016; Vilariño-Güell *et al.*, 2011; Yuan *et al.*, 2016). The onset of symptoms is assymetric, with average AAO of 67 years and slow course of disease progression. They present with typical parkinsonism phenotypes (tremor, rigidity and bradykinesia) and are responsive to L-DOPA therapies (Vilariño-Güell *et al.*, 2014). Additional variants in RME-8 of unknown pathogenecity have been discribed that might contribute to susceptibility of PD development (Gustavsson *et al.*, 2015; Ross *et al.*, 2016). Remarkably, dominant mutations in VPS35, a protein of the VPS retromer trimer, have also been shown to cause PD, with a

similar phenotypic presentation as RME-8 mutation carriers (Vilariño-Güell *et al.*, 2011; Zimprich *et al.*, 2011).

These genetic findings underscore the importance of retromer-mediated endosomal protein sorting in the pathogenesis of PD. N855S RME-8 has been shown to impair endosomal cargo sorting (Yoshida *et al.*, 2018). However, the exact mechanism of how of the N855S RME-8 mutation contributes to disease pathogenesis remains to be elucidated.

Finally, it should be noted that there have been conflicting reports on the association of the N855S RME-8 with PD. An independent re-analysis of the original Mennonite family in which N855S RME-8 was described has pointed to a mutation in TMEM230 to be causative for the disease in this family (Deng *et al.*, 2016). Both proposed variants display imperfect disease segregation, thus further research is required to determine which gene is causative for PD.

1.5.4 Synaptojanin 1 and Parkinson's disease

Synaptojanin 1, encoded by *SYNJ1*, is a presynaptic phosphatase mediating phosphoinositide conversion critical for the shedding of clathrin adaptor proteins from CCVs during uncoating (Figure 1.4) (Cremona *et al.*, 1999; Di Paolo and De Camilli, 2006; McPherson *et al.*, 1996).

A recessive loss of function mutation in *SYNJ1* (R258G) has been described to co-segregate with early onset PD in 4 independent consanguineous families, with AAO ranging between 20 and 30 years old (Krebs *et al.*, 2013; Olgiati *et al.*, 2014; Quadri *et al.*, 2013). In addition to the typical parkinsonian symptoms, patients also presented with atypical neurological features including cognitive decline and

epilepsies. Response to L-DOPA treatment was either poor or limited due to L-DOPA-induced dyskinesias (Krebs *et al.*, 2013; Quadri *et al.*, 2013; Taghavi *et al.*, 2018).

The R258G mutation was shown to drastically impair the phosphatase activity of Synaptojanin 1 (Krebs *et al.*, 2013) and *in vivo* studies of a mouse model with the endogenous mutation showed endocytic deficits impairment of uncoating of CCVs in synapses (Cao *et al.*, 2017). Moreover, these mice exhibited neurological manifestations reminiscent to those of human patients, including early onset motor deficits and seizures (Cao *et al.*, 2017). Impairment of CME in synapses would thus be a plausible mechanism for PD pathogenesis in these patients.

2 OVERVIEW AND AIMS OF THE THESIS

CCVs are ubiquitous across all eukaryotes and cell types and selectively transport cargo from the plasma membrane and the TGN to intracellular destinations. Auxilin is the major neuronal CCV uncoating protein and is required for the successful delivery of cargo to its destination compartments. Whereas its role in the uncoating of CCVs at the synapse has been studied in great detail, the role of Auxilin in the uncoating of TGN-derived CCVs is less established.

Over the past years, homozygous recessive mutations in Auxilin have been found to cause an aggressive form of rare, young onset PD (Edvardson *et al.*, 2012; Elsayed *et al.*, 2016; Köroglu *et al.*, 2013; Olgiati *et al.*, 2016). Two splice-site mutations (T741= and c.801-2A>G) resulting in overall decreased mRNA levels and two C-terminally truncating mutations (Q791X and Q846X) point to a (partial) loss of function mechanism in disease pathogenesis. However, the mechanism of action of the pathogenic point mutation (R927G) is less clear. In addition, the impact of the mutations at the cellular or physiological level has not been studied yet.

One way to address these open questions is to develop a mouse model with endogenous homozygous variant R857G, equivalent to the human pathogenic R927G Auxilin mutation to gain insights into the underlying neuropathology. In addition, cellular models of Auxilin mutations can be utilized to assess the impact of the mutations on biological pathways.

The overarching goal of this PhD thesis is to characterize PD-associated Auxilin mutations in order to gain insight into the mechanisms leading to neurodegeneration. This can be broken down into the following aims:

Aim 1 Test the impact of the pathogenic point mutation R927G in Auxilin in an animal model. This will be achieved by carrying out detailed behavioural analyses to assess neurological phenotypes of a CRISPR/Cas9-based mouse model with homozygous R857G Auxilin variant, equivalent to the human pathogenic R927G Auxilin mutation.

Aim 2 Investigate the neuropathological consequences of the R857G variant in the mouse brain. This will involve assessment of the presence of PD-like neuropathology, such as dopaminergic neurodegeneration and accumulation of intracellular proteinaceous inclusions. Immunohistochemistry and subsequent confocal light microscopy analysis will be performed to gain insight into neuropathology. In addition, electron microscopy will be performed to investigate ultra-structural alterations in the brain of R857G Auxilin mice.

Aim 3 Identification of cellular pathways affected by the pathogenic Auxilin point mutation, via RNAseq-based analysis of transcriptomic alterations in murine primary neurons derived from R857G Auxilin mice. This will test whether there are specific cellular signatures associated with point mutations in Auxilin.

Aim 4 Mapping of the interactome of Auxilin to gain mechanistic insight into the molecular machinery involved with the uncoating of CCVs, both at the synapse and the Golgi apparatus. Proteome-wide analyses will be used to identify the full interactome of Auxilin in an unbiased fashion.

Aim 5 Dissect the pathogenic mechanisms underlying PD in Auxilin mutation carriers, by evaluating the impact of PD mutations on the interactome of Auxilin. This will test whether mutations in Auxilin result in a consistent disease-specific alteration in protein complex biology leading to dysfunction.

Taken together, assessment of the impact of Auxilin mutations at the organismal level, on neuronal pathways and at the cellular and molecular level should provide significant insights in the underlying pathobiology of Auxilin mutation carriers. These findings in turn will contribute to our understanding on the involvement of clathrin trafficking in PD, with the potential to open up novel therapeutic pathways in the future.

3 DEVELOPMENT OF A NOVEL AUXILIN MUTATION MOUSE MODEL

3.1 INTRODUCTION

Auxilin is the major neuronal co-chaperone of HSC70, required for the shedding of the clathrin coat of CCVs. Multiple homozygous recessive mutations in Auxilin have been found to cause a rare, aggressive form of young onset PD, but how Auxilin mutations contribute to PD pathogenesis remains to be elucidated. Some of the described Auxilin mutations are likely to function via a loss of function mechanism, since two nonsense mutations in Auxilin result in C-terminally truncated proteins (Q791X, Q846X) and two additional mutations are splice-site variants (c.801-2A>G, T741=) that are thought to result in decreased mRNA levels (Edvardson *et al.*, 2012; Elsayed *et al.*, 2016; Köroglu *et al.*, 2013; Olgiati *et al.*, 2016). Finally, the homozygous recessive R927G Auxilin mutation lies within the conserved J-domain, required for interaction with HSC70. The mechanism of action in PD of the R927G mutation is less clear (Olgiati *et al.*, 2016).

At the organismal level, complete loss of Auxilin in mice results increased postnatal mortality, with subsequent deviation from the expected 1:2:1 Mendelian inheritance from heterozygous mating in mice (Yim *et al.*, 2010). Surviving Auxilin KO mice showed a decreased body weight, but otherwise normal lifespan (Yim *et al.*, 2010). In addition, GAK, the ubiquitously expressed homologue of Auxilin, was found to be upregulated in the brain, indicating that GAK may compensate for the lack of Auxilin (Yim *et al.*, 2010).

In contrast, GAK KO mice are embryonically lethal (Lee *et al.*, 2008). Selective KO of GAK in the brain of developing mice also results in embryonic and early

postnatal mortality, with all mice dying before the 4th day after birth (Lee *et al.*, 2008). These findings indicate that Auxilin and GAK may not fully compensate for each other in the mouse brain. Either their physiological roles are not fully redundant, or GAK and Auxilin exhibit different cellular expression patterns across cell types in the central nervous system and expression levels are not sufficient to compensate for complete loss of either protein. Whereas Auxilin has been reported to be highly expressed in the brain and more specifically in neurons (Figure 1.12) (Lonsdale *et al.*, 2013; Zhang *et al.*, 2014; Zhang *et al.*, 2016b), GAK has a ubiquitous expression with relatively low expression levels across different brain areas (Figure 1.13) (Lonsdale *et al.*, 2013). Previous RNAseq experiments have indicated very low GAK mRNA levels in acutely isolated cortical neurons from mouse and human brain, respectively (Zhang *et al.*, 2014; Zhang *et al.*, 2016b).

To understand how the R927G Auxilin mutation causes PD, a novel mouse model was developed in collaboration with the Transgenic Core of the National Heart, Lung and Blood Institute (National Institutes of Health), carrying the equivalent murine homozygous R857G Auxilin variant. Remarkably, the R857G Auxilin was found to result in decreased Auxilin levels in the brain. I therefore hypothesized that mice with the homozygous hypomorphic R857G Auxilin allele may recapitulate manifestations seen in mice with complete loss of Auxilin. To understand whether GAK could compensate for the partial loss of Auxilin, RNA and protein levels of GAK and Auxilin in the brain were analysed at different time points. In addition, the expression of GAK and Auxilin in individual cells in the mouse brain were visualized using RNAscope experiments, executed by Dr. Sara Saez-Atienzar. The impact of the R857G Auxilin at the organismal level and

on nigrostriatal pathways will be further discussed in Chapter 4 and Appendix 1, respectively.

3.2 RESULTS

3.2.1 Design of a CRISPR/Cas9-based R857G Auxilin mouse model

The R927 residue of Auxilin lies within a stretch of amino acids in the J-domain that is very well conserved across different J-proteins as well as different species (Figure 3.1 A). I therefore decided to generate a mouse model with the equivalent endogenous homozygous murine R857G variant in collaboration with the transgenic core (National Heart Lung and Blood Institute, National Institutes of Health) using clustered regularly interspaced short palindromic repeats (CRISPR)/Cas9 in a C57BL/6J background. CRISPR-based mutagenesis for R to G substitution was designed for optimal murine glycine codon utilization (AGG>GGC). The AGG codon for the R958 residue served as the protospacer adjacent motif (PAM), critical for target binding and cleavage by CRISPR. Silent mutations were introduced in the PAM sequence to prevent further targeting of Cas9 after CRISPR successful editing (Figure 3.1 B). Correct CRISPR-editing was confirmed by Sanger sequencing of genomic DNA derived from mouse tails (Figure 3.1 C).

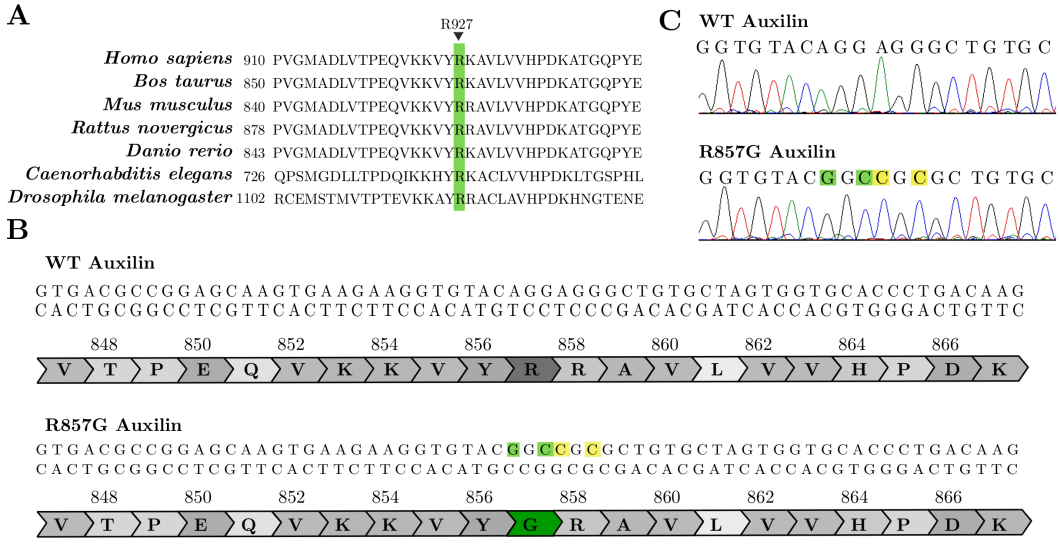

Figure 3.1: **Design of CRISPR-mediated R857G Auxilin mouse** A The human R927 Auxilin residue is conserved across species and is equivalent to the murine R857 residue. Amino acid position is based on the canonical *Mus musculus DNAJC6* transcript ENSMUST00000094953. Silent mutations are indicated in yellow, missense mutations are indicated in green. B Design of the R857G Auxilin mutation mouse at the level of amino acids and basepairs. Silent mutations are indicated in yellow, missense mutations are indicated in green. C Sanger sequencing to confirm correct knockin of R857G Auxilin mutation.

3.2.2 Decreased Auxilin protein levels in neurons of R857G Auxilin animals

Even though Auxilin expression is largely restricted to the brain, and more specifically to neurons, previous work has indicated a dramatic decrease of Auxilin protein levels in primary fibroblasts derived from R927G mutation carriers compared to controls (Olgiati *et al.*, 2016). To understand the effect of the mutation in neurons on Auxilin protein levels, primary neurons were derived from the combined brains from a litter of WT and R857G Auxilin mice each. Western blot (WB) analysis revealed a ∼75% decrease in Auxilin in neurons derived from R857G Auxilin mice compared to WT controls.

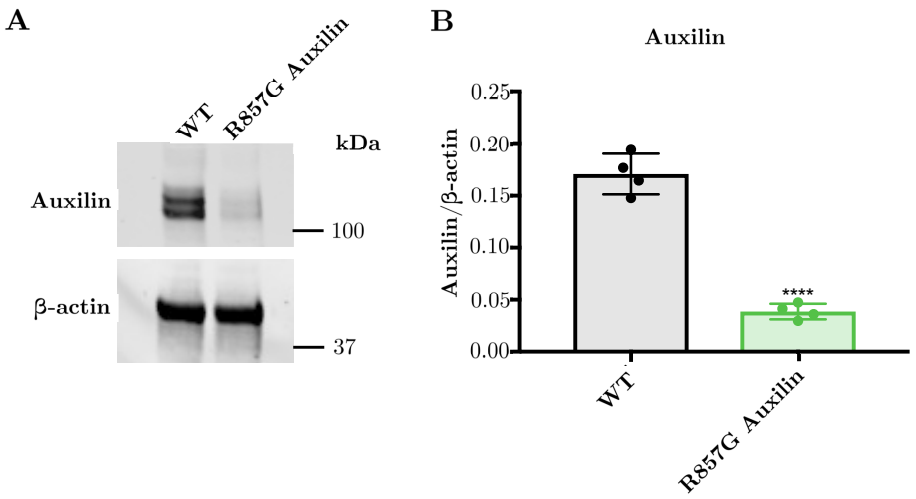

Figure 3.2: **Decreased Auxilin protein levels in R857G Auxilin primary neurons** A WB of Auxilin in primary neurons derived from the combined brains of a full litter of WT and R857G Auxilin mice each. B Quantification of normalized Auxilin levels. n = 4 independent cultures from pooled litters. Welch's t-tests were performed, **** indicates p-value <0.0001. Error bars represent standard deviation (SD).

3.2.3 Age-dependent upregulation of Auxilin in R857G Auxilin mice

To extend these results to the *in vivo* setting, I compared Auxilin levels in mouse brains from litters of WT and R857G Auxilin mice at different time points from birth.

Similarly to primary neurons that are derived from postnatal day 0 (P0) animals, brain lysates of P0 R857G mutant mice showed decreased levels of Auxilin. In four out of five R857G Auxilin animals there was a substantial (∼60%) decrease in Auxilin levels, although in one animal Auxilin protein was more substantially decreased (Figure 3.3).

Analysis of Auxilin in half brain lysates of 2 day old mice (P2) similarly showed that Auxilin was nearly completely absent in the brain of one pup of the R857G Auxilin litter, whereas all other brains displayed a ∼50% decrease in Auxilin levels compared to WT brain lysates (Figure 3.3).

No differences in Auxilin protein levels were observed in half brain lysates of 3 week old animals (Figure 3.3).

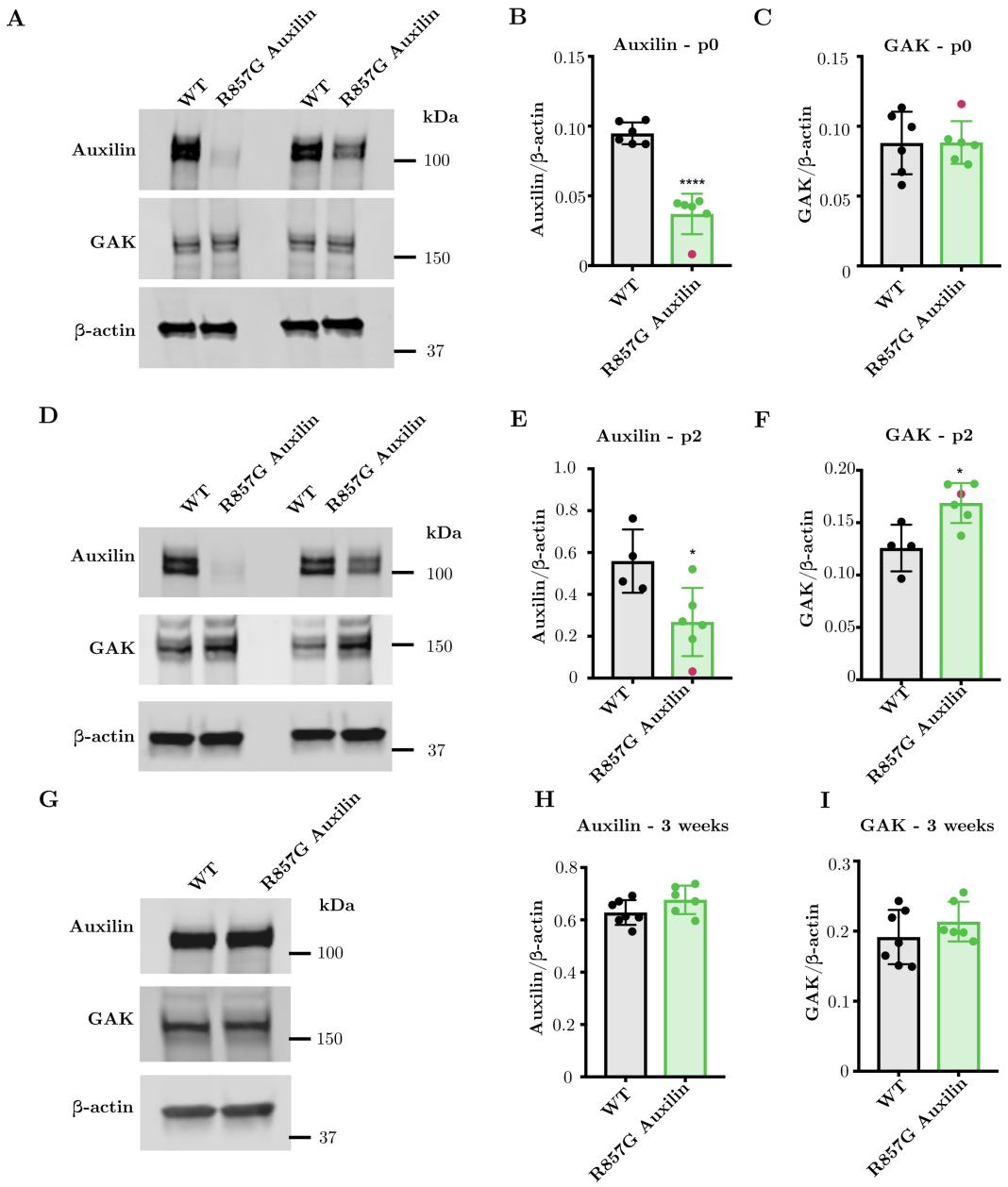

Figure 3.3: **Auxilin and GAK protein levels in the brain of R857G Auxilin mice** A, D, G WB of Auxilin and GAK in brain lysates of P0, P2 and 3 week old WT and R857G Auxilin mice, respectively. n=4-6 mice per genotype. B, C, E, F, H, I Quantification of normalized Auxilin and GAK levels brain lysates of P0, P2 and 3 week old WT and R857G Auxilin mice. Welch's t-tests were performed and p-values indicated when significant, * p-value <0.05, **** p-value <0.0001.

3.2.4 Transient upregulation of GAK in the brain of R857G Auxilin mice

Since GAK was found to be upregulated in the brain of Auxilin KO animals, I analysed protein levels of GAK in the brain in the brain of R857G Auxilin mice at different time points. Whereas no differences in GAK were observed in the brains of P0 or 3 week old mice, GAK protein levels were increased in the brains of P2 R857G Auxilin mice compared to WT mice (Figure 3.3). Interestingly, P0 and P2 R857G Auxilin mice with nearly completely absent Auxilin protein levels, showed high GAK expression levels compared to their littermates (Figure 3.3 B, C, E, F). Thus, GAK appears to be transiently upregulated two days after birth in R857G Auxilin mice, possibly to compensate for the decreased levels of Auxilin protein in early development. This idea is further strengthened by the observation that R857G Auxilin pups with the lowest Auxilin protein levels display the higher GAK levels in the brain.

3.2.5 mRNA expression levels of Auxilin and GAK in the brain of R857G Auxilin mice

To understand whether the observed alterations in Auxilin and GAK protein levels in the brain of R857G Auxilin mice were driven by alterations in mRNA levels, quantitative polymerase chain reactions (qPCR) were performed at different ages (P0, P2 and 3 weeks).

RNA was extracted from full brains from WT and R857G Auxilin litters of P0 mice, or from the remaining hemisphere of the brains that were used for WB analysis of P2 and 3 week old mice.

Even though decreases in Auxilin protein were observed in P0 and P2 R857G Auxilin mice, no differences in Auxilin mRNA levels were observed at any of the time points.

GAK mRNA levels were increased at all time points, in contrast with GAK protein levels that were only found to be significantly increased in P2 R857G Auxilin mice. The P2 R857G Auxilin mouse that showed nearly completely absent Auxilin protein levels (Figure 3.2 D, E), displayed the highest Auxilin mRNA levels compared to its littermates (Figure 3.4 C). GAK protein and mRNA levels were also found to be higher in this animal compared to littermates (Figure 3.3 F, Figure 3.4 D).

Taken together, these data indicate that the decreased levels of Auxilin during early development can not simply be explained by decreased expression in R857G Auxilin mice, as no differences in Auxilin mRNA were observed between genotypes. In contrast, GAK expression was found to be upregulated at all tested time points indicating transcriptional activation in R857G Auxilin mice. However, GAK protein was only found to be transiently increased 2 days after birth in the brain of R857G, indicating that GAK may compensate for decreased Auxilin function in P2 R857G mice.

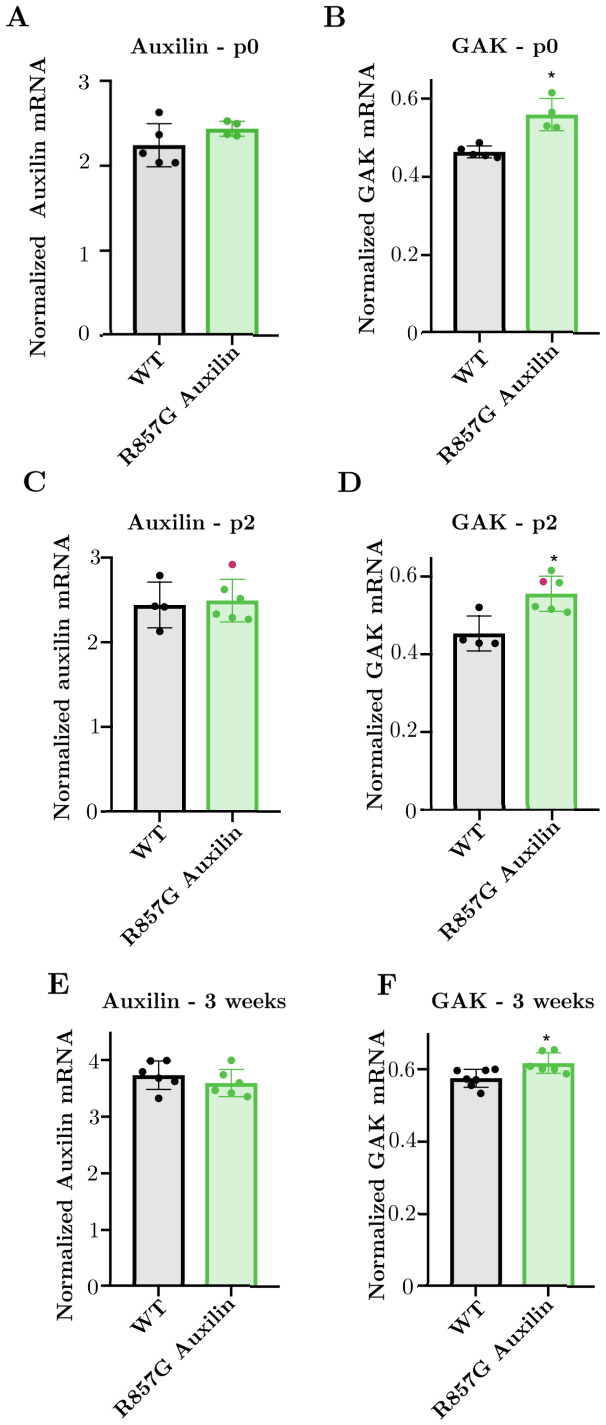

Figure 3.4: **Auxilin and GAK mRNA levels in the brain of R857G Auxilin mice** A, C, E qPCR analysis of Auxilin mRNA normalized against PPID mRNA levels in the brain of P0, P2 and 3 week old WT and R857G Auxilin mice, respectively. n=4-6 mice per genotype. B, D, F qPCR analysis of GAK mRNA normalized against PPID mRNA levels in the brain of P0, P2 and 3 week old WT and R857G Auxilin mice, respectively. Welch's t-tests were performed and p-values indicated when significant, * p-value <0.05.

Auxilin protein levels were found to be decreased in primary R857G Auxilin neurons (Figure 3.2). To address whether GAK expression was increased in neurons derived from R857G Auxilin mice specifically, qPCR was performed of primary cultured prepared from individual brains.

In line with the findings on Auxilin and GAK mRNA levels of total brain RNA, no differences in Auxilin mRNA levels were observed in R857G Auxilin primary neurons, whereas GAK mRNA levels were found to be upregulated (Figure 3.5).

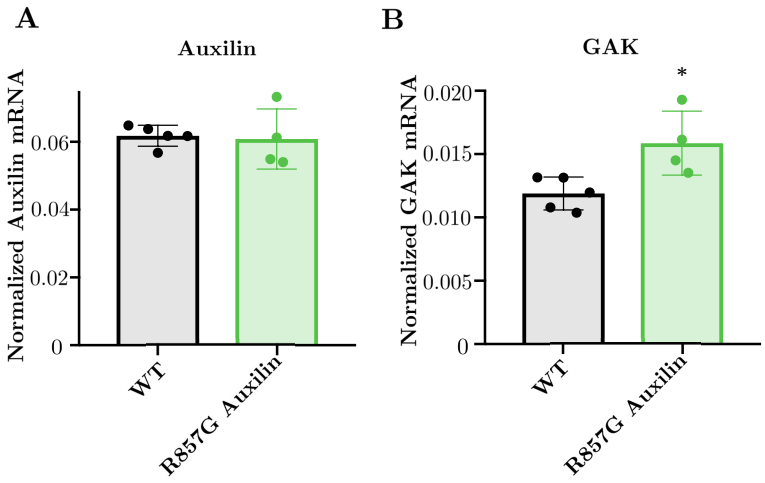

Figure 3.5: **Auxilin and GAK mRNA levels in primary neurons** qPCR analysis of Auxilin mRNA normalized against β-actin mRNA in primary neurons derived from WT and R857G Auxilin mice. Primary neurons were derived from n=4-5 mice per genotype. Welch's t-tests were performed and p-values indicated when significant, * p-value <0.05.

3.2.6 Cellular RNA expression of GAK and Auxilin in the mouse brain

Auxilin expression has previously been reported to be largely restricted to neurons in the mouse brain (Zhang *et al.*, 2014; Zhang *et al.*, 2016b).

Since GAK protein levels were found to be upregulated in the brain of P2 R857G Auxilin mice, it was hypothesized that this could compensate for the decreased Auxilin levels. However, GAK would only be able to partially compensate for loss of Auxilin function when expressed in the same cells, i.e. neurons.

To assess whether Auxilin and GAK are expressed in the same cells in the brain, and in particular in dopaminergic neurons in the SN, the brain area affected in PD, RNAscope was performed to visualize RNA expression in midbrain slices of 2 month old WT mice. Auxilin was found to be highy expressed in dopaminergic neurons in the SN and VTA (Figure 3.6).

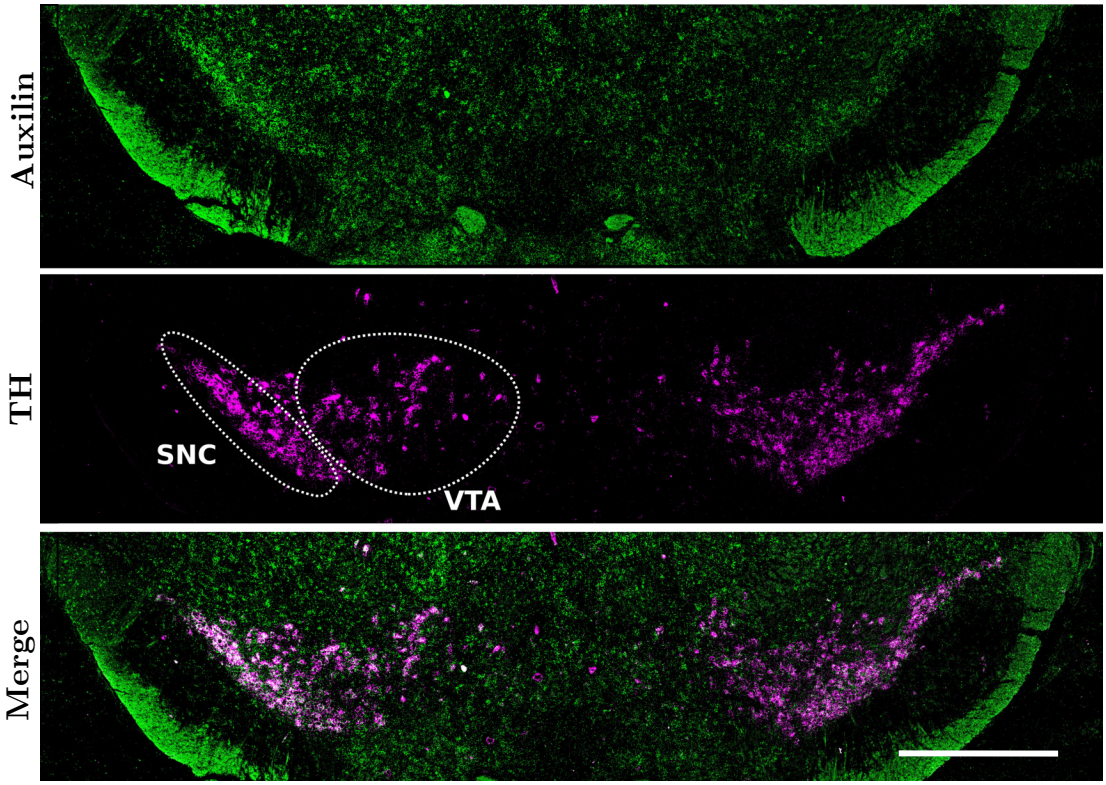

Figure 3.6: **RNAscope of Auxilin in the nigrostriatal pathway** RNAscope experiment was executed by Dr. Sara Saez-Atienzar. Auxilin mRNA (green), the dopaminergic neuronal marker TH mRNA (pink) was visualized in midbrain slices of 2 month old WT mice. Scale bar indicates 800 μm.

RNAscope at higher magnifications of midbrain slices allowed to visualize Auxilin and GAK expression within individual cells. GAK and Auxilin were found to be expressed within the same cells, including in the SN pars compacta and pars reticulata (Figure 3.7).

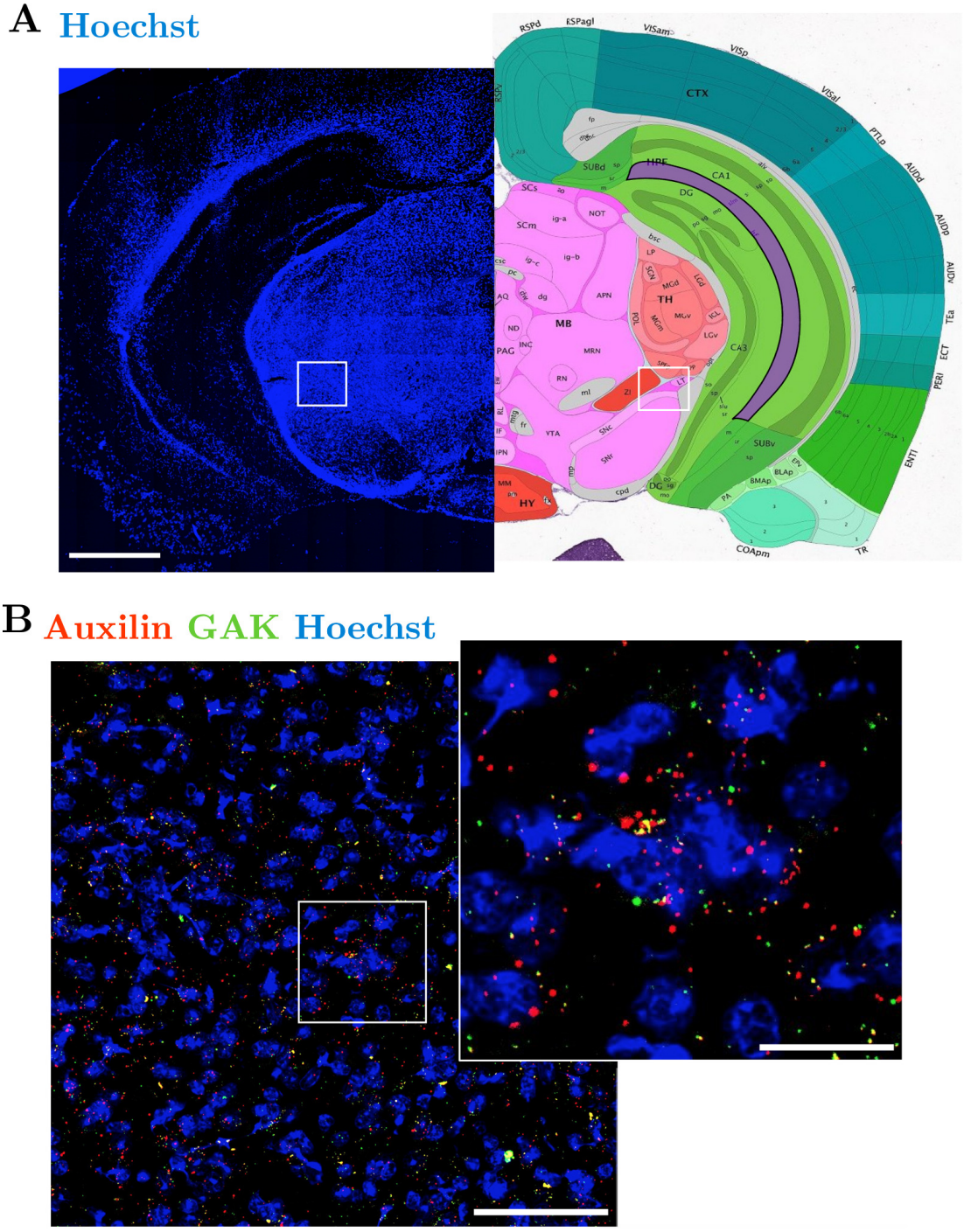

Figure 3.7: **RNAscope GAK and Auxilin in the SN** RNAscope experiment was executed by Dr. Sara Saez-Atienzar. Nucluear marker (DAPI, blue), Auxilin mRNA (red) and GAK mRNA (green) were visualized in the SN in midbrain slices of a 2 month old WT mouse. Scale bars indicate 800 μm, 100 μm and 30 μm in left, middle and right panel respectively.

3.2.7 Deviation from Mendelian inheritance

To evaluate viability of R857G Auxilin mice compared to WT, the offspring of heterozygous R857G Auxilin mice mating were genotyped at 3 weeks old. A significant deviation from the expected 1:2:1 Mendelian inheritance ratio (homozygous R857G:heterozygous R857G Auxilin:WT) was observed, indicating decreased viability of R857G Auxilin mice (Figure 3.8).

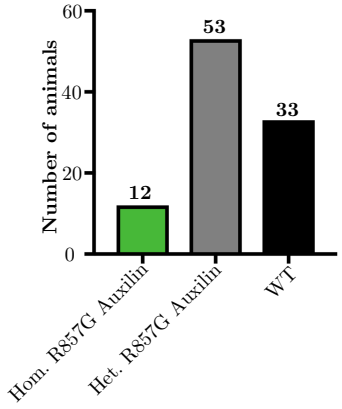

Figure 3.8: **Survival bias of heterozygous R857G Auxilin mating** Survival bias of the offspring of heterozygous R857G Auxilin mating at 3 weeks old. Chi-square test was performed with n = 10 litters and p-value < 0.01.

3.2.8 Decreased birth weight in R857G Auxilin mice

Since a decreased weight at birth was observed in Auxilin KO mice (Yim *et al.*, 2010), the body weight of R857G Auxilin was compared with WT mice at different ages. P0 R857G Auxilin mice displayed a decreased body weight compared to WT mice. Given the large variation in weight between male and female animals at later ages, gender was considered a confounding factor and included as an additional independent variable. A decreased body weight was observed for 6 month old female mice. No differences were observed for 12 month old animals.

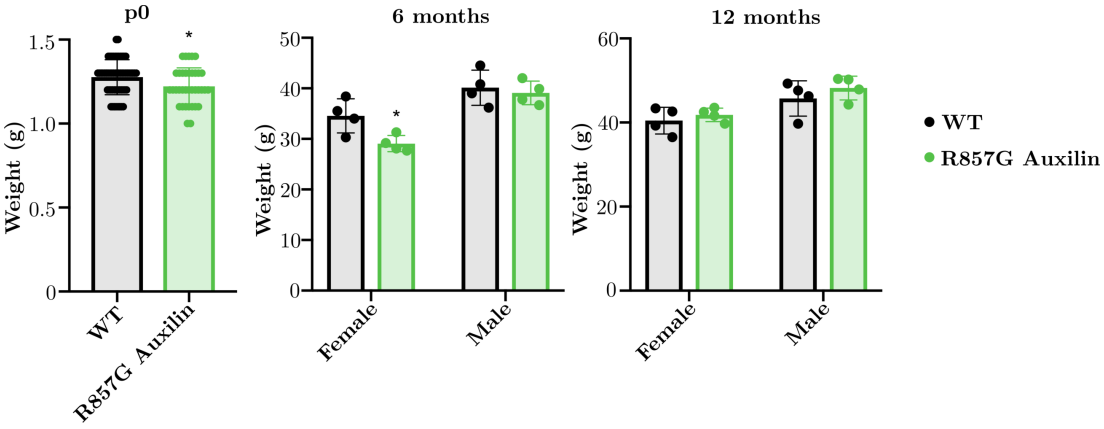

Figure 3.9: **Body weight of R857G Auxilin mice** A Body weight of newborn mice. Welch's t-test was performed, n=5 and 6 litters for WT and R857G Auxilin mice, respectively, * indicates p-value < 0.05. B and C Body weight of 6 and 12 month old mice. Two-way ANOVA was performed with Sidak's *post hoc* analysis, p-value is indicated when significant, * represents $p < 0.05$.

3.3 DISCUSSION

To gain insight into the mechanism of action of the pathogenic R927G Auxilin mutation in PD, a novel CRISPR/Cas9-based mouse model with the equivalent homozygous R857G murine Auxilin mutation was developed.

Decreased Auxilin protein levels were observed in newborn R857G Auxilin mice. Analysis of Auxilin protein levels in P0 R857G Auxilin brains revealed a $\sim 60\%$ decrease compared to WT mice, whereas a $\sim$50% decrease was observed in P2 R857G Auxilin brains. Remarkably, Auxilin appeared to be nearly completely absent in one R857G Auxilin pup per P0 and P2 litter. This points to developmental differences between R857G Auxilin litter mates and a possible explanation is that mutant mice lacking Auxilin are the runts of the litter. No differences in Auxilin protein levels were observed in 3 week old R857G Auxilin mice compared to WT. Taken together, these data show that R857G Auxilin is a hypomorphic allele, but Auxilin levels gradually increase with age in R927G brains and are equivalent to those in WT mice at 3 weeks old (Figure 3.3).

No differences in Auxilin mRNA levels were observed in the brains of P0, P2 or 3 week old R857G Auxilin mice (Figure 3.4). This apparent discrepancy between relative levels of Auxilin mRNA and protein between WT and R857G auxilin mice could be explained in several different ways. First, the R857G Auxilin mutation may decrease the half-life of the Auxilin protein. If this were the case, then the finding that Auxilin protein levels of R857G Auxilin mice gradually increase with age and are equivalent to WT mice in 3 week old animals, would require that R857G Auxilin protein is increasingly stabilized with age. Future experiments should address the impact of the mutation on protein turnover. Second, there might be a delayed onset between translation to protein from Auxilin mRNA in

R857G Auxilin mice. Auxilin expression is largely restricted to neurons in the mouse brain (Zhang *et al.*, 2014; Zhang *et al.*, 2016b) and the transcription of neuron-specific gene products have previously been found to be upregulated around day 10 of embryonic development (Hartl *et al.*, 2008). No differences in Auxilin mRNA levels were observed in newborn pups, however the decrease in Auxilin protein in newborn R857G Auxilin mice might reflect a delay or impairment of translation. Finally, even though no differences in Auxilin mRNA levels were observed, it is possible that mRNA dynamics are altered. Nonsense-mediated decay of mRNA might be counteracted by increased transcription of Auxilin in R857G Auxilin mice. This would result in equal total mRNA levels, but decreased half-life of mRNA levels, which may in turn impact the translation of Auxilin. This idea is further strengthened by the finding that the P2 Auxilin mouse with nearly completely absent Auxilin levels even showed the highest Auxilin mRNA levels as compared to its littermates. In this scenario, increased Auxilin protein levels with age in R857G Auxilin mice might be acquired through increased translational rates.

Analysis of the survivorship of the 3 week old offspring of heterozygous breeding indicates increased mortality of R857G Auxilin mice. Future work will be required to determine whether R857G Auxilin mutation causes embryonic or postnatal mortality. An interesting hypothesis would be that pups that nearly completely lack Auxilin have decreased chances of survival, consistent with the observation that Auxilin KO animals have increased early postnatal mortality (Yim *et al.*, 2010). This hypothesis is further strengthened by the finding that mice completely lacking Auxilin were not observed at the 3 week time-point. However, it can not be ruled out that mice that nearly completely lack Auxilin at P0 or P2 go on to display increased Auxilin levels at later time points.

GAK, the ubiquitous homologue of Auxilin, was found to be increased in the brains of R857G Auxilin mice. Even though GAK mRNA levels were found to be upregulated in newborn mice (P0, P2) as well as 3 week old mice, increased GAK protein levels were only observed in P2 R857G Auxilin mice. Taken together, these data indicate that both GAK and Auxilin protein levels are differentially regulated to compensate for the decrease in Auxilin in newborn R857G mice. Alongside a progressive increase of Auxilin with age, GAK protein levels are transiently increased 2 days after birth. As Auxilin has reached protein levels equivalent to WT mice in 3 week old mice, GAK protein levels have dropped back to equivalent levels as WT controls. A more detailed analysis of the developmental expression of both Auxilin and GAK is required to provide greater insight into the temporal relationship between both genes in the context of the R857G Auxilin mutation. In addition, future work will have to elucidate whether those compensatory changes in GAK and Auxilin levels are mediated through altered dynamics in the synthesis and/or turnover of mRNA and/or protein.

GAK and Auxilin expression in the brain was visualized using RNAscope experiments and were found to be expressed within the same cells, thus indicating that they could compensate for each other. Consistent with this observation, GAK expression was found to be upregulated in primary neurons derived from R857G Auxilin mice. However, endogenous GAK is not sufficient to compensate for a dramatic decrease in Auxilin, as both GAK and Auxilin were found to be upregulated in R857G Auxilin mouse brains. This could be explained by relative expression levels, since GAK expression in the brain is relatively low and may not be sufficient to fully compensate for dramatic decreases in Auxilin. Additionally, it could also indicate that the roles of GAK and Auxilin in the uncoating of CCVs are not fully redundant. As GAK is expressed ubiquitously and Auxilin expression

is largely restricted to neurons, this may indicate a specialized role for Auxilin that is required in neuronal cells only.

3.4 MATERIAL AND METHODS

3.4.1 Animals

All experiments using mice on a C57BL/6J background were conducted in strict accordance with the recommendations in the Guide for the Care and Use of Laboratory Animals of the National Institutes of Health. The specific experiments performed in this chapter were approved by the Institutional Animal Care and Use Committees of the US National Institute on Aging (Animal study protocol number NIH/NIA 463-LNG-2021). The mice were given access to food and water *ad libidum* and housed in a facility with 12 hour light/dark cycles.

3.4.2 Generation of a CRISPR-based knockin mouse model

CRISPR gRNA and donor DNA for CRISPR editing of R857G to G857 were designed using the web-based Benchling software (https://benchling.com). gRNAs were selected based on their proximity to the PAM sequence and based on maximal on-target and minimal off-target effects (score system as described in (Doench *et al.*, 2016)) (Figure 3.10).

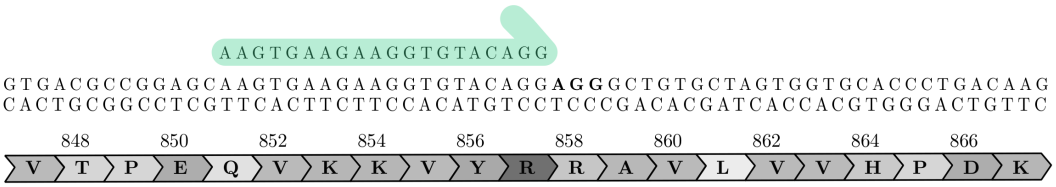

Figure 3.10: **Overview of CRISPR design**

Mouse mating pairs were set up on the day before micro-injection. Females showing vaginal plugs were euthanized and fertilized eggs were harvested. Fertilized eggs were microinjected with Cas9 mRNA (20ng/μl), sgRNA

(10ng/μl, 5'-AAGTGAAGAAGGTGTACAGG-3') and donor DNA (100ng/μl, 5'-GGAGACCAAATGGAAACCCGTGGGCATGGCGGATCTGGTGACGCC GGAGCAAGTGAAGAAGGTGTAC**G**G**C**C**G**CGCTGTGCTAGTG GTGCACCCTGACAAGGTGGGTAGCACCTGCCCTGTCGTAGACT TGCCCGGTCCCTGTTTCAGTGTTC-3', with base pairs to be mutated indicated in bold). Zygotes were cultured overnight in M16 medium at 37°C. The next day, 2-cell stage embryos were implanted into oviducts of pseudo-pregnant surrogate mothers. Two male mice born to the foster mothers with successful homozygous gene editing were bred with C57BL/6J mice to establish the R857G Auxilin knockin mouse line. Mice were crossbred for at least 2 generations.

3.4.3 Genotyping

Genomic DNA was isolated from tails, amplified by PCR and followed by Sanger sequencing.

Genomic DNA from was extracted by overnight incubation of 0.5 cm tail in DirectPCR Lysis Reagent (Tail, Viagen Biotech) with 1 mg/ml Proteinase K, resulting in crude tail lysates.

The region of interest was amplified using Terra PCR Direct Polymerase kit (Takara Biotech). 5 μl of crude lysate was combined with 12.5 μl 2X Terra PCR Direct Buffer, 0.3 μM forward primer (5'-TGTTTGCAGATCCTGGAGTG-3'), 0.3 μM reverse primer (5'-GACAACCTCATGCCTTGTGA-3'), 1.25 U Terra PCR Direct Polymerase Mix and PCR-grade water was added to make up a total reaction volume of 25 μl. 3-step PCR was performed under the cycling conditions outlined in table 3.1.

Cycles	Temperature (°C)	Time
1x	95	3’
38x	95	30”
	57	30”
	72	45”
1	72	5’

Table 3.1: **PCR conditions for genotyping**

The PCR-amplified product was subsequently purified using paramagnetic bead-based PCR cleanup reagents (Agencourt AMPure XP, Beckman Coulter). 45 μl of AMPure paramagnetic beads were mixed with the PCR sample and incubated at room temperature for 5’ to bind the PCR fragments. Beads were separated from the solution using a magnet and samples were subsequently washed three times for 30” with 70% Ethanol to remove contaminants such as dNTPs, salts, polymerases and primers. Beads were air-dried to allow for complete evaporation of ethanol. DNA was subsequently diluted in water.

Purified PCR product was subjected to Sanger sequencing using the BigDye Terminator v3.1 Cycle Sequencing Kit (ThermoFisher Scientific). 3 μl of PCR product was mixed with 2 μl 5X Sequencing Buffer, 0.3 μl BigDye Terminator Ready Reaction Mix, 0.3 μM primer (same as forward primer for PCR, 5’-TGTTTGCAGATCCTGGAGTG-3’) and water was added to make up for a total reaction volume of 10 μl. Cycle sequencing was performed under reaction conditions outlined in table 6.4.4.

Cycles	Temperature (°C)	Time
25x	96	30”
	50	15”
	60	4’

Table 3.2: **Cycle sequencing conditions for Sanger sequencing**

Sequencing samples were cleaned using the Sanger Dye Terminator Removal Agencourt CleanSEQ (Beckman Coulter). Sequencing samples were mixed with 10 μl CleanSEQ paramagnetic beads and 42 μl of 85% Ethanol. Beads were separated from solution using a magnet and were washed 3 times for 30" with 85% Ethanol. Samples were air-dried to remove residual ethanol and DNA was eluted in 40 μl water.

Capillary electrophoresis of sequencing samples was performed using the Hitachi Genetic Analyzer (Applied Biosystems) and data were analysed using the Sequencher software.

3.4.4 Analysis of inheritance

Mating pairs of heterozygous R857G Auxilin mice were set up and tails were collected from 3 week old litters. Genotyping was performed as described above (Section 3.4.3).

3.4.5 Brain retrieval

Newborn and 2 day old mice were euthanized by decapitation, 3 week old mice were euthanized by exposure to CO_2 followed by cervical dislocation. The brain was isolated and dissected into two hemispheres and flash frozen on dry ice. Brain hemispheres were stored at -80°C until experimental use.

3.4.6 Protein sample preparation and gel electrophoresis

Brain hemispheres were homogenized in lysis buffer (20 mM Tris pH7.5, 10% glycerol, 1 mM EDTA, 150 mM NaCl, 1x protease inhibitor cocktail (Halt), 1x

phosphatase inhibitor cocktail (Halt)) with 1% Triton using glass homogenizers and samples were lysed on ice for 20'.

Protein lysates were subsequently cleared (10' centrifugation at 4°C at 21 kg) and protein concentrations were determined using a 660 nm protein assay (Pierce). Protein lysates were diluted to obtain final sample concentration of 30 μg per sample. Samples were boiled in 1x Laemli Sample buffer (Bio-Rad) in a final volume of 20 μl.

Protein samples were loaded on pre-cast 4-20% TGX polyacrylamide gels (Criterion, Bio-Rad) along with a protein standard (Precision Plus Protein Dual Color Standards, Bio-Rad). Electrophoresis was performed in 1x pre-mixed electrophoresis buffer (10 mM Tris, 10 mM Tricine, 0.01% SDS, pH 8.3, diluted with water) and were run at 200 V for 45' using the Criterion Vertical Electrophoresis Cell (Bio-Rad).

3.4.7 Western blot

Following gel electrophoresis, Western blots were performed as described by LI-COR for Near-Infrared Western Blot Detection protocol.

Samples were transferred to 0.45 μm pore-size nitrocellulose membranes (Bio-Rad) using the Trans-Blot Turbo Transfer System (Bio-Rad). Blocking of membranes was performed in a 1:1 solution of phosphate buffered saline (PBS) and Odyssey Blocking Buffer (Li-Cor).

After blocking, membranes were incubated with primary antibodies diluted in antibody buffer (1:1 of Tris buffered saline (TBS) with 0.1% Tween and Odyssey

Blocking Buffer (Li-Cor)) overnight with gentle agitation at 4°C. Primary antibodies and dilutions are shown in table 6.8.

Target	Host	Dilution	Vendor	Catalog number
Auxilin	Rabbit	1/3000	Novus Biologicals	NBP1-81507
GAK	Rabbit	1/500	Gift from Dr. Lois Greene	n/a

Table 3.3: **Primary antibodies used for WB in Chapter 3**

Following primary antibody incubation, membranes were washed 3 times for 5 minutes in TBS-0.1% Tween. Membranes were then incubated with fluorescent secondary antibodies (IRDye, Li-Cor) diluted 1:15000 in antibody buffer for 1 hour at room temperature (RT) under gentle agitation. Secondary antibody incubation was followed by 3 washes of 5' each in TBS-0.1% Tween.

Western blots were imaged using the Odyssey CLx system (Li-Cor) and quantified using Image Studio software.

3.4.8 RNA extraction

RNA extractions were performed as per protocol set forth by Invitrogen Trizol reagent.

Frozen mouse brain hemispheres were homogenized in 1 ml/100 mg tissue ice-cold Trizol reagent (Invitrogen) using glass homogenizers and incubated for 5'. 0.2 ml of chloroform per 1 ml of Trizol was added and incubated for 3', followed by 15' centrifugation at 12 kg at 4°C for phase separation. The resulting upper aqueous phase, containing the RNA, was transferred to a new tube. 0.5 ml of isopropanol per 1 ml of trizol used for lysis was added to the RNA and incubated at RT for 10'. Samples were subsequently centrifuged at 12 kg for 10' at 4°C, resulting in an RNA pellet. The supernatant was removed and the RNA pellet was washed with

75% Ethanol , followed by 5' centrifugation at 7.5 kg at 4°C. The supernatant was discarded and the RNA pellet was air dried for 10' and resuspended in 50 μl water. The concentration of RNA samples was measured using NanoDrop spectrophotometers (ThermoFisher Scientific) and were diluted with water to a final concentration of 1 μg/μl. Resuspended RNA was incubated for 15' at 55°C, before storage at -80°C before proceeding to downstream applications.

3.4.9 cDNA synthesis

1 μg of RNA was used to generate cDNA using the SuperScript III First-Strand Synthesis SuperMix Kit (Invitrogen). For reverse transcription, RNA was mixed with 1 μl of 50 μM oligo$(dT)_{20}$, 1 μl annealing buffer, and water was added to make up a total volume of 8 μl. Reaction was incubated on a thermal cycler for 5' at 65°C and immediately placed on ice for 1'. 10 μl of 2X First-Strand Reaction Mix and 2 μl of SuperScript III/RNaseOUT Enzyme Mix were added to make up a total reaction volume of 20 μl. Reactions were incubated at 50°C for 50' and terminated by 5' incubation at 85°C. cDNA was stored at -20°C until used for downstream applications.

3.4.10 qPCR

Primers were designed using the web-based Primer3Plus software (https://primer3plus.com/). Primers used for qPCR experiments are outlined in table 3.4.

qPCR was performed using the Power SYBR Green RT-PCR Master Mix (ThermoFisher Scientific). 12.5 ng of RNA was mixed with 5 μl Power SYBR Green PCR Master Mix (2X), 3 μM forward primer, 3 μM reverse primer, with

Target	Primers	Exon
CREB3	Fwd 5'-ACGTGCACAGACTTTGAACG-3'	7
	Rvs 5'-TTGACCGCAAGTGGTACATG-3'	8
GBF1	Fwd 5'-ATGCGGAAACAGGAACTTGC-3'	26
	Rvs 5'-ACAGCAGTGCACGAATGTTC-3'	27
β-actin	Fwd 5'-ACGTGCACAGACTTTGAACG-3'	4
	Rvs 5'-TTGACCGCAAGTGGTACATG-3'	5

Table 3.4: **qPCR primers**

water added to make up a total reaction volume of 10 μl. qPCR was analysed using QuantStudio 6 Flex Real-Time PCR System and included Software (ThermoFisher Scientific).

3.4.11 RNAscope

RNAscope is a multiplex RNA *in situ* hybridization method for the visualization of RNA, as described in (Wang *et al.*, 2012) and visualized in figure 3.11. Probes were designed for *DNAJC6*, *GAK* and the DA neuronal marker TH and are shown in table 3.5.

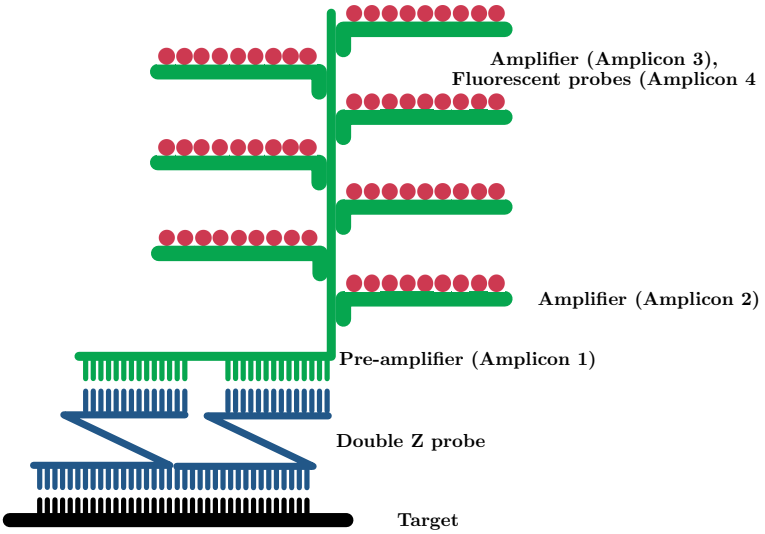

Figure 3.11: **Overview of RNAscope** A total of 20 double Z target probes are designed to hybridize with the target RNA. Each individual Z-probe contains a 18-25-base sequence for hybridization with the RNA, a linker and a 14-base tail. Each double Z probe pair thus forms a 28 base binding site for the pre-amplifier. The pre-amplifier (amplicon 1) subsequently binds to multiple amplifiers (amplicon 2-3) and the amplifiers bind to fluorescent labelled probes (amplicon 4).

Gene	Target region
DNAJC6	235-1177 of NM_001164583.1
GAK	395-1305 of NM_153569.2
TH	483-1603 of NM_009377.1

Table 3.5: **Probes used for RNAscope**

RNAscope experiments were performed on coronal sections of 2 month old WT C57BL/6J mice. Sections were mounted on glass slides and fixed for 15' in 4% PFA. Sections were dried by sequential incubation in 50%, 70%, 100% and 100% Ethanol for 5' each. Protease mix was added for 30' and incubated at RT. Sections were washed with PBS and incubated for 2h at 40°C with primary probes that were pre-equalibrated at 40°C for 10'. Following incubation, slides were washed twice for 5' in 1x wash buffer (ACD Bio). Probes were fluorescently labeled by multiplex amplification, as illustrated in Figure 3.11. Amplicon 1 was incubated for 30' at 40°C, amplicon 2 for 15' at 40°C, amplicon 3 for 30' at 40°C and amplicon for 15' at 40°C. each amplicon incubation step was followed by two

washes of 5' with PBS. Finally, sections were incubated with Hoechst for 30' at RT. Slides were mounted using mounting media and dried at 4°C overnight before visualization using confocal microscopy.

3.4.12 Statistics

Data were plotted and statistical tests were performed using Prism 8 (Graphpad). Error bars represent standard deviation (SD) and points indicate distribution of individual values. The statistical test results are displayed in table 3.6. n represents the number of animals that samples were derived from or independent cultures from pooled litters and is explicitly indicated in the figure legend.

Figure	Variable	Statistical test	Test result	P-value
3.2 B	Genotype	Unpaired t-test	t = 12.56	<0.0001
3.3 B	Genotype	Welch's t-test	t = 8.614	<0.0001
3.3 C	Genotype	Welch's t-test	t = 0.03929	0.9695
3.3 E	Genotype	Welch's t-test	t = 2.888	0.0236
3.3 F	Genotype	Welch's t-test	t = 3.162	0.0203
3.3 H	Genotype	Welch's t-test	t = 1.697	0.1203
3.3 I	Genotype	Welch's t-test	t = 1.188	0.2604
3.4 A	Genotype	Welch's t-test	t = 0.1708	0.1708
3.4 B	Genotype	Welch's t-test	t = 4.407	0.0142
3.4 C	Genotype	Welch's t-test	t = 0.3033	0.7716
3.4 D	Genotype	Welch's t-test	t = 3.503	0.0109
3.4 E	Genotype	Welch's t-test	t = 0.9599	0.3598
3.4 F	Genotype	Welch's t-test	t = 2.826	0.0178
3.5 A	Genotype	Welch's t-test	t = 0.1993	0.8528
3.5 B	Genotype	Welch's t-test	t = 2.858	0.0428
3.8	Genotype	χ^2-test	χ^2 = 9.653	0.0080
3.9 A	Genotype	Welch's t-test	t = 2.370	0.0204
3.9 B	Genotype, gender	2-way ANOVA	F = 5.356, F = 30.85	0.0392, 0.0001
	Genotype	Sidak *post hoc* test	t = 2.757, t = 0.5161	0.0345, 0.8519
3.9 C	Genotype, gender	2-way ANOVA	F = 1.545, F = 14.14	0.2377, 0.0027
	Genotype	Sidak *post hoc* test	t = 0.6277, t = 1.130	0.7902, 0.4824

Table 3.6: **Results of statistical tests**

4 NEUROLOGICAL PHENOTYPES IN R857G AUXILIN MICE

4.1 INTRODUCTION

Although the majority of PD cases are sporadic, insights in familial genetic cases have accelerated our understanding of PD pathogenesis (Hardy *et al.*, 2009; Houlden and Singleton, 2012). In particular, genetic animal models of PD-associated mutations have greatly contributed to dissecting the impact of mutations on nigrostriatal pathways and the pathogenic mechanisms of PD (Chesselet and Richter, 2011; Dawson *et al.*, 2010).

As discussed in Paragraph 1.1, currently only symptomatic treatments for PD are available. A suitable mouse model would be invaluable for the development novel therapeutics that intervene with disease progression, as a platform to screen and validate potential drugs. Ideally, a mouse model should have high construct validity (i.e. based on an established cause of disease, such as genetic mutations) and face validity (i.e. phenocopy of neurological manifestations and pathology as seen in human patients) (Chesselet and Richter, 2011). Remarkably however, the vast majority of animal models with transgenic expression of PD-associated mutant proteins do not fully recapitulate the predominant motor phenotypes of PD, despite many using high levels of transgenic overexpression of mutant genes (Chesselet and Richter, 2011; Dawson *et al.*, 2010).

Two proteins with major roles in the uncoating of CCVs, Auxilin and Synaptojanin 1, have been found to cause young onset atypical PD (Edvardson *et al.*, 2012; Elsayed *et al.*, 2016; Köroglu *et al.*, 2013; Krebs *et al.*, 2013; Olgiati *et al.*, 2014, 2016; Quadri *et al.*, 2013). Whereas Auxilin is a neuronal co-chaperone for HSC70 that catalyzes the ATP-dependent disassembly of the clathrin coat,

Synaptojanin 1 is a presynaptic phosphatase that mediates lipid conversion critical for the shedding of clathrin adaptor proteins. In addition to the parkinsonism phenotypes (bradykinesia, tremor at rest, gait disturbances and rigidity), Auxilin and Synaptojanin 1 mutation carriers also display atypical neurological features, including epilepsies and cognitive decline (Table 1.3) (Edvardson *et al.*, 2012; Elsayed *et al.*, 2016; Köroglu *et al.*, 2013; Krebs *et al.*, 2013; Olgiati *et al.*, 2014, 2016; Quadri *et al.*, 2013).

Recently, Cao and colleagues developed a CRISPR-based mouse model carrying the homozygous recessive Synaptojanin 1 PD mutation (R258Q) (Cao *et al.*, 2017). Strikingly, this model is the first animal model with an endogenous PD mutation to develop neurological phenotypes at young age (before 12 months) resembling manifestations seen in patients. In addition to motor dysfunction, Synaptojanin 1 mutant mice also exhibit seizures (Cao *et al.*, 2017).

To date, no behavioural studies have been reported for Auxilin KO mice (Yim *et al.*, 2010). To understand whether mice with the homozygous R857G Auxilin allele develop neurological phenotypes, a spectrum of behavioural tests were performed to assess motor behaviour, anxiety, startle response and memory (Table 4.1).

Test	Assessment
Beam walk	Balance, motor coordination
Rotarod	Motor learning, balance and coordination
Pole test	Motor coordination and performance
Grip strength	Forelimb strength
Tail suspension test	Hind limb clasping
Open field	Locomotor, exploratory behaviour, anxiety
Startle chamber	Startle response, amplitude of movement
Elevated plus maze	Anxiety
Forced alternation	Spatial memory
Spontaneous alternation	Working memory

Table 4.1: **Behavioural test battery**

R857G Auxilin mice were found to develop neurological phenotypes as early as 6 months old that are reminiscent of clinical features seen in human patients, including motor impairment, seizures, impaired memory and anxiety. No phenotypes were observed in 2 month old animals and so the majority of this chapter will be focused on findings in 6 and 12 month old mice.

4.2 RESULTS

4.2.1 Longitudinal cohort for behavioural testing

Since patients with R927G Auxilin mutations develop early-onset PD, behavioural studies were performed in 2, 6 and 12 month old mice in a longitudinal cohort of age-matched WT and R857G Auxilin mice. All tests at the 12 month time point, with the exception of the beam walk, tail suspension and startle test, were performed by Dr. Melissa Conti. Two WT mice died between the 2 and 6 month time point and one additional WT mice died between the 6 and 12 month time point. All mice were replaced with age, gender and genotype-matched mice. Cohorts at all time points consisted of 8 animals per genotype, with 4 female and 4 male mice each.

4.2.2 Balance and motor impairments in R857G Auxilin mice

The beam walk test was performed to detect deficits in fine motor skills and balance. Animals were trained to cross an elevated beam of 1 m length and 12 mm width three times for three consecutive days. On the 4th day, mice were tested for their ability to traverse the 12 mm beam and time was recorded and averaged for two trials. This process was repeated on the testing day for a 6 mm beam. Age ($p < 0.01$) but not genotype ($p > 0.05$) was found to have a significant impact on the time to traverse the 12 mm beam (Figure 4.1 A, B, Table 4.2). In addition, both age and genotype had a significant impact on the tendency to fall from the 6 mm beam ($p < 0.0001$, $p < 0.0001$). R857G Auxilin mice had an increased tendency to fall at least once when attempting to traverse the 6 mm beam (Figure 4.1 C, D, $p < 0.0001$). In addition, 12 month old mice were more

likely to fall during both trials the 6 mm beam than 6 month old mice (Figure 4.1. Since half of the 6 month old and all of the 12 month old R857G Auxlin mice fell off the beam during both trials on the 6 mm beam, time to traverse the beam could not be assessed. These data indicate progressively decreasing balance and gait disturbances in R857G Auxilin mice, a cardinal motor feature of PD (Lees *et al.*, 2009).

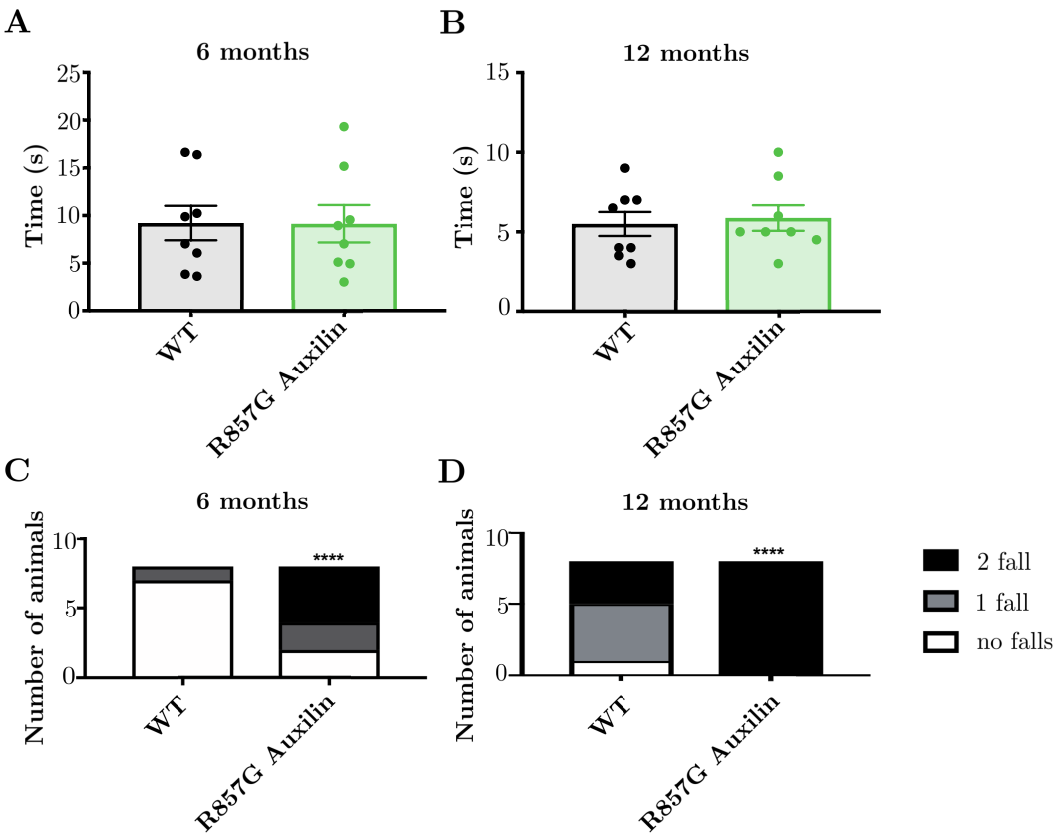

Figure 4.1: **Beam walk** A and B Average time to traverse a 12 mm beam during 2 trials. Two-way ANOVA with Sidak's multiple comparison tests were performed, no significant differences were observed ($p > 0.05$). C and D Number of falls when traversing a 6 mm beam during 2 trials. Multinomial logistic regression was performed, **** indicates $p < 0.0001$ genotype effect.

The pole test was performed to assess agility in R857G Auxilin mice. Mice were placed on a vertical wooden pole and time to turn downward and time to descend the pole were recorded. Whereas no differences were detected in 6 month old

animals (Figure 4.2 A, C), an increased time to turn and to descend was observed in R857G Auxilin mice compared to WT at 12 months (Figure 4.2 B, D), indicating decreased agility and bradykinesia, another cardinal PD motor phenotype (Lees *et al.*, 2009).

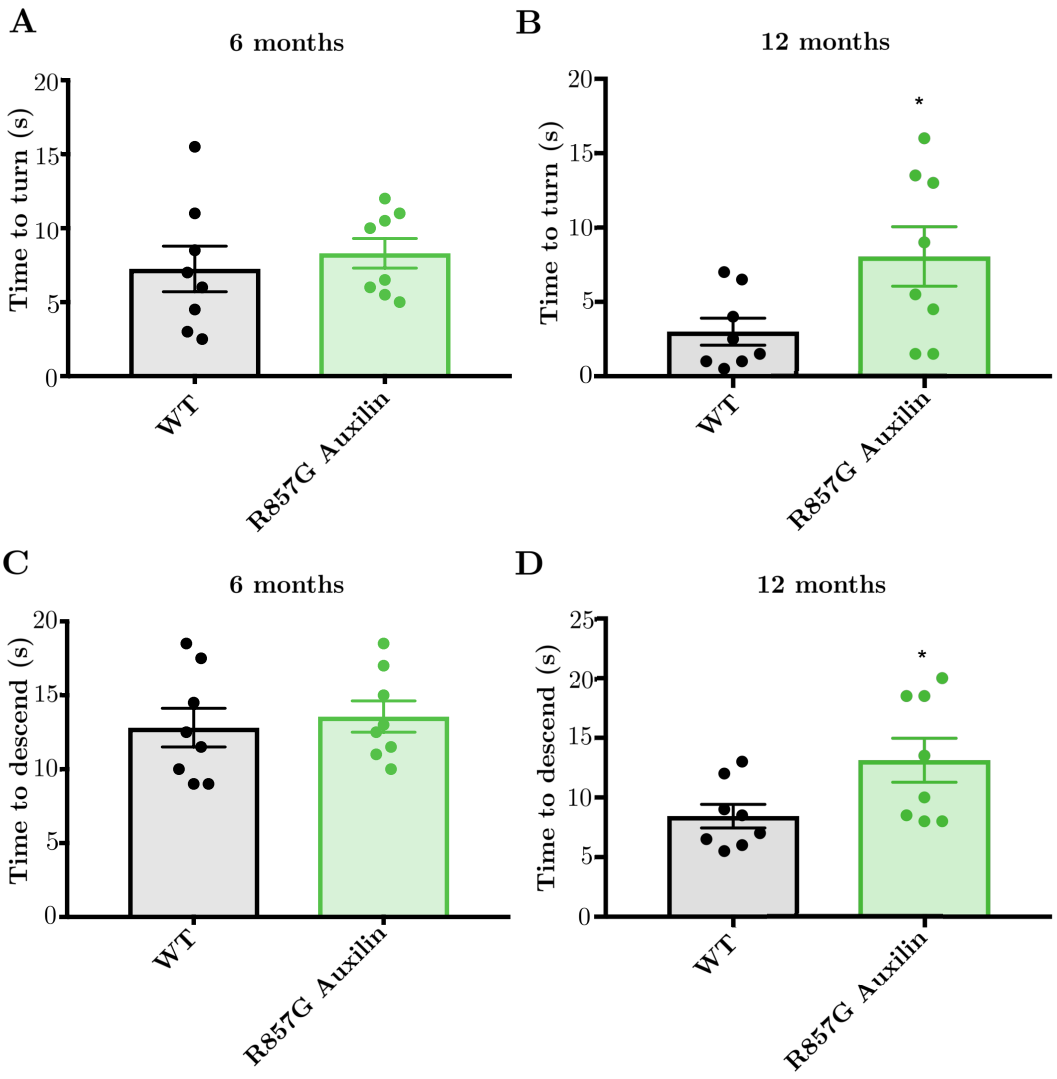

Figure 4.2: **Pole test** A, B Time to turn downwards and C, D time to descend pole. Two-way ANOVA with Sidak's multiple comparison tests were performed and p-values indicated when significant. * indicates $p < 0.05$.

The rotarod test was performed to assess motor learning and motor coordination. Mice were placed on a rod rotating at accelerating speed and latency time to fall was recorded for three trials per day on three consecutive days. Mice showed

increased motor learning ($p < 0.01$), as assessed by three-way ANOVA (Table 4.2). In addition, both age ($p < 0.05$) and genotype ($p < 0.05$) had a significant impact on rotarod performance (Table 4.2, Figure 4.3). Surprisingly, the R857G Auxilin animals showed an increased latency to fall compared to WT animals. This appears to be in contrast with the impaired balance and decreased motor function observed in the beam walk and pole test, respectively. However, it could also point to an inability to stop movement, as is often seen in PD patients (Obeso *et al.*, 2009).

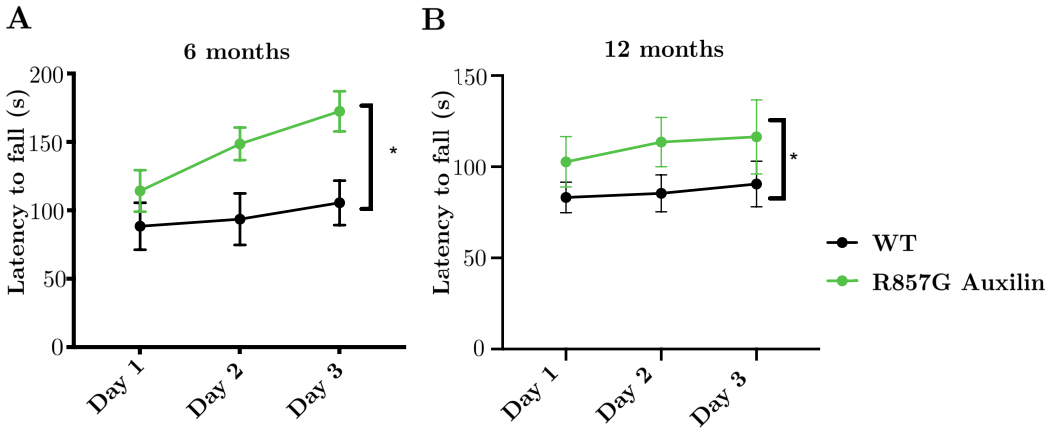

Figure 4.3: **Rotarod test** Average latency to fall off the rotarod during three trials each on three consecutive days. Three-way ANOVA was performed, p-values indicate genotype effect with * $p < 0.05$. Rotarod test at 12 month time point was performed by Dr. Melissa Conti.

4.2.3 Unaltered forelimb strength and hind limb clasping

The grip strength test was performed to assess neuromuscular forelimb function. The animals were subjected to 5 consecutive trials and the average force of grid grasping was measured. Forelimb strength significantly increased with age (Table 4.2), but no differences were detected between WT and R857G Auxilin animals at 6 or 12 months of age (Figure 4.4).

The tail suspension test was performed in 12 month old animals and the hind limb clasping reflex was scored. No clasping phenotypes were observed in WT or R857G Auxilin animals and therefore not quantified.

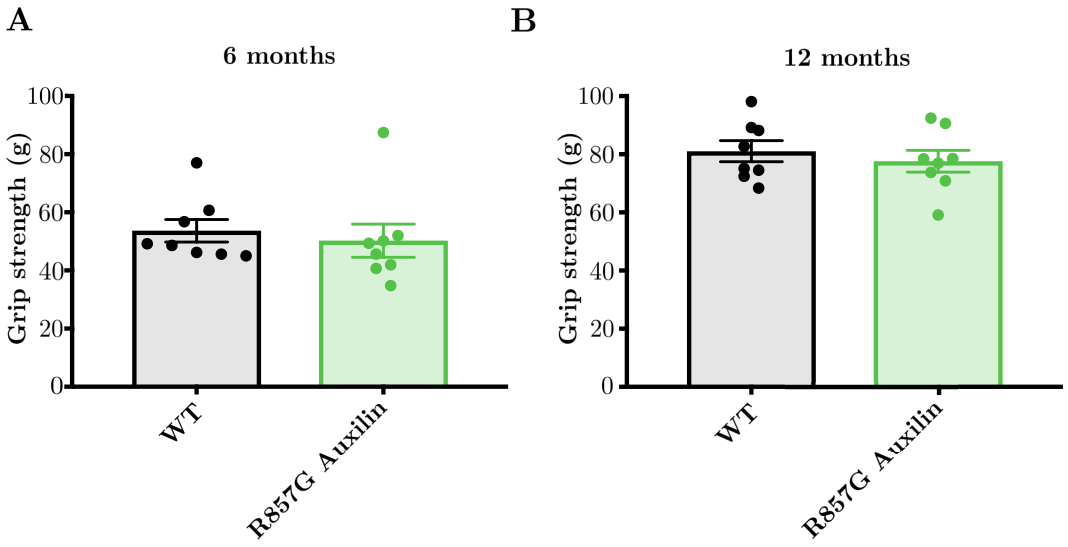

Figure 4.4: **Grip strength** Average forelimb strength of 5 trials. Two-way ANOVA with Sidak's multiple comparison tests were performed, no significant changes were observed ($p > 0.05$). Grip strength test at 12 month time point was performed by Dr. Melissa Conti.

4.2.4 Seizures and startle response in R857G Auxilin mice

R857G Auxilin mice were occasionally observed to suffer spontaneous seizures during weekly cage changes (Supplementary Video 1). The observed seizing mice displayed muscle twitching at a frequency of ∼1.5 Hz, followed by a freezing phenotype and drooling (Figure 4.5).

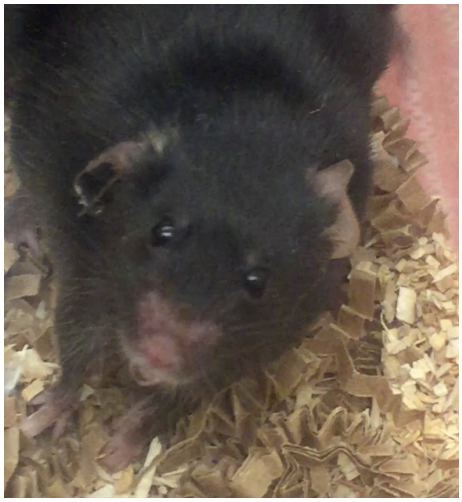

Figure 4.5: **Seizure** Seizure observed in 6 month old female R857G Auxilin mouse. Screen shot captured from Supplementary Video 1, while freezing and drooling.

I hypothesized that seizures might be triggered by exposure to new environments. To gain further insight into the epilepsies, mice were subjected to sound and light stimuli to assess startle responses. Mice were placed in an enclosed cylinder on a piezoelectric accelerometer within a dark startle chamber. The amplitude, which is directly proportional to the amount of displacement of the mouse, was measured per millisecond. Baseline data were recorded for 15 minutes. The mice were then subjected to an acoustic startle of 100 seconds and a light stimulus of 100 seconds, each followed by interval without stimuli of 4 minutes (Figure 4.6).

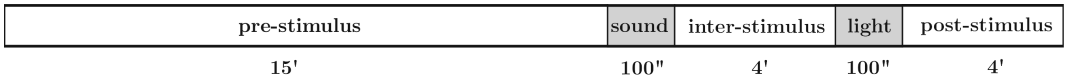

Figure 4.6: **Overview of startle test**

The mean amplitude during the pre-stimulus baseline recordings was compared to the mean amplitude during the light and sound stimuli. Three-way ANOVA revealed a significant impact of the sound and light stimulus on the startle response

($p < 0.0001$) (Figure 4.7, Table 4.2), indicating that the stimuli were successful in evoking a startle response. In addition, three-way ANOVA indicated an interaction between age and genotype ($p < 0.05$), indicating that the startle response R857G Auxilin mice is altered compared to WT controls in an age-dependent matter. However, post-hoc analysis did not reveal significant alterations between genotypes at different time points ($p > 0.05$) (Figure 4.7).

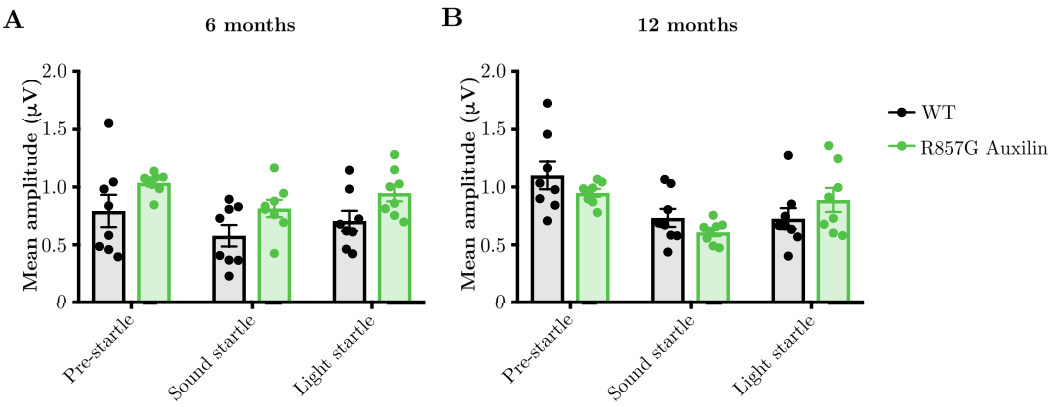

Figure 4.7: **Startle response** Three-way ANOVA with Sidak's multiple comparison tests were performed. No significant alterations between genotypes or stimuli were observed at different time points ($p > 0.05$).

4.2.5 Bi-phasic alterations in the amplitude of movement of R857G Auxilin mice

Because three-way anova of the startle test revealed an interaction between age and genotype, the recorded data of were Fourier transformed to extract frequency information in order to gain further insight in the amplitude of movement of the different genotypes at different ages. To analyse whether there is an intrinsic difference in the amplitude of movement between WT and R857G Auxilin mice, the amplitude over a wide frequency range (0-20 Hz) was analysed during the 15 minutes of pre-startle baseline recordings.

Three-way ANOVA indicated an interaction effect of age, genotype and frequency. Indeed, at 6 months old, an increase in the mean amplitude of movement was observed for R857G Auxilin mice between 0-1 Hz (Figure 4.8 A, B, C). In contrast, a decrease in mean amplitude of movement was observed in 12 month old R857G Auxilin mice at 0-1 Hz (Figure 4.8 D, E, F). The observation of a decreased amplitude of movement at 12 months is in line with the finding that bradykinesia was only apparent during the pole test in 12 month old animals (Figure 4.2).

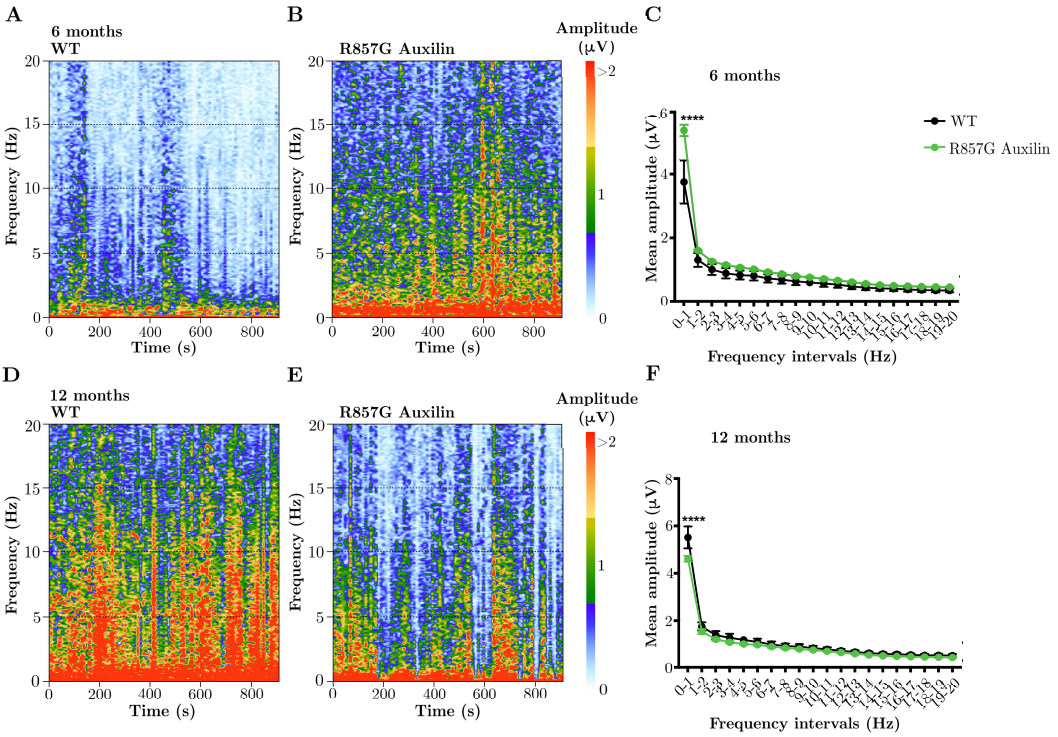

Figure 4.8: **Amplitude of movement** A, B, D, E Representative spectrograms of female WT and R857G Auxilin mice at 6 and 12 month old, displaying amplitude of movement during 15 minutes in the pre-stimulus interval, over a frequency range of 0-20 Hz. C, F Mean amplitude in 1 Hz frequency intervals from 0-20 Hz. Three-way ANOVA was performed, p values indicate results of Sidak's post hoc analysis, with **** $p < 0.0001$. Fourier analysis was performed by Dr. Johann du Hoffmann.

4.2.6 Exploratory behaviour, locomotor activity and thigmotaxis in open field test is unaltered in R857G Auxilin mice

The open field test was performed to examine general locomotor activity, anxiety and exploratory behaviour. Mice were placed in an open field for 30 minutes and overall activity, activity in open center and path length were analysed.

No alterations were observed in total activity counts for WT and R857G Auxilin mice (Figure 4.9 A, B). Total activity counts were further dissected into ambulatory movement, fine movement and rearing counts. No changes were observed in any of the movement counts (Figure 4.9 C-F).

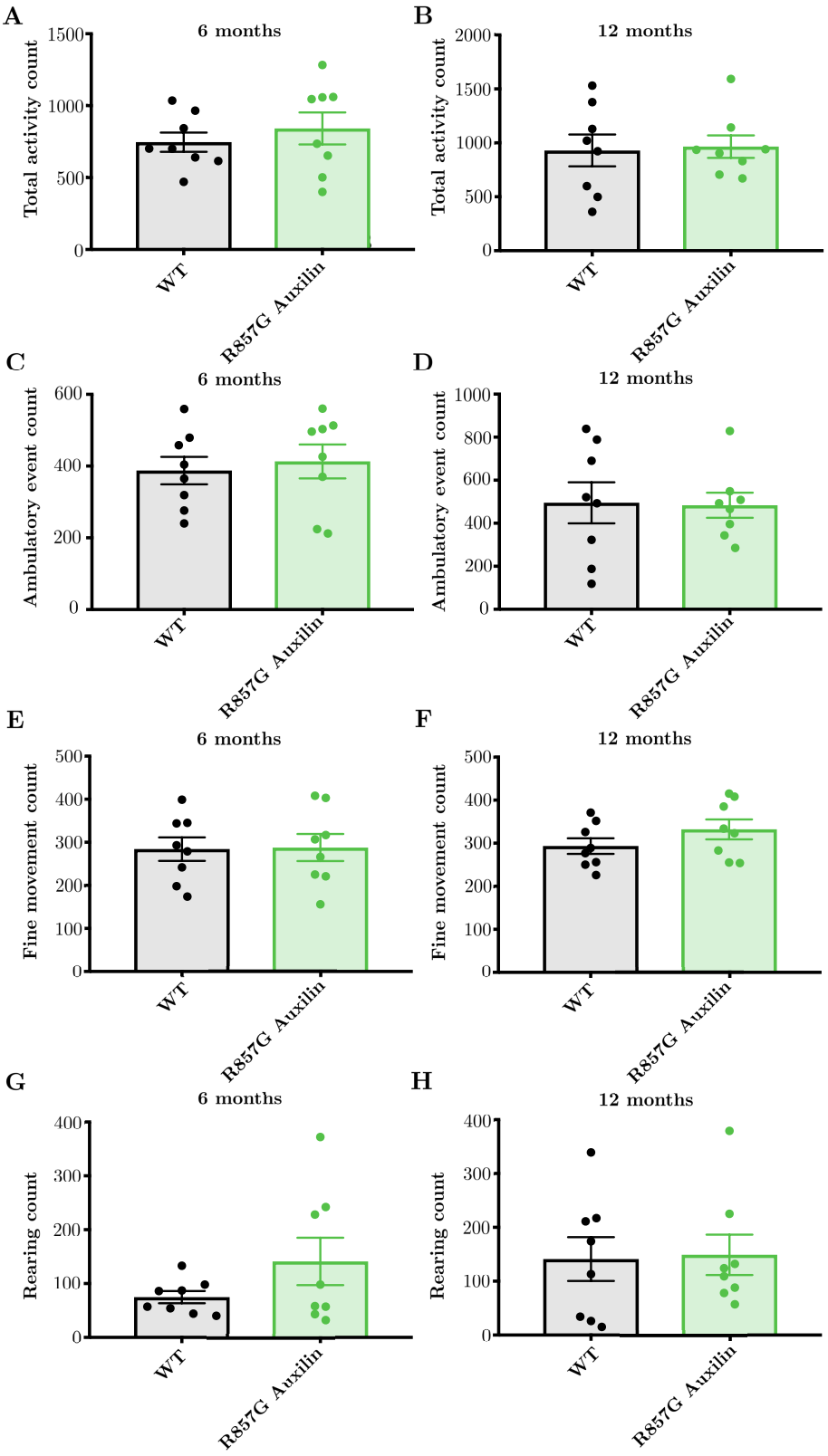

Figure 4.9: **Open field movement counts** A, B Total activity counts. C, D, Ambulatory activity counts. E, F Fine movement counts. G, H Rearing counts. Two-way ANOVA with Sidak's multiple comparison tests were performed, no significant changes were observed ($p > 0.05$). Beam break analysis at all time points was performed by Dr. Jinhui Ding. Open field test at 12 month time point was performed by Dr. Melissa Conti.

No differences in total path length of WT and R857G Auxilin animals were observed (Figure 4.10). This indicates that the observed increase and decrease in amplitude of movement of R857G Auxilin mice at 6 and 12 months, respectively, does not translate into alterations in locomotor activity.

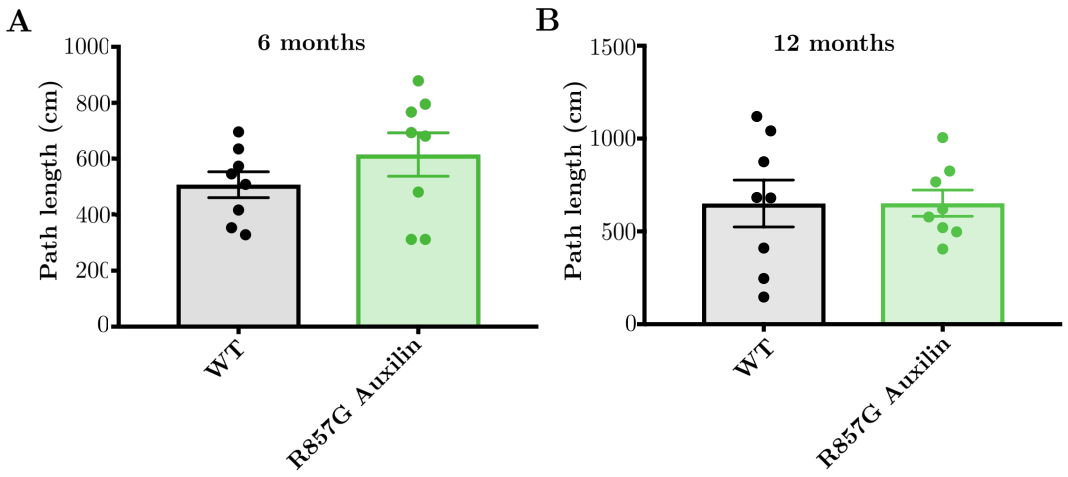

Figure 4.10: **Path length in open field** Two-way ANOVA with Sidak's multiple comparison tests were performed, no significant changes were observed ($p > 0.05$). Open field test at 12 month time point was performed by Dr. Melissa Conti.

The activity and time spent in the center of the open field was analysed to assess thigmotaxis, the tendency of the mice to remain close to the walls, as a measure for exploratory behaviour and anxiety. No differences were observed in the fraction of activity counts in the center and the fraction of time spent in the center between WT and R857G Auxilin mice (Figure 4.11).

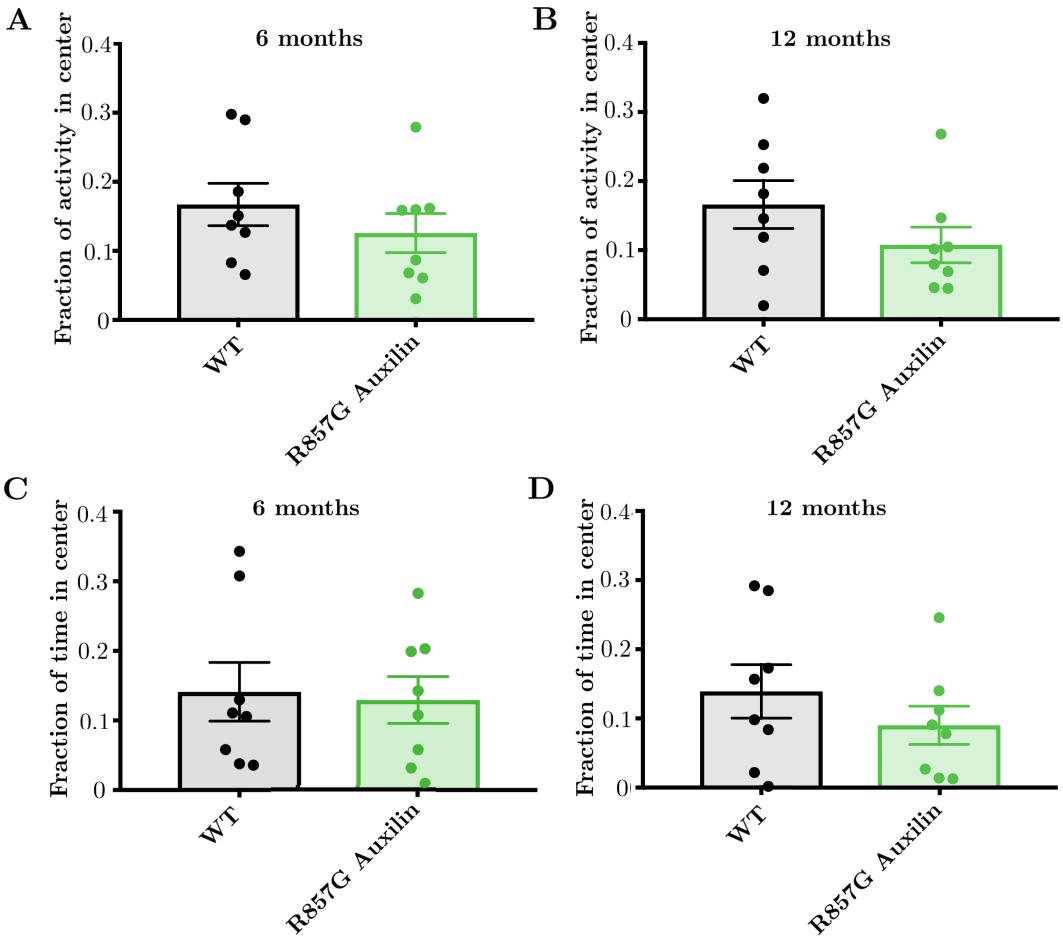

Figure 4.11: **Activity and time spent in center of open field** A, B Fraction of activity in center. C, D Fraction of time spent in center. Two-way ANOVA with Sidak's multiple comparison tests were performed, no significant changes were observed ($p > 0.05$). Beam break analysis at all time points was performed by Dr. Jinhui Ding. Open field test at 12 month time point was performed by Dr. Melissa Conti.

4.2.7 Anxiety phenotypes in R857G Auxilin mice

To further analyse anxiety, mice were placed in an elevated plus maze, with two open and two enclosed arms. The elevated plus maze allows, like the open field, to measure thigmotaxis. However, the elevation component introduces an additional fear-aspect to the test. The fraction of arm entries, distance and time in open

arms was recorded. No alterations in entries, time and distance in open arms were observed (Figure 4.12 A-D).

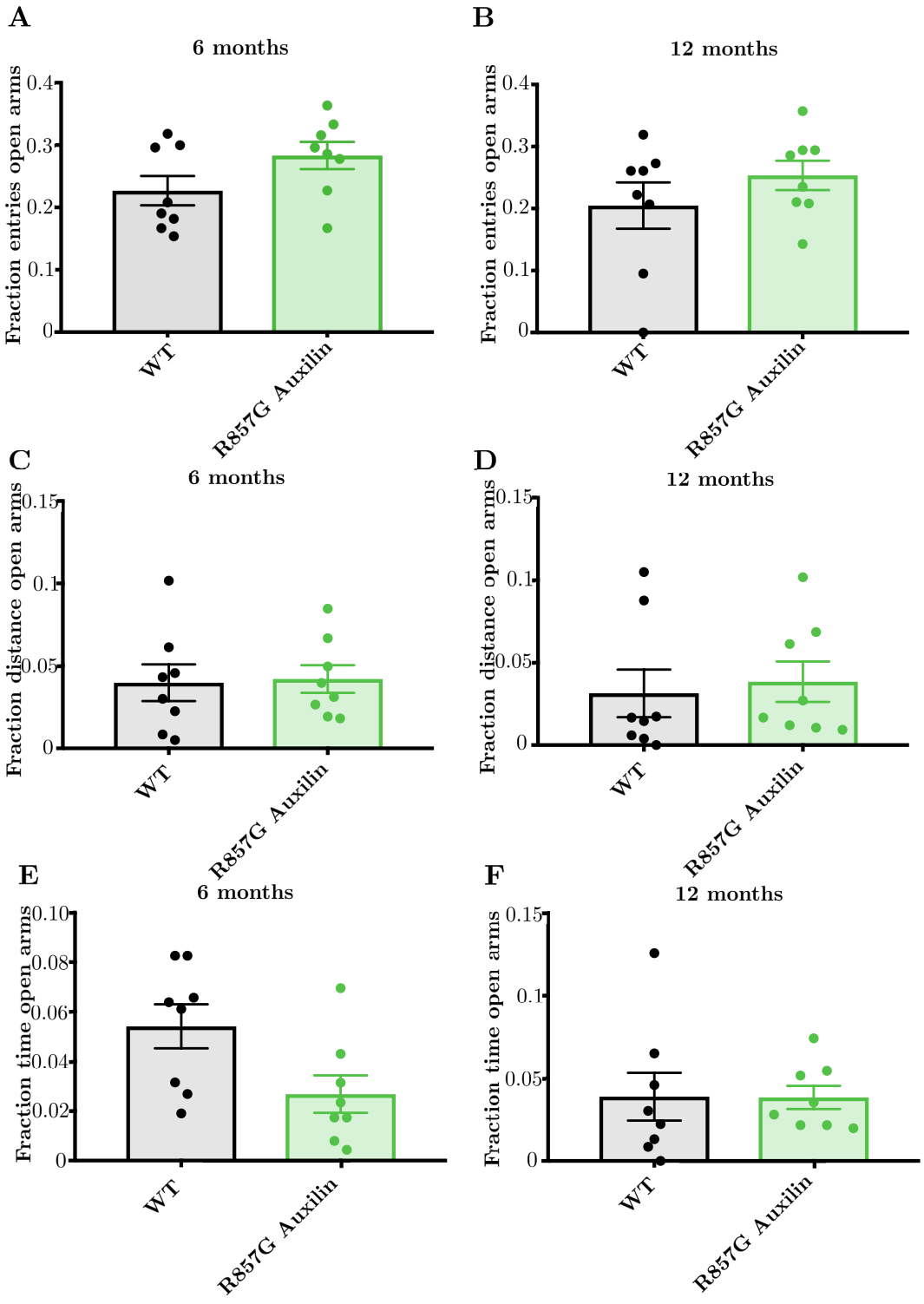

Figure 4.12: **Elevated plus maze** A, B Fraction of open arm entries. C, D Fraction of distance in open arms. E, F Fraction of time spent in open arms. Two-way ANOVA with Sidak's multiple comparison tests were performed. No significant alterations were observed ($p > 0.05$) Elevated plus maze test at 12 month time point was performed by Dr. Melissa Conti.

4.2.8 Memory deficits in R857G Auxilin mice

Finally, Y-maze spontaneous and forced alternation tasks were performed to assess memory deficits in R857G Auxilin mice.

To analyse working memory and exploratory behaviour, spontaneous alternation of arm entries was analysed by placing the mice in a Y-maze with three arms of equal distance and at equal angle for 7 minutes. The ratio of total number of spontaneous alternations (different arm entries in each of three consecutive arm entries) over total number of possible spontaneous alternations (total arm entries - 2) was scored. No alterations in spontaneous alternations were observed (Figure 4.13 A, B).

Spatial memory and exploratory behaviour was assessed using the forced alternation task. One arm of the Y-maze was blocked while the mice were exploring the maze during 8 minutes. After a 45 minute break, mice were reintroduced to the Y-maze with all arms open for 5 minutes. First arm entry and fraction of entries into the initially blocked arm over total arm entries were recorded. For 12 month old mice, three animals (one WT and two R857G Auxilin) did not leave the center of the maze and were not included for analysis. 6 month old, but not 12 month old, displayed a deceased fraction of new arm entries (Figure 4.13 C, D). In addition, genotype but not age had a significant impact on the first arm entry, as R857G Auxilin mice had a decreased tendency to enter the new arm first, indicating impaired working memory (Figure 4.13 E, F).

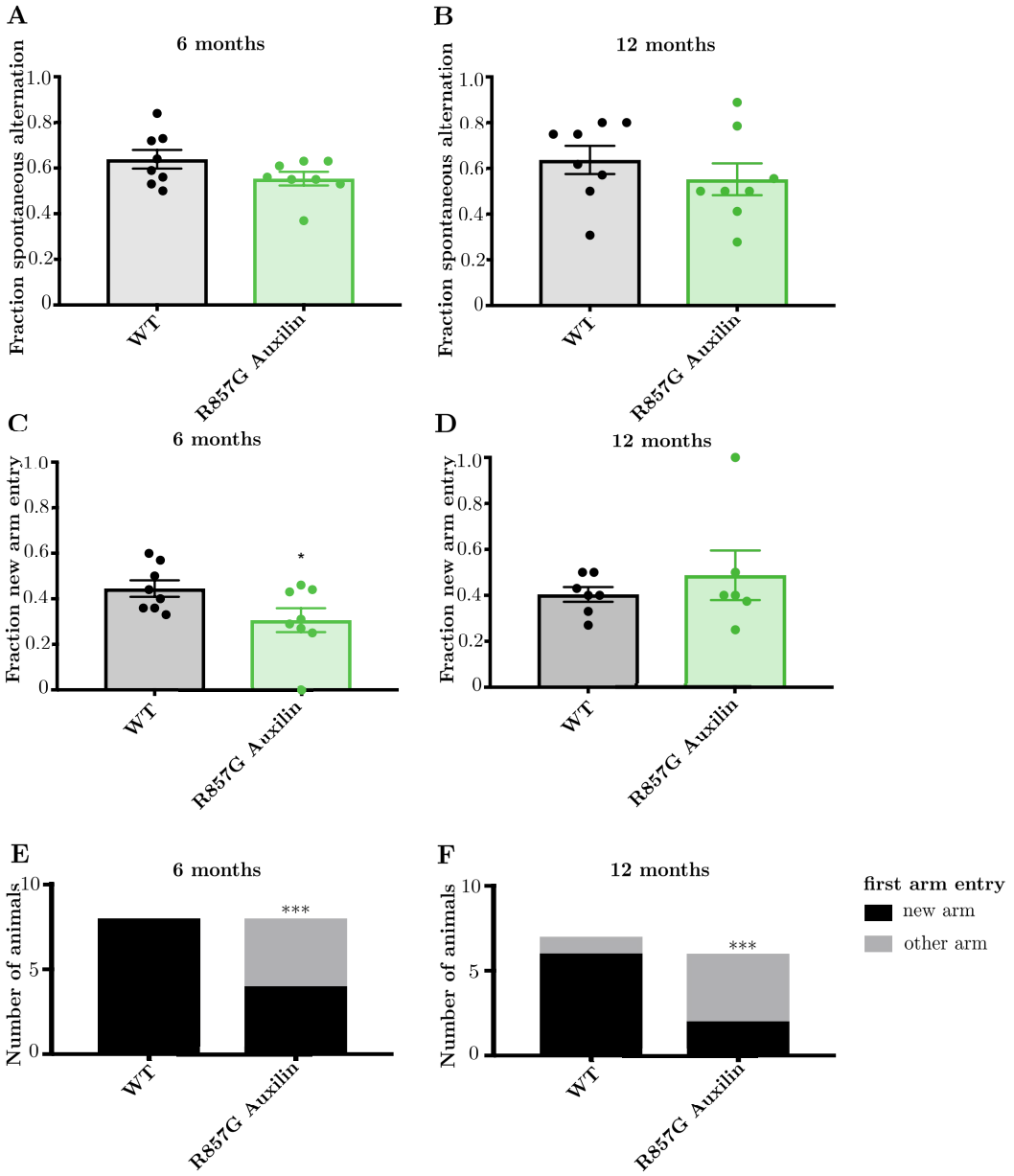

Figure 4.13: **Y-maze spontaneous and forced alternation** A, B Fraction of spontaneous alternation. C, D Fraction of new arm entries. Two-way ANOVA with Sidak's multiple comparison tests, no significant alterations were observed (p-value > 0.05). E, F First arm entries. Binary logistic regression analysis was performed, *** indicates $p < 0.001$ for genotype effect. Y-maze spontaneous and forced alternation tests at 12 month time point were performed by Dr. Melissa Conti.

4.3 DISCUSSION

Loss of function mutations in Auxilin (c.801-2A> G, T741=, Q791X, Q846X, R927G) have been shown to cause juvenile or early onset, atypical PD (Edvardson *et al.*, 2012; Elsayed *et al.*, 2016; Köroglu *et al.*, 2013; Olgiati *et al.*, 2016). In addition to the cardinal motor features of parkinsonism (tremor at rest, bradykinesia, gait disturbances, muscle rigidity), many patients also develop atypical neurological phenotypes including seizures, cognitive decline and pyramidal and cerebellar signs (Table 1.3).

In order to address whether mice with the homozygous endogenous R857G mutation (equivalent to the human R927G PD mutation) recapitulate these neurological manifestations, a battery of behavioural tests was performed (Table 4.1). Tests were performed in a longitudinal cohort of 8 animals per genotype at 2, 6 and 12 months of age. Whereas no phenotypes were observed in 2 month old animals, R857G Auxilin mice developed neurological manifestations resembling clinical features observed in patients in 6 and 12 month old mice.

R857G Auxilin mice showed a progressively increasing tendency to fall with age when traversing an elevated beam, pointing to balance and gait disturbances. The pole test revealed bradykinesia, i.e. slowness of movement, in 12 month old R857G Auxilin mice. Surprisingly, R857G Auxilin mice had an increased latency to fall from the rotarod which seems to be in contrast with the observed balance issues and bradykinesia. However, lesions in the dopaminergic system cause difficulties to initiate and stop movements (Obeso *et al.*, 2000). Increased performance on the rotarod, a test based on forced motor activity, might reflect an inability to stop movement in R857G Auxilin mice. An alternative explanation could be that striatal and other motor circuits compensate for a midbrain defect. No alterations

in grip strength or tail suspension test were observed, indicating that forelimb muscular strength and hind limb clasping reflex were not affected.

Analysis of the amplitude of movement of R857G Auxilin mice using a piezoelectric accelerometer revealed an initial increase at 6 months followed by a decrease in the overall amplitude of movement compared to WT controls at a frequency between 0-1 Hz. An apparent increased agitation and jitter was also observed while handling the R857G Auxilin mice during the behavioural tests at 6 months but not at 12 months. The alterations in amplitude of movement at did not translate into alterations in locomotor activity as assessed with the open field test. The observed decreased amplitude of movement at 12 months points to bradykinesia and is in line with the results of the pole test showing a slowness of movement at 12 months but not 6 months. Hyperkinesia has been observed in other PD animal models based on transgenic overexpression of mutant α-synuclein and LRRK2 and is thought to be caused by impaired dopamine transmission (Longo *et al.*, 2017; Unger *et al.*, 2006; Yue *et al.*, 2015). The initial hyperkinesia followed by bradykinesia in R857G Auxilin mice might reflect bi-phasic alterations in the dopaminergic pathways during disease progression.

Seizures were observed in R857G Auxilin mice when cages were cleaned and changed. Seizing mice were observed to display muscle twitches at a frequency of $\sim$1.5 Hz, followed by a freezing phenotype while drooling. This seizure phenotype resembles the generalized and absence seizures reported in Auxilin mutation carriers. However, no alterations in startle response to sound or light stimuli were observed between genotypes at different time points, indicating that this startle response measurement is not an effective test to measure epileptic activity in R857G Auxilin mice.

Impaired spatial memory was observed in the Y-maze in R857G Auxilin mice, which could indicate cognitive decline, as has been observed in patients. However, R857G Auxilin mice did not display anxiety phenotypes, as measured by the elevated plus maze and open field tests. It is important to note however that behavioural tests assessing anxiety- and exploration-related phenotypes, such as open field, elevated plus maze and Y-maze, rely on introducing the mice to a novel environment. Since all tests were performed in a longitudinal cohort, an important caveat is that repeated testing might attenuate anxiety and exploratory phenotypes due to habituation (Tucker and McCabe, 2017).

In summary, R857G Auxilin mice display multiple neurological phenotypes as early as 6 months old that are reminiscent of clinical features of early onset PD seen in patients. Whereas lesions in the nigrostriatal dopamine pathway may underlie motor impairments, lesions in other brain areas could explain anxiety, seizures and memory impairments. Taken together, animal models with endogenous PD-associated mutations in CCV uncoating proteins Auxilin and Synaptojanin 1 provide a strong link between impairments clathrin trafficking and the development of early onset PD. In addition, they serve as suitable models to investigate the impact of PD mutations on molecular mechanisms underlying PD and as a platform to screen for therapeutics.

4.4 MATERIAL AND METHODS

4.4.1 Animals

All experiments using mice on a C57BL6/J background were conducted in strict accordance with the recommendations in the Guide for the Care and Use of Laboratory Animals of the National Institutes of Health. The specific experiments performed in this chapter were approved by the Institutional Animal Care and Use Committees of the US National Institute on Aging (Animal study protocol number NIH/NIA 463-LNG-2021). The mice were given access to food and water *ad libidum* and housed in a facility with 12 hour light/dark cycles.

All behavioural experiments were performed during the light cycle of the mice. Behavioural tests were performed in the rodent behavioural core (National Institute of Mental Health, National Institutes of Health). All animals were handled for two minutes, three days prior to testing. The longitudinal cohort consisted of 8 WT and 8 R857G Auxilin mice that were age-matched, with 4 male and 4 female mice per genotype. Animals were subjected to behavioural tests at 2, 6 and 12 months of age. All behavioural tests at the 12 month old time point, with the exception of the beam walk, startle test and tail suspension test, were performed by Dr. Melissa Conti.

4.4.2 Beam walk

The beam walk test was performed to measure the motor coordination and balance of the mice (Carter *et al.*, 2001).

The beam walk test platform consists of an elevated square beam of 100 cm in length and 6 or 12 mm in width. An enclosed, dark platform is placed at the end of the beam as the destination box. The mice were placed on one end of the beam to traverse the beam to the destination platform. The middle 80 cm of the beam were marked and the latency to traverse the 80 cm was measured.

The test consisted of 3 training days and 1 testing day. On the training days, the mice were placed on the wide (12 mm) training beam to traverse the beam for 3 consecutive trials. When animals stalled or turned during the training, they were encouraged to traverse the full length of the beam. Platform is cleaned with 70% EtOH between trials. Training was repeated for 3 consecutive days, until mice were able to spontaneously traverse the beam to establish a stable baseline response. On the testing day, the mice traversed the wide (12 mm) beam twice and time to traverse was measured. Mice were then placed on the narrow (6 mm) testing beam for two consecutive trials and the latency to traverse the 80 cm was measured as well.

4.4.3 Rotarod

The rotarod test was performed to assess motor coordination, learning and balance of the mice (Carter *et al.*, 2001).

The rotarod test consisted of 1 training day and 3 testing days and animals were allowed to habituate in the testing room for 60 minutes prior to testing. On training day, the mice were placed on a rotating rod for 5 minutes at a constant speed of 4 rpm (San Diego Instruments). When mice fell, they were placed back on the rotarod. During testing days, mice were placed on the rotarod with constant accelerating speed from 4-40 rpm over 5 minutes for 3 trials, with at least 15

minutes inter-trial intervals. The rotarod was cleaned in between trials with 70% ethanol. Latency time to fall from the rotarod was measured for 3 trials on 3 consecutive days.

4.4.4 Pole test

The pole test was performed to assess motor coordination and performance (Hauser *et al.*, 2015; Matsuura *et al.*, 1997).

Mice were placed head-upward on the top of a vertical pole (1 cm diameter, 0.5 m height). The wooden rough-surfaced pole was mounted into a wooden base and placed into an empty mouse cage covered with bedding. One pre-trial was performed followed by two test trials. Time to descend to the floor of the cage as well as time to turn head-downward was measured and averaged for the two test trials. The pole was cleaned with 70% ethanol in between tests.

4.4.5 Tail suspension test

The tail suspension test was performed to test the hind limb clasping reflex (Cao *et al.*, 2017).

Mice were held by their tail for 30 seconds at 30 cm above a surface and observed for hind limb clasping. Mice were scored per 10 second intervals and allocated a score of 0 in the absence of hindlimb clasped and a score of 1 for abnormal hind limb movement. The score of 3 intervals of 10 seconds was summed, allowing a maximum score of 3.

4.4.6 Grip strength

The grip strength test was performed to measure differences in skeletal muscular forelimb strength (Takeshita *et al.*, 2017).

The grip strength was measured using a digital grip strength gauge (BioSeb). The apparatus was connected to a wire grid of 8 by 8 cm. The mice were lifted by the tail to allow them to grasp the grid with their forelimbs. Mice were pulled backward gently by the tail until the grid was released. The peak full force in grams exerted by the mouse before losing grip was recorded. The mean of 5 consecutive trials was recorded for each mouse.

4.4.7 Open field

Locomotor, exploratory behaviour and anxiety were assessed using the open field test (Dranka *et al.*, 2014).

Mice were allowed to habituate 60 minutes prior to testing in a dark room. Mice were placed in a Flex field photobeam activity system (San Diego Instruments) during 30 minutes with 25.4 x 47 cm dimensions consisting of 4 x 8 photobeams. Open field chambers were cleaned with 70% ethanol between tests.

Activity was tracked when animals broke the photobeams in real time. Total activity count was measured as the arithmetic count of total number of beam breaks, fine movement count as the number of single beam breaks and subtraction of the fine movement counts from total movement counts resulted in the ambulatory event count. Rearing counts indicated the arithmetic count of all beam breaks registered by a second level of photobeams. Dr. Jinhui Ding further analysed the beambreak data to measure path length and activity in center. Path length was

calculated based on the coordinates of the beam breaks. Activity in the center was calculated by breaks of photobeams 2-3 (out of 4 total horizontal beams) and photobeams 3-6 (out of 8 total vertical beams).

4.4.8 Startle test

Sensorimotor gating was measured in the startle test (DeLorey *et al.*, 2011; Kirshenbaum *et al.*, 2013; Veeraragavan *et al.*, 2012).

Startle test was performed using a SR-Lab startle response system (San Diego Instruments). Mice were placed in a non-restrictive plexiglass cylinder (3.2 cm diameter) resting on the sensor platform. A piezo-electric accelerometer was attached to the base of the sensor platform, thus converting mouse displacement and acceleration into a voltage measurement, which was digitized by the SR-Lab software. The cylinder and sensor are isolated in a larger, sound- and light-proof box.

The startle test set-up is visualized in Figure 4.6. Movement of mice without exposure to stimuli was recorded during 15 minutes. Afterwards, the mice were presented with an auditory stimulus burst of 85 dB for 100 ms every 500 ms for a total of 100 s, followed by 4 minutes without stimuli. The mouse was next presented with a light stimulus of 400 lumens for 200 ms every 500 ms for 100 s, followed by another 4 minutes without stimuli. Voltages were measured every ms throughout the entire test. Plexiglass cylinders were cleaned between tests with 70% ethanol.

For analysis, voltage measurements in function of time were Fourier transformed to extract frequency information. Fourier transformations were performed using the

'seewave' and 'rgl' package for R by Dr. Johann du Hoffmann (Rodent Behavioral Core, National Institute of Mental Health, National Institutes of Health).

4.4.9 Elevated plus maze

The elevated plus maze was used to measure anxiety (Walf and Frye, 2007).

The elevated plus maze was set up in a dimly lit room and animals were allowed to habituate in the testing room for 60 minutes prior to testing. Each arm of the maze is 38 cm in length and 10 cm wide. Two arms of the maze opposite to each other were enclosed with 15 cm high walls. The mice were place in the center of the maze facing a closed arm and were allowed to explore the maze for 10 minutes. The number of arm entries, time spent in each arm and percentage of entries into open arms was scored. The maze was cleaned with 70% ethanol in between trials to eliminate odour cues.

4.4.10 Y-maze spontaneous alternation

Working memory was tested using the spontaneous alternation test conducted in a Y-maze (Wolf *et al.*, 2016).

Mice were allowed to habituate in the testing room 60 minutes prior to testing. A symmetrical Y-maze consisted of 3 arms, each 40 cm long, 8 cm wide and enclosed by plexiglass walls that were 12 cm high. Mice were placed in the center of the maze and were allowed to explore all 3 arms of the maze freely during 8 minutes. Spontaneous alternation was defined as conecutive entries in 3 different arms divided by the number of possible alternations (total alternations - 2). Re-entries

into the same arm were scored as separate entries. The maze was cleaned with 70% ethanol in between trials.

4.4.11 Y-maze forced alternation

The forced alternation task was conducted in the same Y-maze as described above to assess spatial memory (Wolf *et al.*, 2016).

Mice were allowed to habituate in the testing room with dimmed lighting 60 minutes prior to testing. The forced alternation task consisted of a 5 minute sample trial and a 5 minute retrieval trial, with a 90 minute inter-trial interval. During the sample trial, the mice were placed in the start arm and were allowed to explore 2 arms of the Y-maze, while the 3rd arm was blocked. During the retrieval, this block was removed and the mouse was placed in the start arm and allowed to freely explore all 3 arms of the Y-maze. Forced alternation was described as the percentage of mice in the retrieval trial entering the arm that was blocked during the sample trial first. In addition, time spent in the novel arm was measured as well. the Y-maze was cleaned with 70% ethanol in between trials.

Since the forced alternation test relies on the novelty aspect exploring the Y-maze, the spontaneous alternation task and forced alternation task were performed at least one week apart.

4.4.12 Statistics

Data were plotted and statistical tests were performed using Prism 8 (Graphpad), or SPSS Statistics (IBM) for binary and multinomial logistic regression analysis. Error bars are displayed as means and standard error of the mean (SEM). The

statistical test results are displayed in table 4.2. n represents the number of animals included in each test.

Figure	Variable	Statistical test	Test result	P-value
4.1 A, B	Genotype	Two-way ANOVA	F = 0.007736	0.9312
	Age	Two-way ANOVA	F = 9.727	0.0075
	Genotype x Age	Two-way ANOVA	F = 0.04029	0.8438
	Genotype at 6 months	Sidak's *post hoc*		0.9992
	Genotype at 12 months	Sidak's *post hoc*		0.9792
4.1 C, D	Genotype, Age	Multinomial logistic regression	χ^2 = 18.117, χ^2 = 18.053	< 0.0001, < 0.0001
4.1 C, D	Genotype (2 compared to 0 falls)		Wald = 209.210	< 0.0001
4.1 C, D	Genotype (1 compared to 0 falls)		Wald = 324.938	< 0.0001
4.1 C, D	Age (2 compared to 0 falls)		Wald = 224.278	< 0.0001
4.2 A, B	Genotype	Two-way ANOVA	F = 4.825	0.0454
	Age	Two-way ANOVA	F = 2.353	0.1474
	Genotype x Age	Two-way ANOVA	F = 1.859	0.1943
	Genotype at 6 months	Sidak's *post hoc*		0.8429
	Genotype at 12 months	Sidak's *post hoc*		0.0366
4.2 C, D	Genotype	Two-way ANOVA	F = 4.116	0.0521
	Age	Two-way ANOVA	F = 3.224	0.0834
	Genotype x Age	Two-way ANOVA	F = 2.158	0.1530
	Genotype at 6 months	Sidak's *post hoc*		0.9072
	Genotype at 12 months	Sidak's *post hoc*		0.0390
4.3 A, B	Genotype	Three-way ANOVA	F = 4.746	0.0469
	Age	Three-way ANOVA	F = 9.845	0.0130
	Trial day	Three-way ANOVA	F = 7.587	0.0023
	Genotype x Age	Three-way ANOVA	F = 3.175	0.0965
	Genotype x Trial day	Three-way ANOVA	F = 2.035	0.1496
	Genotype x Age x Trial day	Three-way ANOVA	F = 1.030	0.3703
4.4 A, B	Genotype	Two-way ANOVA	F = 0.4274	0.5168
	Age	Two-way ANOVA	F = 25.17	< 0.0001
	Genotype x Age	Two-way ANOVA	F = 0.4274	0.5168
	Genotype at 6 months	Sidak's *post hoc*		0.9180
	Genotype at 12 months	Sidak's *post hoc*		0.9142
4.7 A, B	Genotype	Three-way ANOVA	F = 1.927	0.1868
	Age	Three-way ANOVA	F = 0.1938	0.6665
	Stimulus	Three-way ANOVA	F = 13.92	0.0001
	Genotype x Age	Three-way ANOVA	F = 7.890	0.139
	Genotype x Stimulus	Three-way ANOVA	F = 1.276	0.2949
	Age x Stimulus	Three-way ANOVA	F = 1.256	0.3004
	Genotype x Age x Stimulus	Three-way ANOVA	F = 1.565	0.2268
4.8 C, F	Genotype	Three-way ANOVA	F = 0.2658	0.6142
	Age	Three-way ANOVA	F = 1.226	0.2868
	Frequency	Three-way ANOVA	F = 509.8	< 0.0001
	Genotype x Age	Three-way ANOVA	F = 3.824	0.0708
	Genotype x Frequency	Three-way ANOVA	F = 0.8081	0.6970
	Age x Frequency	Three-way ANOVA	F = 1.054	0.3998
	Genotype x Age x Frequency	Three-way ANOVA	F = 8.592	< 0.0001

Figure	Variable	Statistical test	Test result	P-value
	Genotype at 6 months at 0-1 Hz	Sidak's *post hoc*		< 0.0001
	Genotype at 12 months at 0-1 Hz	Sidak's *post hoc*		< 0.0001
4.9 A, B	Genotype	Two-way ANOVA	F = 0.09484	0.7596
	Age	Two-way ANOVA	F = 1.907	0.1611
	Genotype x Age	Two-way ANOVA	F = 0.2874	0.7517
4.9 C, D	Genotype	Two-way ANOVA	F = 0.1059	0.7465
	Age	Two-way ANOVA	F = 3.567	0.0371
	Genotype x Age	Two-way ANOVA	F = 0.2824	0.7554
4.9 E, F	Genotype	Two-way ANOVA	F = 1.080	0.3046
	Age	Two-way ANOVA	F = 1.180	0.3174
	Genotype x Age	Two-way ANOVA	F = 0.2905	0.7494
4.9 G, H	Genotype	Two-way ANOVA	F = 0.6090	0.4396
	Age	Two-way ANOVA	F = 0.9379	0.3995
	Genotype x Age	Two-way ANOVA	F = 0.8245	0.4454
4.10 A, B	Genotype	Two-way ANOVA	F = 0.5403	0.4664
	Age	Two-way ANOVA	F = 1.881	0.1650
	Genotype x Age	Two-way ANOVA	F = 0.1812	0.8349
4.11 A, B	Genotype	Two-way ANOVA	F = 1.927	0.1724
	Age	Two-way ANOVA	F = 2.162	0.1277
	Genotype x Age	Two-way ANOVA	F = 0.9594	0.3913
4.11 C, D	Genotype	Two-way ANOVA	F = 0.01634	0.8989
	Age	Two-way ANOVA	F = 0.2746	0.7612
	Genotype x Age	Two-way ANOVA	F = 1.317	0.2788
4.12 A, B	Genotype	Two-way ANOVA	F = 1.419	0.2534
	Age	Two-way ANOVA	F = 0.5638	0.5733
	Genotype x Age	Two-way ANOVA	F = 1.419	0.2534
4.12 C, D	Genotype	Two-way ANOVA	F = 5.3999	0.0251
	Age	Two-way ANOVA	F = 0.9823	0.3825
	Genotype x Age	Two-way ANOVA	F = 1.171	0.3200
4.12 E, F	Genotype	Two-way ANOVA	F = 0.1635	0.6880
	Age	Two-way ANOVA	F = 2.446	0.0989
	Genotype x Age	Two-way ANOVA	F = 2.493	0.0948
4.13 A, B	Genotype	Two-way ANOVA	F = 0.1424	0.7078
	Age	Two-way ANOVA	F = 0.7778	0.4659
	Genotype x Age	Two-way ANOVA	F = 3.150	0.7078
4.13 C, D	Genotype	Two-way ANOVA	F = 0.3292	0.5694
	Age	Two-way ANOVA	F = 2.067	0.1403
	Genotype x Age	Two-way ANOVA	F = 2.589	0.0879
4.13 E, F	Genotype, Age	Binary logistic regression	$\chi^2 = 10.010$, $\chi^2 = 1.161$	0.002, 0.281
4.13 E, F	Genotype (new compared to old)		Wald = 6.457	0.011

Table 4.2: **Statistical test results**

5 TRANSCRIPTOME ANALYSIS OF MUTANT AUXILIN NEURONS

5.1 INTRODUCTION

Auxilin is a neuronal protein required for the uncoating of CCVs. A novel PD mouse model harbouring the pathogenic PD Auxilin mutation R857G was shown to display neurological symptoms reminiscent of clinical features seen in patients (see Chapter 4). In addition, the R857G Auxilin allele was found to be hypomorphic, indicating a loss of function mechanism in PD pathogenesis (see Chapter 3). However, the exact impact of the R857G Auxilin mutation on cellular pathways remains to be elucidated.

One useful approach to assess pathways affected by the R857G Auxilin mutation in neurons is RNA sequencing (RNAseq). Given the high resolution and broad dynamic range, deep-sequencing methods provide a quantitative way to detect the full transcriptome of samples. Comparison of the full set of transcripts between biological samples thus allows to to detect global alterations in gene expression.

To gain insight into the pathways affected by the pathogenic R857G Auxilin mutation in neurons, RNAseq was performed on primary neuronal cultures derived from R857G Auxilin mice.

RNA samples were converted to a cDNA library by Alice Kaganovich and myself. Subsequent high-throughput sequencing was performed by Alice Kaganovich and sequencing reads were aligned to the reference genome by Dr. Jinhui Ding. Read normalization and differential gene expression analysis was performed by Dr. Mark Cookson.

Following the identification of differentially expressed genes by RNAseq, I also validated top candidates at the RNA-level using quantitative PCR (qPCR). In addition, gene ontology was performed to gain global insight into affected biological pathways, followed by functional experiments to further dissect the underlying mechanisms through which biological pathways are affected.

5.2 RESULTS

5.2.1 RNAseq design

The transcriptome of R857G Auxilin neurons was compared to WT neurons through RNA sequencing (RNAseq) (Figure 5.1).

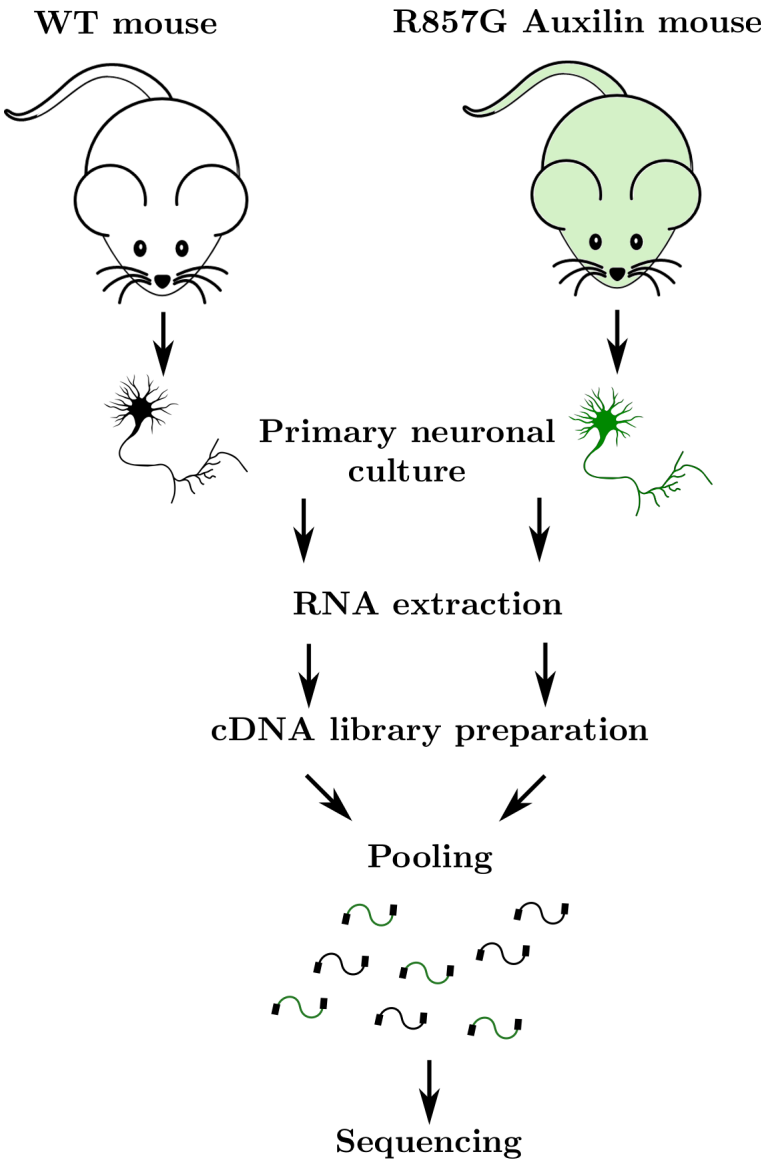

Figure 5.1: **Design of RNAseq experiment for differential gene expression analysis of R857G Auxilin neurons**

Total RNA was extracted from primary cortical neurons derived from n=5 WT and n=6 R857G Auxilin mice. RNA quality was assessed by measurement of the RNA integrity number (RIN). A RIN value of 7 was considered as the cut-off for inclusion in the RNAseq experiment, thus no samples were excluded from analysis (Table 5.1).

Sample	RIN
WT 1	7.3
WT 2	9.4
WT 3	8.6
WT 4	9.0
WT 5	8.8
R857G Auxilin 1	8.3
R857G Auxilin 2	8.7
R857G Auxilin 3	8.5
R857G Auxilin 4	8.7
R857G Auxilin 5	8.6
R857G Auxilin 6	8.9

Table 5.1: **RIN measurements for RNA quality control**

Ribosomal RNA was depleted from all samples followed by RNA fragmentation. Double stranded complementary DNA (cDNA) was synthesized and RNA was depleted from the samples. Indexing adaptors were ligated to both ends of the cDNA to allow for hybridization onto a sequencing flow cell. cDNA with successful adaptor ligation was enriched using primers annealing to the adaptors. cDNA libraries were validated using droplet digital PCR to ensure optimum cluster densities across different lanes of the flow cell. Clonally amplified cDNA fragments hybridized to a flow cell were subsequently subjected to high-throughput sequencing.

5.2.2 Normalization of count data

A count matrix was generated indicating the number of sequencing reads that were unambiguously mapped to a single gene per sample. Counts were analysed using the DESeq2 R package, which assumes a negative binomial distribution of the read counts (Love *et al.*, 2014).

When dealing with count data, an important consideration is that count ratios are inherently noisier when the counts are low. This heteroskedasticity (or variance dependency on mean count) would thus result in stronger differences between groups for weakly expressed genes as compared to strongly expressed genes and would result in potential false positives. Count data were therefore transformed using a regularized logarithm (RLog), which behaves like a Log2 transformation for genes with high counts and shrinks together values for different samples with for genes with low counts (Love *et al.*, 2014). The RLog transformation therefore avoids the spreading apart of data for genes with low counts, as seen with standard transformation such as the Log2 transformation (Figure 5.2 A). The RLog transformation successfully rendered the data homoskedastic, i.e. having stabilized variances (Figure 5.2).

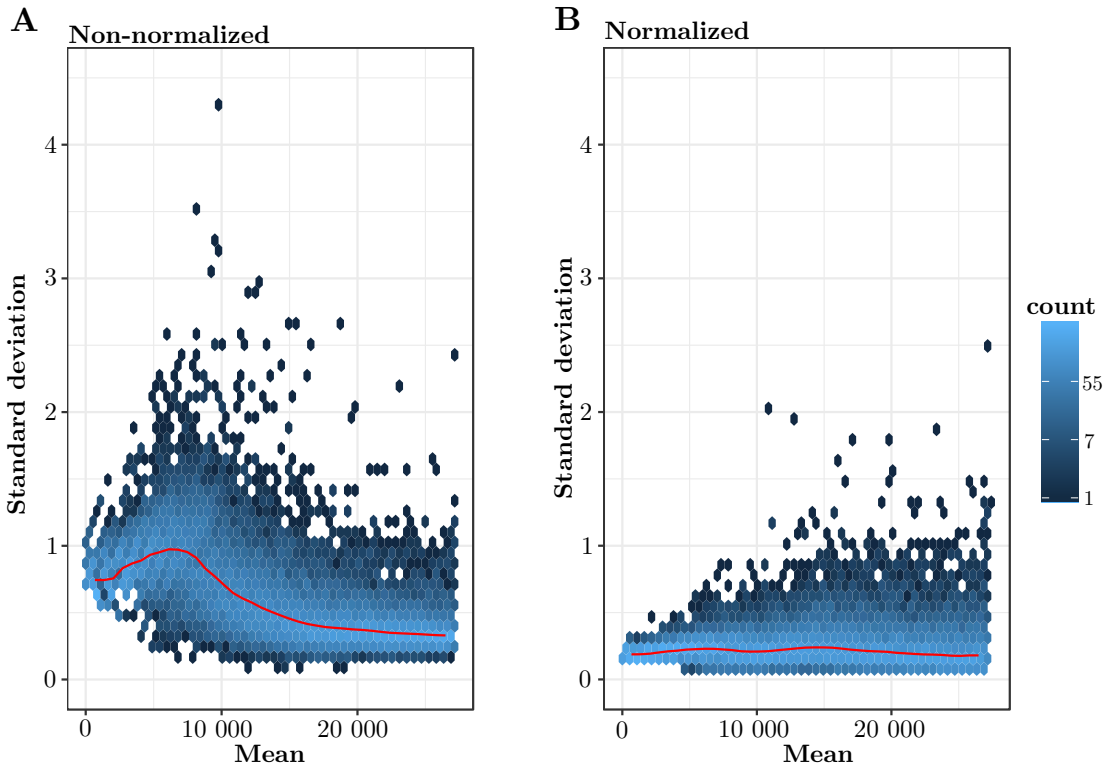

Figure 5.2: **Variance stabilization of RNAseq count data** Mean/Standard deviation plot of A Log2 tranformed and B RLog transformed RNAseq count data.

5.2.3 Relationship between samples and filtering

The homoskedastic data display a similar dynamic range of the variances, allowing for multivariate ordination to assess the relationship between samples and subsequent filtering. First, the Euclidean distance between samples was plotted as a heatmap and subjected to unsupervised hierarchical clustering to observe global differences between samples (Figure 5.3). Strikingly, one WT sample (replicate 1) and two R857G Auxilin samples (replicates 5, 6) clustered separately and displayed large Euclidean distance compared to all other samples. WT samples (replicate 2-5) and R857G Auxilin samples (replicate 1-4) clustered according to genotype.

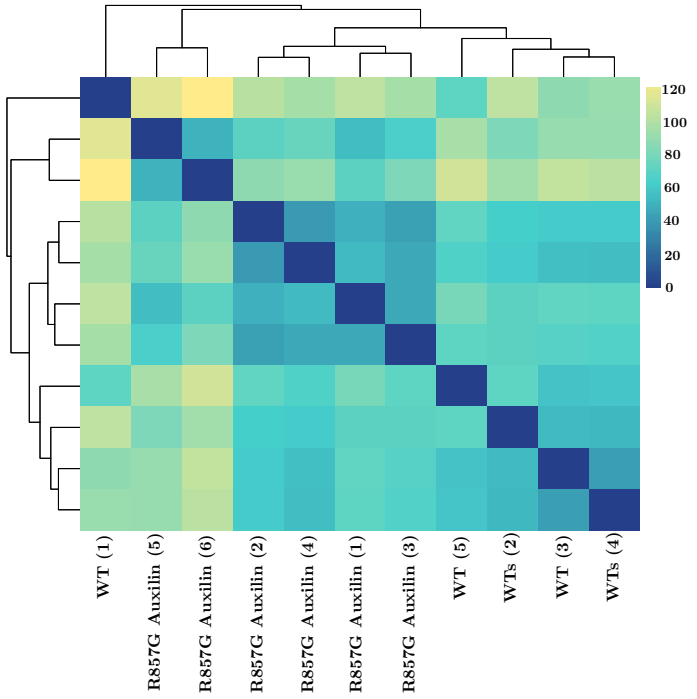

Figure 5.3: **Heat map of the Euclidean distance between samples** Colours indicate Euclidean distance between samples and dendrograms are are scaled to the Euclidean distance between samples.

Principal component analysis (PCA) was performed to analyse the source of variation between samples (Figure 5.4). The first principal component, driving 79% of variation between samples, separated out replicates 5 and 6 from replicates 1-4 R857G Auxilin samples. The second principal component, driving 10% of variation, separated WT sample replicate 1 from replicates 2-5, and R857G Auxilin replicates 5 and 6 from replicates 1-4.

Based on Euclidean distance analysis and PCA, WT replicate 1 and R857G Auxilin replicates 5 and 6 were considered outliers and were excluded from further analysis.

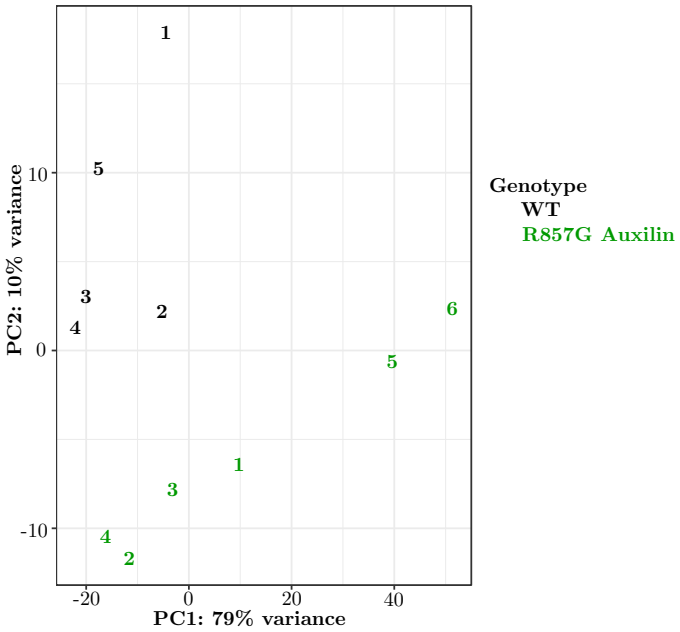

Figure 5.4: **PCA of unfiltered samples**

Euclidean distance analysis and PCA were re-analysed for filtered samples. Unsupervised hierarchical clustering revealed separation by genotype based on Euclidean distance between samples (Figure 5.5). In addition, PCA analysis revealed group separation between genotypes by the first principal component, driving 56% of variation (Figure 5.6).

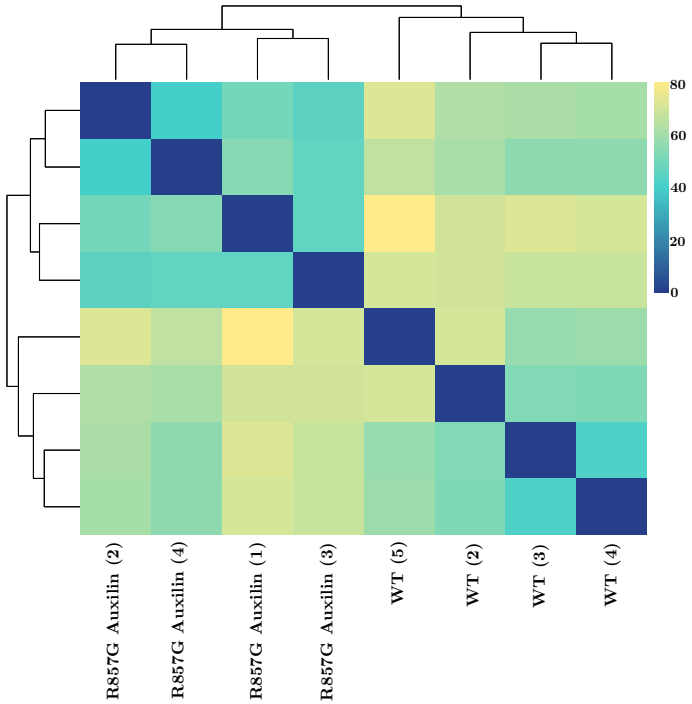

Figure 5.5: **Heat map of the Euclidean distance between filtered samples** Colours indicate Euclidean distance between samples and dendrograms are are scaled to the Euclidean distance between samples.

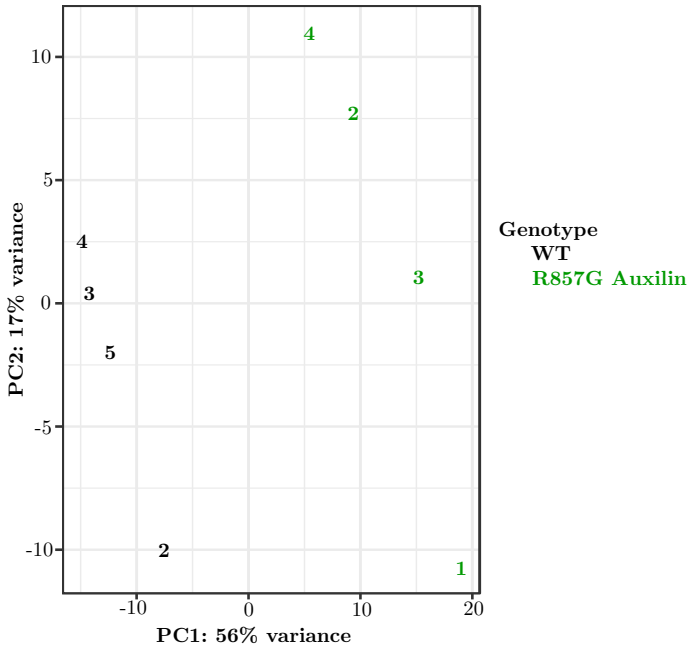

Figure 5.6: **PCA of filtered samples**

5.2.4 Differential gene expression analysis

Normalized counts from filtered samples were subsequently subjected to significance testing using a Wald test, with Benjamini and Hochberg multiple testing adjustment. Out of 27155 detected transcripts, 4666 genes were found to be differentially expressed (adjusted p-value < 0.05), with 2203 genes displaying increased expression in the R857G Auxilin samples (Figure 5.7). The full list of identified transcripts can be found in Supplementary Table 1.

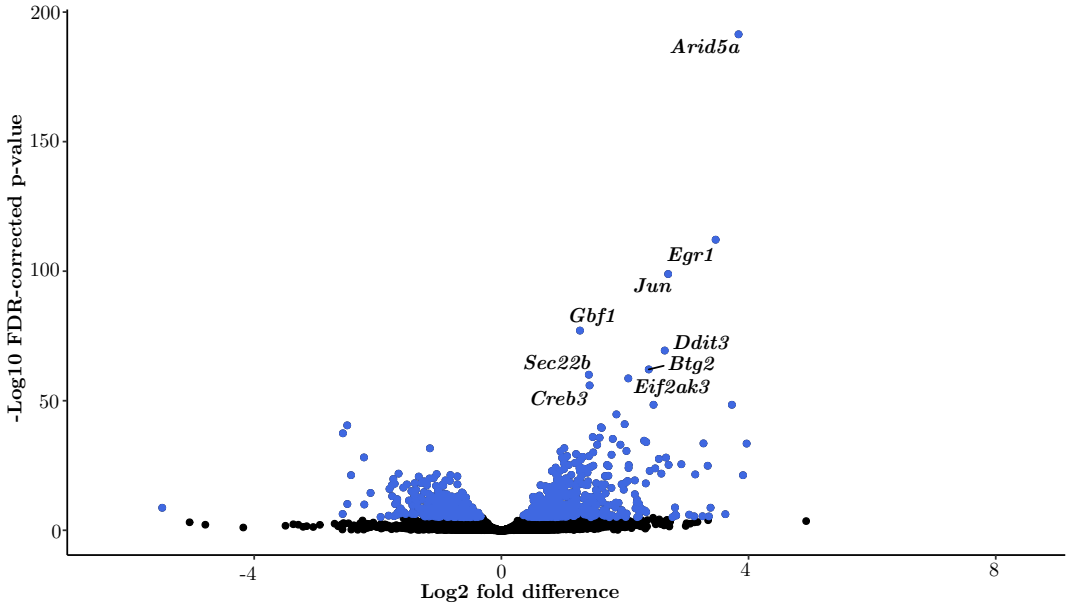

Figure 5.7: **Volcano plot of the impact of R857G Auxilin on transcriptome of primary neurons** Volcano plot of 27155 detected mRNA transcripts quantified using RNAseq isolated from primary neurons (n=4 WT, n=4 R857G Auxilin). The 4666 genes were differentially expressed in R857G Auxilin neurons (Wald test with Benjamini & Hochberg correction, p-value < 0.05) are indicated in blue. Differentially expressed genes with a p-value $< 10^{-50}$ are labeled by gene name.

The z-score of the 50 most significantly differentially expressed genes were plotted on a heat map and subjected to unsupervised hierarchical clustering, revealing large global alterations with opposite relationships to the mean value between WT and R857G Auxilin samples (Figure 5.8).

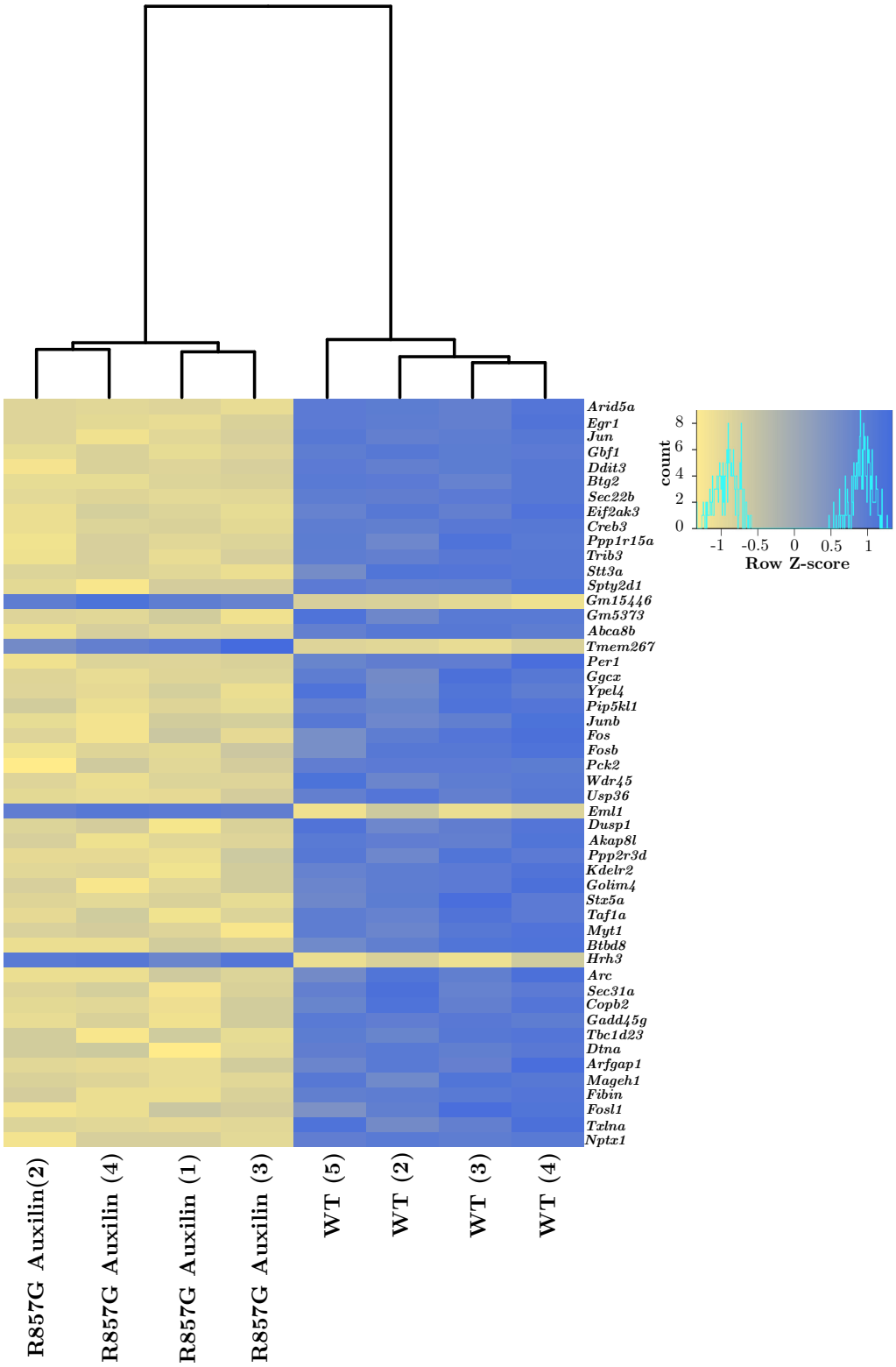

Figure 5.8: **Heat map of the z-score of top 50 differentially expressed genes** Colours indicate the z-score per gene per sample and dendrograms are are scaled to the Euclidean distance between samples based on the top 50 differentially expressed genes.

5.2.5 Gene ontology

To gain further insight into the pathways affected in the R857G Auxilin neurons, the top 50 genes were subjected to gene ontology (GO) analysis (Table 5.2, Figure 5.9) (Reimand *et al.*, 2016). Enrichment analysis for GO term biological process was performed using the Fisher exact test, with Benjamini and Hochberg *post hoc* analysis.

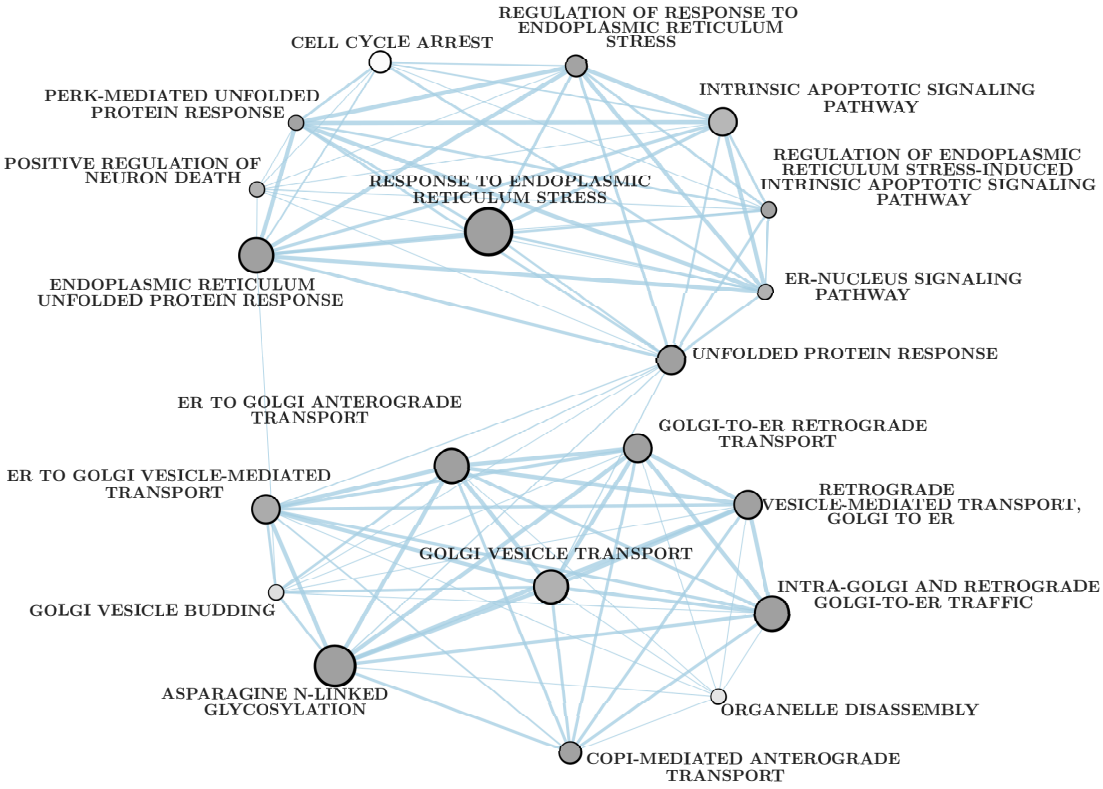

Figure 5.9: **Gene ontology of top 50 differentially upregulated genes in mutant Auxilin neurons** Gene ontology enrichment analysis of the top candidates of Auxilin interactors for biological process and biological pathways. Node size corresponds to number of genes within each gene-set and edge size to number of overlapping genes between connected nodes (larger is more genes). Node colour corresponds to the p-value of the Fisher exact test with Benjamini & Hochberg correction for multiple testing (darker is lower p-value).

Biological process

GO identifier	Description	p-value	Genes
GO:0006986	response to unfolded protein	2.11 x 10^{-4}	*PPP1R15A*, *ARFGAP1*, *CREB3*, *SEC31A*, *EIF2AK3*, *DDIT3*
GO:0034976	response to endoplasmic reticulum stress	4.17 x 10^{-5}	*PPP1R15A*, *ARFGAP1*, *TRIB3*, *CREB3*, *SEC31A*, *EIF2AK3*, *DDIT3*, *JUN*
GO:1905897	regulation of response to endoplasmic reticulum stress	1.81 10^{-3}	*PPP1R15A*, *CREB3*, *EIF2AK3*, *DDIT3*
GO:0006984	ER-nucleus signaling pathway	8 x 10^{-3}	*PPP1R15A*, *EIF2AK3*, *DDIT3*
GO:0097193	intrinsic apoptotic signaling pathway	1.1 x 10^{-2}	*PPP1R15A*, *TRIB3*, *CREB3*, *EIF2AK3*, *DDIT3*
GO:0030968	endoplasmic reticulum unfolded protein response	7.63 x 10^{-5}	*PPP1R15A*, *ARFGAP1*, *CREB3*, *SEC31A*, *EIF2AK3*, *DDIT3*
GO:0036499	PERK-mediated unfolded protein response	1.46 x 10^{-3}	*PPP1R15A*, *EIF2AK3*, *DDIT3*
GO:1902235	regulation of endoplasmic reticulum stress-induced intrinsic apoptotic signaling pathway	1.54 x 10^{-3}	*CREB3*, *EIF2AK3*, *DDIT3*
GO:0048193	Golgi vesicle transport	8 x 10^{-3}	*ARFGAP1*, *GBF1*, *KDELR2*, *SEC31A*, *COPB2*, *SEC22B*
GO:0006890	retrograde vesicle-mediated transport, Golgi to ER	2.41 x 10^{-4}	*ARFGAP1*, *GBF1*, *KDELR2*, *COPB2*, *SEC22B*
GO:0006888	ER to Golgi vesicle-mediated transport	5.4 x 10^{-3}	*ARFGAP1*, *GBF1*, *SEC31A*, *COPB2*, *SEC22B*
GO:0048194	Golgi vesicle budding	3.02 x 10^{-2}	*GBF1*, *SEC31A*, *SEC22B*
GO:1903008	organelle disassembly	3.37 x 10^{-2}	*USP36*, *GBF1*, *WDR45*
GO:0007050	cell cycle arrest	4.44 x 10^{-2}	*PPP1R15A*, *DUSP1*, *BTG2*, *DDIT3*
GO:1901216	positive regulation of neuron death	8.78 x 10^{-3}	*EGR1*, *FOS*, *DDIT3*

Biological pathways reactome

Reactome identifier	Description	p-value	Genes
REAC:R-HSA-	Intra-Golgi and retrograde Golgi-to-ER traffic	1.26 x 10^{-4}	*ARFGAP1*, *GBF1*, *KDELR2*,*GOLIM4*, *COPB2*, *SEC22B*
REAC:R-HSA-	Golgi-to-ER retrograde transport	1.79 x 10^{-4}	*ARFGAP1*, *GBF1*, *KDELR2*, *COPB2*, *SEC22B*
REAC:R-HSA-	Asparagine N-linked glycosylation	1.26 x 10^{-4}	*ARFGAP1*, *GBF1*, *STT3A*, *KDELR2*, *SEC31A*, *COPB2*, *SEC22B*
REAC:R-HSA-	ER to Golgi Anterograde Transport	1.11 x 10^{-4}	*ARFGAP1*, *GBF1*, *KDELR2*, *SEC31A*, *COPB2*, *SEC22B*
REAC:R-HSA-	cCOPI-mediated anterograde transport	9.53 x 10^{-4}	*ARFGAP1*, *GBF1*, *KDELR2*, *COPB2*

Table 5.2: **GO analysis of differentially expressed genes in R857G Auxilin neurons** 50 most significantly differentially expressed genes were subjected to GO analysis. Fischer exact test with Benjamini & Hochberg correction for multiple testing was performed for the enrichment analysis of GO terms for biological process and reactome terms for biological pathways (Reimand *et al.*, 2016).

Two major themes from enriched GO terms appeared: transport and stress response in the early secretory pathway. Indeed, multiple proteins residing in the ER or Golgi network were identified, as well as multiple transcription factors with important roles in regulating the ER and Golgi dynamics (Table 5.2). Table 5.3 and Table 5.4 provide a functional description of the genes involved with two of the larger, overarching GO terms 'response to ER stress' and 'Golgi vesicle transport', respectively.

Gene	Protein	Function
PPP1R15A	Protein phosphatase 1 regulatory subunit 15A	Recruitment of protein phoshpatase 1 for the dephosphorylation of translation initation factor EIF2A to reverse the shut-off stress-induced protein synthesis
ARFGAP1	ADP-ribosylation factor GTPase-activating protein 1	GAP for ARF1, required for the dissociation of coat proteins from Golgi-derived membranes
TRIB3	Tribbles homolog 3	Inhibition of transcriptional activity of DDIT3, involved in cell death regulation during ER stress
CREB3	Cyclic AMP-responsive element-binding protein 3	ER-bound transcription factor promoting cell survival as opposed to ER stress-induced apoptosis
SEC31A	Protein transport protein Sec31A	Component of COPII, promoting the formation of ER-derived vesicles
EIF2AK3	Eukaryotic translation initiation factor 2-alpha kinase 3	Kinase that phosphorylates of translation initiation factor EIF2A in response to stress to decrease overall protein synthesis
DDIT3	DNA damage-inducible transcript 3 protein	Multifunctional transcription factor in ER stress response
JUN	Transcription factor AP-1	Transcription factor regulating gene expression in response to a variety of stimuli, including stress

Table 5.3: **Functional description of the gene-set annotated to GO term 'response to ER stress'** The UniProt database was queried for protein functions (The UniProt Consortium, 2019).

Gene	Protein	Function
ARFGAP1	ADP-ribosylation factor GTPase-activating protein 1	GAP for ARF1, required for the dissociation of coat proteins from Golgi-derived membranes
GBF1	Golgi-specific brefeldin A-resistance guanine nucleotide exchange factor 1	GEF for ARF proteins involved in trafficking in the early secretory pathway
KDELR2	ER lumen protein-retaining receptor 2	Required for the retention of luminal ER proteins and for normal vesicular traffic through the Golgi
SEC31A	Protein transport protein Sec31A	Component of COPII, promoting the formation of ER-derived vesicles
COPB2	Coatomer subunit beta'	Coat protein required for anterograde protein transport from the ER to the TGN via the Golgi stacks, and required for retrograde Golgi-to-ER transport
SEC22B	Vesicle-trafficking protein SEC22b	SNARE involved in targeting and fusion of ER-derived vesicles with the Golgi and Golgi-derived vesicles with the ER

Table 5.4: **Functional description of the gene-set annotated to GO term 'Golgi vesicle transport'** The UniProt database was queried for protein functions (The UniProt Consortium, 2019).

Auxilin plays a specific role in clathrin trafficking from the TGN and the plasma membrane and the R857G Auxilin mutation contributes to PD pathogenesis via a loss of function mechanism. Thus, alterations in ER-cis Golgi trafficking might reflect compensatory mechanisms to restore normal trafficking in cells with diminished Auxilin function. It is conceivable that genes involved in early steps of the secretory pathway are differentially expressed in an attempt to counteract impairments in later steps of the secretory pathway due to impaired clathrin trafficking. In addition, chronic increase of ER-Golgi trafficking may well result in ER stress, with subsequent activation of stress response mechanisms.

5.2.6 Activation of the Golgi stress response

Whereas the ER stress response has been well documented, the signalling cascade during the Golgi stress response is less explored. However, two genes that have been implied as important mediators of the Golgi stress response (*GBF1*, *CREB3*), were found to be among the most significantly differentially expressed genes in R857G Auxilin neurons (Figure 5.7, Figure 5.8) (Reiling *et al.*, 2013).

Validation by quantitative PCR (qPCR) of primary neurons confirmed the upregulation of GBF1 and CREB3 as observed in the RNAseq dataset (Figure 5.10).

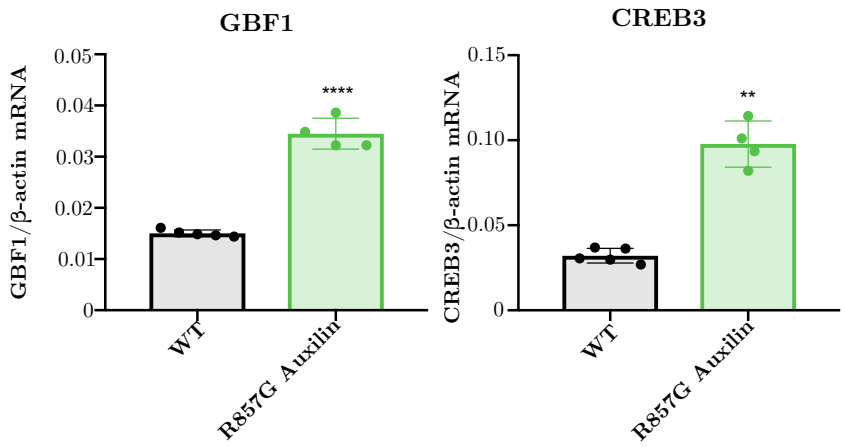

Figure 5.10: **qPCR analysis of GBF1 and CREB3 expression levels** qPCR analysis of n=5 and n=4 RNA samples from WT and R857G Auxilin primary neurons, respectively. Unpaired t-test was performed, with **** indicating a p-value < 0.0001.

CREB3 is an ER-resident transcription factor that is translocated to the cis-Golgi network for cleavage and subsequent activation in response to multiple stressors, including ER and Golgi stress. Activated CREB3 is translocated to the nucleus, for the initiation of gene transcription as part of the stress response. Remarkably, increased expression of ARF4 through activation of CREB3 was found to sensitize cells to apoptosis in response to Golgi stress (Reiling *et al.*, 2013).

The ARFGEF GBF1 is required for GDP to GTP exchange of multiple ARF members, and is the rate-limiting factor to control their activation. GBF1 expression has also been shown to be upregulated in response to Golgi stress. In contrast with CREB3, increased expression of GBF1 was found to protect against Golgi disintegration and apoptosis through activation of ARF1 (Reiling *et al.*, 2013). ARF1 itself is also upregulated in response to Golgi stress and increased expression levels were found to protect against Golgi stress (Reiling *et al.*, 2013).

Thus, ARF1 and ARF4 appear to be upregulated and counteract each other in response to Golgi stress. To address whether ARF1 and ARF4 proteins were upregulated in R857G Auxilin primary neurons too, I looked at differential expression of the genes encoding ARF proteins in the RNAseq dataset (Figure 5.11). Indeed, in contrast with other ARF proteins, ARF1 and ARF4 were found to be upregulated in R857G Auxilin neurons, indicating the activation of the Golgi stress response.

Remarkably, ARF2 and ARF3, which share 96% homology with ARF1, were found to be downregulated in R857G Auxilin neurons (Figure 5.11) (D'Souza-Schorey and Chavrier, 2006). Whereas ARF2 and ARF3 have not been implied in Golgi stress response mechanisms, it is plausible that their downregulation would counteract the upregulation of ARF1, as ARF proteins are thought to provide overlapping functions (D'Souza-Schorey and Chavrier, 2006; Reiling *et al.*, 2013).

5.2.7 Morphological alterations of the Golgi apparatus

Since expression levels of CREB3, GBF1, ARF1 and ARF4 were previously found to correlate with Golgi integrity, the Golgi morphology of R857G Auxilin neurons was analysed by electron microscopy (EM) imaging of striatal brain slices of R857G Auxilin mice (Figure 5.12 A, B) (Reiling *et al.*, 2013). Strikingly, the Golgi apparatus in the striatum of R857G Auxilin mice appeared more swollen as compared to the striatum of WT mice (Figure 5.12 E).

To further address swelling of the Golgi apparatus and to be able to distinguish between cis, medial and trans Golgi stacks, I used confocal microscopy with Airyscan detection to analyse primary neurons stained for endogenous Golgi markers (Figure 5.12 C, D, F, G). Swelling was measured indirectly using

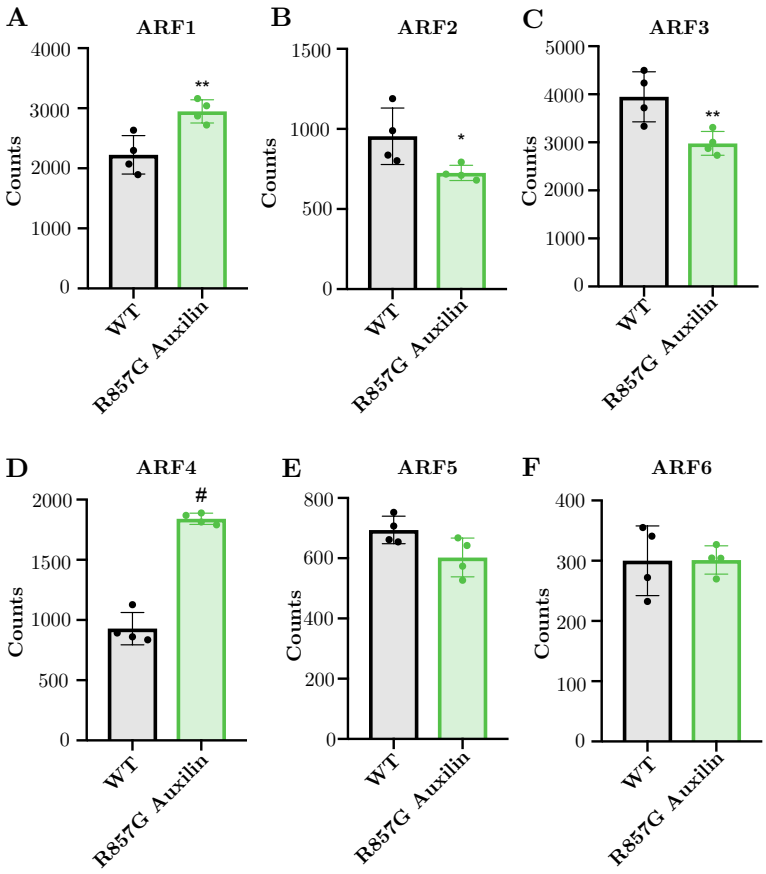

Figure 5.11: **Differential expression of ARF proteins in R857G Auxilin neurons** Differential expression of ARF1-6 in R857G Auxilin neurons as detected by RNAseq. Wald test with Benjamini & Hochberg *post hoc* correction was performed and p-values indicated when significant, with * p-value < 0.05, ** p-value < 0.01, # p-value $< 10^{-17}$.

co-localization analysis: swollen Golgi morphology would result in an increased surface area, with subsequent decrease of co-localization between neighbouring Golgi stacks.

Indeed, a decreased co-localization between cis and medial Golgi stacks (GM130 and GLG1, respectively) and medial Golgi stacks (GLG1 and TGN38, respectively) was observed in primary neurons derived from R857G Auxilin mice compared to WT, indicating swollen Golgi morphology. No alterations in co-localization between cis and trans Golgi stacks were observed (data not shown), which can be expected given the physical distance between both compartments.

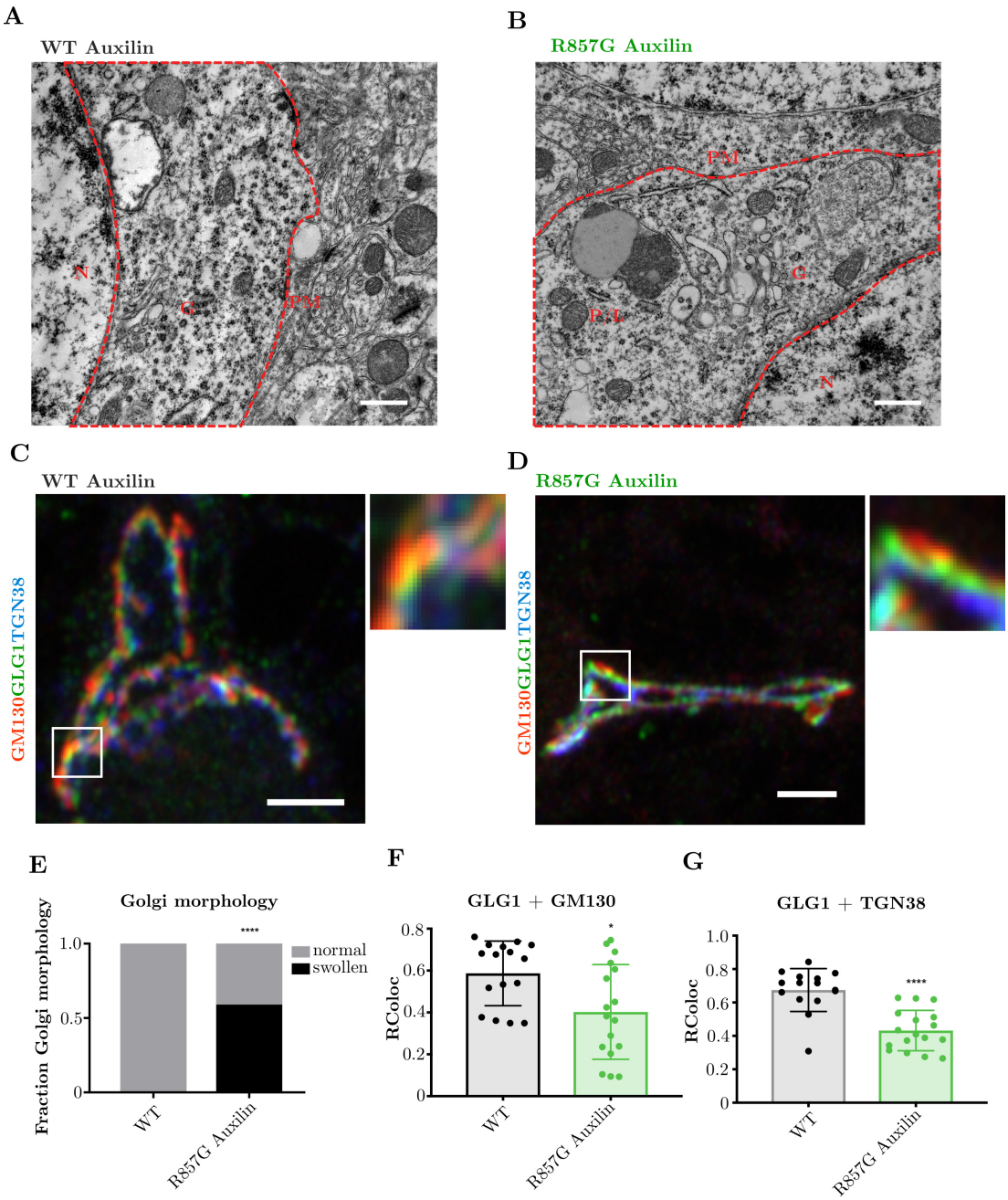

Figure 5.12: **Dystrophic alterations in Golgi morphology in R857G Auxilin neurons** A, B Representative EM images of brain slices of the striatum of WT and R857G Auxilin mice. Scale bar = 600 nm. E Quantification of observed Golgi morphologies of n=10 WT and n=22 R857G Auxilin striatal cells. Binomial test was performed, **** indicates p-value < 0.0001. C, D Representative confocal images with Airy scan detection of WT and R857G Auxilin primary neurons, stained for endogenous GM130 (red), GLG1 (green) and TGN38 (blue) scale bars = 2 μm. F, G Quantification of co-localization of GLG1+GM130 and GLG1+TGN38, respectively, of n=16 WT and n=17 WT R857G Auxilin primary neurons. Unpaired t-tests were performed, * indicates p-value < 0.05, **** indicates p-value < 0.0001.

5.3 DISCUSSION

A novel PD mouse model harbouring the pathogenic R857G Auxilin mutation was developed and RNAseq of primary cultural neurons was performed to assess differential gene expression between WT and R857G Auxilin mice. A total of 4666 genes were found to be differentially expressed, of which 2203 were enriched in the R857G Auxilin neurons (Figure 5.7). GO analysis of the 50 most significantly differentially expressed genes revealed alterations in genes involved in early secretory pathway trafficking, as well as the activation of an early secretory pathway stress response (Figure 5.8).

The early secretory pathway consists of the ER and the Golgi apparatus. Proteins and lipids are synthesized in the ER and are subsequently transported to the Golgi network for processing and sorting and subsequent transport from the TGN to a variety of intracellular compartments. Anterograde and retrograde trafficking between the ER and the Golgi is mediated by COPII and COPI coated vesicles, respectively, whereas clathrin coated vesicles play an important role in vesicular trafficking protein and lipids from the TGN to destination compartments.

Auxilin is required for the uncoating of CCVs in neurons and the R857G Auxilin allele was found to be a hypomorph (see Chapter 3). It is thus conceivable that the R857G Auxilin mutation would result in impaired clathrin trafficking through a partial loss of function mechanism, with subsequent impairments in CCV-mediated trafficking from the TGN and delivery of its cargo to destination compartments.

The observed upregulation of genes involved with trafficking between the ER and the Golgi apparatus might reflect secondary alterations to increase early secretory trafficking in an attempt to compensate for the decreased trafficking from the TGN (Table 5.4). In addition, chronic increase of ER-Golgi trafficking may well

result in the ER and Golgi stress and could explain the observed activation of the early secretory pathway stress response (Figure 5.3).

Whereas the exact mechanisms of the Golgi stress response are not fully understood, two genes that were among the 10 most significantly differentially expressed genes, *CREB3* and *GBF1*, have previously been reported to play an important role in mediating the Golgi stress response (Reiling *et al.*, 2013). Validation by qPCR confirmed the upregulation of those genes in R857G Auxilin neurons (Figure 5.10). Furthermore, electron microscopy and confocal imaging with Airyscan detection revealed dystrophic morphological changes in the Golgi apparatus of R857G Auxilin neurons (Figure 5.12). It is important to note however that the lack of reliable antibodies have prevented me from assessing whether there are alterations of CREB3 and GB1 at the protein level.

The transcription factor CREB3 is activated as a response to Golgi stress and initiates an increase of ARF4 expression, enabling Golgi stress-mediated cell death (Reiling *et al.*, 2013). In contrast, increased expression of GBF1 and its downstream effector ARF1 have been described to protect against Golgi stress (Reiling *et al.*, 2013). GBF1 and ARF1 are also involved in the recruitment of clathrin adaptor proteins to the TGN (see section 1.3.3). Increased expression of GBF1 may therefore indicate a compensatory mechanism to stimulate the recruitment of clathrin adaptor proteins and the formation of CCVs from the TGN, to counteract the decreased efficiency of impaired clathrin trafficking from the Golgi apparatus. However, it should be noted that in addition to ARF1, other ARF proteins including ARF4 are also activated by GBF1. It should be noted that the gene encoding a GAP protein for ARF1 (*ARFGAP1*) was also found to have significantly increased expression levels in R857G Auxilin primary neurons,

potentially counteracting the activation of ARF1 by GBF1 (see Supplementary Table 1).

Taken together, the observed upregulation of CREB3 and GBF1, via activation of ARF4 and ARF1, respectively, may balance each other in the regulation of the Golgi stress response, balancing stress-dependent apoptosis and activation of coping mechanisms in primary R857G Auxilin neurons. Remarkably, in contrast with other ARF proteins, ARF1 and ARF4 were also found to be significantly upregulated in R857G Auxilin neurons. Whereas a modest increase of ARF1 expression was observed, ARF4 was 2-fold higher expressed in R857G Auxilin neurons (figure 5.11). This finding may indicate that the balancing act of ARF1 and ARF4 in the Golgi-stress response is favoured in the direction of apoptosis in R857G Auxilin primary neurons. Future work will have to elucidate the long-term impact of Golgi stress with ageing.

5.4 MATERIAL AND METHODS

5.4.1 Primary neuronal culture

Primary neuronal cultures were derived from the cortex of P0 pups from WT or R857G Auxilin mice. P0 mice were sprayed with 70% ethanol and decapitated. The brains were isolated, cortex was dissected and meninges were removed. Cortices were transferred to a 15 ml falcon with HBSS and washed twice with HBSS to minimize blood contamination, by letting them sink to the bottom and replacing HBSS. HBSS was removed and cortices were incubated with papain solution (BME media (Sigma) with pH 8 with 8 units/ml of papain (Worthington)). 4 cortices were incubated with 2 ml papain solution for 30 minutes at 37°C, with gentle agitation every 10 minutes. After 30 minutes, papain was neutralized by adding plating medium (Basic medium Eagle (BME, Gibco) with 1x B27 supplement (Gibco), 1x N2 supplement (Gibco), 0.45% glucose (Sigma) and 1x glutaMAX-I (Invitrogen)). Cortices were washed twice with plating medium, with centrifugation at 1000 rpm for 1 minute in between washes. Finally, cortices were triturated in plating medium using a 1000 μl pipet. Cells were spun down for 6 minutes at 1000 rpm in a total volume of 10 ml of plating media twice. Supernatant was removed and cell pellet was resuspended in 1 ml of plating media per brain supplemented with 5% FBS (fetal bovine serum, Gemini). 3 million cells were seeded per well of a 12-well plate precoated with poly-D-lysin and laminin (Corning). The following day, media was replaced to plating media without FBS, supplemented with 2.5 μM of glial inhibitor cytosine arabinoside. Media was replaced every 2-3 days.

5.4.2 RNA extraction

RNA was extracted from primary neurons cultured for 7 days *in vitro*. Cells were pelleted ($\sim$ 3 million cells) and RNA was extracted using 500 μl of TRIzol reagent, as described in Section 3.4.8.

The concentration of RNA samples was measured using a NanoDrop spectrophotometer (ThermoFisher Scientific) and were diluted with RNAse-free water to a final concentration of 500 ng/μl.

The quality of the RNA was analysed by the RNA integrity number (RIN). RNA measurements were prepared using the RNA 6000 Nano Kit Guide (Agilent) and measured using the 2100 Bioanalyzer System (Agilent). RNA 6000 nano gel was added to the nano gel matrix, loaded on an RNA nano chip and primed using the priming station. Samples as well as an RNA nano marker as a control were loaded and the nano chip was loaded on the Agilent 2100 bioanalyzer to measure RNA integrity. The bioanalyzer measures the RIN number based on the degradation of 18S and 26S ribosomal RNA.

5.4.3 cDNA library preparation

cDNA libraries were generated from 500 ng RNA using the TruSeq Stranded Total RNA Sample Prep LS (Illumina), according to manufacturers instructions.

Ribosomal RNA binding buffer and removal buffer were added to the RNA samples and ribosomal RNA was depleted from the samples using paramagnetic RiboZero Deplete RNAClean XP Beads. RNA was subsequently fragmented using Fragment High mix. First strand cDNA was synthesized using superscript II reverse transcriptase. Second strand cDNA was synthesized and RNA was

depleted. Double-stranded cDNA was purified using AMPure XP paramagnetic beads and 3' ends were poly-adenylated. Indexing adaptors for 6-fold multiplexing (AR002, AR004, AR005, AR006, AR007, AR012) were ligated at both sides of the cDNA. Fragments with ligated adaptors were enriched by PCR amplification using primers targeting the adaptors. PCR products were purified using AMPure XP paramagnetic beads. The cDNA libary was subsequently validated using digital PCR as described below. Normalized cDNA libraries were multiplexed in 10 nM Tris-HCl with 0.1% Tween20 (6 samples per pool).

5.4.4 Droplet digital PCR

The cDNA library was subjected to serial dilution, with final dilutions of 10^{-6}, 10^{-7} and 10^{-8}. Droplet digital PCR was performed by Alice Kaganovich using the reagents of the droplet digital PCR Library Quantification Kit for Illumina TruSeq (Bio-Rad). Droplets were generated with a QX200 Droplet Generator (Bio-Rad), followed by thermal cycling under the conditions outlined in Table 5.5, allowing for individual PCR reactions per droplet. PCR reads were analysed the QX200 Droplet Reader (Bio-Rad) and number of reads were quantified using the QuantaSoft Software (Bio-Rad), followed by normalization for pooling.

Cycles	Temperature (C)	Time
1x	95	10'
40	94	30"
	60	1'
1x	98	10'

Table 5.5: **Cycle sequencing conditions for droplet digital PCR**

5.4.5 Deep-sequencing

Deep-sequencing was performed by Alice Kaganovich. 7 pM of each pool was hybridized to a flow cell followed by cluster generation using the HiSeq Paired-End Cluster Kit v4 (Illumina) on the cBot cluster amplification system (Illumina), by grafting cDNA with annealed adaptors on the surface of the flow cell. The templates were copied from the adaptor hybridization primers and amplified using high fidelity DNA polymerase to create clonal clusters of ∼1000 copies each. Clusters were subsequently subjected to deep-sequencing using the HiSeq Sequencing by Synthesis Kit V4 (Illumina) reagents and the Illumina HiSeq2500 sequencer.

5.4.6 Read mapping

Sequencing counts were mapped and quantified by Dr. Jinhui Ding. The standard Illumina pipeline was used to generate fastq files, Ensembl GRCm38 annotated transcript abundance were quantified using Salmon in a non-alignment-based mode, and gene level counts were estimated using tximport package (Patro *et al.*, 2017; Soneson *et al.*, 2016).

5.4.7 Differential expression analysis

Differential expression analysis of the cDNA reads resulting from the RNAseq experiment was performed by Dr. Mark Cookson. The DESeq2 R package was used, which assumes a negative binomial distribution of read counts (Love *et al.*, 2014).

Read counts were normalized using an RLog transformation for the stabilization of variances. Differential expression of normalized counts was assessed using a Wald test, with Benjamini and Hochberg multiple testing adjustment.

5.4.8 Functional enrichment analysis

Functional enrichment analysis was performed for the 50 most significantly differentially expressed genes using g:Profiler (Reimand *et al.*, 2016) for gene Ontology terms for 'biological process'. Fischer exact test was performed for functional enrichment analysis with Benjamini and Hochberg *post hoc* correction. Redundant categories (i.e. categories with identical annotated gene sets) and categories with less than 3 annotated genes were removed from analysis. An enrichment map was generated using the 'EnrichmentMap' Cytoscape plug-in.

5.4.9 qPCR

qPCR experiments were performed as described in Section 3.4.10. An overview of the primers used for qPCR experiments in this chapter can be found in Table 5.6.

Target	Primers	Exon
CREB3	Fwd 5'-GTTCTTGGTCTCCAGCAAC-3'	9
	Rvs 5'-TCTGAAAGGTTTGCCTGCAG-3'	9
GBF1	Fwd 5'-ACGTGCACAGACTTTGAACG-3'	11/12
	Rvs 5'-TTGACCGCAAGTGGTACATG-3'	12
β-actin	Fwd 5'-ACGTGCACAGACTTTGAACG-3'	4
	Rvs 5'-TTGACCGCAAGTGGTACATG-3'	5
PPID	Fwd 5'-CTCATCTGGACGGGAAACAT-3'	4
	Rvs 5'-CCAGTCATCCCCTTCTTTCA-3'	5

Table 5.6: **qPCR primers**

5.4.10 Immunocytochemistry

Primary cortical neurons were seeded in 24-well plates containing glass coverslips coated with poly-D lysine (Corning). Cells were fixed for 20 minutes in PBS-CM buffer (PBS with 2 mM CaCl and 20 mM MgCl) containing 4% paraformaldehyde and 120 mM sucrose, followed by permeabilization for 15 minutes in PBS-CM buffer with 0.2% Triton. Cells were blocked for 30 minutes with PBS-CM buffer containing 3% FBS. Next, cells were incubated at RT for 1 hour with primary antibodies diluted in PBS-CM buffer containing 1% FBS Table 5.7). Cells were washed 3 times with PBS. Cells were subsequently incubated with Alexa Fluor secondary antibodies (ThermoFisher Scientific) diluted in PBS-CM buffer containing 1% FBS for 30 minutes, followed by 3 washes with PBS-CM buffer. All secondary antibodies were donkey host and used at 1:500 dilution. Coverslips were mounted on microscope slides using ProLong gold Antifade Mountant (ThermoFisher Scientific) and dried overnight at RT in the dark.

Target	Host	Dilution	Vendor	Catalog number
GM130	Mouse	1/250	Abcam	ab169276
GLG1	Rabbit	1/250	ThermoFisher Scientific	PA5-26838
TGN38	Sheep	1/500	Bio-Rad	ab10552

Table 5.7: **Primary antibodies used for ICC**

5.4.11 Confocal laser-scanning microscopy and Airyscan processing

Super-resolution imaging was acquired using a Zeiss 880 microscope outfitted with an Airyscan detection module. Data were collected using immersion oil optimized for 23°C (Zeiss) and a 63x objective. Fluoresence was detected by sequential laser excitation at wavelengths of 405, 488, 568 and 647 nm to minimize cross talk.

Airyscan processing was performed using the Airyscan module in the included Zen software package (Zeiss).

5.4.12 Electron microscopy

Brain slices for electron microscopy analysis were prepared by Dr. Natalie Landeck (Pallotto *et al.*, 2015). 10 month old mice were anesthetized using ketamine (one WT and one R857G Auxilin mouse). Mice were transcardially perfused with saline for 2 minutes, followed by perfusion with fixation buffer for 5 minutes (2% paraformaldehyde, 2% glutaraldehyde in 150 mM sodium-cacodylate, buffered at pH 7.4). Brains were isolated and postfixed for 8 hours in fixation buffer. Next, brains were rinsed overnight in 150 mM sodium-cacodylate buffer without fixatives. The following day, 200 μm thick coronal brain sections were sliced using a vibratome. Striatal sections around the anterior commissure level were submitted for conventional transmission EM (TEM) imaging.

TEM imaging was performed by the Electron Microscopy Core (National Heart, Lung and Blood Institute, National Institutes of Health) led by Dr. Christopher Bleck. Specimens were rinsed in cacodylate buffer, postfixed with 1% OsO4 in the same buffer on ice, en bloc stained with 1% uranyl acetate, dehydrated in an ethanol series and embedded in EMbed 812 resin (Electron Microscopy Sciences). Thin sections were cut, stained with uranyl acetate and lead citrate, and viewed with a JEM-1200EX (JEOL) transmission electron microscope (accelerating voltage 80 keV) equipped with an AMT 6 megapixel digital camera (Advanced Microscopy Techniques).

5.4.13 Statistics

Data were plotted and statistical tests were performed using Prism 8 (Graphpad) or R version 3.4.3. The statistical test results are displayed in table 5.8. n represents the number of animals samples were derived from or technical replicates and is explicitly indicated in the figure legend. Error bars represent SD.

Figure	Variable	Statistical test	Test result	P-value
5.7	Genotype	Wald test with Benjamini & Hochberg correction	NA	see Supplementary Table 1
5.9	Genes	Fisher exact test with Benjamini & Hochberg correction	NA	see Table 5.2
3.4.10 A	Genotype	Welch's t-test	t = 12.63	0.00007
3.4.10 B	Genotype	Welch's t-test	t = 9.322	0.0014
5.11 A	Genotype	Wald test with Benjamini & Hochberg correction	NA	0.002649183
5.11 B	Genotype	Wald test with Benjamini & Hochberg correction	NA	0.01845598
5.11 C	Genotype	Wald test with Benjamini & Hochberg correction	NA	0.002542252
5.11 D	Genotype	Wald test with Benjamini & Hochberg correction	NA	8.45 x 10-18
5.11 E	Genotype	Wald test with Benjamini & Hochberg correction	NA	0.1674364
5.11 F	Genotype	Wald test with Benjamini & Hochberg correction	NA	0.9946054
5.12 A	Genotype	Binomial test	NA	<0.0001
5.12 B	Genotype	Welch's t-test	t = 0.0104	0.0104
5.12 C	Genotype	Welch's t-test	t = 5.502	<0.0001

Table 5.8: **Statistical test results**

6 IMPACT OF MUTATIONS ON THE INTERACTOME OF AUXILIN

6.1 INTRODUCTION

The formation, maturation and uncoating of CCVs relies on a strict sequence of transient biomolecular interactions. Auxilin-mediated uncoating of synaptic CCVs has been well documented. It is understood that Auxilin is recruited to the newly formed CCVs derived from the plasma membrane through interaction with PI4P, which is abundant on the vesicular membrane after fission, and the clathrin coat (Ahle and Ungewickell, 1990; He *et al.*, 2017; Lee *et al.*, 2006; Scheele *et al.*, 2001). Auxilin in turn binds with the chaperone HSC70 and stimulates its ATPase activity, required for the uncoating reaction (Ahle and Ungewickell, 1990; Braell *et al.*, 1984; Ungewickell, 1985). In addition, Auxilin has been found to interact with the plasma membrane-resident adaptor protein AP2 (Scheele *et al.*, 2001). However, the exact physiological relevance of this interaction is unclear. The ubiquitous homologue of Auxilin, GAK, was also found to interact with AP2, as well as with AP1, a TGN-resident clathrin adaptor (Kametaka *et al.*, 2007).

It remains unclear whether the role of Auxilin at the plasma membrane can simply be extrapolated to the Golgi apparatus. First, it is unknown which PIP species are most abundant on TGN-derived CCVs. Given that the lipid-binding domain of Auxilin is crucial for its CCV recruitment (He *et al.*, 2017; Massol *et al.*, 2006), the according affinity of Auxilin for PIPs on Golgi-derived CCVs would thus play a great role in its recruitment. In addition, as opposed to the finding that GAK interacts with AP1, previous work has not identified any interactions of Auxilin with Golgi clathrin adaptors (Kametaka *et al.*, 2007).

Multiple pathogenic PD mutations in Auxilin have been described young onset, atypical PD (Edvardson *et al.*, 2012; Elsayed *et al.*, 2016; Köroglu *et al.*, 2013; Olgiati *et al.*, 2016). In addition to two splice-site variants (T741=, c.801-2A>G) that are predicted to result in overall decreased levels of Auxilin, two nonsense mutations (Q791X, Q846X) and a point mutation (R927G) reside within the C-terminus of Auxilin. The C-terminus of Auxilin contains the J-domain and clathrin binding domain and is thus involved with multiple protein-protein interactions that are essential for Auxilin function (Figure 6.15). However, the impact of pathogenic Auxilin mutations on the interaction with *bona fide* interactors has not been reported to date.

Results from the RNAseq data have indicated the activation of the Golgi stress response mutant Auxilin neurons (Chapter 5). I therefore hypothesized that Auxilin may indeed play a role in CCV trafficking at the Golgi apparatus. To gain further insight into the molecular machinery involved with the uncoating of CCVs and to examine whether there are any protein-protein interactions indicating a role for Auxilin at the Golgi too, the full interactome of Auxilin was mapped in an unbiased fashion by coupling affinity purification with mass spectometry (AP-MS).

The identification of *bona fide* interactors by AP-MS can be challenging because of the high false positive rates due to background contaminants, including proteins that interact non-specifically with the beads used for co-immunoprecipitation (co-IP) or epitope tags (Mellacheruvu *et al.*, 2013; Trinkle-Mulcahy *et al.*, 2008). Combination of stable isotope labelling with amino acids in cell culture (SILAC) with AP-MS is a semi-quantitative approach provides great accuracy in identifying specific interactors and distinguishing these from false positives, through differential metabolic labelling of cells expressing Auxilin and cells

expressing a negative control. In addition, the contaminant repository for affinity purification (CRAPome) is an online platform of aggregated negative controls from 411 AP-MS studies, providing a more complete and accurate AP-MS background protein set (Mellacheruvu *et al.*, 2013). Comparison of the interactome of Auxilin with the CRAPome database thus further helps to eliminate non-specific interactors.

Newly identified putative Auxilin interactors were further validated to confirm specificity and physiological relevance. Throughout the validation process, the affinities of newly identified interactors were compared for Auxilin and GAK, to gain further insight into the the physiological overlap between both uncoating co-chaperones.

To further understand the impact of pathogenic Auxilin mutations at the molecular level, the effects on the interaction with *bona fide* Auxilin interactors were analysed by co-IPs. In addition, the impact on the co-localization of Auxilin with interacting proteins and CCVs was analysed using confocal microscopy and Airyscan detection. Dr. Nate Smith also modelled the three-dimensional Auxilin structure bound to *bona fide* interactors, to further understand the impact of PD mutations on tertiary protein structure and interactions.

6.2 RESULTS

6.2.1 SILAC-based proteomics to identify interactome of Auxilin

To map the interactome of Auxilin in unbiased fashion, GFP-nanotrap co-IP was combined with mass spectometry-based SILAC proteomics (Figure 6.4.7).

GFP-Auxilin or GFP as a negative control were exogenously expressed through transient transfection in HEK293FT cells labelled with either 'heavy' (R10K8) or 'light' (R0K0) amino acid isotopes, respectively. GFP was used as the tag of choice as it shows minimal non-specific binding with mammalian proteins and because of the availability of GFP-specific nanobody-beads that show high specificity and affinity. In addition, the use of nanobodies eliminates contamination of IgG in the mass spectometry samples. GFP-nanotrap co-IP was performed and the precipitates were mixed at 1:1 ratio. After in-gel trypsin digestion, samples were subjected to liquid chromatography with tandem mass spectometry (LC-MS/MS) (Figure 6.4.7). Trypsin digestion, LC-MS/MS and subsequent protein identification via peptide sequence databases was performed by the Proteomics Core led by Dr. Yan Li (National Institute of Neurological Disorders and Stroke, National Institutes of Health).

Experiments were performed in triplicate and exclusion of proteins that were not identified across all replicates resulted in a list of 412 proteins that were considered for statistical analysis (Figure 6.2 A). However, LC-MS/MS typically identifies a large number of non-specific interactors that are co-purified with the bait (Mellacheruvu *et al.*, 2013). Further bioinformatic filtering was performed to prioritize candidate *bona fide* Auxilin interactors and eliminate background

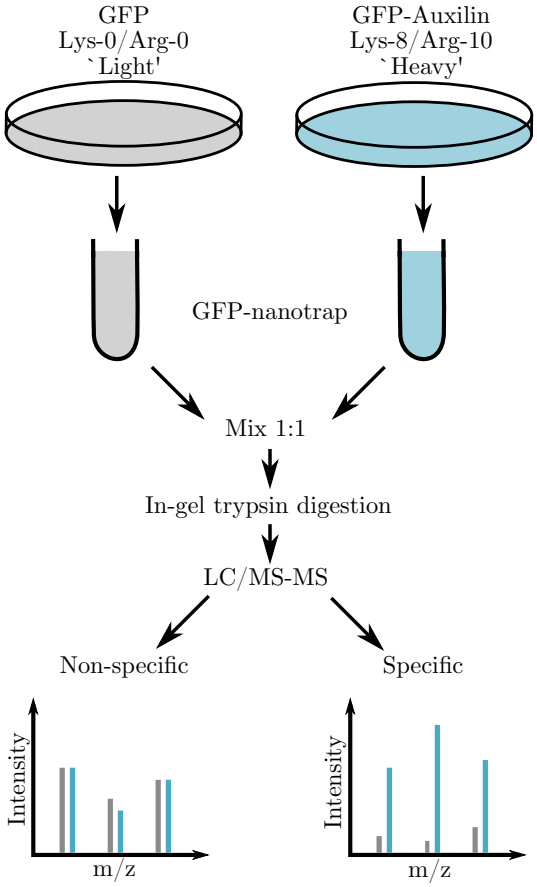

Figure 6.1: **Design of SILAC-based AP-MS approach to identify the interactome of Auxilin** HEK293FT cells were labelled with 'light' or 'heavy' amino acid epitopes and transfected with GFP or GFP-Auxilin, respectively. GFP nanotrap co-IP was performed and precipitates were mixed 1:1. In-gel trypsin digestion, LC-MS/MS and subsequent protein identification via peptide sequence databases was performed by the Proteomics Core led by Dr. Yan Li (National Institute of Neurological Disorders and Stroke, National Institutes of Health).

contaminants (Figure 6.2). A full list of unfiltered candidates can be found in Supplementary Table 2.

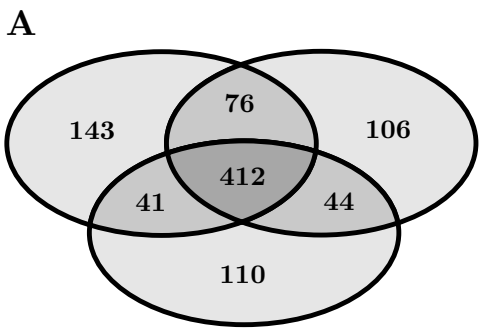

B

412 interactors
↓ Defined L/H SILAC ratio
384 interactors
↓ Protein score > 50
318 interactors
↓ CRAPome fraction < 0.5
269 interactors
↓ FDR P-value < 0.05
153 interactors
↓ L/H SILAC ratio < 0.25
31 interactors

Figure 6.2: **Bio-informatic filtering approach of Auxilin interactome** A Venn diagram indicates number of proteins identified across 3 technical replicates of the SILAC experiment. B Bioinformatic filtering approach to prioritize Auxilin interactors and eliminate background contaminants. L/H SILAC ratio indicates relative abundance ratio in light/heavy labelled SILAC sample. Protein score indicates Mascot protein score. One sample t-test was performed with Benjamini & Hochberg FDR correction for multiple testing.

First, proteins that were solely identified in the GFP negative control were eliminated. Relative abundance of proteins were reported as a light/heavy SILAC ratio. Thus, proteins present in GFP-Auxilin sample only (i.e. abundance in 'light' sample equals zero) would result in a SILAC ratio of 0. In contrast, proteins that were present in the negative control only (i.e. abundance in 'heavy' sample equals zero), were eliminated. Next, proteins were filtered to have a Mascot protein score higher than 50, which represents the -log10 of a probability measurement of random peptide matches to the queried database. In addition, the CRAPome database was used to filter out common contaminants of affinity purification-mass spectometry experiments (Mellacheruvu *et al.*, 2013). 31 proteins with a false discovery rate (FDR)-corrected p-value lower than 0.05 and at least 4-fold enrichment in the GFP-Auxilin samples were considered top candidates for Auxilin interactors (Figure 6.3, Table 6.1).

Among the identified interactors were Auxilin (*DNAJC6*) itself and previously reported interactors clathrin heavy chain (*CLTC*) and AP2 subunit α2 (*AP2A2*), indicating that the experiment had been successful in recovering authentic Auxilin

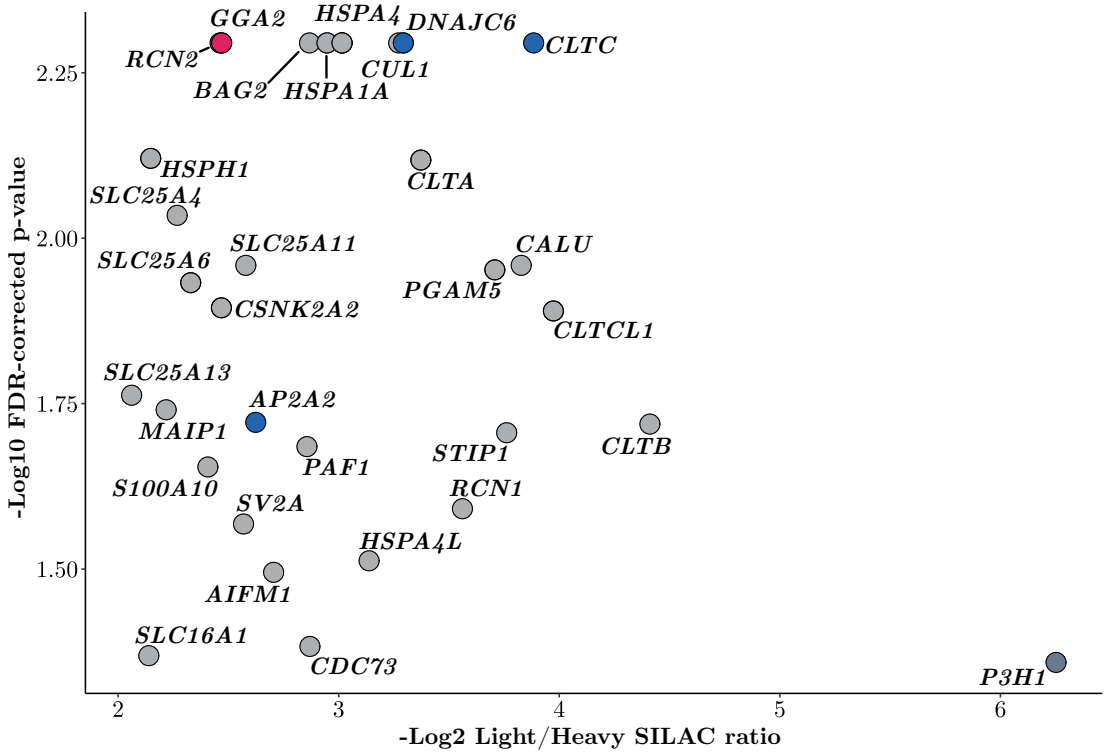

Figure 6.3: **Scatter plot of top candidates Auxilin interactors** Scatterplot indicating the genes of identified proteins. The bait protein Auxilin (*DNAJC6*) and previously identified *bona fide* interactors (*CLTC*, *AP2A2*) are indicated in blue. Novel interactor (*GGA2*) that was followed up on is indicated in pink. P-value indicates one sample t-test statistics with Benjamini & Hochberg FDR correction.

interactors (Scheele *et al.*, 2001) (indicated in blue in Figure 6.3). In addition to *CLTC*, other subunits of clathrin were identified as well (*CLTA*, *CLTB*, *CLTCL*). These are possibly indirect interactors of Auxilin that were co-purified as part of the clathrin complex. HSC70 (*HSPA8*), the chaperone of Auxilin required for its role in uncoating CCVs, showed a low FDR-corrected p-value (0.005067) and high mean enrichment (8.1567) in the GFP-Auxilin sample. Nonetheless, HSC70 was excluded through bioinformatic filtering from the final list of top candidates because of its high abundance in the CRAPome database (fraction of 0.9635) (Supplementary Table 2). However, the HSC70 nucleotide exchange factor BAG2 and HSC70 adaptor protein STIP1, required for HSC70 ADP release and coordination of HSC70 function in protein folding (King *et al.*, 2001; Xu *et al.*,

2008), respectively, were identified in the final list of top candidates, which may indicate an indirect interaction through HSC70 with Auxilin.

In addition to HSC70, Auxilin also requires ATP for the uncoating of CCVs. Multiple protein involved with ADP/ATP exchange were identified. In addition to the aforementioned BAG2, mitochondrial ADP/ATP translocases that mediate the exchange of cytoplasmic ADP for mitochondrial ATP, SLC25A4 and SLC25A6, were also detected. Whereas BAG2 has previously been reported to directly interact with HSC70 (Xu *et al.*, 2008), it is plausible that SLC25A4 and SLC25A6 could be part of a molecular machinery to ensure efficient ADP/ATP exchange of HSC70.

Finally, multiple heat shock proteins were identified (HSPA4, HAPA1A, HSPA4L). One possible explanation is that HSPs, including the *bona fide* Auxilin interactor HSC70, require common molecular machineries for their function and that multiple chaperones were co-purified via common protein interactors. Alternatively, the identified chaperones might interact with the overexpressed Auxilin to enhance correct folding and protein stability.

Gene	Protein	Function
CLTC	Clathrin heavy chain 1	Heavy chain component of the clathrin triskelion in CCVs
DNAJC6	Putative tyrosine-protein phosphatase Auxilin	Neuronal co-chaperon of HSC70 to promote CCV uncoating
CUL1	Cullin-1	Core component of E3 ubuquitin-protein ligase complexes to mediate ubiquitination of proteins in cell cycle progression, signal transduction and transcription
HSPA4	Heat shock 70 kDa protein 4	Chaperone-mediated protein complex assembly and folding, protein insertion in mitochondrial outer membrane
HSPA1A	Heat shock 70 kDa protein 1A	Proteome stress protection, folding and transport of polypeptides, proteolysis of misfolded proteins, formation and dissociation of protein complexes
BAG2	BAG family molecular chaperone regulator 2	Nucleotide-exchange factor promoting release of ADP from HSP70 and HSC70
GGA2	Golgi-localized, γ-ear containing, Arf-binding protein 2	Clathrin adaptor protein that plays a role in protein sorting and trafficking between the TGN and ensosomes
RCN2	Reticulocalbin-2	Calcium ion binding
HSPH1	Heat shock protein 105 kDa	Nucleotide exchange factor for chaperone proteins HSPA1A and HAPA1B promoting release of ADP
CLTA	Clathrin light chain A	Light chain component of the clathrin triskelion in CCVs
SLC25A4	ADP/ATP translocase 1	Catalyzation of exchange of cytoplasmic ADP with mitochondrial ATP across inner mitochondrial membrane
CALU	Calumenin	Regulation of vitamin K-dependent carboxylation of N-terminal glutamate residues
SLC25A11	Mitochondrial 2-oxoglutarate/ malate carrier protein	Catalyzation of transport of 2-oxoglutarate across the inner mitochondrial membrane, role in metabolic processes, maintenance of mitochondrial fusion, fission and morphology
PGAM5	Mitochondrial serine/threonine protein phosphatase PGAM5	Serine/threonine-protein phosphatase of MAP3K5
SLC25A6	ADP/ATP translocase 3	Catalyzation of exchange of cytoplasmic ADP with mitochondrial ATP across inner mitochondrial membrane
CSNK2A2	Casein kinase II subunit alpha'	Serine/threonin-protein kinase with large number of substrates, involved with cellular processes including cell cycle progresion, apoptosis and transcription
CLTCL1	Clathrin heavy chain 2	Clathrin heavy chain involved with membrane organization
SLC25A13	Calcium-binding mitochondrial carrier protein Aralar2	Mitochondrial carrier that catalyzes the calcium-dependent exchange of cytoplasmic glutamate with mitochondrial aspartate across the mitochondrial inner membrane
MAIP1	Mitochondrial m-AAA protease-interacting protein 1	sorting of SMDT1/EMRE in mitochondria by ensuring its maturation
AP2A2	AP-2 complex subunit alpha-2	Plasma membrane-resident clathrin adaptor protein 2 subunit α 2
CLTB	Clathrin light chain B	Light chain component of the clathrin triskelion in CCVs
STIP1	Stress-induced phosphoprotein 1	Co-chaperone of HSP90AA1 that mediates association with HSC70 and HSP90
PAF1	RNA polymerase II-associated factor 1 homolog	Component of the PAF1 complex (PAF1C) which has multiple functions during transcription by RNA polymerase II.
S100A10	Protein S100-A10	Induction of dimerization of ANXA2/p36
RCN1	Reticulocalbin-1	Regulation of calcium-dependent activities in the endoplasmic reticulum lumen or post-ER compartment
SV2A	Synaptic vesicle glycoprotein 2A	Regulation of secretion in neural and endocrine cells, enhancing selectively low-frequency neurotransmission
HSPA4L	Heat shock 70 kDa protein 4L	Chaperone activity, inhibition of aggregation of citrate synthase
AIFM1	Mitochondrial apoptosis-inducing factor 1	NADH oxidoreductase and regulator of apoptosis
CDC73	Parafibromin	Component of PAF1 complex, involved with transcription initiation, elongation and 3'-end formation
SLC16A1	Monocarboxylate transporter 1	Proton-coupled monocarboxylate transporter catalyzing rapid transport across the plasma membrane
P3H1	Prolyl 3-hydroxylase 1	Basement membrane-associated chondroitin sulfate proteoglycan with prolyl 3-hydroxylase activity

Table 6.1: **Top candidates for *bona fide* Auxilin interactors**
Interactors are ranked by the FDR-corrected p-value. The UniProt database was queried for protein functions (The UniProt Consortium, 2019).

6.2.2 Gene ontology analysis of top candidates Auxilin interactors

The 31 top candidates were subjected to gene ontology (GO) analysis for biological process and cellular component terms (The Gene Ontology Consortium, 2019; The Gene Ontology Consortium *et al.*, 2000). Fisher exact test was performed for enrichment analysis with Bonferroni correction for multiple testing. Redundant categories were removed based on hierarchal clustering (subclusters were removed from analysis) (Table 6.2).

Unsurprisingly, clathrin coat assembly, clathrin-dependent endocytosis and membrane organization were the most significantly upregulated GO:Biological process terms (Figure 6.4 A, Table 6.2). Processes involving LDLR, a receptor subject to clathrin-mediated endocytosis, were also found to be enriched. In addition, there was a significant enrichment of the GO term protein folding, largely driven by the presence of heat shock proteins (Table 6.2).

Analysis of the GO cellular component term revealed a significant enrichment of genes localised at the clathrin complex, pre- and postsynaptic zone, endocytic CCVs as well as the TGN and the clathrin coat from TGN-derived vesicles. These findings underscore an important role for Auxilin both at the plasma membrane and the TGN and indicate that Auxilin may interact with Golgi-resident proteins.

Biological process

GO identifier	Description	p-value	Genes
GO:0072583	clathrin-dependent endocytosis	1.18 x 10^{-5}	*AP2A2*,*CLTA*,*DNAJC6*,*CLTB*,*CLTC*
GO:0048268	clathrin coat assembly	3.35 x 10^{-4}	*CLTA*, *CLTB*, *CLTCL1*, *CLTC*
GO:0061024	membrane organization	3.09 x 10^{-3}	*AP2A2*, *S100A10*, *CLTA*, *DNAJC6*, *HSPA1A*, *CLTB*, *MAIP1*, *HSPA4*, *CLTCL1*, *CLTC*
GO:0032802	low-density lipoprotein particle receptor catabolic process	7.93 x 10^{-3}	*AP2*, *CLTA*, *CLTC*
GO:0006457	protein folding	1.05 x 10^{-2}	*HSPH1*, *BAG2*, *HSPA1A1*, *HSPA4L*, *P3H1*, *CSNK2A2*
GO:0006886	intracellular protein transport	1.13 x 10^{-2}	*AP2A2*, *CLTA*, *PAF1*, *CLTB*, *SLC25A6*, *MAIP1*, *HSPA4*, *CLTCL1*, *GGA2*, *CLTC*

Cellular component

GO identifier	Description	p-value	Genes
GO:0030130	clathrin coat of trans-Golgi network vesicle	9.59 x 10^{-8}	*CLTA*, *CLTB*, *CLTC*, *CLTCL1*, *AP2A2*
GO:0030132	clathrin coat of coated pit	6.60 x 10^{-7}	*CLTA*, *CLTB*, *CLTC*, *CLTCL1*, *AP2A2*
GO:0045334	clathrin-coated endocytic vesicle	8.78 x 10^{-5}	*CLTA*, *CLTB*, *CLTC*, *CLTCL1*, *AP2A2*
GO:0098835	presynaptic endocytic zone membrane	7.45 x 10^{-4}	*CLTA*, *CLTB*, *CLTC*
GO:0016593	Cdc73/Paf1 complex	7.45 x 10^{-4}	*PAF1*, *CDC73*
GO:0071439	clathrin complex	9.93 x 10^{-4}	*CLTA*, *CLTCL1*, *CLTC*
GO:0036020	endolysosome membrane	3.05 x 10^{-3}	*CLTA*, *CLTC*, *AP2A2*
GO:0005802	trans-Golgi network	4.39 x 10^{-2}	*CLTA*, *CLTB*, *CLTCL1*, *GGA2*, *CLTC*
GO:0099631	postsynaptic endocytic zone cytoplasmic component	1.91 x 10^{-2}	*CLTA*, *CLTB*

Table 6.2: **GO analysis of *bona fide* Auxilin interactors**
Fischer exact test with Bonferroni correction for multiple testing was performed for the enrichment analysis of GO terms for biological process and cellular component (The Gene Ontology Consortium, 2019; The Gene Ontology Consortium *et al.*, 2000)

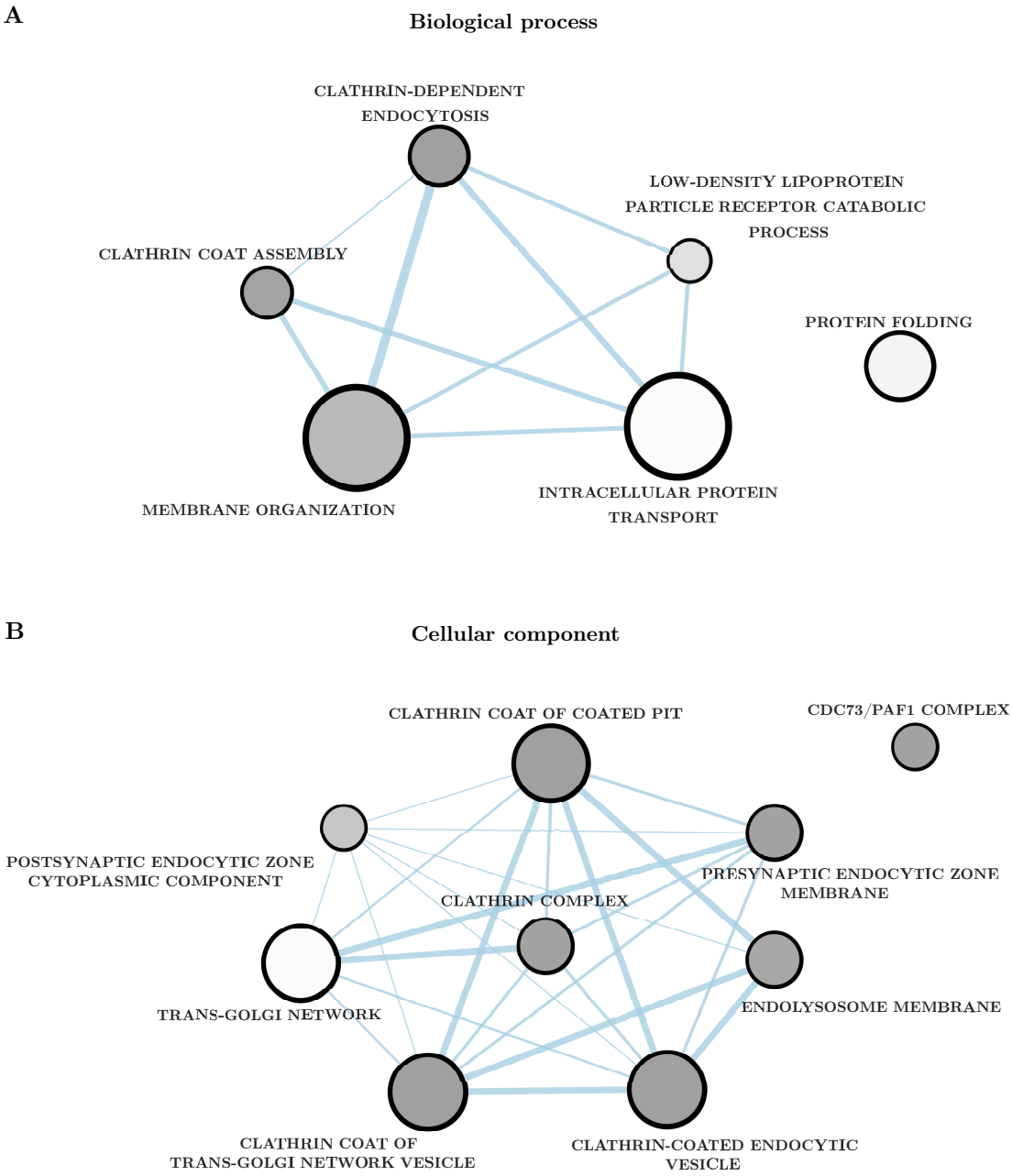

Figure 6.4: **GO enrichment analysis of the interactome of Auxilin** GO enrichment analysis of the top candidates of Auxilin interactors for biological process (A) an cellular component (B). Node size corresponds to number of genes within each geneset and edge size to number of overlapping genes between connected nodes (larger is more genes). Node colour corresponds to the p-value of the Fisher exact test with Bonferroni correction for multiple testing (darker is lower p-value).

6.2.3 Interaction of Auxilin and GAK with clathrin adaptor proteins

Analysis of the GO terms TGN and clathrin coat of TGN vesicle revealed that the Golgi resident clathrin-adaptor protein GGA2 was nominated as an Auxilin interactor top candidate. Interestingly, the Golgi-resident clathrin adaptors (AP1 and GGA1-3) have previously been hypothesized to interact with Auxilin as well as its ubiquitously expressed homologue GAK. Whereas GAK was found to interact with AP1, no Golgi adaptor proteins were found to interact with Auxilin in a prior study (Kametaka *et al.*, 2007).

To validate the interaction of Auxilin with GGA2 and to compare the interaction of Auxilin and GAK with multiple clathrin adaptor proteins, co-IPs were performed from HEK293FT cells transiently expressing GFP-Auxilin or GFP-GAK and WBs were probed for all endogenous adaptor proteins with a reported role in clathrin trafficking (AP1-3 and GGA1-3) (Figure 6.5).

As was previously reported, both Auxilin and GAK were found to interact with the α-subunit of the plasma membrane-resident AP2, whereas only GAK was found to interact with the γ-subunit of AP1 (Greener *et al.*, 2000; Kametaka *et al.*, 2007; Scheele *et al.*, 2001) (Figure 6.5 A, B, C). No interaction was observed of between Auxilin or GAK with the δ-subunit of AP3 (Figure 6.5 A). In addition, co-IP confirmed the interaction of Auxilin with GGA2 and also observed a faint interaction with GGA3, but not GGA1 (Figure 6.5 D, E, F). No interaction between GAK and the GGA proteins was observed (Figure 6.5 D). These data indicate that Auxilin and GAK both interact with the plasma membrane-resident AP2, but display differential binding with Golgi-resident clathrin adaptor proteins.

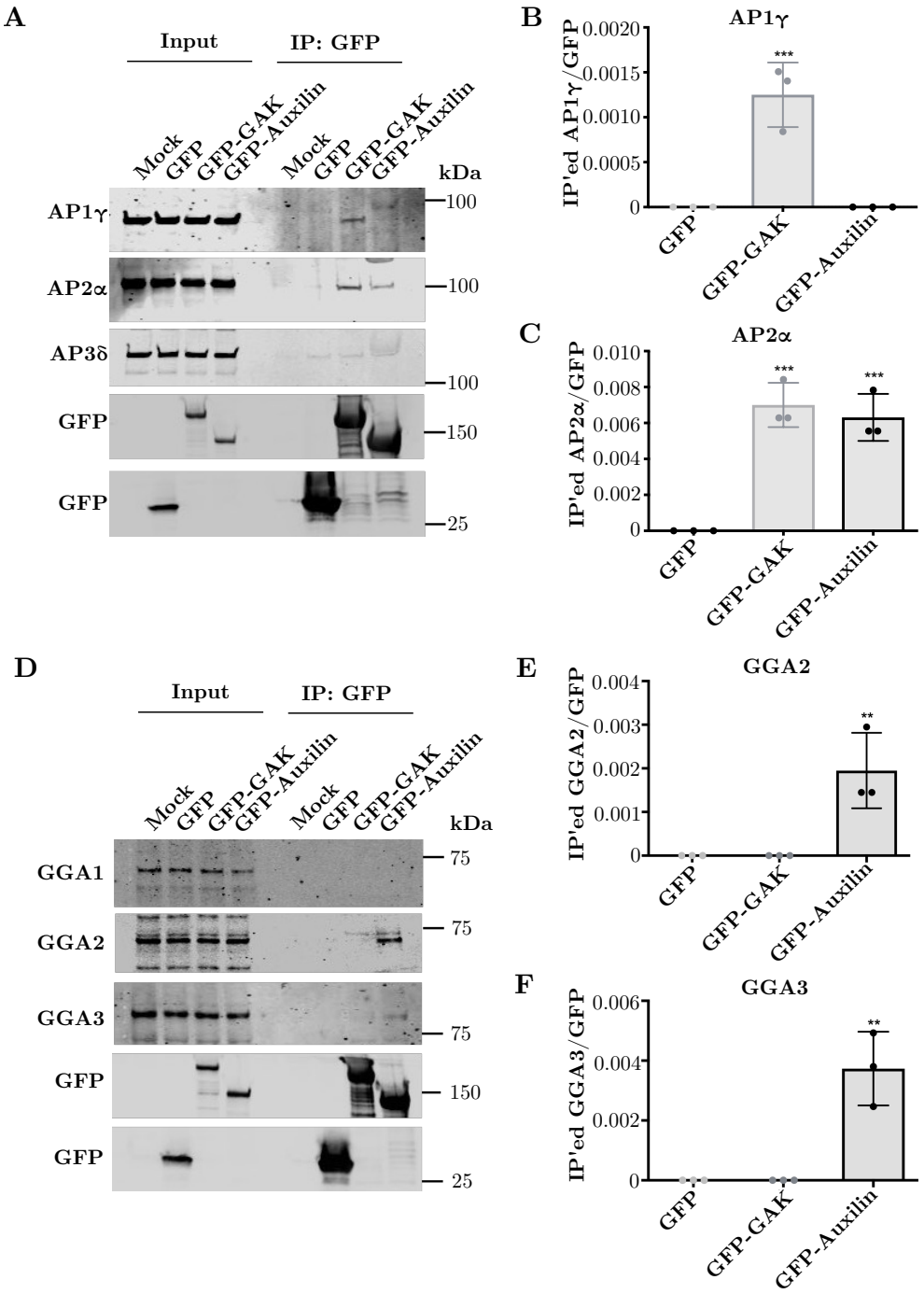

Figure 6.5: **Differential interaction of GAK and Auxilin with clathrin adaptor proteins** A and D GFP, GFP-GAK or GFP-Auxilin were transiently expressed in HEK293FT cells and WB analysis was performed of GFP-nanotrap experiments for interaction with AP and GGA proteins. Images are representative of n = 3 technical replicates. B, C, E, F Quantification AP1, AP2, GGA2, GGA3 interaction with GAK/Auxilin compared to GFP negative control and normalized to bait. One-way ANOVA was performed of n = 3 technical replicates, error bars are standard deviation, p-values represent result from Tukeys multiple comparisons test with *** $p < 0.001$, ** $p < 0.01$.

6.2.4 Defining the Auxilin interaction motif for GGA2

The GGA proteins and the AP1 complex contain γ-ear domains that are structurally similar to each other and bind to multiple accessory proteins (see section 1.3.2). A consensus motif within those accessory proteins that is responsible for interaction with the γ-ear domains has been defined as ψG(P/D/E)(ψ/L/M), with ψ being an aromatic amino acid (Mattera *et al.*, 2004). Indeed, GAK was found to interact with AP1 through two sequences fitting this motif, FGPL and FGEF (Figure 6.6 A) (Kametaka *et al.*, 2007). Blast analysis of GAK and Auxilin showed that this motif was not conserved in Auxilin (Figure 6.6 A) (Altschul *et al.*, 1990). However, since Auxilin but not GAK interacts with GGA proteins, I hypothesized that there might be slight differences in the sequence of the consensus motif or the location of the consensus motif within the protein sequence.

A

GAK	956	AAADP**FGPL**LPSSGNNSQPCSNPDL**FGEF**LNSD	
Auxilin	639	ATFDPFGAPSKPSGQ - - - - - - - -DLLGSFLNTSS	

B

GAK	625	DGKAVIPLGVTVQGDVLIVIYHARSTLGGRLQAKMASMKMFQIQFHTGFVPRNATT
Auxilin	338	DGKI**FIPL**NITVQGDVVVSMYHLRSTIGSRLQAKVTNTQIFQLQFHTG**FIPL**DTTV

C

AAAA	**Auxilin**	338	DGKI**A**I**P**A**P**ANITVQGDVVVSMYHLRSTIGSRLQAKVTNTQIFQLQFHTG**A**I**P**L**A**DTTV

D

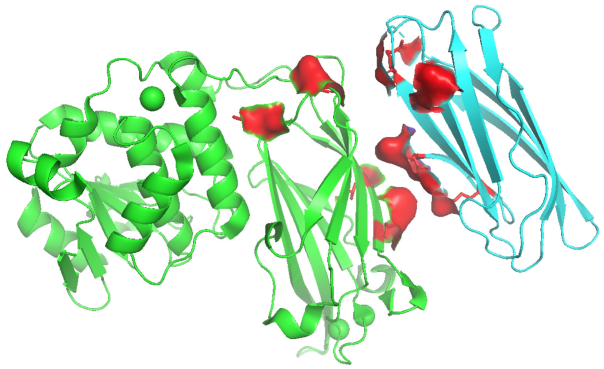

Figure 6.6: **Binding motifs in GAK and Auxilin for interaction with γ-ear domain-containing proteins** A Binding motifs in GAK for AP1 binding are indicated in bold and are not conserved in Auxilin (Altschul *et al.*, 1990; Kametaka *et al.*, 2007). B Putative binding motifs in Auxilin for GGA2 are indicated in bold and are not conserved in GAK (Altschul *et al.*, 1990). C Mutation of putative GGA2 binding motifs in Auxilin, with mutated residues indicated in red. D Modelling of bovine Auxilin (green) with GGA2 (cyan). Putative interacting motifs are indicated in red (F and L from FIPL motifs in Auxilin, AR, K, RR from conserved surface motifs in GGA2 (Nogi *et al.*, 2002). Protein structures were modelled by Dr. Nate Smith.

Analysis of the Auxilin amino acid sequence revealed the presence of two FIPL motifs, similar to the ψG(P/D/E)(ψ/L/M) consensus motif, with the conservative substitution of the glycine residue with isoleucine (Figure 6.6 B). Those motifs are not conserved in GAK, where the aromatic amino acid phenylalanine is replaced with the aliphatic amino acid valine (Figure 6.6 B) (Altschul *et al.*, 1990). Structural modelling of Auxilin and GGA2 showed that the FIPL motifs are present on the surface of the tertiary protein structure (Figure 6.6 D). In addition, the FIPL motifs can be modelled to fit in close proximity with conserved basic residues at the surface of GGA2, previously shown to be required for the recruitment of accessory proteins (Figure 6.6 D) (Nogi *et al.*, 2002). To address whether

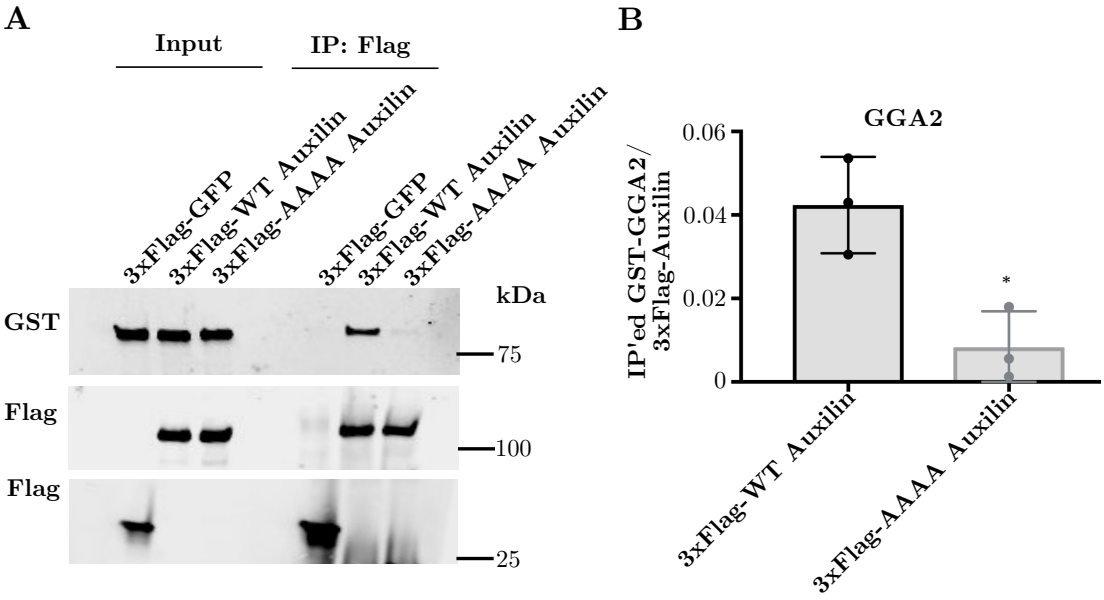

Figure 6.7: **Auxilin interacts with GGA2 is mediated by FIPL motifs** A Recombinant 3xFlag-GFP, 3xFlag-WT Auxilin or 3xFlag-AAAA Auxilin were incubated with recombinant GST-GGA2. 3xFlag co-IP was performed followed by WB analysis to assess interaction with GST-GGA2. Image is representative of n = 3 technical replicates. B Quantification of GGA2 co-purified with 3xFlag-AAAA Auxilin compared with 3xFlag-WT Auxilin normalized to bait. Unpaired t-test was performed of n = 3 technical replicates, error bars are standard deviation, * indicates p-value < 0.05.

the FIPL motifs in Auxilin could be responsible for its interaction with GGA2, both FIPL motifs were mutated to AIPA (referred to as AAAA Auxilin) (Figure 6.6 C). Recombinant GST-GGA2 was incubated with recombinant 3xFlag-GFP

as a negative control, 3x-Flag WT Auxilin or 3xFlag-AAAA Auxilin (Figure 6.7). Co-IP of 3xFlag revealed a direct interaction of GGA2 with Auxilin. This interaction was strongly diminished by mutating the FIPL motifs to AIPL, thus indicating that the FIPL motifs mediate GGA2-Auxilin interaction.

6.2.5 Localization of GGA2-binding deficient Auxilin with the TGN

To address whether Auxilin interaction with the TGN-resident clathrin adaptor GGA2 is required for its recruitment to the TGN, the localization of Auxilin was analysed using confocal microscopy with Airyscan. GFP-WT Auxilin and GFP-AAAA Auxilin (i.e. GGA2 binding deficient Auxilin) were transiently expressed in primary murine neurons and co-stained for the endogenous TGN marker TGN38 (Figure 6.8). Co-localization of both WT and AAAA Auxilin with TGN38 was observed, indicating that interaction with GGA2 is not required for recruitment of Auxilin to the TGN.

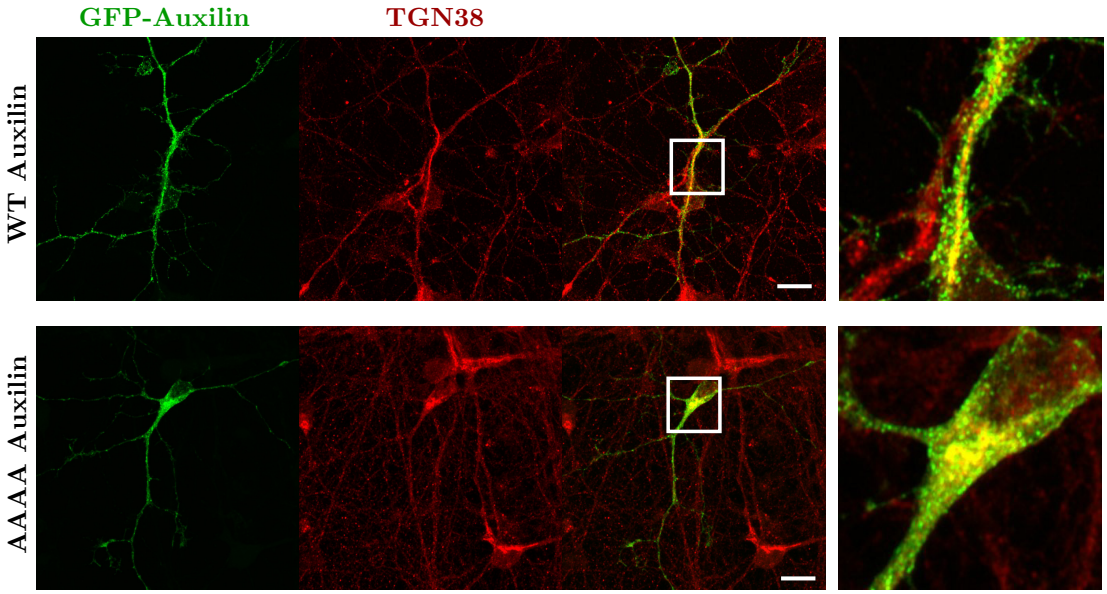

Figure 6.8: **Localization of GGA2-binding deficient Auxilin with the TGN in neurons** Representative images are shown of primary murine neurons transiently transfected with GFP-WT Auxilin (upper panel) or GFP-AAAA (lower panel) Auxilin (green) and co-stained for the endogenous TGN marker TGN38 (red). Scale bar indicates 10 μ m.

6.2.6 Impact of Auxilin mutations on clathrin interaction

Auxilin interacts with the CHC through multiple interaction motifs within its clathrin binding domain (Scheele *et al.*, 2001; Scheele *et al.*, 2003). To address

the effect of pathogenic Auxilin mutations on the interaction with clathrin, GFP-Auxilin was transiently expressed in HEK293FT cells followed by WB analysis of endogenous CHC. Experiments were focused on the Q791X, Q846X and R927G mutations, since the splice-site mutations c.801-2>G and T741 can not be analysed using plasmid constructs of the open reading frame of Auxilin.

Co-IP of GFP-Auxilin revealed a lower strength of interaction of Q791X, Q846X and R927G Auxilin with CHC compared to WT Auxilin (Figure 6.9). The finding that Q791X and Q846X mutations impair clathrin interaction is not surprising given that both nonsense mutations result in a partial truncation of the clathrin binding domain. However, the R927G Auxilin mutation lies outside of the clathrin binding domain and how this mutation results in decreased CHC binding is less clear.

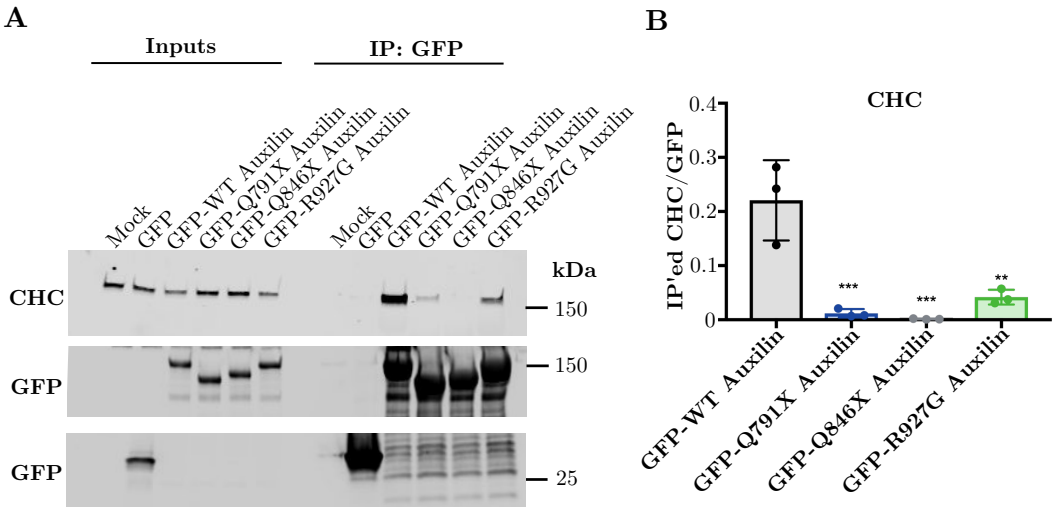

Figure 6.9: **Impact of PD mutations on Auxilin interaction with clathrin** A GFP or WT, Q791X, Q846X, or R927G GFP-Auxilin were transiently expressed in HEK293FT cells and WB analysis was performed of GFP-nanotrap experiments for interaction with endogenous CHC. Images are representative of n = 3 technical replicates. B Quantification CHC interaction with mutant GFP-Auxilin compared to WT GFP-Auxilin and normalized to the bait. One-way ANOVA was performed of n = 3 technical replicates, error bars are standard deviation, p-values represent result from Tukeys multiple comparisons test with *** $p < 0.001$, ** $p < 0.01$.

To analyse the impact of R927G Auxilin mutation on CHC binding, the J-domain of Auxilin, containing the R927G mutation, bound to the assembled clathrin coat was modelled (Figure 6.10).

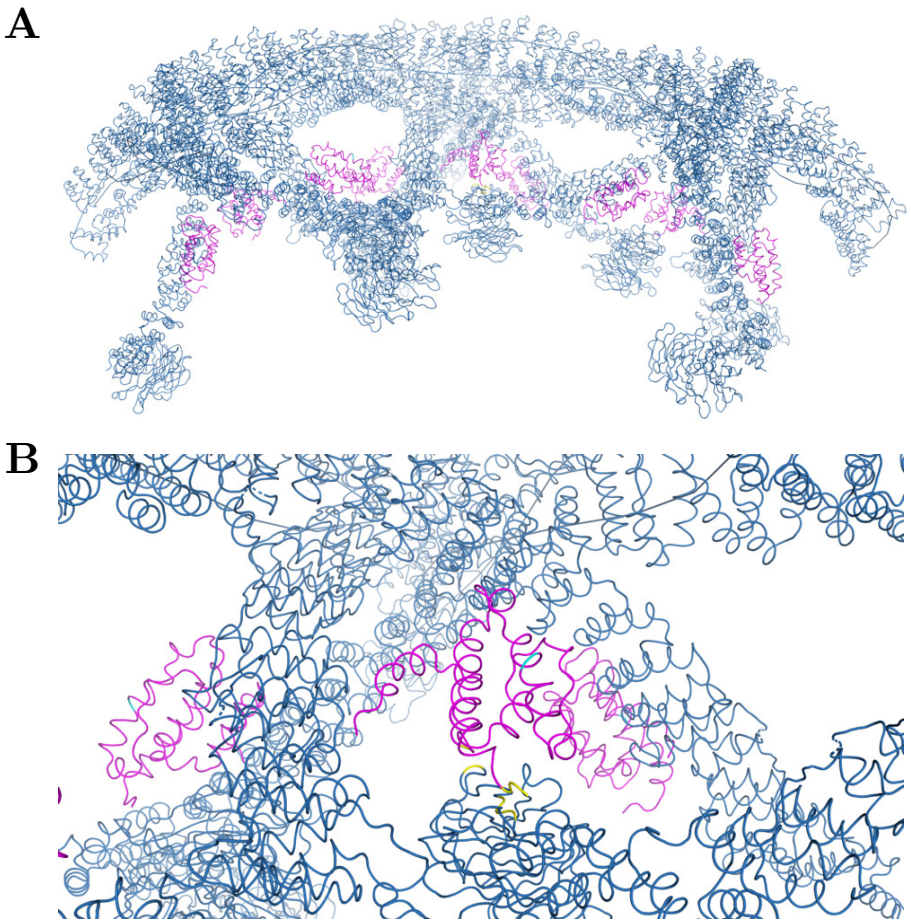

Figure 6.10: **Structural modelling analysis of the impact of R927G mutation on interaction of Auxilin with the clathrin coat** J domain of bovine Auxilin (purple) bound to the assembled clathrin coat (dark blue) (PDB file derived from (Fotin *et al.*, 2004b)). Auxilin residues residing at the interface with the clathrin coat (G825, P908, L909 and Y910, equivalent to human G885, P968, L969 and Y970) are indicated in red. R residue mutated in PD (bovine R867, equivalent of R927G) is indicated in cyan.

The J-domain is composed of highly conserved α-helical structures and R927G resides within one of those α-helices (Figure 6.10) (Gruschus *et al.*, 2004; Jiang *et al.*, 2003). Given that α-helix formation relies on the formation of hydrogen bonds between negatively charged and positively charged amino acids, it is thus conceivable that the substitution of the positively charged R residue to an

uncharged G residue would disrupt the tightly packed α-helical structure of the J-domain.

Further analysis of the J-domain bound to clathrin showed that multiple residues reside at the interface with the N-terminal domain of the CHC and could therefore be important for interaction with clathrin (Figure 6.10). Even though the Auxilin clathrin binding domain appears to be the main determinant for clathrin interaction (Scheele *et al.*, 2001; Scheele *et al.*, 2003), additional low affinity interactions with the Auxilin J-domain may contribute to the binding of Auxilin with clathrin. Disruption of the α-helical structure of the J-domain could therefore explain the observed decreased interaction of R927G Auxilin with clathrin.

6.2.7 Co-localization of mutant Auxilin with CCVs

Since all tested pathogenic Auxilin mutations were shown to impair interaction with clathrin, I hypothesized this could impair the co-localization of Auxilin with CCVs. To adress the impact of mutation on Auxilin localization, murine primary neurons were transiently transfected with WT and mutant GFP-Auxilin and co-stained for endogenous clathrin heavy chain (Figure 6.11). WT Auxilin as well as all Auxilin mutants were found to co-localize with CCVs in neurons. This indicates that impaired interaction of mutant Auxilin with clathrin does not abolish its recruitment to CCVs.

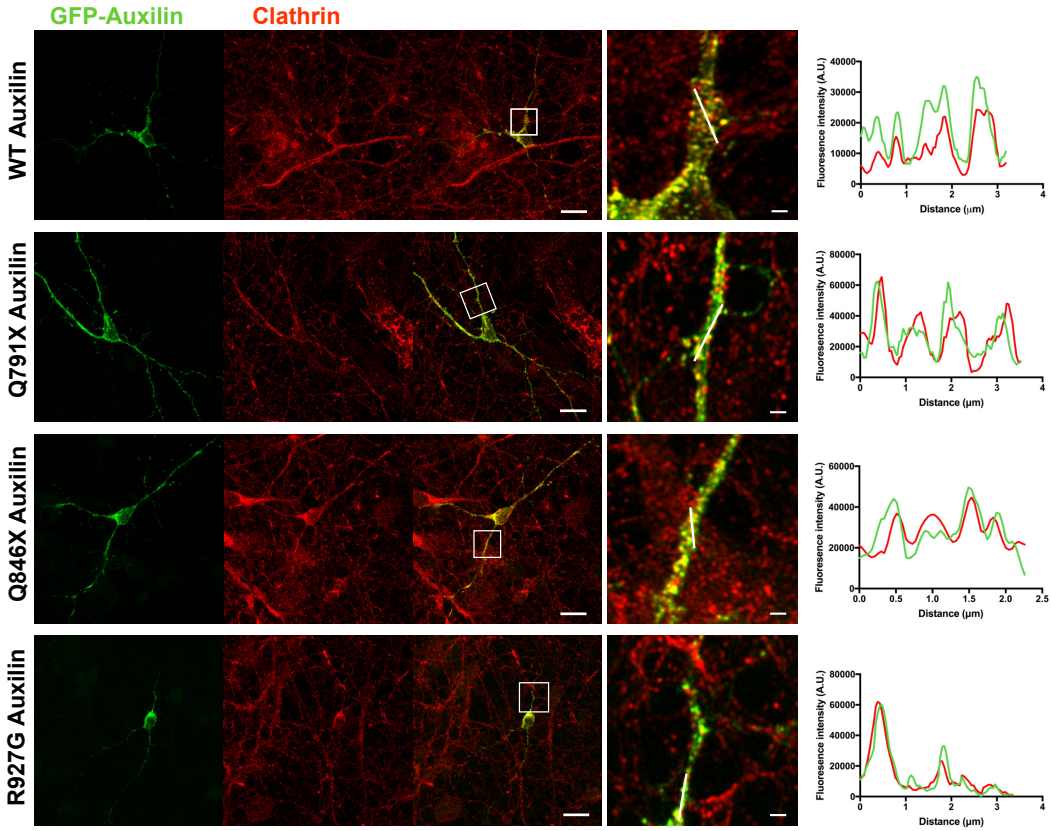

Figure 6.11: **Co-localization of Auxilin with clathrin** WT, Q791X, Q846X or R927G GFP-Auxilin (green) were transiently expressed in murine primary neurons and co-stained for endogenous clathrin heavy chain (red). Scale bar = 20 μm. The right panel shows the fluorescence intensity profiles in function of the distance indicated in the magnified merged image. Scale bar = 2 μm.

6.2.8 Interaction of mutant Auxilin with clathrin adaptor proteins

Auxilin has been found to interact with clathrin adaptor proteins AP2 and GGA2 (Figure 6.5) (Scheele *et al.*, 2001). In addition, a weak interaction with GGA3 was observed (Figure 6.5). WB analysis of co-IP WT and mutant GFP-Auxilin did not reveal an alteration in the interaction with any of the clathrin adaptor proteins (Figure 6.12).

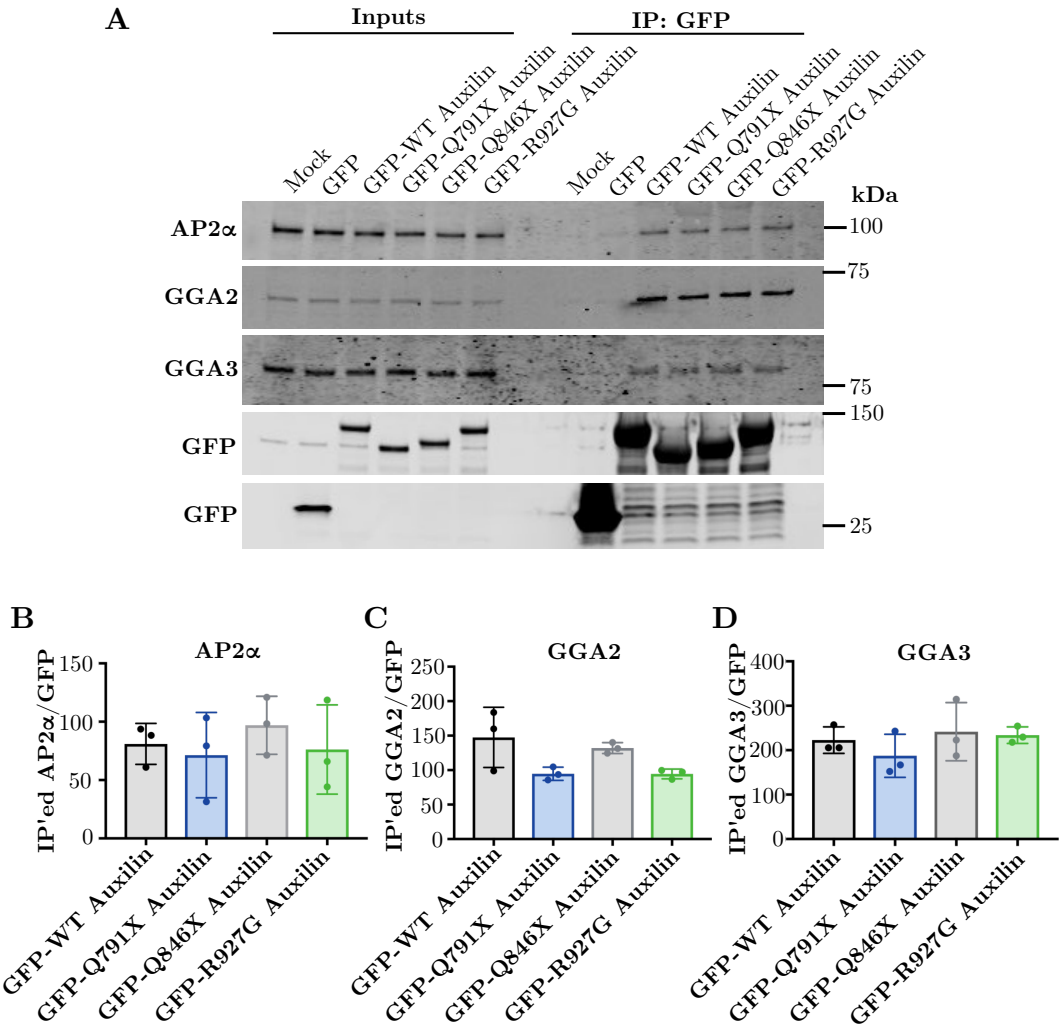

Figure 6.12: **Impact of PD mutations on Auxilin interaction with clathrin adaptor proteins** A GFP or WT, Q791X, Q846X, or R927G GFP-Auxilin were transiently expressed in HEK293FT cells and WB analysis was performed of GFP-nanotrap experiments for interaction with endogenous AP2α, GGA2 or GGA3. Image is representative of n = 3 technical replciates. B, C, D Quantification AP2α, GGA2 or GGA3 interaction with mutant GFP-Auxilin compared to WT GFP-Auxilin and normalized to bait. One-way ANOVA was performed of n = 3 technical replicates, error bars are standard deviation, no significant alterations were observed.

6.2.9 Interaction of mutant Auxilin with HSC70

The J-domain of Auxilin is crucial for the interaction with HSC70 to enable uncoating of CCVs (Figure 6.13) (Jiang *et al.*, 2003, 2007).

The R927G PD point mutation is predicted to disrupt the conserved α-helical structure of the J domain (Figure 6.10) and the PD nonsense mutations Q791X

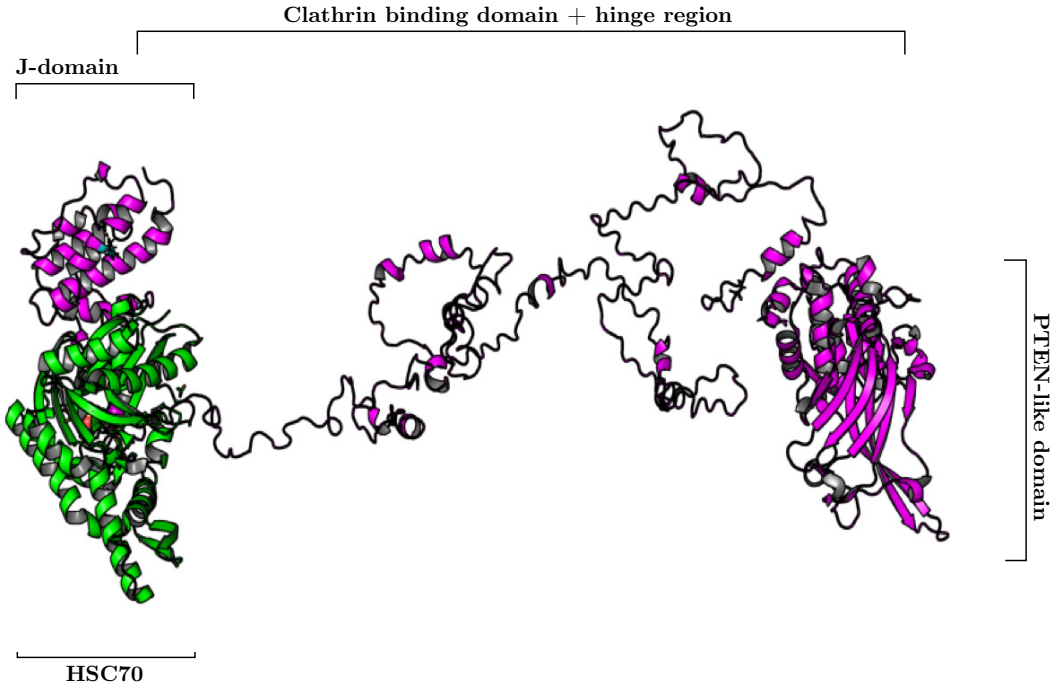

Figure 6.13: **Model of full-length Auxilin interaction with HSC70** Model of full-length human Auxilin (purple) interaction with HSC70 (Green).

and Q846X result in a truncations of Auxilin that completely lack the J-domain. It was therefore hypothesized that those pathogenic Auxilin mutations would disrupt the interaction with HSC70. Surprisingly however, co-IP did not reveal such impairments in HSC70 interaction (Figure 6.14).

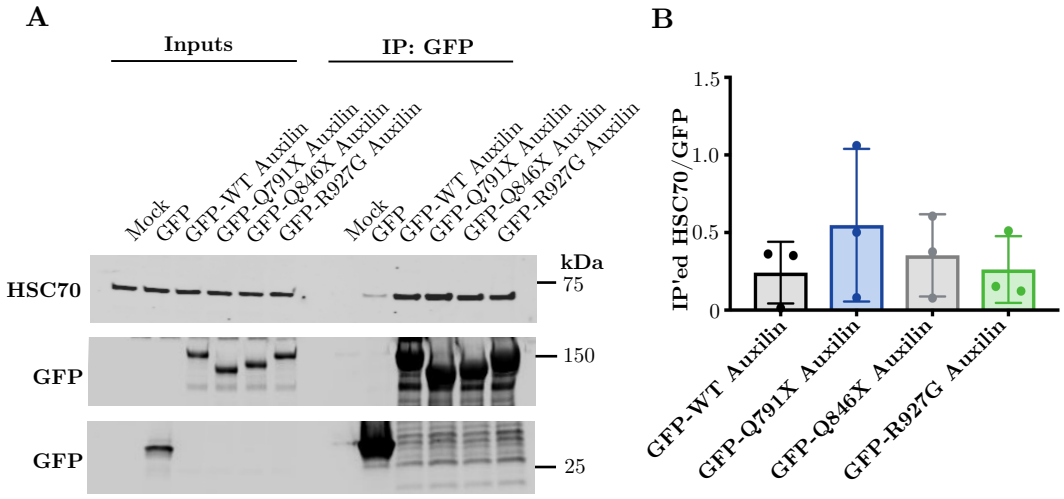

Figure 6.14: **Impact of PD mutations on Auxilin interaction with HSC70** A GFP or WT, Q791X, Q846X, or R927G GFP-Auxilin were transiently expressed in HEK293FT cells and WB analysis was performed of GFP-nanotrap experiments for interaction with endogenous HSC70. Image is representative of n = 3 technical replciates. B Quantification HSC70 interaction with mutant GFP-Auxilin compared to WT GFP-Auxilin and normalized to bait. One-way ANOVA was performed of n = 3 technical replicates, error bars are standard deviation, no significant alterations were observed.

In addition to its role in the assembly and disassembly of macromolecular complexes such as the clathrin coat (see Section 1.4.1), HSC70 also assists in the correct folding of disordered or non-native proteins (Mayer and Bukau, 2005). Pathogenic mutations are likely to have a disruptive impact on the protein structure of Auxilin. Mutant Auxilin may therefore interact with HSC70 as a substrate client protein rather than a co-chaperone.

6.3 DISCUSSION

6.3.1 Mapping the interactome of Auxilin reveals GGA2 as a novel interactor

GFP-nanotrap co-IP was coupled with SILAC-based LC-MS/MS to map the interactome of Auxilin in an unbiased fashion. Co-IPs were performed in mild experimental conditions with low concentrations of detergent to capture weak but potentially physiological relevant Auxilin interactors, at the risk of increasing the number of false positive interactors. A total of 412 proteins were identified across 3 replicates and bioinformatic filtering was applied to remove background contaminants, resulting in a total of 31 top candidates for Auxilin interactors (Table 6.1, Figure 6.3).

One consideration when evaluating these lists is that stringent filtering may result in false negatives, i.e. true interactions that are discarded. The stringent bioinformatic filtering approach has resulted in the exclusion of at least one authentic Auxilin interactor, namely HSC70. It can not be ruled out that more physiological relevant Auxilin interactors were excluded from analysis. In addition, Auxilin was exogenously expressed in HEK293FT cells that do not normally express Auxilin, since its endogenous expression is restricted to neurons. It is therefore possible that neuronal interactors of Auxilin were not identified because of their absence in HEK293FT cells. For example, Auxilin has been reported to interact with the neuronal isoform of dynamin (dynamin 1) (Newmyer *et al.*, 2003). This interaction was not recovered in the SILAC experiment as dynamin 1 is not expressed in HEK293FT. Interaction with the ubiquitously expressed isoform dynamin 2 was also not observed, indicating that the Auxilin interaction motif of dynamin 1 is not conserved across isoforms.

The role of Auxilin has been well-documented for the uncoating of CCVs at the plasma membrane. Even though depletion of Auxilin has previously been suggested to impair TGN-mediated clathrin transport (Zhou *et al.*, 2011), a direct role for Auxilin at the TGN has not been demonstrated to date. GO analysis of the Auxilin interactors revealed an enrichment of proteins at endocytic and TGN-derived CCVs. Indeed, Auxilin was found to interact with both the previously reported clathrin adaptor protein AP2 as well as the newly identified Golgi-resident GGA2 (Figure 6.5) (Scheele *et al.*, 2001). Further validation confirmed that GGA2 directly interacts with Auxilin and is thus a novel *bona fide* interactor of Auxilin (Figure 6.7). These findings highlight a direct role for Auxilin in the uncoating of TGN-derived CCVs.

The finding that PIP binding through the PTEN-domain and clathrin binding via the clathrin-binding domain are the main determinants for Auxilin recruitment to CCVs (He *et al.*, 2017; Massol *et al.*, 2006), raises the question how interactions with clathrin adaptor proteins contribute to the function of Auxilin. In addition, the GGA2 binding sites and lipid binding sites of Auxilin are in close proximity of each other and AP2 shares some of its binding sites with clathrin (Figure 6.15) (Scheele *et al.*, 2003), indicating that interaction of Auxilin with clathrin adaptors could compete with PIP and clathrin interaction. A plausible explanation could be that multiple low-affinity interactions with lipids, clathrin and clathrin adaptor proteins contribute to the recruitment of Auxilin to CCVs. It is possible that these interactions help to distinguish free and coat-associated clathrin triskelia. However, future work will have to elucidate the exact dynamics and the sequential and hierarchical nature of Auxilin interaction with lipids, clathrin and clathrin adaptor proteins.

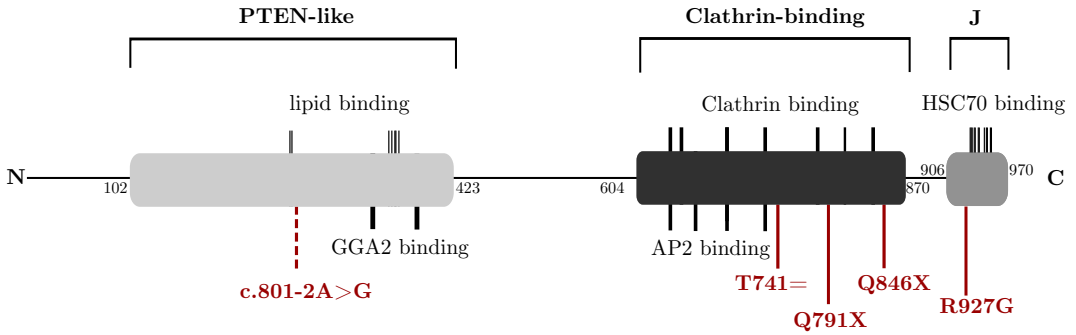

Figure 6.15: **Domain organization of Auxilin with indication of interaction partners and PD mutations** Auxilin domain organization with indication of motifs and residues involved with interaction for lipid, clathrin, HSC70, GGA2 and AP2 binding. Thickness of lines is representative for number of residues involved with interaction. Pathogenic mutations are shown in red, with solid line indicating coding variants and dotted line indicating exonic variant.

6.3.2 Differential interaction of Auxilin and GAK with TGN-resident clathrin adaptor proteins

Comparison of the interaction of Auxilin and its ubiquitously expressed homologue GAK confirmed the interaction of both proteins with plasma membrane-resident clathrin adaptor protein AP2 (Greener *et al.*, 2000; Scheele *et al.*, 2001), but revealed differential interaction with TGN-resident clathrin adaptor proteins. Whereas Auxilin interacts with GGA2, GAK interacts with AP1 as previously reported (Kametaka *et al.*, 2007). AP1 and the GGAs are γ-ear domain containing proteins that recognize a consensus motif, ψG(P/D/E)(ψ/L/M), for binding with accessory proteins. AP1 was found to interact with GAK via two sequences fitting the consensus motif, FGPL and FGEF. BLAST analysis revealed that those sequences are not conserved in Auxilin. However, Auxilin contains two FIPL sequences that closely resemble the consensus motif that were found to mediate interaction with GGA2 (Figure 6.7, Figure 6.15). A weak interaction of Auxilin with GGA3 was observed as well (Figure 6.5), however this interaction may be indirect and further *in vitro* binding experiments will have to confirm a direct interaction between Auxilin and GGA3 and whether this interaction

is mediated by the FIPL binding motifs too. In addition, all interactions were identified by overexpression of Auxilin and GAK. Future experiments should confirm the interaction between Auxilin and GAK and clathrin adaptor proteins at the endogenous level.

It remains to be determined how this differential binding of Auxilin and GAK with TGN-resident clathrin adaptor proteins is acquired. One explanation is that slight differences in binding motifs may result in different affinities for interaction with different γ-ear domain containing proteins. For example, Rabadaptin 5 has previously been described to interact via a single FGPL motif with with AP1, GGA1 and GGA3, but only weakly with GGA2, whereas GAK interacts with AP1 but none of the GGAs via a FGPL and a FGEF motif (Kametaka *et al.*, 2007). On the other hand, Auxilin interacts with GGA2 and only weakly with GGA3, but not with AP1 or GGA1, via two FIPL motifs (Figure 6.5). In addition, the location of the interaction motifs within the protein sequence could be important for binding with γ-ear domain containing proteins. Whereas the binding motifs of GAK for AP1 lies within the unstructured hinge region between the PTEN domain and clathrin-binding domain, the binding motifs of Auxilin for GGA2 are located in within the PTEN domain (Figure 6.15). Interaction of Auxilin with the γ-ear domain of GGA2 would thus take place in close proximity with the vesicular membrane of the CCV, whereas interaction of GAK with the AP1 complex would be closer to the clathrin coat. This may reflect differences in localization of the γ-ear domain of the AP1 complex and GGA proteins relative to the clathrin coat of CCVs. Finally, it can not be ruled out that additional interactions of Auxilin and GAK besides the described motifs contribute to the interaction and differential affinity for GGA2 and AP1, respectively.

Future work will have to elucidate the physiological relevance of the differential interaction of Auxilin and GAK with GGA2 and AP1, respectively. Mutagenesis of the AP1 interaction motif of GAK has been reported to result in a mild reduction of GAK recruitment to the TGN (Kametaka *et al.*, 2007). The GGA2 binding motif lies within the PTEN domain of Auxilin, which is also responsible for PIP binding (Figure 6.15). Auxilin constructs lacking the PTEN domain results in failure of recruitment to CCVs (He *et al.*, 2017). However, Auxilin with mutations in the FIPL motifs that abolish GGA2 interaction can still be recruited to the TGN (Figure 6.8). This likely indicates that interaction of the PTEN domain with lipids is the main determinant of Auxilin recruitment, as has previously been suggested (He *et al.*, 2017). The differential interaction of GAK and Auxilin for different TGN-resident clathrin adaptors raises the question whether this reflects a difference in efficiency for the uncoating of CCVs coated with AP1 or GGA proteins, respectively. About ∼40% colocalization has been observed between AP1 and the GGAs (Daboussi *et al.*, 2012a; Hirst *et al.*, 2001; Mardones *et al.*, 2007; Puertollano *et al.*, 2003; Zhu *et al.*, 2001), however the exact relationship between AP1 and the GGA proteins remains to be elucidated (see Section 1.3.5). Since AP1 and the GGA proteins are ubiquitously expressed across all cell types, it is unlikely that Auxilin or GAK are solely responsible for the uncoating of GGA2 or AP1 coated TGN-derived CCVs, respectively. However, the differential interactions may reflect increased preference in the uncoating of a subset of TGN-derived vesicles and may therefore underscore a particular importance of efficient uncoating of GGA2-coated CCVs by Auxilin in neurons.

6.3.3 Impact of mutations on Auxilin binding with *bona fide* interactors

Multiple homozygous recessive mutations have been identified to cause PD. Two splice site variants (c.801-2A>G, T741=) are thought to result in overall decreased protein levels (Edvardson *et al.*, 2012; Olgiati *et al.*, 2016). Two nonsense mutations (Q791X and Q846X) completely lack the J-domain and part of the clathrin-binding domain (Elsayed *et al.*, 2016; Köroglu *et al.*, 2013). The R927G Auxilin point mutation resides within the J-domain and results in decreased protein levels (Chapter 3) (Olgiati *et al.*, 2016). In addition, the R927G mutation is likely to disrupt the tightly packed α-helical structure of the J-domain (Figure 6.10). Thus, all known coding pathogenic Auxilin mutations cluster around the clathrin-binding domain and the J-domain of Auxilin (Figure 6.15). To address the impact of these mutations on the interactome of Auxilin, co-IPs were performed of WT and mutant Auxilin with *bona fide* Auxilin interactors.

All tested mutations (Q791X, Q846X, R927G) display impaired interaction with clathrin. Modelling of the J-domain within the assembled clathrin coat structure indicates that multiple residues of Auxilin reside at the interface with the clathrin coat and could thus contribute to the interaction of Auxilin with clathrin. The disruption of the tertiary structure of the J-domain by the R927G mutation would result in displacement of the putative clathrin interacting residues in the J-domain (Figure 6.10), with subsequent decreased binding of Auxilin to clathrin. The Q791X Auxilin mutation results in a C-terminal truncation lacking some of the clathrin interaction sites, thus explaining the impaired interaction. The R927G mutation resides in the J-domain, C-terminally of the clathrin binding domain (Figure 6.15). The Q846X mutation also resides in the clathrin binding domain, but does not result in a truncation of any of the reported clathrin binding sites (Figure 6.15). However, the lack of the J-domain and part of the clathrin-binding

domain may result in misfolding of the clathrin binding domain. In addition, similarly to R927G, lack of the putative additional clathrin interaction sites in the J-domain of Auxilin as modelled in Figure 6.10, would also result in decreased clathrin binding.

The clathrin binding domain and PTEN-domain have previously been shown to be crucial for recruitment of Auxilin to CCVs. However, despite decreased interaction of mutant Auxilin with clathrin, Auxilin was still able to be recruited to CCVs. This indicates that residual interaction with clathrin as well as with lipids and clathrin adaptor proteins might be sufficient for CCV recruitment. Indeed, interactions with clathrin adaptor proteins AP2, GGA2 and GGA3 were unaffected by Auxilin mutations. In addition, the PTEN domain that is required for Auxilin recruitment to CCVs via lipid interactions, is not affected by mutations at the sequence level. Since the PTEN-like domain is connected to the clathrin binding domain and J-domain via an unstructured hinge area (Figure 6.13), it is plausible that tertiary structure of the PTEN domain is unaffected, thus preserving interaction with lipids of the vesicular membrane.

Interaction of Auxilin with the HSC70 chaperone via its J-domain is not only crucial for HSC70 recruitment to CCVs, but also to stimulate HSC70 ATPase activity for the uncoating of CCVs. Interaction of Auxilin with the clathrin coat is also required to guide HSC70 to a correct position within the clathrin coat. Auxilin interacts with the clathrin coat via multiple contacts (Figure 6.15), ultimately resulting in the placement of its J-domain underneath the tripod of a clathrin triskelion, thereby placing HSC70 in close proximity of a set of critical clathrin interactions (Fotin *et al.*, 2004b). It is thus conceivable that impaired interaction with clathrin would result in a failure of correct positioning of HSC70. In addition, two pathogenic Auxilin mutations (Q791X, Q846X) are nonsense

mutations that completely lack the J domain and the R927G Auxilin mutation is thought to result in dramatic conformational alterations of the highly conserved α-helical structure J-domain (Figure 6.10). These pathogenic Auxilin mutations could therefore result in an impaired recruitment of HSC70 to CCVs.

However, no decrease of interaction of mutant Auxilin with HSC70 was observed (Figure 6.14). One explanation could be that HSC70 interacts with Auxilin as a substrate rather than a client protein, to assist in correct folding of the mutant protein. In addition, increased interaction of Auxilin with HSC70 could also be an overexpression artefact, where HSC70-assisted folding is part of a cellular response to sudden increased Auxilin protein levels, to enhance solubility and correct assembly of the Auxilin.

In summary, these data indicate that even though pathogenic Auxilin mutants with a truncation or disruption of the J-domain (Q791X, Q846X, R927G) can still be recruited to CCVs, they are likely to be unable to fulfill their function as co-chaperones of HSC70, resulting in an impairment of the uncoating of CCVs derived from both the Golgi apparatus and the plasma membrane. In addition, there is evidence that c.801-2A>G, T741= and R927G are hypomorphic alleles, resulting in an overall decreased efficiency of CCV uncoating (see Chapter 3) (Edvardson *et al.*, 2012; Olgiati *et al.*, 2016). Inefficient uncoating of CCVs would impede delivery of its cargo to destination compartments, ultimately resulting in decreased cellular function.

6.4 MATERIAL AND METHODS

6.4.1 pCR8 cloning of Auxilin

The open reading frame of full-length Auxilin (NP_001243793.1) was amplified using PCR from a pCR-BluntII-TOPO vector (plasmid identification HsCD00346779, Harvard Medical School plasmid repository). The PCR reaction contained 30 ng of plasmid, PCR buffer, dNTPs, forward primer (5'-atgaaagattctgaaaataaaggtgc-3'), reverse primer (5'-ttaatataagggcttttggcctt-3') Pfu Ultra II polymerase and Pfu Ultra PCR buffer (Agilent).

The PCR-amplified product was subsequently purified using paramagnetic bead-based PCR cleanup reagents (Agencourt AMPure XP, Beckman Caoulter). AMPure paramagnetic beads were mixed with the PCR sample and incubated at room temperature for 5' to bind the PCR fragments. Beads were separated from the solution using a magnet and samples were subsequently washed three times for 30" with 70% Ethanol to remove contaminants such as dNTPs, salts, polymerases and primers. Beads were air-dried to allow for complete evaporation of ethanol. DNA was subsequently diluted in water.

The purified Auxilin fragment was subjected to poly-A-tailing. The poly-A-tailing reaction mixture contained dATP, Taq polymerase and Taq polymerase buffer (Invitrogen). The reaction was incubated at 72°C for 40 minutes.

Next, the Auxilin fragment was cloned into a pCR8 backbone (Invitrogen) containing a spectinomycin resistance cassette, by incubation of the Auxilin fragment with the vector and a salt solution at RT for 1 hour.

6.4.2 Transformation of competent bacteria

NEB5α competent *Escherichia coli* bacteria (High efficiency, New England BioLabs) were thawed on ice and 2 μl of the pCR8-Auxilin reaction was mixed with 50 μl of the bacteria and incubated on ice for 15 minutes. The bacteria were then subjected to a heat shock by 30 second incubation at 42°C, followed by another incubation on ice for 5 minutes. 100 μl of SuperBroth (KD Medical) was mixed with the bacteria, poured and spread on Agar plates (KD Medical) containing 50 μg/ml spectinomycin and incubated overnight at 37°C.

6.4.3 Plasmid purification

For small scale pCR8 plasmid purification, a colony from an agar plate incubated overnight was used to inoculate 5 ml of SuperBroth media containing 50 μg/ml spectinomycin overnight at 37°C. The following day, 1 ml of the inoculated SuperBroth was used to make glycerol stocks (800 μl of inoculated broth with 200 μl of 80% glycerol diluted in SuperBroth). The QIAprep Spin Miniprep Kit (Qiagen) was used for plasmid preparation, resulting in $\sim$20 μg of plasmid.

For large scale pCR8 plasmid purification, 50 ml of SuperBroth containing 50 μg/ml spectinomycin was inoculated overnight at 37°C with transformed bacteria scraped from the glycerol stock. Plasmid Plus Kits (Qiagen) was used for plasmid preparation, resulting in $\sim$500 μg of plasmid.

6.4.4 Sanger sequencing

Purified PCR product was subjected to Sanger sequencing using the BigDye Terminator v3.1 Cycle Sequencing Kit (ThermoFisher Scientific). 500 ng of

purified plasmid was mixed with 2 μl 5X Sequencing Buffer, 0.3 μl BigDye Terminator Ready Reaction Mix, 0.3 μM primer and water was added to make up for a total reaction volume of 10 μl. Cycle sequencing was performed under reaction conditions outlined in table 3.2.

As Sanger sequencing resulted in ∼600 base pair reads, primers were designed to be spaced ∼400 base pairs apart, to cover the full sequence (total of 2910 base pairs). In addition, primers were designed to cover the junction of the Auxilin fragment and the plasmid backbone, to confirm correct insertion of the Auxilin fragment. Table 6.3 gives an overview of the primers used for sequencing Auxilin.

Start	Direction	Exon
34	Fwd	5'-ggagctaccggaaaaagacc-3'
419	Fwd	5'-tgtcctttcctctggacaatg-3'
927	Fwd	5'-caaacagaggaatggatgtcg-3'
1400	Fwd	5'-cttaggaggacaggctccaa-3'
1895	Fwd	5'-tgcgtctccaaccctaagag-3'
2417	Fwd	5'-cactcctctccccagaacc-3'
2899	Fwd	5'-ctcaatgatgcctggtctga-3'
34	Rvs	5'-ggtctttttccggtagctcc-3'
147	Rvs	5'-gcgttcactctctgcttgc-3'
245	Rvs	5'-atagctgggctccatgtctg-3'
763	Rvs	5'-gctgggccaggagtagagta-3'
1273	Rvs	5'-tgtcacctgaaatagctgagga-3'
1757	Rvs	5'-ttcagaattggtgggaggag-3'
2269	Rvs	5'-ttgctggcaaaggaagaact-3'
2751	Rvs	5'-ctggtttccacttggtctcc-3'
2899	Rvs	5'-tcagaccaggcatcattgag-3'

Table 6.3: **Sequencing primers used for Auxilin plasmids**

Sequencing samples were cleaned using the Sanger Dye Terminator Removal Agencourt CleanSEQ (Beckman Coulter). Sequencing samples were mixed with 10 μl CleanSEQ paramagnetic beads and 42 μl of 85% Ethanol. Beads were separated from solution using a magnet and were washed 3 times for 30" with

85% Ethanol. Samples were air-dried to remove residual ethanol and DNA was eluted in 40 μl water.

Capillary electrophoresis of sequencing samples was performed using the Hitachi Genetic Analyzer (Applied Biosystems) and data were analysed using the Sequencher software to confirm correct sequence of the Auxilin fragment and correct insertion into the backbone.

6.4.5 Site-directed mutagenesis

For mutagenesis of a single point mutation (e.g. pathogenic Auxilin mutations), the QuickChange IIXL Site-Directed Mutagenesis Kit (Agilent). 10 ng of the pCR8 Auxilin plasmid was mixed with 1X reaction buffer, 2.5 units of PfuUltra High Fidelity DNA polymerase, 6% QuikSolution, 1 μl of dNTP and 125 ng each of forward and reverse mutagenesis primers (Table 6.4), in a total reaction volume of 50 μl. Mutagenesis primers were designed using the web-based Agilent software (www.agilent.com/genomics/gcpd). Mutagenesis PCR was performed using the cycling parameters outlined in Table 6.5.

Mutation	Direction	Exon
Q791X	Fwd	5'-gaggcttaggctatggctgctgccagttgta-3'
	Rvs	5'-tacaactggcagcagccatagcctaagcctc-3'
Q8846X	Fwd	5'-tgtgagcattgaaaccttaaccagagagtaggtcttc-3'
	Rvs	5'-gaagacctactctctggttaaggtttcaatgctcaca-3'
R927G	Fwd	5'-ccaggacagccttcccgtacaccttcttcac-3'
	Rvs	5'-gtgaagaaggtgtacgggaaggctgtcctgg-3'

Table 6.4: **Mutagenesis primers used for pathogenic variants Auxilin**

For mutagenesis of multiple base pairs (e.g. GGA2 binding-deficient Auxilin required mutagenesis of a total of 6 basepairs, resulting in 4 amino acid changes), the QuikChange Lightning Multi Site-Directed Mutagenesis Kit (Agilent) was

Cycles	Temperature (C)	Time
1x	95	2’
30x	95	20”
	55	30”
	65	10’
1x	65	5’

Table 6.5: **Cycle sequencing conditions for single-site mutagenesis**

used. Two primer pairs were designed to change 3 base pairs each (Table 6.6) and all primers were combined in during a single mutagenesis reaction for simultaneous mutagenesis of all 6 basepairs. Multi site-directed mutagenesis was performed using 50 ng of plasmid, mixed with 1X reaction buffer, 1 μl QuikChange Lightning Multi enzyme blend, 50 ng of each primer and 1 μl dNTP mix, in a total reaction volume of 50 μl. Mutagenesis PCR was performed using the cycling parameters outlined in Table 6.7.

Mutations	Direction	Exon
F342A, L345A	Fwd	5’-tctccttgcacagtgatgttcgcgggaatggcgatttttccatcttggacacg-3’
	Rvs	5’-cgtgtccaagatggaaaaatcgccattcccgcgaacatcactgtgcaaggaga-3’
F386A, L389A	Fwd	5’-gaactttaaaactgttgtgtccgctggtatggctccagtgtgaaactgaagctggaa-3’
	Rvs	5’-ttccagcttcagtttcacactggagccataccagcggacacaacagttttaaagttc-3’

Table 6.6: **Primers used for multi-site mutagenesis for GGA2 binding-deficient Auxilin**

Cycles	Temperature (°C)	Time
1x	95	2’
30x	95	1’
	55	1’
	65	6’
1x	65	5’

Table 6.7: **Cycle sequencing conditions for multi-site mutagenesis**

Following mutagenesis, the parental plasmid DNA was degraded using DpnI. The parental plasmid was purified from *Eschericia coli* and is methylated and therefore

susceptible to DpnI digestion, whereas the newly synthesized mutagenized plasmid is not. Mutagenesis reaction mixtures were incubated with 10 units of DpnI for 1 hour at 37°C.

Next, competent bacteria were transformed with 2 μl of the mutagenesis reaction mixture (see Section 6.4.2), followed by plasmid purification (see Section 6.4.3) and correct mutagenesis was confirmed using Sanger sequencing (see Section 6.4.4).

6.4.6 Gateway recombination

Gateway LR Clonase II Enzyme Mix (Invitrogen) was used for Gateway recombination of the Gateway donor vector (pCR8-Auxilin) with a Gateway compatible destination vector. The Gateway destination vectors pCMV-AcGFP and pCMV-3xFlag (previously constructed in the lab) contained a CMV promotor and a kanamycin or ampicilin resistance cassette, respectively, and were used for N-terminal AcGFP or 3x-Flag tagging of Auxilin.

150 ng of donor vector (pCR8-Auxilin) was mixed with 150 ng of destination vector (pCMV-AcGFP or pCMV-3xFlag), 2 μl of Gateway LR Clonase II Enzyme Mix, and TE buffer was added to make up a total reaction volume of 10 μl. The Gateway reaction mixture was incubated for 1 hour at RT.

Bacteria were transformed with 2 μl of mutagenesis reaction mixture as described in Section 6.4.2, using 50 μg/ml kanamycin or 100 μg/ml ampicilin for the selection of pCMV-AcGFP-Auxilin or pCMV-3xFlag-Auxilin, respectively. Gateway destination vectors contain a Gateway cassette with the ccdB gene, toxic for *Escherichia coli*. When recombination of the donor vector with the recombination

vector is successful, the ccdB gene is replaced with the gene of interest (i.e. Auxilin), thereby positively selecting for successfully recombined plasmid constructs.

Plasmids were purified as described in Section 6.4.3 and correct mutagenesis was confirmed using Sanger sequencing as described in Section 6.4.4.

6.4.7 SILAC labelling of HEK293FT

HEK293FT cells were cultured in DMEM (Gibco) supplemented with 10% FBS (Gemini). For the metabolic incorporation of 'light' and 'heavy' stable isotopes in HEK293FT, the SILAC Protein Quantitation Kit (LysC), DMEM (ThermoFisher Scientific) was used. DMEM was supplemented with 10% dialysed FBS. For labelling with 'light' SILAC isotopes, the media was supplemented with $^{12}C_6$ L-Lysine-2HCl (Lys-0) and $^{12}C_6$ L-Arginine-HCl (Arg-0), for 'heavy' SILAC isotopes, the media was supplemented with $^{13}C_6$ L-Lysine-2HCl (Lys-8) and $^{13}C_6$ L-Arginine-Hcl (Arg-10) (resulting in a 8 and 10 Dalton mass-shift compared to 'light' L-Lysine-2HCl and L-Arginine-HCl, respectively).

HEK293FT cells were grown in light or heavy SILAC media for at least 10 doublings, allowing for 98% efficient incorporation of the light or heavy stable isotopes.

6.4.8 Co-immunoprecipitations

HEK293FT cells were grown in a 10-cm dish at a density of ∼10 million cells per plate and transfected with 8 μg GFP-Auxilin plasmid using lipofectamin 2000, as per manufacturer instructions. Co-IPs were performed 24 hours after transfection.

Cells were resuspended gentle lysis buffer (20 mM Tris pH7.5, 10% glycerol, 1 mM EDTA, 150 mM NaCl, 0.3% Triton) supplemented with 1x protease inhibitor cocktail (Halt) and 1x phosphatase inhibitor cocktail (Halt) and rotated at 4°C for 30 minutes.

Protein lysates were cleared (10' centrifugation at 4°C at 21kg) and protein concentrations were determined using a 660 nm protein assay (Pierce). Input samples were prepared by diluting 10 μg of protein in a total volume of 20 μl containing 1x Laemli sample buffer and were boiled for 5 minutes at 95°C.

For co-IPs, equal amounts of protein lysates were mixed with GFP-Trap agarose beads (Chromotek) and rotated at 4°C for one hour. Beads were subsequently washed 5 times with gentle lysis buffer and boiled for 5 minutes at 95°C in 2X Laemli sample buffer.

Input samples and co-IP samples were subjected to gel electrophoresis and western blot analysis as described below on the same day (Sections 6.4.11 and 6.4.12).

6.4.9 Recombinant protein synthesis

HEK293FT cells were transfected with 3xFlag-Auxilin constructs or 3xFlag-GFP as described above, followed by co-IP.

Cells were resuspended lysis buffer (20 mM Tris pH7.5, 10% glycerol, 1 mM EDTA, 150 mM NaCl, 1% Triton) supplemented with 1x protease inhibitor cocktail (Halt) and 1x phosphatase inhibitor cocktail (Halt) and rotated at 4°C for 30 minutes.

Protein lysates were cleared (10' centrifugation at 4°C at 21 kg) and protein concentrations were determined using a 660 nm protein assay (Pierce). Input

samples were prepared by diluting 10 μg of protein in a total volume of 20 μl containing 1x Laemli sample buffer and were boiled for 5 minutes at 95°C.

For co-IPs, equal amounts of protein lysates were mixed with Flag-M2 magnetic beads (Sigma) and rotated at 4°C for one hour. Beads were subsequently washed 5 times with lysis buffer. Protein was eluted from the beads by incubation of the beads with Flag peptide (Sigma). Recombinant protein eluates were stored at -80°C until experimental use.

6.4.10 *In vitro* protein-protein binding experiments

Recombinant 3x-Flag-Auxilin protein was generated as described above and GST-GGA2 was purchased from Novus Biologicals. 20 ng of recombinant 3xFlag-Auxilin or 3xFlag-GFP was mixed with 100 ng recombinant GST-GGA2 and lysis buffer (20 mM Tris pH7.5, 10% glycerol, 1 mM EDTA, 150 mM NaCl, 1% Triton) supplemented with 1x protease inhibitor cocktail (Halt) and 1x phosphatase inhibitor cocktail (Halt). 1% of the reaction was used for input samples, and the remainder was incubated with 20 μl Flag-M2 beads and rotated at 4°C for 1 hour.

Flag-M2 beads were washed 5 times with lysis buffer and boiled in 2X Laemli sample buffer. Input samples and co-IPs were subjected to gel electrophoresis and western blot analysis as described below on the same day (Sections 6.4.11 and 6.4.12).

6.4.11 Gel electrophoresis

Protein samples were loaded on pre-cast 4-20% TGX polyacrylamide gels (Criterion, Bio-Rad) along with a protein standard (Precision Plus Protein

Dual Color Standards, Bio-Rad). Electrophoresis was performed in 1x premixed electrophoresis buffer (10 mM Tris, 10 mM Tricine, 0.01% SDS, pH 8.3, diluted with water) and were run at 200 V for 45 minutes using the Criterion Vertical Electrophoresis Cell (Bio-Rad).

6.4.12 Western blot

Western blots were performed as described in section 3.4.7. Primary antibodies used in this chapter for WB are shown in Table 6.8.

Target	Host	Dilution	Vendor	Catalog number
CHC	Mouse	1/3000	Abcam	ab21679
HSC70	Rat	1/3000	Abcam	ab19136
AP1γ	Mouse	1/1000	B & D Biosciences	610385
AP2α	Mouse	1/1000	Abcam	ab2730
AP3β	Mouse	1/1000	Aviva Systems biology	ARP33647
GGA1	Mouse	1/1000	Abcam	ab10551
GGA2	Rabbit	1/1000	Abcam	ab10552
GGA3	Mouse	1/1000	B & D Biosciences	612311
GFP	Rabbit	1/5000	Sigma	ab290
GST	Goat	1/5000	Sigma	27-4577-01
Flag	Mouse	1/5000	Sigma	F1804

Table 6.8: **Primary antibodies used for WB**

6.4.13 SILAC proteomics

HEK293FT cells were labelled with 'light' or 'heavy' SILAC isotopes (Section 6.4.7) and were transfected with GFP or GFP-Auxilin, respectively, using lipofectamin 2000 according to manufacturer's instructions. GFP nano-trap co-IPs were performed as described in Section 6.4.8 and co-IPs were mixed at 1:1 ratio. Experiments were performed in triplicate, and the resulting 3 samples were loaded

on a polyacrylamide gel for electrophoresis (as described in section 6.4.11) were allowed to migrate for 5 minutes.

Samples were subsequently cut out from the gel and subjected to in-gel trypsin digestion, followed by liquid chromatography tandem mass spectometry analysis (LC-MS/MS). The LC-MS/MS data were searched against the NCBI Human database and Mascot Distiller software was used to calculated the protein Light/Heavy ratios (O'Leary *et al.*, 2016; Perkins *et al.*, 1999).

In gel trypsin digestion, LC-MS/MS and subsequent protein identification via peptide sequence databases was performed by the Proteomics Core led by Dr. Yan Li (National Institute of Neurological Disorders and Stroke, National Institutes of Health).

6.4.14 Functional enrichment analysis

Functional enrichment analysis was performed for the 50 most significantly differentially expressed genes using Gene Ontology (The Gene Ontology Consortium, 2019; The Gene Ontology Consortium *et al.*, 2000) for gene Ontology terms 'biological process' and 'cellular component'. Fischer exact test was performed for functional enrichment analysis with Bonferroni *post hoc* correction. An enrichment map was generated using the 'EnrichmentMap' Cytoscape plug-in.

6.4.15 Immunocytochemistry

Primary neurons were cultured as described in Section 5.4.1 and transfected using lipofectamin 2000 (Invitrogen), according to manufacturer's instructions. 2 μg plasmid was transfected for a 12 mm coverslip in a single well of a 24-well plate

of primary neurons cultured 7 DIV. Culturing media was replaced 4 hours after transfection and immunocytochemistry was performed 40 hours after transfection as described in Section 5.4.10. Primary antibody rabbit-CHC (Abcam, ab21679) was used for immunocytochemistry in this chapter.

6.4.16 Confocal laser-scanning microscopy with Airyscan detection

Super-resolution microscopy using the Zeiss 880 Confocoal microscope outfitted with Airyscan module was performed as described in Section 5.4.11.

6.4.17 Structural protein modelling

Protein structures were modelled by Dr. Nate Smith. All models were generated using PyMOL (Version 2.0, Schrödinger, LLC).

Modeling of the interaction between the Clathrin triskelion (Blue) and the J-domain (Pink) of Auxilin was performed utilizing the structure from *Bos Taurus* (PDB:1XI5) emphasizing the pathogenic mutation (Cyan) and interaction domain (Yellow) (Figure 1.5) (Fotin *et al.*, 2004b).

Representational modeling of potential interaction between GGA2 and Auxilin was performed using the previously solved structures (PDB: 3N0A-Auxilin and the S. Cerevisiae GGA2 PDB: 3MNM) and based on predicted interaction sites (Figure 6.7) (Fang *et al.*, 2010; Guan *et al.*, 2010; Kametaka *et al.*, 2007; Nogi *et al.*, 2002).

I-TASSER was utilized to predict the structure of human Auxilin and the strongest match was selected. The generated model was based on the Auxilin structure

from *Bos taurus* (PDB: 3N0A) (Guan *et al.*, 2010; Roy *et al.*, 2010; Yang *et al.*, 2015; Zhang, 2008).

Heterodimeric complex (Hsc70 and Auxilin) was modelled in PyMol overlaying the J-domain of the generated model with the Hsc70-J-domain structure available in the Protein Data Bank (PDB: 2QWO) (Figure 6.13) (Jiang *et al.*, 2007).

6.4.18 Statistics

Data were plotted and statistical tests were performed using Prism 8 (Graphpad) or R version 3.4.3. The statistical test results are displayed in table 6.9. n represents the number of technical replicates.

Figure	Variable	Statistical test	Test result	P-value
6.3	Genotype	One-sample t-test with Benjamini & Hochberg correction	NA	See Supplementary Table 2
6.4	Genotype	Fisher exact test with Bonferroni correction	NA	See Table 6.2
6.5 B	Genotype	1-way ANOVA	F = 36.42	0.0004
	Genotype	Sidak *post hoc* test	t = 7.391, t = 0.000	0.0009, >0.9999
6.5 C	Genotype	1-way ANOVA	F = 41.37	0.0003
	Genotype	Sidak *post hoc* test	t = 8.251, t = 7.440	0.0005, 0.0009
6.5 E	Genotype	1-way ANOVA	F = 15.23	0.0045
	Genotype	Sidak *post hoc* test	t = 0.000, t = 4.780	>0.9999, 0.00992
6.5 F	Genotype	1-way ANOVA	F = 3.914	0.0817
	Genotype	Sidak *post hoc* test	t = 0.000, t = 6.430	>0.9999, 0.0020
6.7	Genotype	Unpaired t-test	t = 4.094	0.0149
6.9 A	Genotype	1-way ANOVA	F = 22.02	0.0003
	Genotype	Sidak *post hoc* test	t = 6.752, t = 7.095, t = 5.785	0.0007, 0.0005, 0.0018
6.12 A	Genotype	1-way ANOVA	F = 0.3947	0.7604
	Genotype	Sidak *post hoc* test	t = 0.3851, t = 0.6394, t = 0.1896	0.9994, 0.99906, >0.9999
6.12 B	Genotype	1-way ANOVA	F = 4.088	0.0494
	Genotype	Sidak *post hoc* test	t = 2.814, t = 0.8265, t = 2.825	0.1287, 0.9666, 0.1267
6.12 C	Genotype	1-way ANOVA	F = 0.8754	0.4931
	Genotype	Sidak *post hoc* test	t = 0.9770, t = 0.5198, t = 0.3041	0.9292, 0.9969, 0.9998
6.14 F	Genotype	1-way ANOVA	F = 0.5876	0.6400
	Genotype	Sidak *post hoc* test	t = 1.186, t = 0.4307, t = 0.07584	0.8483, 0.9989, >0.9999

Table 6.9: **Statistical test results**

7 GENERAL DISCUSSION

A detailed analysis and discussion of the results has been presented individually in each chapter. In this section, I will highlight the key findings of this thesis and discuss interrelated data from the different chapters. Based on the results of this thesis, I will present a model for PD pathogenesis in Auxilin mutation carriers. In addition, I will highlight questions that arise from the data presented in this thesis. Finally, I will present an outlook on how future work might address the remaining open questions.

7.1 KEY FINDINGS

7.1.1 PD-associated R927G Auxilin variant is a loss of function mutation

Auxilin is the major neuronal clathrin uncoating protein and requires interaction with HSC70 via its J-domain for its function. Over the past seven years, 5 recessive Auxilin mutations have been described to cause an aggressive form of young onset PD. Two of those mutations are splice-site mutations (T741=, c.801-2A>G) that have been predicted to result in an overall decrease in mRNA and are thus hypomorphic Auxilin alleles (Edvardson *et al.*, 2012; Olgiati *et al.*, 2016). In addition, two C-terminally truncating mutations (Q791X, Q846X) completely lack the J-domain of Auxilin required for HSC70 binding, pointing to a loss of function mechanism (Elsayed *et al.*, 2016; Köroglu *et al.*, 2013). Finally, a point mutation within the J-domain (R927G) was described to cause PD, however the mechanism of action of this mutation is less clear (Olgiati *et al.*, 2016).

A novel CRISPR-based mouse model was generated carrying the homozygous R857G Auxilin variant, equivalent to the human pathogenic R927G Auxilin

mutation (Figure 3.1). Auxilin levels were found to be decreased in the brain of newborn R857G Auxilin mice, indicating that R857G Auxilin might be a hypomorphic allele in early development (Figure 3.3). Even though Auxilin protein levels were upregulated with age to equivalent levels as WT mice in 3 week old animals, it is possible that the stability and/or half life of Auxilin protein may be affected in R857G Auxilin mice.

Structural modelling of Auxilin revealed that the R927G mutation resides in one of the α-helices that make up the tightly packed J-domain of Auxilin (Figure 6.13). α-helices are formed through hydrogen bonds between positively and negatively charged residues, it is conceivable that substitution of the positively charged R927 to an uncharged G927 would break up the α-helical formation of the J-domain. Disruption of the highly conserved J-domain of Auxilin in turn would weaken interaction of Auxilin with HSC70, thereby impairing its function in the uncoating of CCVs.

7.1.2 Auxilin interacts with synaptic and Golgi-resident clathrin adaptor proteins

Whereas the role of Auxilin in CME is well-established, less is known about its function in the uncoating of TGN-derived CCVs. To gain further insight into the physiological role of Auxilin, the interactome of Auxilin was mapped using unbiased proteomics (Figure 6.3). As has previously been reported, Auxilin was found to interact with the plasma membrane-resident clathrin adaptor protein AP2 (Figure 6.5). In addition, the TGN-resident clathrin adaptor protein GGA2 was found to be a novel interactor of Auxilin (Figure 6.7). These data thus indicate for the first time a direct role for Auxilin in the uncoating of Golgi-derived CCVs.

7.1.3 GAK does not fully compensate for loss of Auxilin function

Whereas Auxilin levels were decreased in newborn R857G Auxilin mice, GAK protein levels were found to be transiently upregulated 2 days after birth (Figure 3.3). At 3 weeks of age, Auxilin protein in R857G Auxilin mice was upregulated to equivalent levels as age-matched WT mice and GAK protein levels dropped back to normal as well. These findings indicate that GAK protein levels are transiently upregulated to compensate for decreased Auxilin protein levels. However, upregulation of GAK does not appear to be sufficient to fully compensate for decreased Auxilin protein, as R857G Auxilin mice exhibit increased mortality (Figure 3.8).

One possible explanation is that GAK protein levels might not be high enough to compensate for a partial loss of Auxilin. Indeed, even whilst taking into account the increase in GAK in p2 R857G mice, GAK expression levels are still ∼5 times lower than Auxilin expression levels (Figure 3.4). In addition, GAK has previously been shown to be less efficient in the uncoating of CCVs compared to Auxilin (Yim *et al.*, 2010).

In contrast, it is also possible that Auxilin and GAK are not fully redundant in function. Both GAK and Auxilin were found to interact with the plasma-membrane resident clathrin adaptor protein AP2, however they interact with a different subset of TGN-resident clathrin adaptor proteins. GAK was found to interact with AP1, whereas Auxilin was found to interact with GGA2 (Figure 6.5). An intriguing possibility is therefore that GAK might efficiently compensate for Auxilin in the uncoating of plasma membrane-derived, AP2-coated CCVs, but might not fully compensate for the uncoating of TGN-derived, GGA2-coated CCVs in neurons.

7.1.4 Activation of the Golgi stress response in Auxilin neurons

Similarly to newborn R857G mice, primary R857G Auxilin neurons were found to have decreased Auxilin protein levels, thus likely resulting in an overall decreased efficiency of CCV uncoating (Figure 3.2). Dystrophic morphological alterations were observed in the Golgi apparatus of R857G Auxilin mice (Figure 5.12) and transcriptome analysis of revealed significant upregulation of genes involved with the Golgi stress response (*GBF1*, *CREB3*) (Figure 5.7, Figure 5.10). Whereas GBF1 protects against Golgi stress, CREB3 is involved with the initiation of Golgi stress-dependent apoptosis (Reiling *et al.*, 2013). In addition to its role in protecting against Golgi-stress, GBF1 is also required for the recruitment of GGA proteins, but not AP1 to the TGN (Lefrançois and McCormick, 2007). Since Auxilin specifically interacts with GGA2 (Figure 3.3), upregulation of GBF1 might mediate increased recruitment of GGA proteins to compensate for inefficient uncoating of GGA-coated CCVs.

Golgi stress in R857G Auxilin neurons could be a direct consequence of impaired clathrin trafficking at the TGN. Inefficient uncoating of TGN-derived CCVS may result in the inefficient recycling of TGN-resident clathrin-adaptor proteins such as GGA2. In contrast, Golgi stress could also be an indirect consequence of impaired clathrin trafficking, both at the TGN and the plasma membrane. Both endolysosomal and synaptically targeted proteins are sorted and transported through the Golgi apparatus. Impaired uncoating of CCVs would result in inefficient delivery of its cargo to intracellular destination compartments, such as the endolysosomal system and the synapse. As a compensatory mechanism, R857G Auxilin neurons may upregulate trafficking in the early secretory pathway, to compensate for decreased efficiency in Golgi and post-Golgi trafficking. Indeed, multiple genes involved with ER-Golgi transport were found to be upregulated

in R857G Auxilin neurons (Figure 5.7). It is conceivable that chronic increased activation of ER-Golgi trafficking would result in Golgi stress.

7.1.5 Pathogenic Auxilin mutations impair its interaction with clathrin

Stimulation of the ATPase activity of HSC70 by Auxilin is required for the uncoating of CCVs in neurons. Auxilin interacts with clathrin to allow for the correct positioning of the J-domain that mediates interaction of HSC70 (Figure 6.13, Figure 6.10). HSC70 in turn is placed in close proximity to a set of critical clathrin interactions. Subsequent stimulation of the ATPase activity of HSC70 by Auxilin mediates a distortion in the clathrin coat to allow for the uncoating of CCVs.

Remarkably, all tested pathogenic Auxilin mutations (Q791X, Q846X, R927G) were found to impair interaction with clathrin (Figure 6.9). It is plausible that decreased interaction with clathrin would impair the correct positioning of the J-domain and HSC70, thereby decreasing the efficiency of CCV uncoating.

7.1.6 Neuropathological lesions underlie PD-like phenotypes in R857G Auxilin mice

Behavioural analysis revealed the development of neurological phenotypes in R857G Auxilin mice, as early as 6 months of age (see chapter 4). R857G Auxilin mice displayed motor impairments reminiscent of the typical motor features seen in PD patients, including bradykinesia, gait disturbances, and an inability to terminate movements. R857G Auxilin mice also exhibited phenotypes that phenocopy atypical neurological features seen in Auxilin mutation carriers, such as seizures and memory deficits. Remarkably, a mouse model harbouring an

endogenous PD-associated mutation in Synaptojanin 1, another neuronal protein required for the uncoating of CCVs, was also found to display motor impairment and seizure phenotypes (Cao *et al.*, 2017).

Lesions in the nigrostriatal pathway are thought to underlie the cardinal motor features of PD (see Section 1.1.3). The first major neuropathological hallmark of PD is the neurodegeneration of DA neurons in the nigrostriatal pathway. No neurodegeneration was observed in one year old R857G Auxilin mice (Figure A.1, Figure A.2). However, a decreased number of synaptic vesicles was observed in the presynapse of DA neurons in the striatum of R857G Auxilin mice (Figure A.4). Given that clathrin trafficking plays an important role in the recycling of synaptic vesicles, the decreased number of synaptic vesicles might be a consequence of impaired clathrin trafficking at the synapse in R857G Auxilin mice.

The second major neuropathological hallmark is the presence of intracellular aggregates composed of proteins and lipids in DA neurons in the nigrostriatal pathway. Large protein/lipid accumulations were observed in the striatum of R857G Auxilin mice, and lipids were also found to be increased in DA neurons in the SN of R857G Auxilin mice (Figure A.3). Impaired clathrin uncoating of TGN-derived CCVs might result in impaired delivery of its cargo, including proteins and lipids, to their intracellular destination compartments. TGN-derived CCVs are particularly important for the delivery of hydrolases to the lysosomes (Braulke and Bonifacino, 2009). Impaired delivery of those hydrolases may decrease the neuronal degradative capacity and aggravate the accumulation of intracellular cargo.

Taken together, impairments in clathrin trafficking in DA neurons in the SN and striatum due to partial loss of Auxilin function may underlie motor phenotypes

observed in R857G Auxilin mice. However, Auxilin is expressed in all neurons and lesions in other neuronal subtypes may well underlie some of the atypical phenotypes. The observed memory impairments might be caused by lesions in brain regions such as the neocortex, amygdala, cerebellum and basal ganglia. Spontaneous absence seizures as observed in R857G Auxilin mice might involve brain areas including the cortex and thalamus.

7.2 MODEL

Based on the key findings presented in the thesis, I would propose the following model for PD pathogenesis in Auxilin mutation carriers (Figure 7.1).

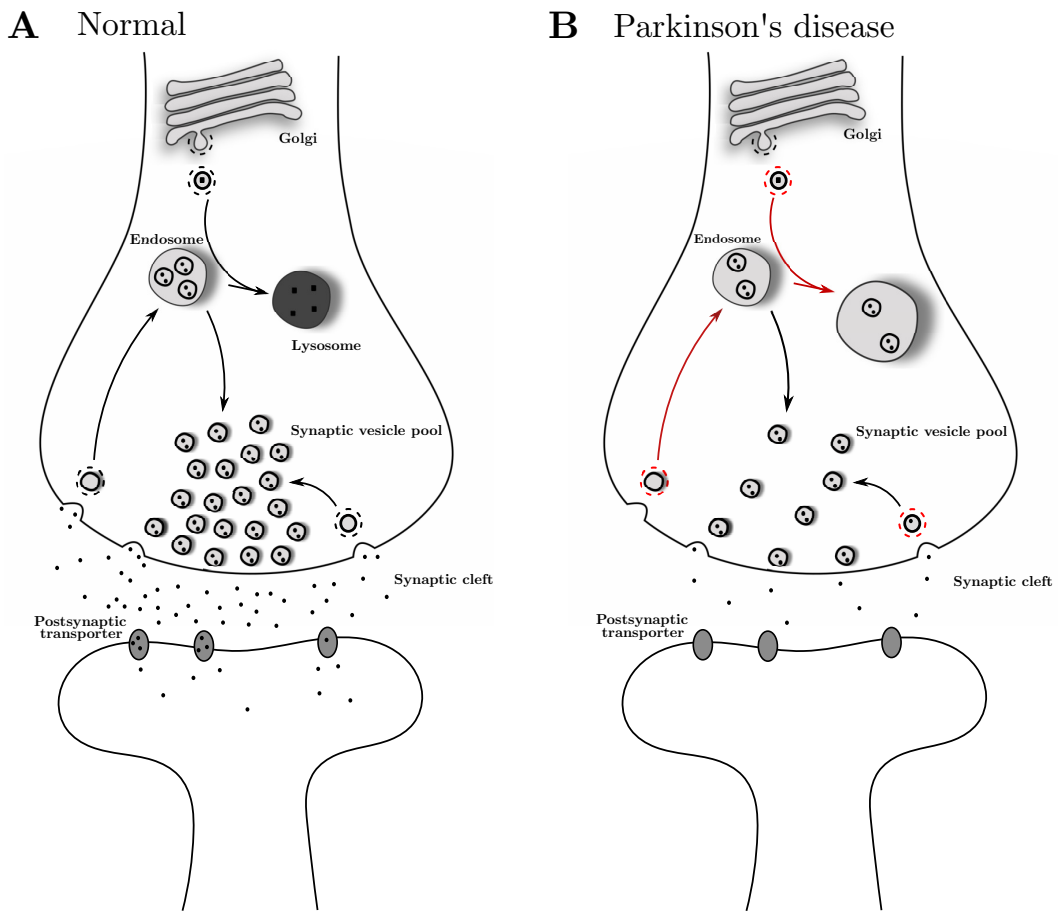

Figure 7.1: **Model for PD pathogenesis in Auxilin mutation carriers** Clathrin trafficking in neurons of normal population (A) and PD patients (B). Impaired clathrin trafficking due to PD-associated Auxilin mutations would result in inefficient synaptic vesicle recycling, with subsequent decrease in number of vesicles in the pre-synaptic intracellular synaptic vesicle pool. In addition, inefficient clathrin trafficking from the TGN would result in impaired delivery of lysosomal hydrolases and therefore impair lysosomal maturation, resulting in an accumulation of intracellular cargo.

Based on the genetic findings, PD-associated Auxilin mutations can be categorized into two groups. Whereas the truncating mutations (Q791X, Q846X) would result in a complete loss of function due to the complete absence of the J-domain, the splice-site mutations (c.801-2A>G, T741=) and point mutation (R927G) may function through a partial loss of function, via decreased protein levels or decreased functionality of the J-domain, respectively. Indeed, there appears to be a strong genotype-phenotype correlation in Auxilin mutation carriers. Splice-site mutation carriers (T741=, c.801A>G) develop PD with AAO ranging between 13 and 29 years, and R927G mutation carriers develop PD in their 20s (Edvardson *et al.*, 2012; Olgiati *et al.*, 2016). On the other hand, Q791X and Q846X mutation carriers result in juvenile onset PD (AAO 10-11 years) (Elsayed *et al.*, 2016; Köroglu *et al.*, 2013). In addition to the typical PD motor symptoms, Q791X and Q846X mutation carriers also develop additional neurological phenotypes, such as pyramidal and cerebellar signs, suffer from spontaneous seizures and present with cognitive decline (Elsayed *et al.*, 2016; Köroglu *et al.*, 2013).

Taken together, all described pathogenic Auxilin mutations are likely to function through a loss of function mechanism, resulting in inefficient uncoating of CCVs. Inefficient uncoating of CCVs would result in impairments in the delivery of CCV cargo to its intracellular destination compartments, which in turn would be detrimental for cellular function. Indeed, depletion of Auxilin and its homologue GAK have previously been found to result in an accumulation of clathrin structures that are depleted of cargo and packed with clathrin-binding proteins (Borner *et al.*, 2006; Borner *et al.*, 2012; Hirst *et al.*, 2008).

Inefficient uncoating of CCVs derived from CME at the synapse might result in impairments of synaptic vesicle recycling. Indeed, a decrease of synaptic vesicles was observed in the pre-synapse of R857G Auxilin mice (Figure A.4). Subsequent

impairments in synaptic transmission in the SN may underlie some of the cardinal motor phenotypes seen in patients, such as bradykinesia, tremor and balance impairments. In addition, impaired synaptic transmission in other brain regions may well underlie additional atypical neurological phenotypes observed in Auxilin mutations carriers, such as seizures and cognitive decline.

Impaired uncoating of Golgi-derived CCVs would result in inefficient delivery of a wide range of clathrin cargo, both lipids and proteins, to their intracellular destination compartments. In addition, Golgi stress was observed in neurons from R857G Auxilin mice (Figure 5.12), which may result in overall impaired Golgi function and subsequent impaired sorting of non-clathrin cargo as well. Indeed, cytosolic accumulations of lipids and proteins were observed in the nigrostriatal pathway of R857G Auxilin mice, which might be a direct consequence of impaired post-Golgi trafficking (Figure A.3). In addition, TGN-derived CCVs have previously been found to be important for the sorting of lysosome-targeted hydrolases (Braulke and Bonifacino, 2009), and thus impaired delivery to the lysosomes might further contribute to an overall decreased degradative capacity of neurons. Transcriptome analysis revealed the upregulation of genes involved in the early secretory pathway for ER-Golgi trafficking (Figure 5.7). This might indicate that mutant Auxilin neurons increase ER to cis-Golgi trafficking to compensate for decreased efficiency of post-Golgi trafficking.

Impaired lysosomal clearance and impaired post-Golgi trafficking have been shown to be important for both familial and idiopathic PD pathogenesis, suggesting a mechanistic overlap with disease pathogenesis in Auxilin mutation carriers (see Section 1.1.5). Indeed, Mendelian PD genes, including *LRRK2* and *VPS35*, have been found to play a prominent role in trafficking between Golgi apparatus and endosomes (Beilina *et al.*, 2014; Zavodszky *et al.*, 2014). In addition, multiple

PD risk factors, including *GBA* and *CTSB*, are lysosomal hydrolases and rely on clathrin trafficking for correct sorting to the lysosomes (Nalls *et al.*, 2018). It is thus plausible that impaired post-Golgi clathrin trafficking in the SN may underlie Parkinsonian phenotypes seen in Auxilin mutation carriers. In contrast, impaired clathrin trafficking in other brain regions may well underlie the atypical neurological phenotypes seen in patients, such as seizures and cognitive decline. Deficient retrieval of lipids and proteins may well be detrimental for neuronal survival. In addition, chronic Golgi-stress could result in Golgi stress-mediated apoptosis, ultimately leading to neurodegeneration.

7.3 OPEN QUESTIONS

The data presented in this thesis raise a number of important research questions that fall into two categories, namely research questions related to the role of Auxilin in the aetiology of PD, and research questions related to the physiological function of Auxilin and the functional overlap with its ubiquitous homologue GAK.

Within this thesis the murine R857G Auxilin allele was found to result in decreased Auxilin protein levels in the brain of newborn but not 3 week old mice. It should therefore be addressed whether the equivalent R927G Auxilin allele in human patients may act as a hypomorph as well. In addition, it remains to be elucidated how Auxilin levels are upregulated with age in R857G Auxilin mice. Pathogenic Auxilin splice-site mutations T741= and c.801-2A>G are predicted to result in overall decreased Auxilin expression, but have not formally been shown to result in decreased Auxilin protein levels to prove hypomorphism.

The truncating mutations Q791X and Q846X Auxilin lack the J-domain and it was shown that the R927G mutation likely disrupts the J-domain structure, responsible for interaction with HSC70. However, co-IPs did not reveal impaired interaction with HSC70. It is possible that mutant Auxilin still interacts with HSC70 as a substrate rather than a co-chaperone to aid in solubility and folding of the mutant protein. The exact nature of those interactions should be further explored.

Human neuropathology in Auxilin mutation carriers is unknown to date. However, the R857G animal model presented in this thesis has provided insights into possible underlying neuropathology, including lipid accumulation and synaptic dysfunction. Future experiments will have to elucidate whether the observed

neurological phenotypes can be explained by merely an impaired function of neurons or whether neurodegeneration contributes to disease pathology in R857G Auxilin mice. As Auxilin mutation carriers display an atypical form of PD, different brain regions underlying the variety of phenotypes remain to be studied. In addition, future work is required to determine whether the observed neurological phenotypes are the result of impaired Golgi trafficking, synaptic trafficking or a combination of both.

Golgi stress was observed in neurons derived from R857G Auxilin mice. Two mediators of the Golgi stress response were found to be upregulated, namely GBF1 and CREB3. Whereas GBF1 is involved with protection against Golgi stress, CREB3 initiates Golgi stress-mediated cell death. Thus, coping mechanisms appear to counteract cell death mechanisms in response to Golgi stress. The response to chronic Golgi stress with age should therefore be further analysed.

Pathogenic Auxilin mutations are thought to act through a loss of function mechanism resulting in impaired uncoating of CCV, resulting in inefficient delivery of its cargo to intracellular destination compartments. However, further experiments are required to assess the direct impact on clathrin trafficking pathways and cargo delivery.

Even though this thesis has provided new insights into the physiological role of Auxilin, there are some remaining open questions regarding the exact role of Auxilin and its ubiquitous homologue GAK, in particular at the Golgi apparatus.

Whereas Auxilin interacts with Golgi-resident clathrin adaptor proteins GGA2 and GGA3, GAK interacts with AP1. The exact functional diversity of the different Golgi-resident clathrin adaptor proteins, as well as the physiological relevance of Auxilin and GAK interaction with clathrin adaptor proteins, remains to be

fully understood (see Section 1.3.5). Regardless, the finding that Auxilin and GAK interact with a different subset of Golgi-resident clathrin adaptor proteins raises questions as to the relative uncoating efficiency of Auxilin and GAK of Golgi-derived CCVs with different clathrin adaptor coats. Since all clathrin adaptor proteins are expressed across all cell types, it seems unlikely that Auxilin and GAK would exclusively be involved in the uncoating of GGA-coated or AP1-coated CCVs, respectively. Recently, WDR11 and TBC1D23 were found to regulate the tethering of AP1-coated CCVs (Navarro Negredo *et al.*, 2018; Shin *et al.*, 2017). Whereas WDR11 was detected in the proteomics screen of Auxilin interactors (Supplementary Table 2), *TBC1D23* was found to be upregulated in neurons of R857G Auxilin mice (Supplementary Table 1). These findings indicate that Auxilin may indeed play an important role in the uncoating of AP1-coated CCVs. However, the finding that the neuron-specific Auxilin specifically interacts with GGA2/3 might point to a relative importance of efficient uncoating of GGA2/3-coated vesicles in neurons.

Related to the question of how great a degree of functional redundancy there is between GAK and Auxilin, it is not clear to what extent GAK can compensate for loss of Auxilin function in mutation carriers. Auxilin levels were found to be drastically decreased in the brain of newborn R857G Auxilin mice, and GAK protein levels were transiently upregulated in p2 R857G Auxilin mice. In addition, GAK mRNA levels were found to be upregulated both in newborn and 3 week old R857G Auxilin mice, suggesting the activation of transcriptional mechanisms for the upregulation of GAK in response to loss of Auxilin function. Future work will be required to determine the regulation of Auxilin and GAK levels with age in R857G mice. In addition, it would be interesting to measure GAK and Auxilin levels in the brain of human patients.

Finally, GAK is a risk factor candidate for PD. However, the GAK locus contains multiple other genes, including TMEM175, and it remains to be determined which of those genes is associated with PD. In the light of the findings presented in this thesis, I would argue that the current evidence is slightly against GAK being the risk gene. Under the assumption that variants in the GAK locus were to result in a partial loss of function of GAK and contribute to disease pathogenesis via similar mechanisms as Auxilin loss of function variants, it would be highly likely that mutation carriers would present with multiple systemic manifestations given the ubiquitous expression of GAK. Moreover, since Auxilin is neuron-specific, Auxilin might be able to partially compensate for lack of GAK function in neurons, partially alleviating neurological phenotypes as a consequence of GAK loss of function. However, it can not be ruled out that GAK contributes to PD pathogenesis as a risk factor via different mechanisms than presented for the Auxilin loss-of-function mechanism. More research is thus required to shed light on this complex genetic situation.

7.4 OUTLOOK

The work of this thesis can be continued using different experimental approaches to address the remaining open questions.

In the long term, it would be interesting to address the impact of other pathogenic Auxilin mutations (Q791X, Q846X, T741=. c.801-2A>G) at the cellular level and organismal level. Models with endogenous mutations would be particular suitable for this purpose, since the synonymous T741= mutation and the intronic c.801-2A>G mutation can not be studied using overexpression models that only express the open reading frame of Auxilin. In addition, the impact of pathogenic Auxilin mutations should also be addressed in alternative models with a human background. CRISPR-editing of induced pluripotent stem cells, or stem cells derived from patients and controls, can be differentiated to neurons or brain organoids and would provide a great alternative models to study PD-associated Auxilin mutations.

To gain further insight into the neuropathology of Auxilin mutation carriers, the presented R857G Auxilin mouse model could be analysed for neurological lesions. For example, neuronal firing and neurodegeneration can be analysed using electrophysiology and stereological neuron counts, respectively. In addition, *post mortem* analysis of the brain of human patients would greatly contribute to a neuropathological understanding of PD in Auxilin mutation carriers.

Further research is required to address the temporal regulation of Auxilin and GAK protein levels in R857G Auxilin mice. As Auxilin and GAK levels were only assessed in mice up to 3 weeks of age, more time points should be analysed to elucidate protein dynamics in older mice. In addition, it remains to be elucidated through which mechanisms Auxilin protein is decreased in newborn R857G

mice and primary cultures. Treatment of primary neurons with lysosomal or proteasomal inhibitors would address whether Auxilin is degraded via either of those major protein degradation pathways. In contrast, treatment with translational inhibitors could assess whether Auxilin protein is decreased via impaired or delayed translation of Auxilin mRNA.

The interaction of mutant Auxilin with HSC70 should also be further explored. Even though multiple pathogenic Auxilin mutation result in a complete lack or disruption of the J-domain that is required for Auxilin interaction as a co-chaperone with HSC70, no impairment of interaction was observed using co-IPs. It is possible however that mutant Auxilin becomes a substrate of HSC70, to prevent misfolding of the mutant protein. Generation of HSC70 constructs with mutagenesis of residues that are critical for interaction with Auxilin either as a co-chaperone or as a substrate could be generated to further explore the nature of the interaction of HSC70 with Auxilin.

The impact of mutations on clathrin trafficking pathways and the delivery of clathrin-dependent cargo should also be explored in more detail. For example, impaired Golgi trafficking might result in impaired delivery of multiple cargoes, including (but not limited to) synaptically targeted proteins (e.g. VMAT2) and lysosomal hydrolases (e.g. CTSD). Experiments analysing the transport of individual proteins using the RUSH (retention using selective hooks) system combined with live cell imaging might provide further insight into the impact of Auxilin mutations on cargo delivery (Boncompain *et al.*, 2012). In addition, synaptic vesicular recycling could be assessed using extracellular fluorescent probes, e.g. FM dyes, in combination with TIRF microscopy (Gaffield and Betz, 2006).

One of the main problems in the interpretation on functional relevance of the interaction of Auxilin and GAK with GGA2/3 and AP1, respectively, is the incomplete understanding of the functional differences between different Golgi-resident clathrin adaptor proteins. Endogenous labelling of Auxilin/GAK and clathrin adaptor proteins in combination with (live) super-resolution microscopy could be leveraged to gain further insight into the temporal and spatial organization in the uncoating of CCVs.

Taken together, the findings in this thesis underscore an important role for clathrin trafficking in PD pathogenesis and open up new avenues for therapeutic strategies. Response to L-DOPA, the first-line treatment in PD, is either absent or limited due to severe side-effects in Auxilin mutation carriers. Further dissection of clathrin-dependent pathways in neurons is therefore of particular interest to find novel potential therapeutic targets. Moreover, the presented R857G Auxilin mouse model could be a valuable platform to screen for potential drugs, given its high construct and face validity.

8 REFERENCES

Ahle, S and Ungewickell, E (1990). "Auxilin, a newly identified clathrin-associated protein in coated vesicles from bovine brain". In: *The Journal of Cell Biology* 111.1, pp. 19–29

Ahle, S., Mann, A., Eichelsbacher, U., and Ungewickell, E. (1988). "Structural relationships between clathrin assembly proteins from the Golgi and the plasma membrane". In: *The EMBO Journal* 7.4, pp. 919–929

Altschul, S. F., Gish, W., Miller, W., Myers, E. W., and Lipman, D. J. (1990). "Basic local alignment search tool". In: *Journal of Molecular Biology* 215.3, pp. 403–410

Alvarez, E, Gironès, N, and Davis, R. J. (1990a). "A point mutation in the cytoplasmic domain of the transferrin receptor inhibits endocytosis". In: *Biochemical Journal* 267.1, pp. 31–35

Alvarez, E, Gironès, N, and Davis, R. J. (1990b). "Inhibition of the receptor-mediated endocytosis of diferric transferrin is associated with the covalent modification of the transferrin receptor with palmitic acid". In: *The Journal of biological chemistry* 265.27, pp. 16644–55

Anderson, R. G., Goldstein, J. L., and Brown, M. S. (1977a). "A mutation that impairs the ability of lipoprotein receptors to localise in coated pits on the cell surface of human fibroblasts". In: *Nature* 270.5639, pp. 695–9

Anderson, R. G. W., Goldstein, J. L., and Brown, M. S. (1977b). "A mutation that impairs the ability of lipoprotein receptors to localise in coated pits on the cell surface of human fibroblasts". In: *Nature* 270.5639, pp. 695–699

Arighi, C. N., Hartnell, L. M., Aguilar, R. C., Haft, C. R., and Bonifacino, J. S. (2004). "Role of the mammalian retromer in sorting of the cation-independent mannose 6-phosphate receptor". In: *Journal of Cell Biology* 165.1, pp. 123–133

Austin, C, Hinners, I, and Tooze, S. A. (2000). "Direct and GTP-dependent interaction of ADP-ribosylation factor 1 with clathrin adaptor protein AP-1 on immature secretory granules". In: *The Journal of Biological Chemistry* 275.29, pp. 21862–21869

Avinoam, O., Schorb, M., Beese, C. J., Briggs, J. A. G., and Kaksonen, M. (2015). "Endocytic sites mature by continuous bending and remodeling of the clathrin coat". In: *Science* 348.6241, pp. 1369–1372

Bai, H., Doray, B., and Kornfeld, S. (2004). "GGA1 interacts with the adaptor protein AP-1 through a WNSF sequence in its hinge region". In: *The Journal of Biological Chemistry* 279.17, pp. 17411–17447

Beilina, A., Rudenko, I. N., Kaganovich, A., Civiero, L., Chau, H., Kalia, S. K., Kalia, L. V., Lobbestael, E., Chia, R., Ndukwe, K., Ding, J., Nalls, M. a., Olszewski, M., Hauser, D. N., Kumaran, R., Lozano, A. M., Baekelandt, V., Greene, L. E., Taymans, J.-M., Greggio, E., and Cookson, M. R. (2014). "Unbiased screen for interactors of leucine-rich repeat kinase 2 supports a common pathway for sporadic and familial Parkinson disease". In: *Proceedings of the National Academy of Sciences of the United States of America* 111.7, pp. 2626–2631

Bertler, A and Rosengren, E (1959). "Occurrence and distribution of catechol amines in brain". In: *Acta Physiologica Scandinavica* 47, pp. 350–361

Böcking, T., Aguet, F., Harrison, S. C., and Kirchhausen, T. (2011). "Single-molecule analysis of a molecular disassemblase reveals the mechanism of Hsc70-driven clathrin uncoating". In: *Nature Structural & Molecular Biology* 18.3, pp. 295–301

Boll, W., Ohno, H., Songyang, Z., Rapoport, I., Cantley, L. C., Bonifacino, J. S., and Kirchhausen, T. (1996). "Sequence requirements for the recognition of tyrosine-based endocytic signals by clathrin AP-2 complexes". In: *The EMBO Journal* 15.21, pp. 5789–5795

Boll, W., Rapoport, I., Brunner, C., Modis, Y., Prehn, S., and Kirchhausen, T. (2002). "The mu2 Subunit of the Clathrin Adaptor AP-2 Binds to FDNPVY and YppO Sorting Signals at Distinct Sites". In: *Traffic* 3.8, pp. 590–600

Boman, A. L., Zhang, C. j., Zhu, X, and Kahn, R. A. (2000). "A family of ADP-ribosylation factor effectors that can alter membrane transport through the trans-Golgi". In: *Molecular Biology of the Cell* 11.4, pp. 1241–1255

Boncompain, G., Divoux, S., Gareil, N., Forges, H. DE, Lescure, A., Latreche, L., Mercanti, V., Jollivet, F., Raposo, G., and Perez, F. (2012). "Synchronization

of secretory protein traffic in populations of cells". In: *Nature Methods* 9.5, pp. 493–498

Bonifacino, J. S. (2004). "The GGA proteins: adaptors on the move". In: *Nature Reviews Molecular Cell Biology* 5.1, pp. 23–32

Bonifacino, J. S. and Traub, L. M. (2003). "Signals for Sorting of Transmembrane Proteins to Endosomes and Lysosomes". In: *Annual Review of Biochemistry* 72.1, pp. 395–447

Bonifati, V., Rizzu, P., Baren, M. J. VAN, Schaap, O., Breedveld, G. J., Krieger, E., Dekker, M. C. J., Squitieri, F., Ibanez, P., Joosse, M., Dongen, J. W. VAN, Vanacore, N., Swieten, J. C. VAN, Brice, A., Meco, G., Duijn, C. M. VAN, Oostra, B. a., and Heutink, P. (2003). "Mutations in the DJ-1 gene associated with autosomal recessive early-onset parkinsonism". In: *Science* 299, pp. 256–259

Borner, G. H. H., Harbour, M., Hester, S., Lilley, K. S., and Robinson, M. S. (2006). "Comparative proteomics of clathrin-coated vesicles." In: *The Journal of cell biology* 175.4, pp. 571–8

Borner, G. H., Antrobus, R., Hirst, J., Bhumbra, G. S., Kozik, P., Jackson, L. P., Sahlender, D. A., and Robinson, M. S. (2012). "Multivariate proteomic profiling identifies novel accessory proteins of coated vesicles". In: *The Journal of Cell Biology* 197.1, pp. 141–160

Braak, H., Tredici, K. D., Rüb, U., Vos, R. A.I DE, Jansen Steur, E. N., and Braak, E. (2003). "Staging of brain pathology related to sporadic Parkinson's disease". In: *Neurobiology of Aging* 24, pp. 197–211

Braak, H., Ghebremedhin, E., Rüb, U., Bratzke, H., and Del Tredici, K. (2004). "Stages in the development of Parkinson's disease-related pathology". In: *Cell and Tissue Research* 318, pp. 121–134

Braak, H., Vos, R. A. DE, Bohl, J., and Del Tredici, K. (2006). "Gastric α-synuclein immunoreactive inclusions in Meissner's and Auerbach's plexuses in cases staged for Parkinson's disease-related brain pathology". In: *Neuroscience Letters* 396.1, pp. 67–72

Braell, W. A., Schlossman, D. M., Schmid, S. L., and Rothman, J. E. (1984). "Dissociation of clathrin coats coupled to the hydrolysis of ATP: role of an uncoating ATPase". In: *The Journal of Cell Biology* 99.2, pp. 734–741

Braulke, T. and Bonifacino, J. S. (2009). "Sorting of lysosomal proteins". In: *Biochimica et Biophysica Acta* 1793.4, pp. 605–614

Brown, M. S. and Goldstein, J. L. (1976). "Analysis of a mutant strain of human fibroblasts with a defect in the internalization of receptor-bound low density lipoprotein". In: *Cell* 9.4, pp. 663–674

Bucher, D., Frey, F., Sochacki, K. A., Kummer, S., Bergeest, J.-P., Godinez, W. J., Kräusslich, H.-G., Rohr, K., Taraska, J. W., Schwarz, U. S., and Boulant, S. (2018). "Clathrin-adaptor ratio and membrane tension regulate the flat-to-curved transition of the clathrin coat during endocytosis". In: *Nature Communications* 9.1109

Burré, J., Sharma, M., Tsetsenis, T., Buchman, V., Etherton, M. R., and Südhof, T. C. (2010). "α-Synuclein promotes SNARE-complex assembly in vivo and in vitro". In: *Science* 329, pp. 107–110

Busch, D. J., Houser, J. R., Hayden, C. C., Sherman, M. B., Lafer, E. M., and Stachowiak, J. C. (2015). "Intrinsically disordered proteins drive membrane curvature". In: *Nature Communications* 6.7875

Cao, M., Wu, Y., Ashrafi, G., Ellisman, M. H., Ryan, T. A., Camilli, P. D., Cao, M., Wu, Y., Ashrafi, G., Mccartney, A. J., Wheeler, H., Bushong, E. A., Boassa, D., Ellisman, M. H., Ryan, T. A., and Camilli, P. D. (2017). "Parkinson Sac Domain Mutation in Synaptojanin 1 Impairs Clathrin Uncoating at Synapses and Triggers Dystrophic Changes in Dopaminergic Axons Article Parkinson Sac Domain Mutation in Synaptojanin 1 Impairs Clathrin Uncoating at Synapses and Triggers Dystro". In: *Neuron* 93.4, pp. 882–896

Carlsson, A, Lindqvist, M, Magnusson, T, and Waldeck, B (1958). "On the presence of 3-hydroxytyramine in brain". In: *Science* 127.3296, p. 471

Carter, R. J., Morton, J., and Dunnett, S. B. (2001). "Motor Coordination and Balance in Rodents". In: *Current Protocols in Neuroscience* 15.1

Chappie, J. S., Acharya, S., Leonard, M., Schmid, S. L., and Dyda, F. (2010). "G domain dimerization controls dynamin's assembly-stimulated GTPase activity". In: *Nature* 465.7297, pp. 435–440

Chappie, J. S., Mears, J. A., Fang, S., Leonard, M., Schmid, S. L., Milligan, R. A., Hinshaw, J. E., and Dyda, F. (2011). "A pseudoatomic model of the dynamin polymer identifies a hydrolysis-dependent powerstroke". In: *Cell* 147.1, pp. 209–222

Charcot, J.-M. (1872). "De la paralysie agitante". In: *Oeuvres Complètes: Leçons sur les maladies du système nerveux*, pp. 155–188

Chartier-Harlin, M.-C., Kachergus, Jennifer Roumier, C., Mouroux, V., Douay, X., Lincoln, S., Levecque, C., Larvor, L., Andrieux, J., Hulihan, M., Waucquier, N., Defebvre, D., Amouyel, P., and Farrer, M. (2004). "α-synuclein locus duplication as a cause of familial Parkinson's disease". In: *Lancet* 364.9440, pp. 1167–1169

Chen, C.-Y., Reese, M. L., Hwang, P. K., Ota, N., Agard, D., and Brodsky, F. M. (2002). "Clathrin light and heavy chain interface: alpha-helix binding superhelix loops via critical tryptophans". In: *The EMBO journal* 21.22, pp. 6072–6082

Chen, H. J., Yuan, J, and Lobel, P (1997). "Systematic mutational analysis of the cation-independent mannose 6-phosphate/insulin-like growth factor II receptor cytoplasmic domain". In: *The Journal of Biological Chemistry* 272.11, pp. 7003–7012

Chen, W. J., Goldstein, J. L., and Brown, M. S. (1990). "NPXY, a sequence often found in cytoplasmic tails, is required for coated pit-mediated internalization of the low density lipoprotein receptor". In: *The Journal of Biological Chemistry* 265, pp. 3116–3123

Cheng, Y., Boll, W., Kirchhausen, T., Harrison, S. C., and Walz, T. (2007). "Cryo-electron Tomography of Clathrin-coated Vesicles: Structural Implications for Coat Assembly". In: *Journal of Molecular Biology* 365.3, pp. 892–899

Chesselet, M.-F. and Richter, F. (2011). "Modelling of Parkinson's disease in mice". In: *Lancet Neurology* 10, pp. 1108–1118

Chin, L. S., Raynor, M. C., Wei, X, Chen, H. Q., and Li, L (2001). "Hrs interacts with sorting nexin 1 and regulates degradation of epidermal growth factor receptor". In: *The Journal of Biological Chemistry* 276.10, pp. 7069–7078

Cocucci, E., Aguet, F., Boulant, S., and Kirchhausen, T. (2012). "The first five seconds in the life of a clathrin-coated pit". In: *Cell* 150.3, pp. 495–507

Collawn, J. F., Stangel, M., Kuhn, L. A., Esekogwu, V., Jing, S., Trowbridge, I. S., and Tainer, J. A. (1990). "Transferrin receptor internalization sequence YXRF implicates a tight turn as the structural recognition motif for endocytosis". In: *Cell* 63.5, pp. 1061–1072

Collins, B. M., McCoy, A. J., Kent, H. M., Evans, P. R., and Owen, D. J. (2002). "Molecular Architecture and Functional Model of the Endocytic AP2 Complex". In: *Cell* 109.4, pp. 523–535

Collins, B. M., Praefcke, G. J. K., Robinson, M. S., and Owen, D. J. (2003a). "Structural basis for binding of accessory proteins by the appendage domain of GGAs". In: *Nature Structural & Molecular Biology* 10.8, pp. 607–613

Collins, B. M., Watson, P. J., and Owen, D. J. (2003b). "The Structure of the GGA1-GAT Domain Reveals the Molecular Basis for ARF Binding and Membrane Association of GGAs". In: *Developmental Cell* 4.3, pp. 321–332

Conway, K. a., Harper, J. D., and Lansbury, P. T. (1998). "Accelerated in vitro fibril formation by a mutant α-synuclein linked to early-onset Parkinson disease". In: *Nature Medicine* 4.11, pp. 1318–1320

Costaguta, G., Stefan, C. J., Bensen, E. S., Emr, S. D., and Payne, G. S. (2001). "Yeast Gga Coat Proteins Function with Clathrin in Golgi to Endosome Transport". In: *Molecular Biology of the Cell* 12.6, pp. 1885–1896

Cremona, O, Di Paolo, G, Wenk, M. R., Lüthi, A, Kim, W. T., Takei, K, Daniell, L, Nemoto, Y, Shears, S. B., Flavell, R. A., McCormick, D. A., and De Camilli, P (1999). "Essential role of phosphoinositide metabolism in synaptic vesicle recycling". In: *Cell* 99.2, pp. 179–188

Crowther, R., Pinch, J., and Pearse, B. (1976). "On the structure of coated vesicles". In: *Journal of Molecular Biology* 103.4, pp. 785–798

Daboussi, L., Costaguta, G., and Payne, G. S. (2012a). "Phosphoinositide-mediated clathrin adaptor progression at the trans-Golgi network". In: *Nature Cell Biology* 14.3, pp. 239–248

Daboussi, L., Costaguta, G., and Payne, G. S. (2012b). "Phosphoinositide-mediated clathrin adaptor progression at the trans-Golgi network". In: *Nature Cell Biology* 14.3, pp. 239–248

Dauer, W. and Przedborski, S. (2003). "Parkinson's disease: mechanisms and models". In: *Neuron* 39, pp. 889–909

Davis, C. G., Lehrman, M. A., Russell, D. W., Anderson, R. G., Brown, M. S., and Goldstein, J. L. (1986). "The J.D. mutation in familial hypercholesterolemia: amino acid substitution in cytoplasmic domain impedes internalization of LDL receptors". In: *Cell* 45.1, pp. 15–24

Dawson, T. M., Ko, H. S., and Dawson, V. L. (2010). "Genetic animal models of Parkinson's disease". In: *Neuron* 66.5, pp. 646–661

Dell'Angelica, E. C., Ohno, H., Ooi, C. E., Rabinovich, E., Roche, K. W., and Bonifacino, J. S. (1997a). "AP3: an adaptorlike protein complex with ubiquitous expression". In: *The EMBO Journal* 16.5, pp. 917–928

Dell'Angelica, E. C., Ooi, C. E., and Bonifacino, J. S. (1997b). "Beta3A-adaptin, a subunit of the adaptor-like complex AP-3". In: *The Journal of Biological Chemistry* 272.24, pp. 15078–15084

Dell'Angelica, E. C., Klumperman, J, Stoorvogel, W, and Bonifacino, J. S. (1998). "Association of the AP-3 adaptor complex with clathrin". In: *Science* 280.5362, pp. 431–434

Dell'Angelica, E. C., Mullins, C, and Bonifacino, J. S. (1999). "AP-4, a novel protein complex related to clathrin adaptors". In: *The Journal of Biological Chemistry* 274.11, pp. 7278–7285

Dell'Angelica, E. C., Puertollano, R, Mullins, C, Aguilar, R. C., Vargas, J. D., Hartnell, L. M., and Bonifacino, J. S. (2000). "GGAs: a family of ADP ribosylation factor-binding proteins related to adaptors and associated with the Golgi complex". In: *The Journal of Cell Biology* 149.1, pp. 81–94

DeLorey, T. M., Sahbaie, P., Hashemi, E., Li, W.-W., Salehi, A., and Clark, D. J. (2011). "Somatosensory and sensorimotor consequences associated with the

heterozygous disruption of the autism candidate gene, Gabrb3". In: *Behavioural Brain Research* 216.1, pp. 36–45

Deng, H.-X., Shi, Y., Yang, Y., Ahmeti, K. B., Miller, N., Huang, C., Cheng, L., Zhai, H., Deng, S., Nuytemans, K., Corbett, N. J., Kim, M. J., Deng, H., Tang, B., Yang, Z., Xu, Y., Chan, P., Huang, B., Gao, X.-P., Song, Z., Liu, Z., Fecto, F., Siddique, N., Foroud, T., Jankovic, J., Ghetti, B., Nicholson, D. A., Krainc, D., Melen, O., Vance, J. M., Pericak-Vance, M. A., Ma, Y.-C., Rajput, A. H., and Siddique, T. (2016). "Identification of TMEM230 mutations in familial Parkinson's disease". In: *Nature Genetics* 48.7, pp. 733–739

Derivery, E., Sousa, C., Gautier, J. J., Lombard, B., Loew, D., and Gautreau, A. (2009). "The Arp2/3 Activator WASH Controls the Fission ofEndosomes through a Large Multiprotein Complex". In: *Developmental Cell* 17.5, pp. 712–723

Di Fonzo, A., Rohe, C., Ferreira, J., Chien, H., Vacca, L., Stocchi, F., Guedes, L., Fabrizio, E., Manfredi, M., and Vanacore, N. (2005). "A frequent gene mutation associated with autosomal dominant Parkinson's disease". In: *The Lancet* 365, pp. 412–415

Di Fonzo, A, Dekker, M. C. J., Montagna, P, Baruzzi, A, Yonova, E. H., Correia Guedes, L, Szczerbinska, A, Zhao, T, Dubbel-Hulsman, L. O. M., Wouters, C. H., Graaff, E DE, Oyen, W. J. G., Simons, E. J., Breedveld, G. J., Oostra, B. A., Horstink, M. W., and Bonifati, V (2009). "FBXO7 mutations cause autosomal recessive, early-onset parkinsonian-pyramidal syndrome". In: *Neurology* 72.3, pp. 240–245

Di Paolo, G. and De Camilli, P. (2006). "Phosphoinositides in cell regulation and membrane dynamics". In: *Nature* 443.7112, pp. 651–657

Dick, R. J., Byron, K. a., and Dear, a. E. (2013). "A novel α-synuclein missense mutation in Parkinson disease". In: *Neurology* 80, pp. 1062–1064

Doench, J. G., Fusi, N., Sullender, M., Hegde, M., Vaimberg, E. W., Donovan, K. F., Smith, I., Tothova, Z., Wilen, C., Orchard, R., Virgin, H. W., Listgarten, J., and Root, D. E. (2016). "Optimized sgRNA design to maximize activity and minimize off-target effects of CRISPR-Cas9". In: *Nature Biotechnology* 34.2, pp. 184–191

Donaldson, J. G. and Jackson, C. L. (2000). "Regulators and effectors of the ARF GTPases". In: *Current Opinion in Cell Biology* 12.4, pp. 475–482

Doray, B., Bruns, K., Ghosh, P., and Kornfeld, S. A. (2002a). "Autoinhibition of the ligand-binding site of GGA1/3 VHS domains by an internal acidic cluster-dileucine motif". In: *Proceedings of the National Academy of Sciences of the United States of America* 99.12, pp. 8072–8077

Doray, B., Ghosh, P., Griffith, J., Geuze, H. J., and Kornfeld, S. (2002b). "Cooperation of GGAs and AP-1 in packaging MPRs at the trans-Golgi network". In: *Science* 297.5587, pp. 1700–1703

Dorsey, E. R., Constantinescu, R, Thompson, J. P., Biglan, K. M., Holloway, R. G., Kieburtz, K, Marshall, F. J., Ravina, B. M., Schifitto, G, Siderowf, A, and Tanner, C. M. (2007). "Projected number of people with Parkinson disease in the most populous nations, 2005 through 2030". In: *Neurology* 68.5, pp. 384–386

Drake, M. T., Downs, M. A., and Traub, L. M. (2000). "Epsin binds to clathrin by associating directly with the clathrin-terminal domain. Evidence for cooperative binding through two discrete sites". In: *The Journal of Biological Chemistry* 275.9, pp. 6479–6489

Dranka, B. P., Gifford, A., McAllister, D., Zielonka, J., Joseph, J., O'Hara, C. L., Stucky, C. L., Kanthasamy, A. G., and Kalyanaraman, B. (2014). "A novel mitochondrially-targeted apocynin derivative prevents hyposmia and loss of motor function in the leucine-rich repeat kinase 2 (LRRK2 R1441G) transgenic mouse model of Parkinson's disease". In: *Neuroscience Letters* 583, pp. 159–164

D'Souza-Schorey, C. and Chavrier, P. (2006). "ARF proteins: roles in membrane traffic and beyond". In: *Nature Reviews Molecular Cell Biology* 7.5, pp. 347–358

Edvardson, S., Cinnamon, Y., Ta-Shma, A., Shaag, A., Yim, Y. I., Zenvirt, S., Jalas, C., Lesage, S., Brice, A., Taraboulos, A., Kaestner, K. H., Greene, L. E., and Elpeleg, O. (2012). "A deleterious mutation in DNAJC6 encoding the neuronal-specific clathrin-uncoating co-chaperone auxilin, is associated with juvenile parkinsonism". In: *PLoS ONE* 7.5, pp. 4–8

Ehringer, H and Hornykiewicz, O (1960). "Distribution of noradrenaline and dopamine (3-hydroxytyramine) in the human brain and their behavior in

diseases of the extrapyramidal system". In: *Klinische Wochenschrift* 38, pp. 1236–1239

Ehrlich, M., Boll, W., Oijen, A. VAN, Hariharan, R., Chandran, K., Nibert, M. L., and Kirchhausen, T. (2004). "Endocytosis by random initiation and stabilization of clathrin-coated pits". In: *Cell* 118.5, pp. 591–605

Elsayed, L. E. O., Drouet, V., Usenko, T., Mohammed, I. N., Hamed, A. A. A., Elseed, M. A., Salih, M. A., Koko, M. E., Mohamed, A. Y. O., Siddig, R. A., Elbashir, M. I., Ibrahim, M. E., Durr, A., Stevanin, G., Lesage, S., Ahmed, A. E., and Brice, A. (2016). "A novel nonsense mutation in DNAJC6 expands the phenotype of autosomal-recessive juvenile-onset Parkinson's disease". In: *Annals of Neurology* 79.2, pp. 335–337

Faelber, K., Posor, Y., Gao, S., Held, M., Roske, Y., Schulze, D., Haucke, V., Noé, F., and Daumke, O. (2011). "Crystal structure of nucleotide-free dynamin". In: *Nature* 477.7366, pp. 556–560

Fahn, S. (2003). "Description of Parkinson's disease as a clinical sydrome". In: *Annals New York Academy of Sciences* 991, pp. 1–14

Fang, P., Li, X., Wang, J., Niu, L., and Teng, M. (2010). "Structural Basis for the Specificity of the GAE Domain of yGGA2 for Its Accessory Proteins Ent3 and Ent5". In: *Biochemistry* 49.36, pp. 7949–7955

Fearnley, J. M. and Lees, A. J. (1991). "Ageing and Parkinson's disease: substantia nigra regional selectivity". In: *Brain* 114, pp. 2283–2301

Feigin, V. L. *et al.* (2017). "Global, regional, and national burden of neurological disorders during 19902015: a systematic analysis for the Global Burden of Disease Study 2015". In: *The Lancet Neurology* 16.11, pp. 877–897

Fernandes, H., Hartfield, E., Christian, H., Emmanoulidou, E., Zheng, Y., Booth, H., Bogetofte, H., Lang, C., Ryan, B., Sardi, S., Badger, J., Vowles, J., Evetts, S., Tofaris, G., Vekrellis, K., Talbot, K., Hu, M., James, W., Cowley, S., and Wade-Martins, R. (2016). "ER Stress and Autophagic Perturbations Lead to Elevated Extracellular α-Synuclein in GBA-N370S Parkinson's iPSC-Derived Dopamine Neurons". In: *Stem Cell Reports* 6.3, pp. 342–356

Fingerhut, A, Figura, K von, and Honing, S (2001). "Binding of AP2 to sorting signals is modulated by AP2 phosphorylation". In: *The Journal of Biological Chemistry* 276.8, pp. 5476–5482

Fjorback, A. W., Seaman, M., Gustafsen, C., Mehmedbasic, A., Gokool, S., Wu, C., Militz, D., Schmidt, V., Madsen, P., Nyengaard, J. R., Willnow, T. E., Christensen, E. I., Mobley, W. B., Nykjær, A., and Andersen, O. M. (2012). "Retromer binds the FANSHY sorting motif in SorLA to regulate amyloid precursor protein sorting and processing". In: *The Journal of Neuroscience* 32.4, pp. 1467–1480

Follett, J., Norwood, S. J., Hamilton, N. A., Mohan, M., Kovtun, O., Tay, S., Zhe, Y., Wood, S. A., Mellick, G. D., Silburn, P. A., Collins, B. M., Bugarcic, A., and Teasdale, R. D. (2014). "The VPS35 D620N mutation linked to Parkinson's disease disrupts the cargo sorting function of retromer". In: *Traffic* 15.2, pp. 230–244

Foo, J. N., Liany, H., Tan, L. C., Au, W.-L., Prakash, K.-M., Liu, J., and Tan, E.-K. (2014). "DNAJ mutations are rare in Chinese Parkinson's disease patients and controls". In: *Neurobiology of Aging* 35.4

Ford, M. G. J., Mills, I. G., Peter, B. J., Vallis, Y., Praefcke, G. J. K., Evans, P. R., and McMahon, H. T. (2002). "Curvature of clathrin-coated pits driven by epsin". In: *Nature* 419.6905, pp. 361–366

Ford, M. G. J., Jenni, S., and Nunnari, J. (2011). "The crystal structure of dynamin". In: *Nature* 477.7366, pp. 561–566

Fotin, A., Cheng, Y., Sliz, P., Grigorieff, N., Harrison, S. C., Kirchhausen, T., and Walz, T. (2004a). "Molecular model for a complete clathrin lattice from electron cryomicroscopy". In: *Nature* 432.7017, pp. 573–579

Fotin, A., Cheng, Y., Grigorieff, N., Walz, T., Harrison, S. C., and Kirchhausen, T. (2004b). "Structure of an auxilin-bound clathrin coat and its implications for the mechanism of uncoating". In: *Nature* 432.7017, pp. 649–653

Freeman, C. L., Hesketh, G., and Seaman, M. N. J. (2014). "RME-8 coordinates the activity of the WASH complex with the function of the retromer SNX dimer to control endosomal tubulation". In: *Journal of Cell Science* 127.9, pp. 2053–70

Frost, A., Perera, R., Roux, A., Spasov, K., Destaing, O., Egelman, E. H., De Camilli, P., and Unger, V. M. (2008). "Structural basis of membrane invagination by F-BAR domains". In: *Cell* 132.5, pp. 807–817

Fujibayashi, A., Taguchi, T., Misaki, R., Ohtani, M., Dohmae, N., Takio, K., Yamada, M., Gu, J., Yamakami, M., Fukuda, M., Waguri, S., Uchiyama, Y., Yoshimori, T., and Sekiguchi, K. (2008). "Human RME-8 Is Involved in Membrane Trafficking through Early Endosomes". In: *Cell Structure and Function* 33.1, pp. 35–50

Fujita, H., Saeki, M., Yasunaga, K., Ueda, T., Imoto, T., and Himeno, M. (1999). "In Vitro Binding Study of Adaptor Protein Complex (AP-1) to Lysosomal Targeting Motif (LI-Motif)". In: *Biochemical and Biophysical Research Communications* 255.1, pp. 54–58

Gaffield, M. A. and Betz, W. J. (2006). "Imaging synaptic vesicle exocytosis and endocytosis with FM dyes". In: *Nature Protocols* 1.6, pp. 2916–2921

Gaidarov, I and Keen, J. H. (1999). "Phosphoinositide-AP-2 interactions required for targeting to plasma membrane clathrin-coated pits". In: *The Journal of Cell Biology* 146.4, pp. 755–764

Gall, W. E., Higginbotham, M. A., Chen, C, Ingram, M. F., Cyr, D. M., and Graham, T. R. (2000). "The auxilin-like phosphoprotein Swa2p is required for clathrin function in yeast." In: *Current biology : CB* 10.21, pp. 1349–58

Gallop, J. L., Jao, C. C., Kent, H. M., Butler, P. J. G., Evans, P. R., Langen, R., and McMahon, H. T. (2006). "Mechanism of endophilin NBAR domainmediated membrane curvature". In: *The EMBO Journal* 25.12, pp. 2898–2910

GBD 2016 Parkinson's Disease Collaborators, E. R., Elbaz, A., Nichols, E., Abd-Allah, F., Abdelalim, A., Adsuar, J. C., Ansha, M. G., Brayne, C., Choi, J.-Y. J., Collado-Mateo, D., Dahodwala, N., Do, H. P., Edessa, D., Endres, M., Fereshtehnejad, S.-M., Foreman, K. J., Gankpe, F. G., Gupta, R., Hankey, G. J., Hay, S. I., Hegazy, M. I., Hibstu, D. T., Kasaeian, A., Khader, Y., Khalil, I., Khang, Y.-H., Kim, Y. J., Kokubo, Y., Logroscino, G., Massano, J., Ibrahim, N. M., Mohammed, M. A., Mohammadi, A., Moradi-Lakeh, M., Naghavi, M., Nguyen, B. T., Nirayo, Y. L., Ogbo, F. A., Owolabi, M. O., Pereira, D. M., Postma, M. J., Qorbani, M., Rahman, M. A., Roba, K. T., Safari, H., Safiri, S., Satpathy, M., Sawhney, M., Shafieesabet, A., Shiferaw, M. S., Smith,

M., Szoeke, C. E. I., Tabarés-Seisdedos, R., Truong, N. T., Ukwaja, K. N., Venketasubramanian, N., Villafaina, S., Weldegwergs, K. GIDEY, Westerman, R., Wijeratne, T., Winkler, A. S., Xuan, B. T., Yonemoto, N., Feigin, V. L., Vos, T., and Murray, C. J. L. (2018). "Global, regional, and national burden of Parkinson's disease, 1990-2016: a systematic analysis for the Global Burden of Disease Study 2016". In: *The Lancet Neurology*

Ghosh, P. and Kornfeld, S. (2003). "AP-1 binding to sorting signals and release from clathrin-coated vesicles is regulated by phosphorylation". In: *The Journal of Cell Biology* 160.5, pp. 699–708

Ghosh, P., Griffith, J., Geuze, H. J., and Kornfeld, S. (2003). "Mammalian GGAs act together to sort mannose 6-phosphate receptors". In: *The Journal of Cell Biology* 163.4, pp. 755–766

Giasson, B. I., Uryu, K., Trojanowski, J., and Lee, V. (1999). "Mutant and wild type human α-synucleins assemble into elongated filaments with distinct morphologies in vitro". In: *The Journal of Biological Chemistry* 274.12, pp. 7619–7622

Gibb, W. R. and Lees, A. J. (1988). "The relevance of the Lewy body to the pathogenesis of idiopathic Parkinson's disease". In: *Journal of Neurology, Neurosurgery, and Psychiatry* 51.6, pp. 745–752

Girard, M., Poupon, V., Blondeau, F., and McPherson, P. S. (2005). "The DnaJ-domain protein RME-8 functions in endosomal trafficking". In: *The Journal of Biological Chemistry* 280.48, pp. 40135–40143

Goldman, J. G. and Postuma, R. (2014). "Premotor and nonmotor features of Parkinsons disease". In: *Current Opinion in Neurology* 27.4, pp. 434–441

Goldstein, J. L., Brown, M. S., and Stone, N. J. (1977). "Genetics of the LDL receptor: evidence that the mutations affecting binding and internalization are allelic". In: *Cell* 12.3, pp. 629–41

Goldstein, J. L., Anderson, R. G., and Brown, M. S. (1979). "Coated pits, coated vesicles, and receptor-mediated endocytosis". In: *Nature* 279.5715, pp. 679–85

Gomez, T. S. and Billadeau, D. D. (2009). "A FAM21-Containing WASH Complex Regulates Retromer-Dependent Sorting". In: *Developmental Cell* 17.5, pp. 699–711

Govero, J., Doray, B., Bai, H., and Kornfeld, S. (2012). "Analysis of Gga Null Mice Demonstrates a Non-Redundant Role for Mammalian GGA2 during Development". In: *PLoS ONE* 7.1

Greenbaum, E. a., Graves, C. L., Mishizen-Eberz, A. J., Lupoli, M. a., Lynch, D. R., Englander, S. W., Axelsen, P. H., and Giasson, B. I. (2005). "The E46K mutation in α-synuclein increases amyloid fibril formation". In: *Journal of Biological Chemistry* 280.9, pp. 7800–7807

Greener, T, Zhao, X, Nojima, H, Eisenberg, E, and Greene, L. E. (2000). "Role of cyclin G-associated kinase in uncoating clathrin-coated vesicles from non-neuronal cells". In: *The Journal of Biological Chemistry* 275.2, pp. 1365–1370

Greener, T., Grant, B., Zhang, Y., Wu, X., Greene, L. E., Hirsh, D., and Eisenberg, E. (2001). "Caenorhabditis elegans auxilin: a J-domain protein essential for clathrin-mediated endocytosis in vivo". In: *Nature Cell Biology* 3.2, pp. 215–219

Greenfield, J. G. and Bosanquet, F. D. (1953). "The brain-stem lesions in Parkinsonism". In: *Journal of Neurology, Neurosurgery, and Psychiatry* 16.4, pp. 213–226

Gruschus, J. M., Han, C. J., Greener, T., Ferretti, J. A., Greene, L. E., and Eisenberg, E. (2004). "Structure of the Functional Fragment of Auxilin Required for Catalytic Uncoating of Clathrin-Coated Vesicles". In: *Biochemistry* 43.11, pp. 3111–3119

Guan, R., Dai, H., Han, D., Harrison, S. C., and Kirchhausen, T. (2010). "Structure of the PTEN-like region of auxilin, a detector of clathrin-coated vesicle budding". In: *Structure* 18.9, pp. 1191–1198

Gustavsson, E. K., Trinh, J., Guella, I., Vilariño-Güell, C., Appel-Cresswell, S., Stoessl, A. J., Tsui, J. K., McKeown, M., Rajput, A., Rajput, A. H., Aasly, J. O., and Farrer, M. J. (2015). "DNAJC13 genetic variants in parkinsonism". In: *Movement Disorders* 30.2, pp. 273–278

Haar, E ter, Harrison, S. C., and Kirchhausen, T (2000). "Peptide-in-groove interactions link target proteins to the beta-propeller of clathrin". In: *Proceedings of the National Academy of Sciences of the United States of America* 97.3, pp. 1096–1100

Haar, E. ter, Musacchio, A., Harrison, S. C., and Kirchhausen, T. (1998). "Atomic Structure of Clathrin: A β Propeller Terminal Domain Joins an α Zigzag Linker". In: *Cell* 95.4, pp. 563–573

Hagedorn, E. J., Bayraktar, J. L., Kandachar, V. R., Bai, T., Englert, D. M., and Chang, H. C. (2006). "Drosophila melanogaster auxilin regulates the internalization of Delta to control activity of the Notch signaling pathway". In: *The Journal of Cell Biology* 173.3, pp. 443–452

Harbour, M. E., Breusegem, S. Y. A., Antrobus, R., Freeman, C., Reid, E., and Seaman, M. N. J. (2010). "The cargo-selective retromer complex is a recruiting hub for protein complexes that regulate endosomal tubule dynamics". In: *Journal of Cell Science* 123.21, pp. 3703–3717

Hardy, J., Lewis, P., Revesz, T., Lees, A., and Paisan-Ruiz, C. (2009). "The genetics of Parkinson's syndromes: a critical review". In: *Current Opinion in Genetics and Development* 19, pp. 254–265

Harter, C and Mellman, I (1992). "Transport of the lysosomal membrane glycoprotein lgp120 (lgp-A) to lysosomes does not require appearance on the plasma membrane". In: *The Journal of Cell Biology* 117.2, pp. 311–325

Hartl, D., Irmler, M., Römer, I., Mader, M. T., Mao, L., Zabel, C., Angelis, M. H. de, Beckers, J., and Klose, J. (2008). "Transcriptome and proteome analysis of early embryonic mouse brain development". In: *Proteomics* 8.6, pp. 1257–1265

Hartl, F. U. and Hayer-Hartl, M. (2002). "Molecular chaperones in the cytosol: from nascent chain to folded protein". In: *Science* 295.5561, pp. 1852–1858

Hattori, N., Kitada, T., Matsumine, H., Asakawa, S., Yamamura, Y., Yoshino, H., Kobayashi, T., Yokochi, M., Wang, M., Yoritaka, A., Kondo, T., Kuzuhara, S., Nakamura, S., Shimizu, N., and Mizuno, Y. (1998a). "Molecular genetic analysis of a novel Parkin gene in Japanese families with autosomal recessive juvenile parkinsonism: evidence for variable homozygous deletions in theParkin gene in affected individuals". In: *Annals of Neurology* 44.6, pp. 935–941

Hattori, N., Matsumine, H., Asakawa, S., Kitada, T., Yoshino, H., Elibol, B., Brookes, A. J., Yamamura, Y., Kobayashi, T., Wang, M., Yoritaka, A., Minoshima, S., Shimizu, N., and Mizuno, Y. (1998b). "Point Mutations

(Thr240Arg and Ala311Stop) in the Parkin gene". In: *Biochemical and Biophysical Research Communications* 249.3, pp. 754–758

Haucke, V. and Kozlov, M. M. (2018). "Membrane remodeling in clathrin-mediated endocytosis". In: *Journal of Cell Science* 131.17

Hauser, D. N., Primiani, C. T., Langston, R. G., Kumaran, R., and Cookson, M. R. (2015). "The Polg Mutator Phenotype Does Not Cause Dopaminergic Neurodegeneration in DJ-1-Deficient Mice". In: *eNeuro* 2.1

Hauser, D. N., Mamais, A., Conti, M. M., Primiani, C. T., Kumaran, R., Dillman, A. A., Langston, R. G., Beilina, A., Garcia, J. H., Diaz-Ruiz, A., Bernier, M., Fiesel, F. C., Hou, X., Springer, W., Li, Y., Cabo, R. DE, and Cookson, M. R. (2017). "Hexokinases link DJ-1 to the PINK1/parkin pathway". In: *Molecular Neurodegeneration* 12.70

He, K., Marsland III, R., Upadhyayula, S., Song, E., Dang, S., Capraro, B. R., Wang, W., Skillern, W., Gaudin, R., Ma, M., and Kirchhausen, T. (2017). "Dynamics of phosphoinositide conversion in clathrin-mediated endocytic traffic". In: *Nature* 552, pp. 410–414

Heilker, R, Manning-Krieg, U, Zuber, J. F., and Spiess, M (1996). "In vitro binding of clathrin adaptors to sorting signals correlates with endocytosis and basolateral sorting." In: *The EMBO journal* 15.11, pp. 2893–2899

Henne, W. M., Boucrot, E., Meinecke, M., Evergren, E., Vallis, Y., Mittal, R., and McMahon, H. T. (2010). "FCHo Proteins Are Nucleators of Clathrin-Mediated Endocytosis". In: *Science* 328.5983, pp. 1281–1284

Heuser, J (1980). "Three-dimensional visualization of coated vesicle formation in fibroblasts". In: *The Journal of Cell Biology* 84.3, pp. 560–583

Heuser, J (1989). "Effects of cytoplasmic acidification on clathrin lattice morphology". In: *The Journal of Cell Biology* 108.2, pp. 401–411

Heuser, J and Kirchhausen, T (1985). "Deep-etch views of clathrin assemblies". In: *Journal of Ultrastructure Research* 92.1-2, pp. 1–27

Heuser, J. E. and Keen, J (1988). "Deep-etch visualization of proteins involved in clathrin assembly". In: *The Journal of Cell Biology* 107.3, pp. 877–886

Heuser, J. E. and Reese, T. S. (1973). "Evidence for recycling of synaptic vesicle membrane during transmitter release at the frog neuromuscular junction". In: *The Journal of Cell Biology* 57.2, pp. 315–344

Heymann, J. B., Winkler, D. C., Yim, Y.-I., Eisenberg, E., Greene, L. E., and Steven, A. C. (2013). "Clathrin-coated vesicles from brain have small payloads: A cryo-electron tomographic study". In: *Journal of Structural Biology* 184.1, pp. 43–51

Hida, T., Ikeda, H., Kametaka, S., Akazawa, C., Kohsaka, S., Ebisu, S., Uchiyama, Y., and Waguri, S. (2007). "Specific depletion of GGA2 causes cathepsin D missorting in HeLa cells". In: *Archives of Histology and Cytology* 70.5, pp. 303–312

Hinshaw, J. E. and Schmid, S. L. (1995). "Dynamin self-assembles into rings suggesting a mechanism for coated vesicle budding". In: *Nature* 374.6518, pp. 190–192

Hirst, J., Bright, N. A., Rous, B., and Robinson, M. S. (1999). "Characterization of a Fourth Adaptor-related Protein Complex". In: *Molecular Biology of the Cell* 10.8, pp. 2787–2802

Hirst, J., Lui, W. W., Bright, N. A., Totty, N, Seaman, M. N., and Robinson, M. S. (2000). "A family of proteins with gamma-adaptin and VHS domains that facilitate trafficking between the trans-Golgi network and the vacuole/lysosome". In: *The Journal of Cell Biology* 149.1, pp. 67–80

Hirst, J., Lindsay, M. R., and Robinson, M. S. (2001). "Golgi-localized, γ-Ear-containing, ADP-Ribosylation Factor-binding Proteins: Roles of the Different Domains and Comparison with AP-1 and Clathrin". In: *Molecular Biology of the Cell* 12.11, pp. 3573–3588

Hirst, J., Seaman, M. N. J., Buschow, S. I., and Robinson, M. S. (2007). "The Role of Cargo Proteins in GGA Recruitment". In: *Traffic* 8.5, pp. 594–604

Hirst, J., Sahlender, D. A., Li, S., Lubben, N. B., Borner, G. H. H., and Robinson, M. S. (2008). "Auxilin depletion causes self-assembly of clathrin into membraneless cages in vivo." In: *Traffic (Copenhagen, Denmark)* 9.8, pp. 1354–71

Hirst, J., Sahlender, D. A., Choma, M., Sinka, R., Harbour, M. E., Parkinson, M., and Robinson, M. S. (2009). "Spatial and Functional Relationship of GGAs and AP-1 in Drosophila and HeLa Cells". In: *Traffic* 10.11, pp. 1696–1710

Hirst, J., D. Barlow, L., Francisco, G. C., Sahlender, D. A., Seaman, M. N. J., Dacks, J. B., and Robinson, M. S. (2011). "The Fifth Adaptor Protein Complex". In: *PLoS Biology* 9.10

Hirst, J., Borner, G., Antrobus, R., Peden, A., Hodson, N., Sahlender, D., and Robinson, M. (2012). "Distinct and Overlapping Roles for AP-1 and GGAs Revealed by the Knocksideways System". In: *Current Biology* 22.18, pp. 1711–1716

Hirst, J., Irving, C., and Borner, G. H. (2013). "Adaptor Protein Complexes AP-4 and AP-5: New Players in Endosomal Trafficking and Progressive Spastic Paraplegia". In: *Traffic* 14.2, pp. 153–164

Hoehn, M. and Yahr, M. D. (1967). "Parkinsonism: onset, progression and mortality". In: *Neurology* 17.5, pp. 427–442

Hofmann, M. W., Höning, S, Rodionov, D, Dobberstein, B, Figura, K VON, and Bakke, O (1999). "The leucine-based sorting motifs in the cytoplasmic domain of the invariant chain are recognized by the clathrin adaptors AP1 and AP2 and their medium chains". In: *The Journal of Biological Chemistry* 274.51, pp. 36153–36158

Holstein, S. E., Ungewickell, H, and Ungewickell, E (1996). "Mechanism of clathrin basket dissociation: separate functions of protein domains of the DnaJ homologue auxilin". In: *The Journal of Cell Biology* 135.4, pp. 925–937

Höning, S., Griffith, J., Geuze, H. J., and Hunziker, W. (1996). "The tyrosine-based lysosomal targeting signal in lamp-1 mediates sorting into Golgi-derived clathrin-coated vesicles". In: *The EMBO Journal* 15.19, pp. 5230–5239

Houlden, H. and Singleton, A. B. (2012). "The genetics and neuropathology of Parkinson's disease". In: *Acta Neuropathologica* 124.3, pp. 325–338

Hughes, A. J., Daniel, S. E., Kilford, L, and Lees, A. J. (1992). "Accuracy of clinical diagnosis of idiopathic Parkinson's disease: a clinico-pathological study of 100 cases". In: *Journal of Neurology, Neurosurgery, and Psychiatry* 55.3, pp. 181–184

Hughes, A. J., Ben-Shlomo, Y, Daniel, S. E., and Lees, A. J. (2001). "Improved accuracy of clinical diagnosis of Lewy body Parkinson's disease". In: *Neurology* 57.8, pp. 1497–1499

Ibáñez, P, Bonnet, A.-M., Débarges, B, Lohmann, E, Tison, F, Agid, Y, Dürr, A, Brice, A, and Pollak, P (2004). "Causal relation between α-synuclein locus duplication as a cause of familial Parkinson's disease". In: *The Lancet* 364.9440, pp. 1169–1171

Jackson, A. P., Seow, H.-F., Holmes, N., Drickamer, K., and Parham, P. (1987). "Clathrin light chains contain brain-specific insertion sequences and a region of homology with intermediate filaments". In: *Nature* 326.6109, pp. 154–159

Jackson, L. P., Kelly, B. T., McCoy, A. J., Gaffry, T., James, L. C., Collins, B. M., Höning, S., Evans, P. R., and Owen, D. J. (2010). "A Large-Scale Conformational Change Couples Membrane Recruitment to Cargo Binding in the AP2 Clathrin Adaptor Complex". In: *Cell* 141.7, pp. 1220–1229

Jellinger, K. A. (2012). "Neuropathology of sporadic Parkinson's disease: Evaluation and changes of concepts". In: *Movement Disorders* 27.1, pp. 8–30

Jiang, J., Taylor, A. B., Prasad, K., Ishikawa-Brush, Y., Hart, P. J., Lafer, E. M., and Sousa, R. (2003). "Structure Function Analysis of the Auxilin J-Domain Reveals an Extended Hsc70 Interaction Interface". In: *Biochemistry* 42.19, pp. 5748–5753

Jiang, J., Prasad, K., Lafer, E. M., and Sousa, R. (2005). "Structural Basis of Interdomain Communication in the Hsc70 Chaperone". In: *Molecular Cell* 20.4, pp. 513–524

Jiang, J., Maes, E. G., Taylor, A. B., Wang, L., Hinck, A. P., Lafer, E. M., and Sousa, R. (2007). "Structural Basis of J Cochaperone Binding and Regulation of Hsp70". In: *Molecular Cell* 28.3, pp. 422–433

Jin, A. J. and Nossal, R. (2000). "Rigidity of Triskelion Arms and Clathrin Nets". In: *Biophysical Journal* 78.3, pp. 1183–1194

Jing, S. Q., Spencer, T, Miller, K, Hopkins, C, and Trowbridge, I. S. (1990). "Role of the human transferrin receptor cytoplasmic domain in endocytosis: localization of a specific signal sequence for internalization". In: *The Journal of Cell Biology* 110.2, pp. 283–294

Jinn, S., Drolet, R. E., Cramer, P. E., Wong, A. H.-K., Toolan, D. M., Gretzula, C. A., Voleti, B., Vassileva, G., Disa, J., Tadin-Strapps, M., and Stone, D. J. (2017). "TMEM175 deficiency impairs lysosomal and mitochondrial function and increases α-synuclein aggregation". In: *Proceedings of the National Academy of Sciences of the United States of America* 114.9, pp. 2389–2394

Johnson, K. F. and Kornfeld, S (1992). "The cytoplasmic tail of the mannose 6-phosphate/insulin-like growth factor-II receptor has two signals for lysosomal enzyme sorting in the Golgi". In: *The Journal of Cell Biology* 119.2, pp. 249–257

Kachergus, J., Mata, I. F., Hulihan, M., Taylor, J. P., Lincoln, S., Aasly, J., Gibson, J. M., Ross, O. A., Lynch, T., Wiley, J., Payami, H., Nutt, J., Maraganore, D. M., Czyzewski, K., Styczynska, M., Wszolek, Z. K., Farrer, M. J., and Toft, M. (2005). "Identification of a Novel LRRK2 Mutation Linked to Autosomal Dominant Parkinsonism: Evidence of a Common Founder across European Populations". In: *The American Journal of Human Genetics* 76.4, pp. 672–680

Kaksonen, M. and Roux, A. (2018). "Mechanisms of clathrin-mediated endocytosis". In: *Nature Reviews Molecular Cell Biology* 19.5, pp. 313–326

Kametaka, S., Moriyama, K., Burgos, P. V., Eisenberg, E., Greene, L. E., Mattera, R., and Bonifacino, J. S. (2007). "Canonical interaction of cyclin G associated kinase with adaptor protein 1 regulates lysosomal enzyme sorting". In: *Molecular Biology of the Cell* 18.8, pp. 2991–3001

Kampinga, H. H. and Craig, E. A. (2010). "The HSP70 chaperone machinery: J proteins as drivers of functional specificity". In: *Nature Reviews Molecular Cell Biology* 11.8, pp. 579–592

Kanaseki, T and Kadota, K (1969). "The 'vesicle in a basket'. A morphological study of the coated vesicle isolated from the nerve endings of the guinea pig brain, with special reference to the mechanism of membrane movements". In: *The Journal of Cell Biology* 42.1, pp. 202–220

Keen, J. H. (1987). "Clathrin assembly proteins: affinity purification and a model for coat assembly". In: *The Journal of Cell Biology* 105.5, pp. 1989–1998

Keen, J. H., Willingham, M. C., and Pastan, I. H. (1979). "Clathrin-coated vesicles: Isolation, dissociation and factor-dependent reassociation of clathrin baskets". In: *Cell* 16.2, pp. 303–312

Kelley, W. L. (1998). "The J-domain family and the recruitment of chaperone power". In: *Trends in Biochemical Sciences* 23.6, pp. 222–227

Kent, H. M., McMahon, H. T., Evans, P. R., Benmerah, A., and Owen, D. J. (2002). "γ-Adaptin Appendage Domain: Structure and Binding Site for Eps15 and γ-Synergin". In: *Structure* 10.8, pp. 1139–1148

Kiely, A. P., Asi, Y. T., Kara, E., Limousin, P., Ling, H., Lewis, P., Proukakis, C., Quinn, N., Lees, A. J., Hardy, J., Revesz, T., Houlden, H., and Holton, J. L. (2013). "α-Synucleinopathy associated with G51D SNCA mutation: a link between Parkinson's disease and multiple system atrophy?" In: *Acta Neuropathologica* 125.5, pp. 753–769

King, F. W., Wawrzynow, A, Höhfeld, J, and Zylicz, M (2001). "Co-chaperones Bag-1, Hop and Hsp40 regulate Hsc70 and Hsp90 interactions with wild-type or mutant p53". In: *The EMBO journal* 20.22, pp. 6297–6305

Kirchhausen, T and Toyoda, T (1993). "Immunoelectron microscopic evidence for the extended conformation of light chains in clathrin trimers". In: *The Journal of Biological Chemistry* 268.14, pp. 10268–10273

Kirchhausen, T, Harrison, S. C., Parham, P, and Brodsky, F. M. (1983). "Location and distribution of the light chains in clathrin trimers". In: *Proceedings of the National Academy of Sciences of the United States of America* 80.9, pp. 2481–2485

Kirchhausen, T, Harrison, S. C., Chow, E. P., Mattaliano, R. J., Ramachandran, K. L., Smart, J, and Brosius, J (1987a). "Clathrin heavy chain: molecular cloning and complete primary structure". In: *Proceedings of the National Academy of Sciences of the United States of America* 84.24, pp. 8805–8809

Kirchhausen, T, Scarmato, P, Harrison, S. C., Monroe, J. J., Chow, E. P., Mattaliano, R. J., Ramachandran, K. L., Smart, J. E., Ahn, A. H., and Brosius, J (1987b). "Clathrin light chains LCA and LCB are similar, polymorphic, and share repeated heptad motifs". In: *Science* 236.4799, pp. 320–324

Kirchhausen, T. (2012). "Bending membranes". In: *Nature Cell Biology* 14.9, pp. 906–908

Kirchhausen, T., Owen, D., and Harrison, S. C. (2014). "Molecular structure, function, and dynamics of clathrin-mediated membrane traffic". In: *Cold Spring Harbor Perspectives in Biology* 6.5

Kirchhausen, T. (1993). "Coated pits and coated vesicles sorting it all out". In: *Current Opinion in Structural Biology* 3.2, pp. 182–188

Kirchhausen, T. and Harrison, S. C. (1981). "Protein organization in clathrin trimers". In: *Cell* 23.3, pp. 755–761

Kirshenbaum, G. S., Dawson, N., Mullins, J. G. L., Johnston, T. H., Drinkhill, M. J., Edwards, I. J., Fox, S. H., Pratt, J. A., Brotchie, J. M., Roder, J. C., and Clapcote, S. J. (2013). "Alternating Hemiplegia of Childhood-Related Neural and Behavioural Phenotypes in Na+,K+-ATPase α3 Missense Mutant Mice". In: *PLoS ONE* 8.3

Kordower, J. H., Chu, Y., Hauser, R. a., Freeman, T. B., and Olanow, C. W. (2008). "Lewy body-like pathology in long-term embryonic nigral transplants in Parkinson's disease". In: *Nature medicine* 14.5, pp. 504–506

Kornfeld, S. (1992). "Structure and Function of the Mannose 6-Phosphate/Insulinlike Growth Factor II Receptors". In: *Annual Review of Biochemistry* 61.1, pp. 307–330

Köroglu, Ç., Baysal, L., Cetinkaya, M., Karasoy, H., and Tolun, A. (2013). "DNAJC6 is responsible for juvenile parkinsonism with phenotypic variability". In: *Parkinsonism and Related Disorders* 19.3, pp. 320–324

Korolchuk, V. I. and Banting, G. (2002). "CK2 and GAK/auxilin2 are Major protein kinases in clathrin-coated vesicles". In: *Traffic* 3.6, pp. 428–439

Kotzbauer, P. T., Trojanowski, J. Q., and Lee, V. M. (2001). "Lewy body pathology in Alzheimer's disease". In: *Journal of Molecular Neuroscience* 17.2, pp. 225–232

Krauss, M., Kinuta, M., Wenk, M. R., De Camilli, P., Takei, K., and Haucke, V. (2003). "ARF6 stimulates clathrin/AP-2 recruitment to synaptic membranes by activating phosphatidylinositol phosphate kinase type Igamma". In: *The Journal of Cell Biology* 162.1, pp. 113–124

Krebs, C. E., Karkheiran, S., Powell, J. C., Cao, M., Makarov, V., Darvish, H., Di Paolo, G., Walker, R. H., Shahidi, G. A., Buxbaum, J. D., De Camilli, P.,

Yue, Z., and Paisán-Ruiz, C. (2013). "The Sac1 domain of SYNJ1 identified mutated in a family with early-onset progressive parkinsonism with generalized seizures". In: *Human Mutation* 34.9, pp. 1200–1207

Krüger, R., Kuhn, W., Müller, T., Woitalla, D., Graeber, M., Kösel, S., Przuntek, H., Epplen, Jörg, T., Schöls, L., and Riess, O. (1998). "Ala30Pro mutation in the gene encoding α-synuclein in Parkinson's disease". In: *Nature Genetics* 18.2, pp. 106–108

Kumaran, R. and Cookson, M. R. (2015). "Pathways to parkinsonism redux: convergent pathobiological mechanisms in genetics of Parkinson's disease". In: *Human Molecular Genetics* 9, pp. 1–37

Kurten, R. C., Cadena, D. L., and Gill, G. N. (1996). "Enhanced degradation of EGF receptors by a sorting nexin, SNX1". In: *Science* 272.5264, pp. 1008–1010

Langston, J. W., Ballard, P, Tetrud, J. W., and Irwin, I (1983a). "Chronic Parkinsonism in humans due to a product of meperidine-analog synthesis". In: *Science* 219.4587, pp. 979–980

Langston, J., Ballard, P., Tetrud, J., and Irwin, I. (1983b). "Chronic Parkinsonism in humans due to a product of meperidine-analog synthesis". In: *Science* 219, pp. 979–980

Larkin, J. M., Donzell, W. C., and Anderson, R. G. (1986). "Potassium-dependent assembly of coated pits: new coated pits form as planar clathrin lattices". In: *The Journal of Cell Biology* 103.6, pp. 2619–2627

Lau, L. M. L. DE and Breteler, M. M. B. (2006). "Epidemiology of Parkinson's disease". In: *The Lancet Neurology* 5, pp. 525–535

Lee, D.-W., Wu, X., Eisenberg, E., and Greene, L. E. (2006). "Recruitment dynamics of GAK and auxilin to clathrin-coated pits during endocytosis". In: *Journal of Cell Science* 119.17, pp. 3502–3512

Lee, D.-W., Zhao, X., Yim, Y.-I., Eisenberg, E., and Greene, L. E. (2008). "Essential role of cyclin-G-associated kinase (Auxilin-2) in developing and mature mice". In: *Molecular Biology of the Cell* 19.7, pp. 2766–2776

Lees, A. J., Hardy, J., and Revesz, T. (2009). "Parkinson's disease". In: *Lancet* 373.9680, pp. 2055–2066

Lefrançois, S. and McCormick, P. J. (2007). "The Arf GEF GBF1 Is Required for GGA Recruitment to Golgi Membranes". In: *Traffic* 8.10, pp. 1440–1451

Leroy, E., Anastasopoulos, D., Konitsiotis, S., Lavedan, C., and Polymeropoulos, M. H. (1998). "Deletions in the Parkin gene and genetic heterogeneity in a Greek family with early onset Parkinson's disease". In: *Human Genetics* 103.4, pp. 424–427

Lewy, F. (1912). "Paralysis agitans Patholgische anatomie". In: *Handbuch der Neurologie*, pp. 920–933

Li, J.-Y., Englund, E., Holton, J. L., Soulet, D., Hagell, P., Lees, A. J., Lashley, T., Quinn, N. P., Rehncrona, S., Björklund, A., Widner, H., Revesz, T., Lindvall, O., and Brundin, P. (2008). "Lewy bodies in grafted neurons in subjects with Parkinson's disease suggest host-to-graft disease propagation". In: *Nature Medicine* 14.5, pp. 501–503

Lobel, P., Fujimoto, K., Ye, R. D., Griffiths, G., and Kornfeld, S. (1989). "Mutations in the cytoplasmic domain of the 275 kd mannose 6-phosphate receptor differentially alter lysosomal enzyme sorting and endocytosis". In: *Cell* 57.5, pp. 787–796

Long, K. R., Trofatter, J. A., Ramesh, V., McCormick, M. K., and Buckler, A. J. (1996). "Cloning and Characterization of a Novel Human Clathrin Heavy Chain Gene (CLTCL)". In: *Genomics* 35.3, pp. 466–472

Longo, F., Mercatelli, D., Novello, S., Arcuri, L., Brugnoli, A., Vincenzi, F., Russo, I., Berti, G., Mabrouk, O. S., Kennedy, R. T., Shimshek, D. R., Varani, K., Bubacco, L., Greggio, E., and Morari, M. (2017). "Age-dependent dopamine transporter dysfunction and Serine129 phospho-α-synuclein overload in G2019S LRRK2 mice". In: *Acta Neuropathologica Communications* 5.1, p. 22

Lonsdale, J. *et al.* (2013). "The Genotype-Tissue Expression (GTEx) project". In: *Nature Genetics* 45.6, pp. 580–585

Lorenzo-Betancor, O., Ogaki, K., Soto-Ortolaza, A. I., Labbe, C., Walton, R. L., Strongosky, A. J., Gerpen, J. A. VAN, Uitti, R. J., McLean, P. J., Springer, W., Siuda, J., Opala, G., Krygowska-Wajs, A., Barcikowska, M., Czyzewski, K., McCarthy, A., Lynch, T., Puschmann, A., Rektorova, I., Sanotsky, Y., Vilariño-Güell, C., Farrer, M. J., Ferman, T. J., Boeve, B. F., Petersen, R. C.,

Parisi, J. E., Graff-Radford, N. R., Dickson, D. W., Wszolek, Z. K., and Ross, O. A. (2015). "DNAJC13 p.Asn855Ser mutation screening in Parkinson's disease and pathologically confirmed Lewy body disease patients". In: *European Journal of Neurology* 22.9, pp. 1323–1325

Love, M. I., Huber, W., and Anders, S. (2014). "Moderated estimation of fold change and dispersion for RNA-seq data with DESeq2". In: *Genome Biology* 15.12, p. 550

Lu, C.-S., Lai, S.-C., Wu, R.-M., Weng, Y.-H., Huang, C.-L., Chen, R.-S., Chang, H.-C., Wu-Chou, Y.-H., and Yeh, T.-H. (2012). "PLA2G6 mutations in PARK14-linked young-onset parkinsonism and sporadic Parkinson's disease". In: *American Journal of Medical Genetics: Neuropsychiatric Genetics* 159.2, pp. 183–191

Lücking, C., Abbas, N, Dürr, A, Bonifati, V, Bonnet, A.-M., Broucker, T DE, De Michele, G, Wood, N., Agid, Y, and Brice, A (1998). "Homozygous deletions in parkin gene in European and North African families with autosomal recessive juvenile parkinsonism". In: *The Lancet* 352.9137, pp. 1355–1356

Manzoni, C., Mamais, A., Dihanich, S., Abeti, R., Soutar, M. P. M., Plun-Favreau, H., Giunti, P., Tooze, S. a., Bandopadhyay, R., and Lewis, P. A. (2013). "Inhibition of LRRK2 kinase activity stimulates macroautophagy". In: *Biochimica et Biophysica Acta* 1833.12, pp. 2900–2910

Manzoni, C., Mamais, A., Roosen, D. A., Dihanich, S., Soutar, M. P. M., Plun-Favreau, H., Bandopadhyay, R., Hardy, J., Tooze, S. A., Cookson, M. R., and Lewis, P. A. (2016). "mTOR independent regulation of macroautophagy by Leucine Rich Repeat Kinase 2 via Beclin-1". In: *Scientific Reports* 6.35106

Mardones, G. A., Burgos, P. V., Brooks, D. A., Parkinson-Lawrence, E., Mattera, R., and Bonifacino, J. S. (2007). "The trans-Golgi Network Accessory Protein p56 Promotes Long-Range Movement of GGA/Clathrin-containing Transport Carriers and Lysosomal Enzyme Sorting". In: *Molecular Biology of the Cell* 18.9, pp. 3486–3501

Marks, M. S., Roche, P. A., Donselaar, E VAN, Woodruff, L, Peters, P. J., and Bonifacino, J. S. (1995). "A lysosomal targeting signal in the cytoplasmic tail of the beta chain directs HLA-DM to MHC class II compartments". In: *The Journal of Cell Biology* 131.2, pp. 351–369

Massol, R. H., Boll, W., Griffin, A. M., and Kirchhausen, T. (2006). "A burst of auxilin recruitment determines the onset of clathrin-coated vesicle uncoating". In: *Proceedings of the National Academy of Sciences of the United States of America* 103.27, pp. 10265–10270

Matsuura, K, Kabuto, H, Makino, H, and Ogawa, N (1997). "Pole test is a useful method for evaluating the mouse movement disorder caused by striatal dopamine depletion". In: *Journal of Neuroscience Methods* 73.1, pp. 45–48

Mattera, R., Ritter, B., Sidhu, S. S., McPherson, P. S., and Bonifacino, J. S. (2004). "Definition of the consensus motif recognized by gamma-adaptin ear domains". In: *The Journal of Biological Chemistryhemistry* 279.9, pp. 8018–8028

Mayer, M. P. and Bukau, B (2005). "Hsp70 chaperones: cellular functions and molecular mechanism". In: *Cellular and Molecular Life Sciences* 62.6, pp. 670–684

Mazzio, E. A., Close, F., and Soliman, K. F. A. (2011). "The biochemical and cellular basis for nutraceutical strategies to attenuate neurodegeneration in Parkinson's disease". In: *International Journal of Molecular Sciences* 12.1, pp. 506–569

McGough, I. J. and Cullen, P. J. (2011). "Recent Advances in Retromer Biology". In: *Traffic* 12.8, pp. 963–971

McGough, I. J., Steinberg, F., Jia, D., Barbuti, P. A., McMillan, K. J., Heesom, K. J., Whone, A. L., Caldwell, M. A., Billadeau, D. D., Rosen, M. K., and Cullen, P. J. (2014). "Retromer binding to FAM21 and the WASH complex is perturbed by the Parkinson disease-linked VPS35(D620N) mutation". In: *Current Biology* 24.14, pp. 1670–1676

McGraw, T. E., Greenfield, L, and Maxfield, F. R. (1987). "Functional expression of the human transferrin receptor cDNA in Chinese hamster ovary cells deficient in endogenous transferrin receptor". In: *The Journal of cell biology* 105.1, pp. 207–14

McMahon, H. T. and Boucrot, E. (2011). "Molecular mechanism and physiological functions of clathrin-mediated endocytosis". In: *Nature Reviews Molecular Cell Biology* 12.8, pp. 517–533

McPherson, P. S., Garcia, E. P., Slepnev, V. I., David, C., Zhang, X., Grabs, D., Sossini, W. S., Bauerfeind, R., Nemoto, Y., and De Camilli, P. (1996). "A presynaptic inositol-5-phosphatase". In: *Nature* 379.6563, pp. 353–357

Meinecke, M., Boucrot, E., Camdere, G., Hon, W.-C., Mittal, R., and McMahon, H. T. (2013). "Cooperative recruitment of dynamin and BIN/amphiphysin/Rvs (BAR) domain-containing proteins leads to GTP-dependent membrane scission". In: *The Journal of Biological Chemistry* 288.9, pp. 6651–6661

Mellacheruvu, D., Wright, Z., Couzens, A. L., Lambert, J.-P., St-Denis, N. A., Li, T., Miteva, Y. V., Hauri, S., Sardiu, M. E., Low, T. Y., Halim, V. A., Bagshaw, R. D., Hubner, N. C., Al-Hakim, A., Bouchard, A., Faubert, D., Fermin, D., Dunham, W. H., Goudreault, M., Lin, Z.-Y., Badillo, B. G., Pawson, T., Durocher, D., Coulombe, B., Aebersold, R., Superti-Furga, G., Colinge, J., Heck, A. J. R., Choi, H., Gstaiger, M., Mohammed, S., Cristea, I. M., Bennett, K. L., Washburn, M. P., Raught, B., Ewing, R. M., Gingras, A.-C., and Nesvizhskii, A. I. (2013). "The CRAPome: a contaminant repository for affinity purificationmass spectrometry data". In: *Nature Methods* 10.8, pp. 730–736

Messa, M., Fernández-Busnadiego, R., Sun, E. W., Chen, H., Czapla, H., Wrasman, K., Wu, Y., Ko, G., Ross, T., Wendland, B., and De Camilli, P. (2014). "Epsin deficiency impairs endocytosis by stalling the actin-dependent invagination of endocytic clathrin-coated pits". In: *eLife*

Meyer, C, Zizioli, D, Lausmann, S, Eskelinen, E. L., Hamann, J, Saftig, P, Figura, K VON, and Schu, P (2000). "μ1A-adaptin-deficient mice: lethality, loss of AP-1 binding and rerouting of mannose 6-phosphate receptors". In: *The EMBO journal* 19.10, pp. 2193–2203

Miele, A. E., Watson, P. J., Evans, P. R., Traub, L. M., and Owen, D. J. (2004). "Two distinct interaction motifs in amphiphysin bind two independent sites on the clathrin terminal domain β-propeller". In: *Nature Structural & Molecular Biology* 11.3, pp. 242–248

Miller, G. J., Mattera, R., Bonifacino, J. S., and Hurley, J. H. (2003). "Recognition of accessory protein motifs by the γ-adaptin ear domain of GGA3". In: *Nature Structural & Molecular Biology* 10.8, pp. 599–606

Miller, S., Sahlender, D., Graham, S., Höning, S., Robinson, M., Peden, A., and Owen, D. (2011). "The Molecular Basis for the Endocytosis of Small R-SNAREs by the Clathrin Adaptor CALM". In: *Cell* 147.5, pp. 1118–1131

Misra, S., Puertollano, R., Kato, Y., Bonifacino, J. S., and Hurley, J. H. (2002). "Structural basis for acidic-cluster-dileucine sorting-signal recognition by VHS domains". In: *Nature* 415.6874, pp. 933–937

Morgan, J. R., Prasad, K, Jin, S, Augustine, G. J., and Lafer, E. M. (2001). "Uncoating of clathrin-coated vesicles in presynaptic terminals: roles for Hsc70 and auxilin." In: *Neuron* 32.2, pp. 289–300

Mullins, C. and Bonifacino, J. S. (2001). "Structural Requirements for Function of Yeast GGAs in Vacuolar Protein Sorting, α-Factor Maturation, and Interactions with Clathrin". In: *Molecular and Cellular Biology* 21.23, pp. 7981–7994

Musacchio, A., Smith, C. J., Roseman, A. M., Harrison, S. C., Kirchhausen, T., and Pearse, B. M. (1999). "Functional Organization of Clathrin in Coats: Combining Electron Cryomicroscopy and X-Ray Crystallography". In: *Molecular Cell* 3.6, pp. 761–770

Nagle, M. W., Latourelle, J. C., Labadorf, A., Dumitriu, A., Hadzi, T. C., Beach, T. G., and Myers, R. H. (2016). "The 4p16.3 Parkinson Disease Risk Locus Is Associated with GAK Expression and Genes Involved with the Synaptic Vesicle Membrane". In: *PloS ONE* 11.8

Nalls, M. A., Pankratz, N., Lill, C. M., Do, C. B., Hernandez, D. G., Saad, M., DeStefano, A. L., Kara, E., Bras, J., Sharma, M., Schulte, C., Keller, M. F., Arepalli, S., Letson, C., Edsall, C., Stefansson, H., Liu, X., Pliner, H., Lee, J. H., Cheng, R., Ikram, M. A., Ioannidis, J. P. A., Hadjigeorgiou, G. M., Bis, J. C., Martinez, M., Perlmutter, J. S., Goate, A., Marder, K., Fiske, B., Sutherland, M., Xiromerisiou, G., Myers, R. H., Clark, L. N., Stefansson, K., Hardy, J. A., Heutink, P., Chen, H., Wood, N. W., Houlden, H., Payami, H., Brice, A., Scott, W. K., Gasser, T., Bertram, L., Eriksson, N., Foroud, T., and Singleton, A. B. (2014). "Large-scale meta-analysis of genome-wide association data identifies six new risk loci for Parkinson's disease". In: *Nature Genetics* 46.9, pp. 989–993

Nalls, M. A., Blauwendraat, C., Vallerga, C. L., Heilbron, K., Bandres-Ciga, S., Chang, D., Tan, M., Kia, D. A., Noyce, A. J., Xue, A., Bras, J., Young,

E., Coelln, R. von, Simon-Sanchez, J., Schulte, C., Sharma, M., Krohn, L., Pihlstrom, L., Siitonen, A., Iwaki, H., Leonard, H., Faghri, F., Gibbs, J. R., Hernandez, D. G., Scholz, S. W., Botia, J. A., Martinez, M., Corvol, J.-C., Lesage, S., Jankovic, J., Shulman, L. M., Team, T. a. R., Consortium, S. G.o.P.D. S., Sutherland, M., Tienari, P., Majamaa, K., Toft, M., Brice, A., Yang, J., Gan-Orr, Z., Gasser, T. M., Heutink, P. M., Shulman, J. M., Wood, N. A., Hinds, D. A., Hardy, J. R., Morris, H. R., Gratten, J. M., Visscher, P. M., Graham, R. R., Singleton, A. B., and Consortium, I. P.D. G. (2018). "Parkinson's disease genetics: identifying novel risk loci, providing causal insights and improving estimates of heritable risk". In: *bioRxiv*

Narendra, D. P., Jin, S. M., Tanaka, A., Suen, D.-F., Gautier, C. A., Shen, J., Cookson, M. R., and Youle, R. J. (2010). "PINK1 Is Selectively Stabilized on Impaired Mitochondria to Activate Parkin". In: *PLoS Biology* 8.1

Navarro Negredo, P., Edgar, J. R., Manna, P. T., Antrobus, R., and Robinson, M. S. (2018). "The WDR11 complex facilitates the tethering of AP-1-derived vesicles". In: *Nature Communications* 9.1, p. 596

Newmyer, S. L., Christensen, A., and Sever, S. (2003). "Auxilin-Dynamin Interactions Link the Uncoating ATPase Chaperone Machinery with Vesicle Formation". In: *Developmental Cell* 4.6, pp. 929–940

Nielsen, M. S., Gustafsen, C., Madsen, P., Nyengaard, J. R., Hermey, G., Bakke, O., Mari, M., Schu, P., Pohlmann, R., Dennes, A., and Petersen, C. M. (2007). "Sorting by the cytoplasmic domain of the amyloid precursor protein binding receptor SorLA". In: *Molecular and cellular biology* 27.19, pp. 6842–51

Nogi, T., Shiba, Y., Kawasaki, M., Shiba, T., Matsugaki, N., Igarashi, N., Suzuki, M., Kato, R., Takatsu, H., Nakayama, K., and Wakatsuki, S. (2002). "Structural basis for the accessory protein recruitment by the γ-adaptin ear domain". In: *Nature Structural Biology* 9.7, p. 527

Norris, A., Tammineni, P., Wang, S., Gerdes, J., Murr, A., Kwan, K. Y., Cai, Q., and Grant, B. D. (2017). "SNX-1 and RME-8 oppose the assembly of HGRS-1/ESCRT-0 degradative microdomains on endosomes". In: *Proceedings of the National Academy of Sciences of the United States of America* 114.3

Obeso, J. A., Rodriguez-Oroz, M. C., Rodriguez, M., Lanciego, J. L., Artieda, J., Gonzalo, N., and Olanow, C. W. (2000). "Pathophysiology of the basal ganglia in Parkinson's disease". In: *Trends in Neuroscience* 23.10

Obeso, J. A., Marin, C., Rodriguez-Oroz, C., Blesa, J., Benitez-Temiño, B., Mena-Segovia, J., Rodríguez, M., and Olanow, C. W. (2009). "The basal ganglia in Parkinson's disease: Current concepts and unexplained observations". In: *Annals of Neurology* 64.2

Ohno, H, Stewart, J, Fournier, M. C., Bosshart, H, Rhee, I, Miyatake, S, Saito, T, Gallusser, A, Kirchhausen, T, and Bonifacino, J. S. (1995). "Interaction of tyrosine-based sorting signals with clathrin-associated proteins". In: *Science* 269.5232, pp. 1872–1875

O'Leary, N. A., Wright, M. W., Brister, J. R., Ciufo, S., Haddad, D., McVeigh, R., Rajput, B., Robbertse, B., Smith-White, B., Ako-Adjei, D., Astashyn, A., Badretdin, A., Bao, Y., Blinkova, O., Brover, V., Chetvernin, V., Choi, J., Cox, E., Ermolaeva, O., Farrell, C. M., Goldfarb, T., Gupta, T., Haft, D., Hatcher, E., Hlavina, W., Joardar, V. S., Kodali, V. K., Li, W., Maglott, D., Masterson, P., McGarvey, K. M., Murphy, M. R., O'Neill, K., Pujar, S., Rangwala, S. H., Rausch, D., Riddick, L. D., Schoch, C., Shkeda, A., Storz, S. S., Sun, H., Thibaud-Nissen, F., Tolstoy, I., Tully, R. E., Vatsan, A. R., Wallin, C., Webb, D., Wu, W., Landrum, M. J., Kimchi, A., Tatusova, T., DiCuccio, M., Kitts, P., Murphy, T. D., and Pruitt, K. D. (2016). "Reference sequence (RefSeq) database at NCBI: current status, taxonomic expansion, and functional annotation". In: *Nucleic Acids Research* 44.1, pp. 733–745

Olgiati, S., De Rosa, A., Quadri, M., Criscuolo, C., Breedveld, G. J., Picillo, M., Pappatà, S., Quarantelli, M., Barone, P., De Michele, G., and Bonifati, V. (2014). "PARK20 caused by SYNJ1 homozygous Arg258Gln mutation in a new Italian family". In: *Neurogenetics* 15.3, pp. 183–188

Olgiati, S., Quadri, M., Fang, M., Rood, J. P.M. A., Saute, J. A., Chien, H. F., Bouwkamp, C. G., Graafland, J., Minneboo, M., Breedveld, G. J., Zhang, J., International Parkinsonism Genetics Network, Verheijen, F. W., Boon, A. J. W., Kievit, A. J. A., Jardim, L. B., Mandemakers, W., Barbosa, E. R., Rieder, C. R. M., Leenders, K. L., Wang, J., and Bonifati, V. (2016). "DNAJC6

mutations associated with early-onset Parkinson's disease". In: *Annals of Neurology* 79.2, pp. 244–256

Olusanya, O., Andrews, P. D., Swedlow, J. R., and Smythe, E. (2001). "Phosphorylation of threonine 156 of the μ2 subunit of the AP2 complex is essential for endocytosis in vitro and in vivo". In: *Current Biology* 11.11, pp. 896–900

Otter, W. K. DEN and Briels, W. J. (2011). "The Generation of Curved Clathrin Coats from Flat Plaques". In: *Traffic* 12.10, pp. 1407–1416

Owen, D. J., Vallis, Y., Noble, M. E., Hunter, J. B., Dafforn, T. R., Evans, P. R., and McMahon, H. T. (1999). "A Structural Explanation for the Binding of Multiple Ligands by the α-Adaptin Appendage Domain". In: *Cell* 97.6, pp. 805–815

Owen, D. J., Collins, B. M., and Evans, P. R. (2004). "Adaptors for clathrin coats: structure and function". In: *Annual Review of Cell and Developmental Biology* 20.1, pp. 153–191

Owen, D., Vallis, Y., Pearse, B., McMahon, H., and Evans, P. (2000). "The structure and function of the β2adaptin appendage domain". In: *The EMBO Journal* 19.16, pp. 4216–4227

Padrón, D., Wang, Y. J., Yamamoto, M., Yin, H., and Roth, M. G. (2003). "Phosphatidylinositol phosphate 5-kinase Ibeta recruits AP-2 to the plasma membrane and regulates rates of constitutive endocytosis". In: *The Journal of Cell Biology* 162.4, pp. 693–701

Page, L. J. and Robinson, M. S. (1995). "Targeting signals and subunit interactions in coated vesicle adaptor complexes". In: *The Journal of Cell Biology* 131.3, pp. 619–630

Paisán-Ruíz, C., Jain, S., Evans, E. W., Gilks, W. P., Simón, J., Van Der Brug, M., De Munain, A. L., Aparicio, S., Gil, A. M., Khan, N., Johnson, J., Martinez, J. R., Nicholl, D., Carrera, I. M., Pea, A. S., De Silva, R., Lees, A., Martí-Massó, J. F., Pérez-Tur, J., Wood, N. W., and Singleton, A. B. (2004). "Cloning of the gene containing mutations that cause PARK8-linked Parkinson's disease". In: *Neuron* 44.4, pp. 595–600

Paleotti, O., Macia, E., Luton, F., Klein, S., Partisani, M., Chardin, P., Kirchhausen, T., and Franco, M. (2005). "The small G-protein Arf6GTP recruits the AP-2 adaptor complex to membranes". In: *The Journal of Biological Chemistry* 280.22, pp. 21661–21666

Pallotto, M., Watkins, P. V., Fubara, B., Singer, J. H., and Briggman, K. L. (2015). "Extracellular space preservation aids the connectomic analysis of neural circuits". In: *eLife* 4

Parkinson, J. (1817). *An essay on the shaking palsy*. Sherwood, Neely, and Jones

Patro, R., Duggal, G., Love, M. I., Irizarry, R. A., and Kingsford, C. (2017). "Salmon provides fast and bias-aware quantification of transcript expression". In: *Nature Methods* 14.4, pp. 417–419

Pearse, B. M. (1975). "Coated vesicles from pig brain: purification and biochemical characterization". In: *Journal of Molecular Biology* 97.1, pp. 93–98

Pearse, B. M. (1988). "Receptors compete for adaptors found in plasma membrane coated pits". In: *The EMBO Journal* 7.11, pp. 3331–3336

Pearse, B. and Robinson, M. (1984). "Purification and properties of 100-kd proteins from coated vesicles and their reconstitution with clathrin". In: *The EMBO Journal* 3.9, pp. 1951–1957

Peden, A. A., Rudge, R. E., Lui, W. W. Y., and Robinson, M. S. (2002). "Assembly and function of AP-3 complexes in cells expressing mutant subunits". In: *The Journal of Cell Biology* 156.2, pp. 327–336

Perkins, D. N., Pappin, D. J. C., Creasy, D. M., and Cottrell, J. S. (1999). "Probability-based protein identification by searching sequence databases using mass spectrometry data". In: *Electrophoresis* 20.18, pp. 3551–3567

Peter, B. J., Kent, H. M., Mills, I. G., Vallis, Y., Butler, P. J. G., Evans, P. R., and McMahon, H. T. (2004). "BAR domains as sensors of membrane curvature: the amphiphysin BAR structure". In: *Science* 303.5657, pp. 495–499

Pihlstrøm, L., Blauwendraat, C., Cappelletti, C., Berge-Seidl, V., Langmyhr, M., Henriksen, S. P., Berg, W. D. J. VAN DE, Gibbs, J. R., Cookson, M. R., Singleton, A. B., Nalls, M. A., Toft, M., Nalls, M. A., and Toft, M. (2018). "A comprehensive analysis of SNCA-related genetic risk in sporadic Parkinson's disease". In: *Annals of Neurology* 84.1, pp. 117–129

Pishvaee, B., Costaguta, G., Yeung, B. G., Ryazantsev, S., Greener, T., Greene, L. E., Eisenberg, E., McCaffery, J. M., and Payne, G. S. (2000). "A yeast DNA J protein required for uncoating of clathrin-coated vesicles in vivo". In: *Nature Cell Biology* 2.12, pp. 958–963

Polymeropoulos, M. H., Higgins, J. J., Golbe, L. I., Johnson, W. G., Ide, S. E., Di Iorio, G., Sanges, G., Stenroos, E. S., Pho, L. T., Schaffer, A. A., Lazzarini, A. M., Nussbaum, R. L., and Duvoisin, R. C. (1996). "Mapping of a gene for Parkinson's disease to chromosome 4q21-q23". In: *Science* 274, pp. 1197–1199

Polymeropoulos, M. H., Lavedant, C., Leroyt, E., Ide, S. E., Dehejia, A., Dutra, A., Pike, B., Root, H., Rubenstein, J., Boyer, R., Stenroos, E. S., Chandrasekharappa, S., Athanassiadou, A., Papapetropoulos, T., Johnson, W. G., Lazzarini, A. M., Duvoisin, R. C., Di, G., Golbe, L. I., and Nussbaum, R. L. (1997). "Mutation in the α-synuclein gene identified in families with Parkinson's disease". In: *Science* 276.June, pp. 2045–2048

Popoff, V., Mardones, G. A., Bai, S.-K., Chambon, V, Tenza, D, Burgos, P. V., Shi, A., Benaroch, P., Urbe, S., Lamaze, C., Grant, B. D., Raposo, G., and Johannes, L. (2009). "Analysis of Articulation Between Clathrin and Retromer in Retrograde Sorting on Early Endosomes". In: *Traffic* 10.12, pp. 1868–1880

Posor, Y., Eichhorn-Gruenig, M., Puchkov, D., Schöneberg, J., Ullrich, A., Lampe, A., Müller, R., Zarbakhsh, S., Gulluni, F., Hirsch, E., Krauss, M., Schultz, C., Schmoranzer, J., Noé, F., and Haucke, V. (2013). "Spatiotemporal control of endocytosis by phosphatidylinositol-3,4-bisphosphate". In: *Nature* 499.7457, pp. 233–237

Poussu, A, Lohi, O, and Lehto, V. P. (2000). "Vear, a novel Golgi-associated protein with VHS and gamma-adaptin ear domains." In: *The Journal of Biological Chemistry* 275.10, pp. 7176–7183

Prag, G., Lee, S., Mattera, R., Arighi, C. N., Beach, B. M., Bonifacino, J. S., and Hurley, J. H. (2005). "Structural mechanism for ubiquitinated-cargo recognition by the Golgi-localized, gamma-ear-containing, ADP-ribosylation-factor-binding proteins". In: *Proceedings of the National Academy of Sciences of the United States of America* 102.7, pp. 2334–2339

Pringsheim, T., Jette, N., Frolkis, A., and Steeves, T. D. (2014). "The prevalence of Parkinson's disease: A systematic review and meta-analysis". In: *Movement Disorders* 29.13, pp. 1583–1590

Puertollano, R, Aguilar, R. C., Gorshkova, I, Crouch, R. J., and Bonifacino, J. S. (2001a). "Sorting of mannose 6-phosphate receptors mediated by the GGAs". In: *Science* 292.5522, pp. 1712–1716

Puertollano, R. and Bonifacino, J. S. (2004). "Interactions of GGA3 with the ubiquitin sorting machinery". In: *Nature Cell Biology* 6.3, pp. 244–251

Puertollano, R., Randazzo, P. A., Presley, J. F., Hartnell, L. M., and Bonifacino, J. S. (2001b). "The GGAs Promote ARF-Dependent Recruitment of Clathrin to the TGN". In: *Cell* 105.1, pp. 93–102

Puertollano, R., Wel, N. N. VAN DER, Greene, L. E., Eisenberg, E., Peters, P. J., and Bonifacino, J. S. (2003). "Morphology and Dynamics of Clathrin/GGA1-coated Carriers Budding from the trans-Golgi Network". In: *Molecular Biology of the Cell* 14.4, pp. 1545–1557

Quadri, M., Fang, M., Picillo, M., Olgiati, S., Breedveld, G. J., Graafland, J., Wu, B., Xu, F., Erro, R., Amboni, M., Pappatà, S., Quarantelli, M., Annesi, G., Quattrone, A., Chien, H. F., Barbosa, E. R., Oostra, B. A., Barone, P., Wang, J., and Bonifati, V. (2013). "Mutation in the SYNJ1 gene associated with autosomal recessive, early-onset parkinsonism". In: *Human Mutation* 34.9, pp. 1208–1215

Raiborg, C., Bache, K. G., Mehlum, A, Stang, E, and Stenmark, H (2001). "Hrs recruits clathrin to early endosomes". In: *The EMBO Journal* 20.17, pp. 5008–5021

Ramirez, A., Heimbach, A., Gründemann, J., Stiller, B., Hampshire, D., Cid, L. P., Goebel, I., Mubaidin, A. F., Wriekat, A.-L., Roeper, J., Al-Din, A., Hillmer, A. M., Karsak, M., Liss, B., Woods, C. G., Behrens, M. I., and Kubisch, C. (2006). "Hereditary parkinsonism with dementia is caused by mutations in ATP13A2, encoding a lysosomal type 5 P-type ATPase". In: *Genetics* 38.10, pp. 1184–1191

Rapoport, I., Boll, W., Yu, A., Böcking, T., and Kirchhausen, T. (2008). "A Motif in the Clathrin Heavy Chain Required for the Hsc70/Auxilin Uncoating Reaction". In: *Molecular Biology of the Cell* 19.1, pp. 405–413

Reiling, J. H., Olive, A. J., Sanyal, S., Carette, J. E., Brummelkamp, T. R., Ploegh, H. L., Starnbach, M. N., and Sabatini, D. M. (2013). "A CREB3/ARF4 signalling pathway mediates the response to Golgi stress and susceptibility to pathogens". In: *Nature Cell Biology* 15.12, pp. 1473–1485

Reimand, J., Arak, T., Adler, P., Kolberg, L., Reisberg, S., Peterson, H., and Vilo, J. (2016). "g:Profiler: a web server for functional interpretation of gene lists (2016 update)". In: *Nucleic Acids Research* 44.W1, W83–W89

Ren, X., Farías, G., Canagarajah, B., Bonifacino, J., and Hurley, J. (2013). "Structural Basis for Recruitment and Activation of the AP-1 Clathrin Adaptor Complex by Arf1". In: *Cell* 152.4, pp. 755–767

Ringstad, N, Gad, H, Löw, P, Di Paolo, G, Brodin, L, Shupliakov, O, and De Camilli, P (1999). "Endophilin/SH3p4 is required for the transition from early to late stages in clathrin-mediated synaptic vesicle endocytosis". In: *Neuron* 24.1, pp. 143–154

Robinson, M. S. (1987). "100-kD coated vesicle proteins: molecular heterogeneity and intracellular distribution studied with monoclonal antibodies". In: *The Journal of Cell Biology* 104.4, pp. 887–895

Robinson, M. S. and Pearse, B. M. (1986). "Immunofluorescent localization of 100K coated vesicle proteins". In: *The Journal of Cell Biology* 102.1, pp. 48–54

Robinson, M. S. (2004). "Adaptable adaptors for coated vesicles". In: *Trends in Cell Biology* 14.4, pp. 167–174

Robinson, M. S. (2015). "Forty Years of Clathrin-coated Vesicles". In: *Traffic* 16.12, pp. 1210–1238

Ross, J. P., Dupre, N., Dauvilliers, Y., Strong, S., Ambalavanan, A., Spiegelman, D., Dionne-Laporte, A., Pourcher, E., Langlois, M., Boivin, M., Leblond, C. S., Dion, P. A., Rouleau, G. A., and Gan-Or, Z. (2016). "Analysis of DNAJC13 mutations in French-Canadian/French cohort of Parkinson's disease". In: *Neurobiology of Aging* 45, 212.e13–212.e17

Roth, T. F. and Porter, K. R. (1964). "Yolk protein uptake in the oocyte of the mosquito Aedes Egypti. L." In: *The Journal of Cell Biology* 20.2, pp. 313–332

Roy, A., Kucukural, A., and Zhang, Y. (2010). "I-TASSER: a unified platform for automated protein structure and function prediction". In: *Nature Protocols* 5.4, pp. 725–738

Russo, I., Bubacco, L., and Greggio, E. (2014). "LRRK2 and neuroinflammation: partners in crime in Parkinson's disease?" In: *Journal of neuroinflammation* 11.1, p. 52

Saffarian, S., Cocucci, E., and Kirchhausen, T. (2009). "Distinct Dynamics of Endocytic Clathrin-Coated Pits and Coated Plaques". In: *PLoS Biology* 7.9

Saleem, M., Morlot, S., Hohendahl, A., Manzi, J., Lenz, M., and Roux, A. (2015). "A balance between membrane elasticity and polymerization energy sets the shape of spherical clathrin coats". In: *Nature Communications* 6.1, p. 6249

Sanders, W. R. (1865). "Case of an unusual form of nervous disease, dystaxia or pseudo-paralysis agitans, with remarks". In: *Edinburgh Medical Journal* 10, pp. 987–997

Sano, I, Gamo, T, Kakimoto, Y, Taniguchi, K, Takesada, M, and Nishinuma, K (1959). "Distribution of catechol compounds in human brain". In: *Biochimica et Biophysica Acta* 32, pp. 586–587

Scheele, U, Kalthoff, C, and Ungewickell, E (2001). "Multiple interactions of auxilin 1 with clathrin and the AP-2 adaptor complex". In: *The Journal of Biological Chemistry* 276.39, pp. 36131–36138

Scheele, U., Alves, J., Frank, R., Duwel, M., Kalthoff, C., and Ungewickell, E. (2003). "Molecular and functional characterization of clathrin- and AP-2-binding determinants within a disordered domain of auxilin". In: *The Journal of Biological Chemistry* 278.28, pp. 25357–25368

Schlossman, D. M., Schmid, S. L., Braell, W. A., and Rothman, J. E. (1984). "An enzyme that removes clathrin coats: purification of an uncoating ATPase". In: *The Journal of Cell Biology* 99.2, pp. 723–733

Scholz, S., Bras, J., Scholz, S. W., and Bras, J. (2015). "Genetics Underlying Atypical Parkinsonism and Related Neurodegenerative Disorders". In: *International Journal of Molecular Sciences* 16.10, pp. 24629–24655

Schultheis, P. J., Fleming, S. M., Clippinger, A. K., Lewis, J., Tsunemi, T., Giasson, B., Dickson, D. W., Mazzulli, J. R., Bardgett, M. E., Haik, K. L., Ekhator, O., Chava, A. K., Howard, J., Gannon, M., Hoffman, E., Chen, Y., Prasad, V., Linn, S. C., Tamargo, R. J., Westbroek, W., Sidransky, E., Krainc, D., and Shull, G. E. (2013). "Atp13a2-deficient mice exhibit neuronal ceroid lipofuscinosis, limited α-synuclein accumulation and age-dependent sensorimotor deficits". In: *Human Molecular Genetics* 22.10, pp. 2067–2082

Scott, B. L., Sochacki, K. A., Low-Nam, S. T., Bailey, E. M., Luu, Q., Hor, A., Dickey, A. M., Smith, S., Kerkvliet, J. G., Taraska, J. W., and Hoppe, A. D. (2018). "Membrane bending occurs at all stages of clathrin-coat assembly and defines endocytic dynamics". In: *Nature Communications* 9.419

Scott, P. M., Bilodeau, P. S., Zhdankina, O., Winistorfer, S. C., Hauglund, M. J., Allaman, M. M., Kearney, W. R., Robertson, A. D., Boman, A. L., and Piper, R. C. (2004). "GGA proteins bind ubiquitin to facilitate sorting at the trans-Golgi network". In: *Nature Cell Biology* 6.3, pp. 252–259

Seaman, M. N., Ball, C. L., and Robinson, M. S. (1993). "Targeting and mistargeting of plasma membrane adaptors in vitro". In: *The Journal of Cell Biology* 123.5, pp. 1093–1105

Seaman, M. N. J., Marcusson, E. G., Cereghino, J. L., and Emr, S. D. (1997). "Endosome to Golgi Retrieval of the Vacuolar Protein Sorting Receptor, Vps10p, Requires the Function of the VPS29, VPS30, and VPS35 Gene Products". In: 137.1, pp. 79–92

Seaman, M. N. (2004). "Cargo-selective endosomal sorting for retrieval to the Golgi requires retromer". In: *J Cell Biol* 165.1, pp. 111–122

Seaman, M. N. (2005). "Recycle your receptors with retromer". In: *Trends in Cell Biology* 15.2, pp. 68–75

Seaman, M. N. and Williams, H. P. (2002). "Identification of the Functional Domains of Yeast Sorting Nexins Vps5p and Vps17p". In: *Molecular Biology of the Cell* 13.8. Ed. by C. Kaiser, pp. 2826–2840

Seaman, M. N., McCaffery, J. M., and Emr, S. D. (1998). "A Membrane Coat Complex Essential for Endosome-to-Golgi Retrograde Transport in Yeast". In: *The Journal of Cell Biology* 142.3, pp. 665–681

Shi, A., Sun, L., Banerjee, R., Tobin, M., Zhang, Y., and Grant, B. D. (2009). "Regulation of endosomal clathrin and retromer-mediated endosome to Golgi retrograde transport by the J-domain protein RME-8". In: *The EMBO journal* 28.21, pp. 3290–3302

Shiba, T., Takatsu, H., Nogi, T., Matsugaki, N., Kawasaki, M., Igarashi, N., Suzuki, M., Kato, R., Earnest, T., Nakayama, K., and Wakatsuki, S. (2002). "Structural basis for recognition of acidic-cluster dileucine sequence by GGA1". In: *Nature* 415.6874, pp. 937–941

Shiba, T., Kawasaki, M., Takatsu, H., Nogi, T., Matsugaki, N., Igarashi, N., Suzuki, M., Kato, R., Nakayama, K., and Wakatsuki, S. (2003). "Molecular mechanism of membrane recruitment of GGA by ARF in lysosomal protein transport". In: *Nature Structural & Molecular Biology* 10.5, pp. 386–393

Shiba, Y., Katoh, Y., Shiba, T., Yoshino, K., Takatsu, H., Kobayashi, H., Shin, H.-W., Wakatsuki, S., and Nakayama, K. (2004). "GAT (GGA and Tom1) domain responsible for ubiquitin binding and ubiquitination". In: *The Journal of Bological Chemistry* 279.8, pp. 7105–7111

Shih, W, Gallusser, A, and Kirchhausen, T (1995). "A clathrin-binding site in the hinge of the beta 2 chain of mammalian AP-2 complexes". In: *The Journal of Biological Chemistry* 270.52, pp. 31083–31090

Shimada, A., Niwa, H., Tsujita, K., Suetsugu, S., Nitta, K., Hanawa-Suetsugu, K., Akasaka, R., Nishino, Y., Toyama, M., Chen, L., Liu, Z.-J., Wang, B.-C., Yamamoto, M., Terada, T., Miyazawa, A., Tanaka, A., Sugano, S., Shirouzu, M., Nagayama, K., Takenawa, T., and Yokoyama, S. (2007). "Curved EFC/F-BAR-domain dimers are joined end to end into a filament for membrane invagination in endocytosis." In: *Cell* 129.4, pp. 761–72

Shin, H.-W., Morinaga, N., Noda, M., and Nakayama, K. (2004). "BIG2, a guanine nucleotide exchange factor for ADP-ribosylation factors: its localization to recycling endosomes and implication in the endosome integrity". In: *Molecular Biology of the Cell* 15.12, pp. 5283–5294

Shin, J. J. H., Gillingham, A. K., Begum, F., Chadwick, J., and Munro, S. (2017). "TBC1D23 is a bridging factor for endosomal vesicle capture by golgins at the trans-Golgi". In: *Nature Cell Biology* 19.12, pp. 1424–1432

Shinotsuka, C., Yoshida, Y., Kawamoto, K., Takatsu, H., and Nakayama, K. (2002). "Overexpression of an ADP-ribosylation factor-guanine nucleotide exchange factor, BIG2, uncouples brefeldin A-induced adaptor protein-1 coat dissociation and membrane tubulation". In: *The Journal of Biological Chemistry* 277.11, pp. 9468–9473

Shupliakov, O, Löw, P, Grabs, D, Gad, H, Chen, H, David, C, Takei, K, De Camilli, P, and Brodin, L (1997). "Synaptic vesicle endocytosis impaired by disruption of dynamin-SH3 domain interactions". In: *Science* 276.5310, pp. 259–263

Simpson, F., Bright, N. A., West, M. A., Newman, L. S., Darnell, R. B., and Robinson, M. S. (1996). "A novel adaptor-related protein complex". In: *The Journal of Cell Biology* 133.4, pp. 749–760

Simpson, F., Peden, A. A., Christopoulou, L., and Robinson, M. S. (1997). "Characterization of the Adaptor-related Protein Complex, AP-3". In: *The Journal of Cell Biology* 137.4, pp. 835–845

Sina, F., Shojaee, S., Elahi, E., and Paisán-Ruiz, C. (2009). "R632W mutation in PLA2G6 segregates with dystonia-parkinsonism in a consanguineous Iranian family". In: *European Journal of Neurology* 16.1, pp. 101–104

Singleton, A. B., Farrer, M, Johnson, J, Singleton, A, Hague, S, Kachergus, J, Hulihan, M, Peuralinna, T, Dutra, A, Nussbaum, R, Lincoln, S, Crawley, A, Hanson, M, Maraganore, D, Adler, C, Cookson, M. R., Muenter, M, Baptista, M, Miller, D, Blancato, J, Hardy, J, and Gwinn-Hardy, K. (2003). "α-Synuclein locus triplication causes Parkinson's disease". In: *Science* 302.October, p. 841

Singleton, A. and Hardy, J. (2016). "The Evolution of Genetics: Alzheimer's and Parkinson's Diseases". In: *Neuron* 90.6, pp. 1154–1163

Smith, C. J., Grigorieff, N, and Pearse, B. M. (1998). "Clathrin coats at 21 A resolution: a cellular assembly designed to recycle multiple membrane receptors". In: *The EMBO journal* 17.17, pp. 4943–4953

Smith, C. J., Dafforn, T. R., Kent, H., Sims, C. A., Khubchandani-Aswani, K., Zhang, L., Saibil, H. R., and Pearse, B. M. (2004). "Location of Auxilin Within a Clathrin Cage". In: *Journal of Molecular Biology* 336.2, pp. 461–471

Sochacki, K. A., Dickey, A. M., Strub, M.-P., and Taraska, J. W. (2017). "Endocytic proteins are partitioned at the edge of the clathrin lattice in mammalian cells". In: *Nature Cell Biology* 19.4, pp. 352–361

Soldner, F., Stelzer, Y., Shivalila, C. S., Abraham, B. J., Latourelle, J. C., Barrasa, M. I., Goldmann, J., Myers, R. H., Young, R. A., and Jaenisch, R. (2016). "Parkinson-associated risk variant in distal enhancer of α-synuclein modulates target gene expression". In: *Nature* 533.7601, pp. 95–99

Soneson, C., Love, M. I., and Robinson, M. D. (2016). "Differential analyses for RNA-seq: transcript-level estimates improve gene-level inferences". In: *F1000Research* 4.1521

Song, L., He, Y., Ou, J., Zhao, Y., Li, R., Cheng, J., Lin, C.-H., and Ho, M. S. (2017). "Auxilin Underlies Progressive Locomotor Deficits and Dopaminergic Neuron Loss in a Drosophila Model of Parkinson's Disease". In: *Cell Reports* 18.5, pp. 1132–1143

Spillantini, M. G., Schmidt, M. L., Lee, V. M. Y., Trojanowski, J. Q., Jakes, R., and Goedert, M. (1997). "α-Synuclein in Lewy bodies". In: *Nature* 388, pp. 839–840

Stachowiak, J. C., Schmid, E. M., Ryan, C. J., Ann, H. S., Sasaki, D. Y., Sherman, M. B., Geissler, P. L., Fletcher, D. A., and Hayden, C. C. (2012). "Membrane bending by protein protein crowding". In: *Nature Cell Biology* 14.9, pp. 944–949

Stamnes, M. A. and Rothman, J. E. (1993). "The binding of AP-1 clathrin adaptor particles to Golgi membranes requires ADP-ribosylation factor, a small GTP-binding protein". In: *Cell* 73.5, pp. 999–1005

Stetler, R. A., Gan, Y., Zhang, W., Liou, A. K., Gao, Y., Cao, G., and Chen, J. (2010). "Heat shock proteins: Cellular and molecular mechanisms in the central nervous system". In: *Progress in Neurobiology* 92.2, pp. 184–211

Suer, S., Misra, S., Saidi, L. F., and Hurley, J. H. (2003). "Structure of the GAT domain of human GGA1: A syntaxin amino-terminal domain fold in an endosomal trafficking adaptor". In: *Proceedings of the National Academy of Sciences* 100.8, pp. 4451–4456

Taghavi, S., Chaouni, R., Tafakhori, A., Azcona, L. J., Firouzabadi, S. G., Omrani, M. D., Jamshidi, J., Emamalizadeh, B., Shahidi, G. A., Ahmadi, M., Habibi,

S. A. H., Ahmadifard, A., Fazeli, A., Motallebi, M., Petramfar, P., Askarpour, S., Askarpour, S., Shahmohammadibeni, H. A., Shahmohammadibeni, N., Eftekhari, H., Shafiei Zarneh, A. E., Mohammadihosseinabad, S., Khorrami, M., Najmi, S., Chitsaz, A., Shokraeian, P., Ehsanbakhsh, H., Rezaeidian, J., Ebrahimi Rad, R., Madadi, F., Andarva, M., Alehabib, E., Atakhorrami, M., Mortazavi, S. E., Azimzadeh, Z., Bayat, M., Besharati, A. M., Harati-Ghavi, M. A., Omidvari, S., Dehghani-Tafti, Z., Mohammadi, F., Mohammad Hossein Pour, B., Noorollahi Moghaddam, H., Esmaili Shandiz, E., Habibi, A., Taherian-Esfahani, Z., Darvish, H., and Paisán-Ruiz, C. (2018). "A Clinical and Molecular Genetic Study of 50 Families with Autosomal Recessive Parkinsonism Revealed Known and Novel Gene Mutations". In: *Molecular Neurobiology* 55.4, pp. 3477–3489

Takatsu, H, Katoh, Y, Shiba, Y, and Nakayama, K (2001). "Golgi-localizing, gamma-adaptin ear homology domain, ADP-ribosylation factor-binding (GGA) proteins interact with acidic dileucine sequences within the cytoplasmic domains of sorting receptors through their Vps27p/Hrs/STAM (VHS) domains". In: *The Journal of biological chemistry* 276.30, pp. 28541–5

Takei, K., Slepnev, V. I., Haucke, V., and De Camilli, P. (1999). "Functional partnership between amphiphysin and dynamin in clathrin-mediatedendocytosis". In: *Nature Cell Biology* 1.1, pp. 33–39

Takeshita, H., Yamamoto, K., Nozato, S., Inagaki, T., Tsuchimochi, H., Shirai, M., Yamamoto, R., Imaizumi, Y., Hongyo, K., Yokoyama, S., Takeda, M., Oguro, R., Takami, Y., Itoh, N., Takeya, Y., Sugimoto, K., Fukada, S.-I., and Rakugi, H. (2017). "Modified forelimb grip strength test detects aging-associated physiological decline in skeletal muscle function in male mice". In: *Scientific Reports* 7.42323

Tansey, M. G. and Goldberg, M. S. (2011). "Neuroinflammation in Parkinson's disease: its role in neuronal death and implications for therapeutic intervention". In: *Neurobiological Disorders* 37.3, pp. 510–518

Taschenberger, G., Garrido, M., Tereshchenko, Y., Bähr, M., Zweckstetter, M., and Kügler, S. (2012). "Aggregation of αSynuclein promotes progressive in vivo neurotoxicity in adult rat dopaminergic neurons". In: *Acta Neuropathologica* 123, pp. 671–683

Taylor, M. J., Perrais, D., and Merrifield, C. J. (2011). "A High Precision Survey of the Molecular Dynamics of Mammalian Clathrin-Mediated Endocytosis". In: *PLoS Biology* 9.3

The Gene Ontology Consortium (2019). "The Gene Ontology Resource: 20 years and still GOing strong". In: *Nucleic Acids Research* 47.D1, pp. D330–D338

The Gene Ontology Consortium, Ashburner, M, Ball, C. A., Blake, J. A., Botstein, D, Butler, H, Cherry, J. M., Davis, A. P., Dolinski, K, Dwight, S. S., Eppig, J. T., Harris, M. A., Hill, D. P., Issel-Tarver, L, Kasarskis, A, Lewis, S, Matese, J. C., Richardson, J. E., Ringwald, M, Rubin, G. M., Sherlock, G, and Sherlock, G. (2000). "Gene ontology: tool for the unification of biology". In: *Nature Genetics* 25.1, pp. 25–9

The UniProt Consortium (2019). "UniProt: a worldwide hub of protein knowledge". In: *Nucleic Acids Research* 47.D1, pp. D506–D515

Towler, M. C., Gleeson, P. A., Hoshino, S., Rahkila, P., Manalo, V., Ohkoshi, N., Ordahl, C., Parton, R. G., and Brodsky, F. M. (2004). "Clathrin isoform CHC22, a component of neuromuscular and myotendinous junctions, binds sorting nexin 5 and has increased expression during myogenesis and muscle regeneration". In: *Molecular Biology of the Cell* 15.7, pp. 3181–3195

Traub, L. M., Ostrom, J. A., and Kornfeld, S (1993). "Biochemical dissection of AP-1 recruitment onto Golgi membranes". In: *The Journal of Cell Biology* 123.3, pp. 561–573

Tretiakoff, K. (1919). "Contribution a l'etude de l'anatomie pathologique du locus niger de Soemmering avec quelques deduction relatives a la pathogenie des troubles du tonus musculaire et la maladie de Parkinson". In: *Doctoral Dissertation, University of Paris*

Trinkle-Mulcahy, L., Boulon, S., Lam, Y. W., Urcia, R., Boisvert, F.-M., Vandermoere, F., Morrice, N. A., Swift, S., Rothbauer, U., Leonhardt, H., and Lamond, A. (2008). "Identifying specific protein interaction partners using quantitative mass spectrometry and bead proteomes". In: *The Journal of Cell Biology* 183.2, pp. 223–239

Tucker, L. B. and McCabe, J. T. (2017). "Behavior of Male and Female C57BL/6J Mice Is More Consistent with Repeated Trials in the Elevated Zero Maze than in the Elevated Plus Maze". In: *Frontiers in Behavioral Neuroscience* 11.13

Umeda, A., Meyerholz, A., and Ungewickell, E. (2000). "Identification of the universal cofactor (auxilin 2) in clathrin coat dissociation". In: *European Journal of Cell Biology* 79.5, pp. 336–342

Unger, E. L., Eve, D. J., Perez, X. A., Reichenbach, D. K., Xu, Y., Lee, M. K., and Andrews, A. M. (2006). "Locomotor hyperactivity and alterations in dopamine neurotransmission are associated with overexpression of A53T mutant human α-synuclein in mice". In: *Neurobiology of Disease* 21.2, pp. 431–443

Ungewickell, E (1985). "The 70-kd mammalian heat shock proteins are structurally and functionally related to the uncoating protein that releases clathrin triskelia from coated vesicles". In: *The EMBO journal* 4.13, pp. 3385–3391

Ungewickell, E, Ungewickell, H, and Holstein, S. E. (1997). "Functional interaction of the auxilin J domain with the nucleotide- and substrate-binding modules of Hsc70". In: *The Journal of Biological Chemistry* 272.31, pp. 19594–19600

Ungewickell, E. and Branton, D. (1981). "Assembly units of clathrin coats". In: *Nature* 289.5796, pp. 420–422

Usenovic, M., Tresse, E., Mazzulli, J. R., Taylor, J. P., and Krainc, D. (2012). "Deficiency of ATP13A2 leads to lysosomal dysfunction, α-synuclein accumulation, and neurotoxicity". In: *The Journal of Neuroscience* 32.12, pp. 4240–4246

Valente, E. M., Abou-Sleiman, P. M., Caputo, V., Muqit, M. M. K., Harvey, K., Gispert, S., Ali, Z., Del Turco, D., Bentivoglio, A. R., Healy, D. G., Albanese, A., Nussbaum, R., González-Maldonado, R., Deller, T., Salvi, S., Cortelli, P., Gilks, W. P., Latchman, D. S., Harvey, R. J., Dallapiccola, B., Auburger, G., and Wood, N. W. (2004). "Hereditary early-onset Parkinson's disease caused by mutations in PINK1". In: *Science* 304, pp. 1158–1160

Vauthier, V., Jaillard, S., Journel, H., Dubourg, C., Jockers, R., and Dam, J. (2012). "Homozygous deletion of an 80kb region comprising part of DNAJC6 and LEPR genes on chromosome 1P31.3 is associated with early onset obesity,

mental retardation and epilepsy". In: *Molecular Genetics and Metabolism* 106.3, pp. 345–350

Veeraragavan, S., Graham, D., Bui, N., Yuva-Paylor, L. A., Wess, J., and Paylor, R. (2012). "Genetic reduction of muscarinic M4 receptor modulates analgesic response and acoustic startle response in a mouse model of fragile X syndrome (FXS)". In: *Behavioural Brain Research* 228.1, pp. 1–8

Vigers, G. P., Crowther, R. A., and Pearse, B. M. (1986). "Three-dimensional structure of clathrin cages in ice". In: *The EMBO journal* 5.3, pp. 529–534

Vilariño-Güell, C., Wider, C., Ross, O. A., Dachsel, J. C., Kachergus, J. M., Lincoln, S. J., Soto-Ortolaza, A. I., Cobb, S. A., Wilhoite, G. J., Bacon, J. A., Bahareh Behrouz, Melrose, H. L., Hentati, E., Puschmann, A., Evans, D. M., Conibear, E., Wasserman, W. W., Aasly, J. O., Burkhard, P. R., Djaldetti, R., Ghika, J., Hentati, F., Krygowska-Wajs, A., Lynch, T., Melamed, E., Rajput, A., Rajput, A. H., Solida, A., Wu, R. M., Uitti, R. J., Wszolek, Z. K., Vingerhoets, F., and Farrer, M. J. (2011). "VPS35 mutations in parkinson disease". In: *American Journal of Human Genetics* 89.1, pp. 162–167

Vilariño-Güell, C., Rajput, A., Milnerwood, A. J., Shah, B., Szu-Tu, C., Trinh, J., Yu, I., Encarnacion, M., Munsie, L. N., Tapia, L., Gustavsson, E. K., Chou, P., Tatarnikov, I., Evans, D. M., Pishotta, F. T., Volta, M., Beccano-Kelly, D., Thompson, C., Lin, M. K., Sherman, H. E., Han, H. J., Guenther, B. L., Wasserman, W. W., Bernard, V., Ross, C. J., Appel-Cresswell, S., Stoessl, A. J., Robinson, C. A., Dickson, D. W., Ross, O. A., Wszolek, Z. K., Aasly, J. O., Wu, R.-M., Hentati, F., Gibson, R. A., McPherson, P. S., Girard, M., Rajput, M., Rajput, A. H., and Farrer, M. J. (2014). "DNAJC13 mutations in Parkinson's disease". In: *Human Molecular Genetics* 23.7, pp. 1794–1801

Wakeham, D. E., Abi-Rached, L., Towler, M. C., Wilbur, J. D., Parham, P., and Brodsky, F. M. (2005). "Clathrin heavy and light chain isoforms originated by independent mechanisms of gene duplication during chordate evolution". In: *Proceedings of the National Academy of Sciences* 102.20, pp. 7209–7214

Walf, A. A. and Frye, C. A. (2007). "The use of the elevated plus maze as an assay of anxiety-related behavior in rodents". In: *Nature Protocols* 2.2, pp. 322–328

Wang, F., Flanagan, J., Su, N., Wang, L.-C., Bui, S., Nielson, A., Wu, X., Vo, H.-T., Ma, X.-J., and Luo, Y. (2012). "RNAscope: A Novel in Situ RNA

Analysis Platform for Formalin-Fixed, Paraffin-Embedded Tissues". In: *The Journal of Molecular Diagnostics* 14.1, pp. 22–29

Wang, Y. J., Wang, J., Sun, H. Q., Martinez, M., Sun, Y. X., Macia, E., Kirchhausen, T., Albanesi, J. P., Roth, M. G., and Yin, H. L. (2003). "Phosphatidylinositol 4 Phosphate Regulates Targeting of Clathrin Adaptor AP-1 Complexes to the Golgi". In: *Cell* 114.3, pp. 299–310

Williams, M. A. and Fukuda, M (1990). "Accumulation of membrane glycoproteins in lysosomes requires a tyrosine residue at a particular position in the cytoplasmic tail". In: *The Journal of Cell Biology* 111.3, pp. 955–966

Wilms, H., Rosenstiel, P., Sievers, J., Deuschl, G., Zecca, L., and Lucius, R. (2003). "Activation of microglia by human neuromelanin is NF-κB dependent and involves p38 mitogen-activated protein kinase: implications for Parkinson's disease". In: *The FASEB Journal* 17.3, pp. 500–502

Winkler, F. and Stanley, K. (1983). "Clathrin heavy chain, light chain interactions". In: *The EMBO Journal* 2.8, pp. 1393–1400

Winner, B., Jappelli, R., Maji, S. K., Desplats, P. A., Boyer, L., and Aigner, S. (2011). "In vivo demonstration that α-synuclein oligomers are toxic". In: *Proceedings of the National Academy of Sciences* 108.10, pp. 4194–4199

Wolf, A., Bauer, B., Abner, E. L., Ashkenazy-Frolinger, T., and Hartz, A. M. S. (2016). "A Comprehensive Behavioral Test Battery to Assess Learning and Memory in 129S6/Tg2576 Mice". In: *PLOS ONE* 11.1, e0147733

Xing, Y., Böcking, T., Wolf, M., Grigorieff, N., Kirchhausen, T., and Harrison, S. C. (2010). "Structure of clathrin coat with bound Hsc70 and auxilin: mechanism of Hsc70-facilitated disassembly". In: *The EMBO Journal* 29.3, pp. 655–665

Xu, Z., Page, R. C., Gomes, M. M., Kohli, E., Nix, J. C., Herr, A. B., Patterson, C., and Misra, S. (2008). "Structural basis of nucleotide exchange and client binding by the Hsp70 cochaperone Bag2". In: *Nature Structural & Molecular Biology* 15.12, pp. 1309–1317

Yang, J., Yan, R., Roy, A., Xu, D., Poisson, J., and Zhang, Y. (2015). "The I-TASSER Suite: protein structure and function prediction". In: *Nature Methods* 12.1, pp. 7–8

Yim, Y.-I., Sun, T., Wu, L.-G., Raimondi, A., De Camilli, P., Eisenberg, E., and Greene, L. E. (2010). "Endocytosis and clathrin-uncoating defects at synapses of auxilin knockout mice". In: *Proceedings of the National Academy of Sciences of the United States of America* 107.9, pp. 4412–4417

Yoshida, S., Hasegawa, T., Suzuki, M., Sugeno, N., Kobayashi, J., Ueyama, M., Fukuda, M., Ido-Fujibayashi, A., Sekiguchi, K., Ezura, M., Kikuchi, A., Baba, T., Takeda, A., Mochizuki, H., Nagai, Y., and Aoki, M. (2018). "Parkinson's disease-linked DNAJC13 mutation aggravates alpha-synuclein-induced neurotoxicity through perturbation of endosomal trafficking". In: *Human Molecular Genetics* 27.5, pp. 823–836

Yuan, L., Song, Z., Deng, X., Zheng, W., Guo, Y., Yang, Z., and Deng, H. (2016). "Systematic analysis of genetic variants in Han Chinese patients with sporadic Parkinson's disease". In: *Scientific Reports* 6.33850

Yue, M., Hinkle, K., Davies, P., Trushina, E., Fiesel, F., Christenson, T., Schroeder, A., Zhang, L., Bowles, E., Behrouz, B., Lincoln, S., Beevers, J., Milnerwood, A., Kurti, A., McLean, P., Fryer, J., Springer, W., Dickson, D., Farrer, M., and Melrose, H. (2015). "Progressive dopaminergic alterations and mitochondrial abnormalities in LRRK2 G2019S knock-in mice". In: *Neurobiology of Disease* 78, pp. 172–195

Zarranz, J. J., Alegre, J., Gómez-Esteban, J. C., Lezcano, E., Ros, R., Ampuero, I., Vidal, L., Hoenicka, J., Rodriguez, O., Atarés, B., Llorens, V., Gomez Tortosa, E., Ser, T. DEL, Muñoz, D. G., and Yebenes, J. G. DE (2004). "The new mutation, E46K, of alpha-synuclein causes Parkinson and Lewy body dementia". In: *Annals of Neurology* 55, pp. 164–173

Zavodszky, E., Seaman, M. N., Moreau, K., Jimenez-Sanchez, M., Breusegem, S. Y., Harbour, M. E., and Rubinsztein, D. C. (2014). "Mutation in VPS35 associated with Parkinson's disease impairs WASH complex association and inhibits autophagy". In: *Nature Communications* 5.3828

Zhang, Y, Grant, B, and Hirsh, D (2001). "RME-8, a conserved J-domain protein, is required for endocytosis in Caenorhabditis elegans". In: *Molecular Biology of the Cell* 12.7, pp. 2011–2021

Zhang, Y., Chen, K., Sloan, S. A., Bennett, M. L., Scholze, A. R., O'Keeffe, S., Phatnani, H. P., Guarnieri, P., Caneda, C., Ruderisch, N., Deng, S.,

Liddelow, S. A., Zhang, C., Daneman, R., Maniatis, T., Barres, B. A., and Wu, J. Q. (2014). "An RNA-Sequencing Transcriptome and Splicing Database of Glia, Neurons, and Vascular Cells of the Cerebral Cortex". In: *Journal of Neuroscience* 34.36, pp. 11929–11947

Zhang, Y. (2008). "I-TASSER server for protein 3D structure prediction". In: *BMC Bioinformatics* 9.40

Zhang, Y., Sloan, S. A., Clarke, L. E., Caneda, C., Plaza, C. A., Blumenthal, P. D., Vogel, H., Steinberg, G. K., Edwards, M. S. B., Li, G., Duncan, J. A., Cheshier, S. H., Shuer, L. M., Chang, E. F., Grant, G. A., Gephart, M. G. H., and Barres, B. A. (2016a). "Purification and Characterization of Progenitor and Mature Human Astrocytes Reveals Transcriptional and Functional Differences with Mouse". In: *Neuron* 89.1, pp. 37–53

Zhang, Y. *et al.* (2016b). "Purification and Characterization of Progenitor and Mature Human Astrocytes Reveals Transcriptional and Functional Differences with Mouse". In: *Neuron* 89.1, pp. 37–53

Zhou, X., Fabian, L., Bayraktar, J. L., Ding, H.-M., Brill, J. A., and Chang, H. C. (2011). "Auxilin is required for formation of Golgi-derived clathrin-coated vesicles during Drosophila spermatogenesis". In: *Development* 138.6, pp. 1111–1120

Zhu, G., He, X., Zhai, P., Terzyan, S., Tang, J., and Zhang, X. C. (2003a). "Crystal structure of GGA2 VHS domain and its implication in plasticity in the ligand binding pocket". In: *FEBS Letters* 537.1-3, pp. 171–176

Zhu, G., Zhai, P., He, X., Terzyan, S., Zhang, R., Joachimiak, A., Tang, J., and Zhang, X. C. (2003b). "Crystal Structure of the Human GGA1 GAT Domain". In: *Biochemistry* 42.11, pp. 6392–6399

Zhu, Y, Doray, B, Poussu, A, Lehto, V. P., and Kornfeld, S (2001). "Binding of GGA2 to the lysosomal enzyme sorting motif of the mannose 6-phosphate receptor". In: *Science* 292.5522, pp. 1716–1718

Zimprich, A., Biskup, S., Leitner, P., Lichtner, P., Farrer, M., Lincoln, S., Kachergus, J., Hulihan, M., Uitti, R. J., Calne, D. B., Stoessl, a. J., Pfeiffer, R. F., Patenge, N., Carbajal, I. C., Vieregge, P., Asmus, F., Müller-Myhsok, B., Dickson, D. W., Meitinger, T., Strom, T. M., Wszolek, Z. K., and Gasser, T.

(2004). “Mutations in LRRK2 cause autosomal-dominant parkinsonism with pleomorphic pathology”. In: *Neuron* 44, pp. 601–607

Zimprich, A., Benet-Pagès, A., Struhal, W., Graf, E., Eck, S. H., Offman, M. N., Haubenberger, D., Spielberger, S., Schulte, E. C., Lichtner, P., Rossle, S. C., Klopp, N., Wolf, E., Seppi, K., Pirker, W., Presslauer, S., Mollenhauer, B., Katzenschlager, R., Foki, T., Hotzy, C., Reinthaler, E., Harutyunyan, A., Kralovics, R., Peters, A., Zimprich, F., Brücke, T., Poewe, W., Auff, E., Trenkwalder, C., Rost, B., Ransmayr, G., Winkelmann, J., Meitinger, T., and Strom, T. M. (2011). “A mutation in VPS35, encoding a subunit of the retromer complex, causes late-onset parkinson disease”. In: *American Journal of Human Genetics* 89.1, pp. 168–175

A APPENDIX 1: NEUROPATHOLOGY IN R857G AUXILIN MICE

A.1 INTRODUCTION

R857G Auxilin mice were found to develop neurological phenotypes reminiscent of young onset PD, including the typical Parkinsonian phenotypes bradykinesia, balance impairments and a decreased ability to terminate movements (see Chapter 4).

Even though the neuropathology underlying PD in Auxilin mutation carriers is unknown to date, typical PD is characterized by neurodegeneration of DA neurons in the SN and Lewy pathology (i.e. intracellular aggregates consisting of proteins and lipids) in surviving neurons. DA neurons in the SN project to the striatum, where they release the neurotransmitter dopamine. The resulting depletion of DA in the striatum is thought to underlie motor symptoms in PD, through abnormalities in basal ganglia signaling (see section 1.1.3) (Obeso *et al.*, 2009).

To gain further insight into the neuropathology in one year old R857G Auxilin mice, light microscopy and electron microscopy were used to analyse neuropathology and ultra-structural morphology, respectively, in brain slices of the nigrostriatal pathway in one year old R857G Auxilin mice. All immunohistochemistry experiments were performed by Dr. Natalie Landeck. Electron microscopy was performed in collaboration with the Electron Microscopy Core (National Heart, Lung and Blood Institute), led by Dr. Cristopher Bleck.

A.2 RESULTS

A.2.1 No signs of neurodegeneration in one year old R857G Auxilin mice

To address neurodegeneration in the SN, brain slices of one year old mice were stained with tyrosine hydroxylase (TH). TH is the rate-limiting enzyme in catecholamine biosynthesis, including the conversion of tyrosine to DA, and is therefore a DA neuronal marker. Comparison of midbrain slices of R857G Auxilin mice with age-matched WT controls did not reveal obvious alterations in DA neuron density in the SN (Figure A.1).

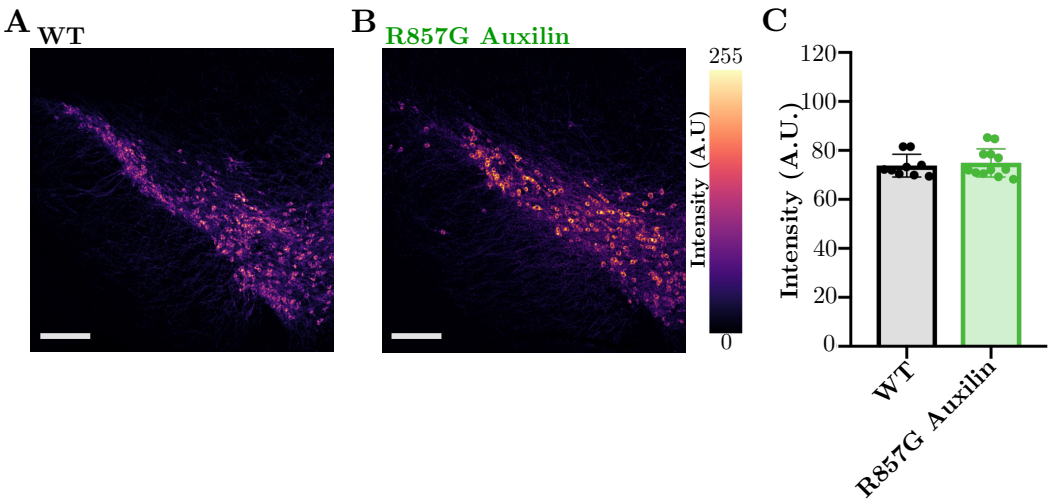

Figure A.1: **Staining for TH in the SN** A, B Staining for TH in the SN of WT and R857G Auxilin mice were performed by Dr. Natalie Landeck. Representative images are shown of 3 sections of n = 3 and n = 4 WT and R857G Auxilin mice, respectively. Scale bar indicates 200 μm. C Fluoresence intensity was quantified and Welch's t-test were performed. No significant alterations were observed.

Since DA neurons in the SN project to the striatum, projections of TH-positive neurons were analysed in the striatum. However, fiber density analysis did not reveal significant differences between WT and R857G Auxilin mice (Figure A.2 A-C).

In addition to TH, striatal brain sections were also stained for two dopaminergic presynaptic proteins, namely DAT (dopamine transporter) and VMAT2 (vesicular monoamine transporter 2). DAT transports extracellular dopamine in the synaptic cleft back into the cytosol. VMAT2 transports monoamine neurotransmitters, including dopamine, from the cytosol into synaptic vesicles. However, VMAT2 is not only a marker for DA neurons, but also for norepinephrinic, serotonergic and histaminergic neurons. Fiber density analysis of DAT and VMAT2 positive neurons in striatal sections also did not reveal differences between WT and R857G Auxilin mice (Figure A.2 C-I).

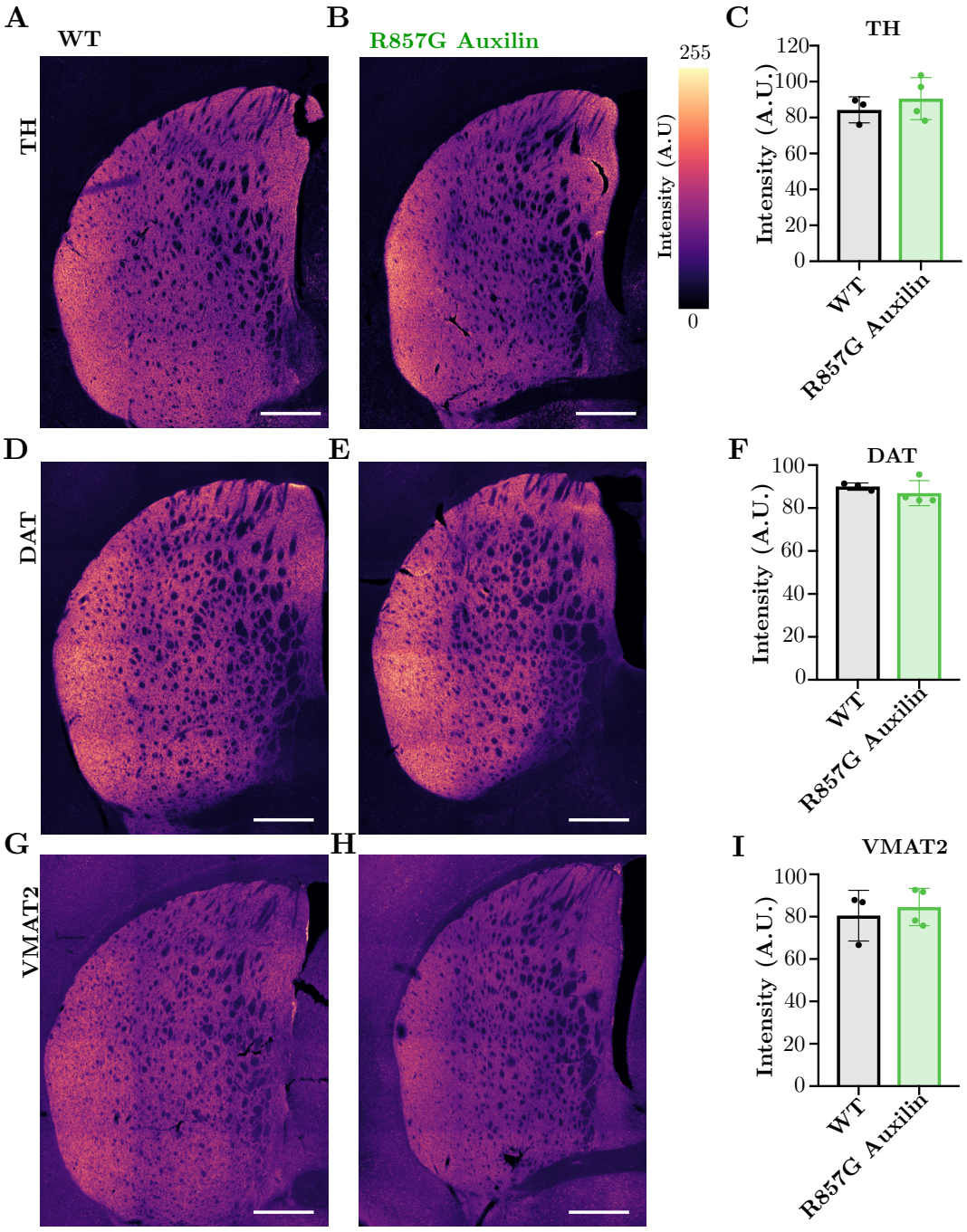

Figure A.2: **Staining for dopaminergic markers in the striatum** Staining for TH (A, B), DAT (D, E) and VMAT2 (G,H) in the striatum of WT and R857G Auxilin mice were performed by Dr. Natalie Landeck. Representative images are shown of n = 3 and n = 4 WT and R857G Auxilin mice, respectively. Scale bar indicates 500 μm. Fluorescence intensity (C, F, I) was quantified and Welch's t-test was performed. No significant alterations were observed.

A.2.2 Accumulation of lipid/proteinaceous aggregates in the striatum of R857G Auxilin mice

To analyse neuropathology in one year old R857G Auxilin mice at the ultra-structural level, striatal sections were analysed using EM. Large intracellular accumulations of lipid and protein, surrounded by limiting membrane, were apparent in R857G Auxilin mice, but not in WT mice (Figure A.3 A). Further analysis of lipid accumulation in DA neurons in the SN was performed using the boron-dipyrromethen (BODIPY) staining (i.e. a neutral lipid staining). Confocal microscopy analysis of BODIPY staining revealed a decrease in the number of lipid droplets in the striatum of R857G Auxilin mice, but the size of each droplet is significantly increased, resulting in an overall increase of total lipid content per cell in DA neurons in the SN in R857G Auxilin mice (Figure A.3 B-F).

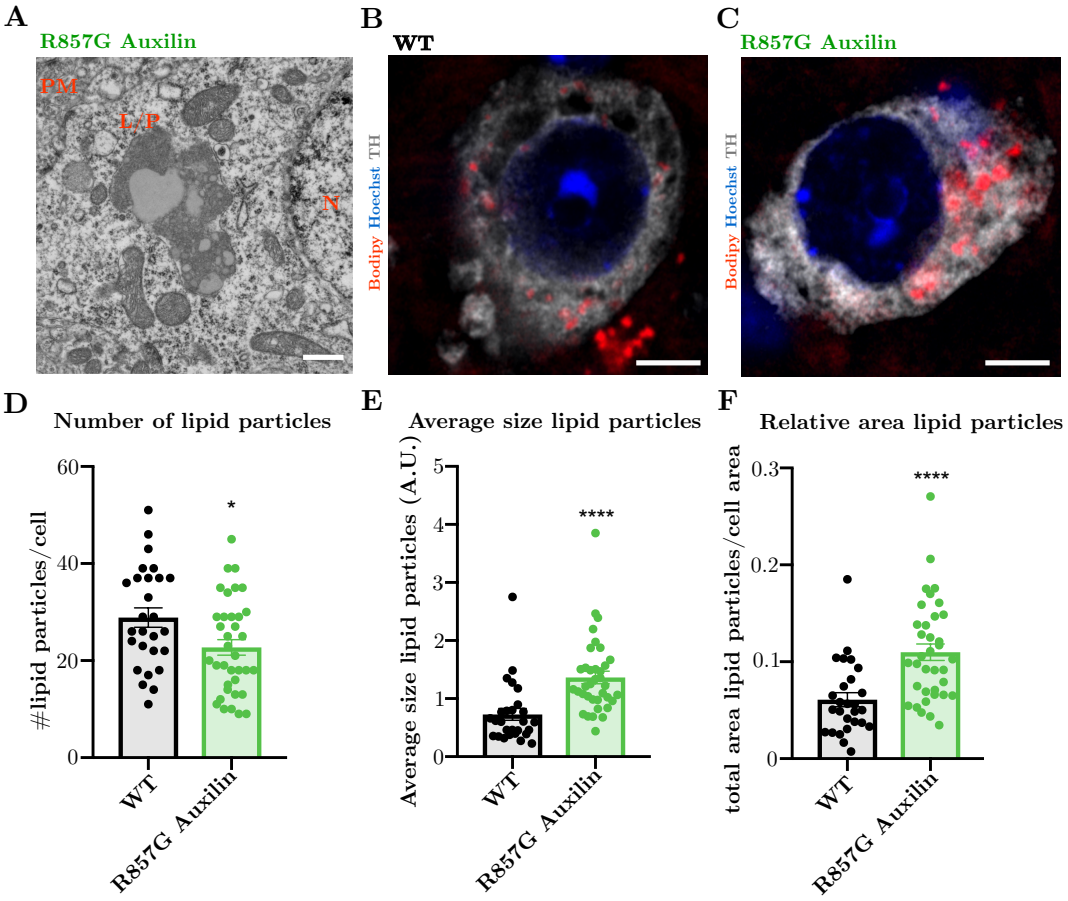

Figure A.3: **Accumulation of lipids in dopaminergic neurons** A EM analysis of striatal sections of a R857G Auxilin mouse. PM indicates plasma membrane, L/P lipid protein aggregate, N nucleus. Scale bar indicates 300 nm. EM analysis was performed in collaboration with the Electron Microscopy Core (National Heart, Lung and Blood Institute). B, C BODIPY staining and confocal imaging with Airyscan detection of DA neurons in sections of the SN of WT and R857G Auxilin mice was performed by Dr. Natalie Landeck. Scale bar indicates 5 μm. D, E, F Quantification of number of particles, particle size and lipid content per DA cell in the SN, respectively. 27 and 36 cells of n = 3 and n = 4 WT and R857G Auxilin mice, respectively, were analysed. Welch's t-test was performed, * indicates p-value <0.05, **** indicates p-value <0.0001.

A.2.3 Decreased number of synaptic vesicles in the striatum of R857G Auxilin mice

Ultra-structural analysis of synapses in the striatum revealed a decreased number of synaptic vesicles in the pre-synaptic area (Figure A.4). Given that the SN is the main input nucleus of the striatum, this indicates that DA neurons of the SN have a decreased number of SV in the pre-synaptic area.

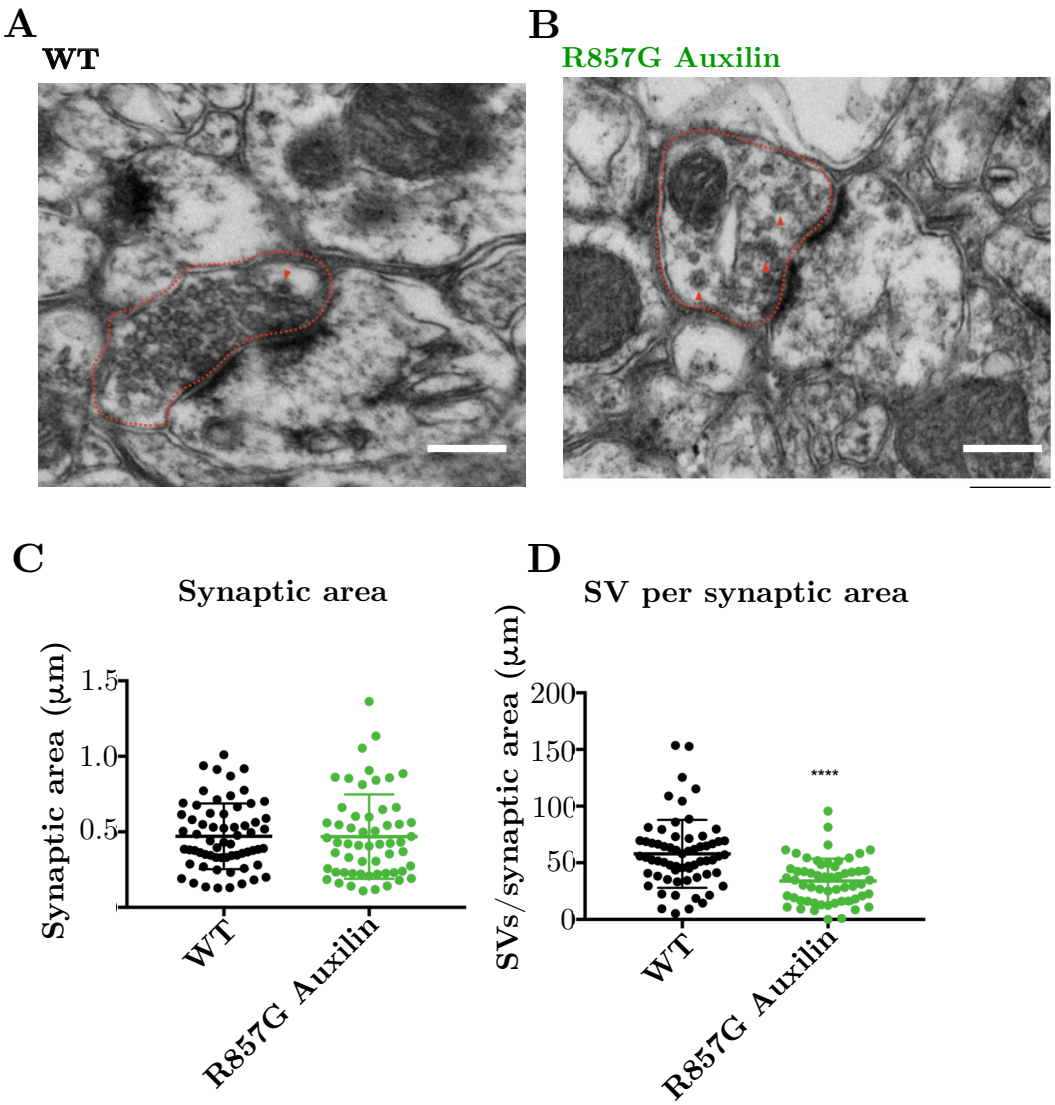

Figure A.4: **Decreased number of synaptic vesicles** A, B EM analysis of synaptic terminals of DA neurons in the *striatum* of WT and R857G Auxilin mice, respectively. EM analysis was performed by the Electron Microscopy Core (National Heart, Lung and Blood Institute). Presynapse is circled by red dotted line. Scale bar indicates 300 nm. C Quantification of pre-synaptic area. D Quantification of number of synaptic vesicles per pre-synaptic area. 64 and 57 synapses were analysed of n = 1 WT and R857G Auxilin mouse, respectively. Welch's t-test was performed, **** indicates p-value <0.0001. EM analysis was performed by the Electron Microscopy Core (National Heart, Lung and Blood Institute).

One-year old R857G Auxilin mice develop neurological phenotypes resembling young onset PD (see Chapter 4). The first neuropathological hallmark underlying motor phenotypes in human PD patients is the neurodegeneration of DA neurons in the SN that project to the striatum, with subsequent loss of DA fibers and depletion of DA in the striatum, but no such deterioration of DA neurons and projections were observed in the SN or striatum of R857G Auxilin mice. However, it is possible that synaptic defects underlie neurological phenotypes in R857G Auxilin mice. Indeed, a decreased number of synaptic vesicles was observed in R857G Auxilin mice. Given that CME is crucial for maintenance of the SV pool, it is thus conceivable that impaired CME may cause alterations in the number of CCVs. It is important to note that the EM experiments were performed in one animal per genotype. More experiments are required in additional mice to confirm the observed phenotype, for example by immunohistochemistry for synaptic vesicle markers. In addition, higher-resolution EM microscopy would greatly contribute to distinguish between clathrin coated and uncoated synaptic vesicles in the synapse, to analyse the impact of the R857G Auxilin mutation on the abundance of CCVs. Electrophysiology experiments would provide further insight into the synaptic activity of R857G Auxilin mice.

The second pathological hallmark of PD in patients is the accumulation of intracellular protein/lipid aggregates known as Lewy bodies. Remarkably, large intracellular lipid/protein aggregates were observed in the striatum of R857G Auxilin mice, and lipid staining revealed the accumulation of neutral lipids in the SN of R857G Auxilin mice. These aggregates might be the result of impaired clathrin trafficking at the TGN. The ER and Golgi apparatus are required for the synthesis and modifications of proteins and lipids, which are subsequently be

transported to intracellular destinations via the TGN. Impaired uncoating of CCVs derived from the TGN by R857G Auxilin mice might result of inefficient delivery of CCV cargo, including proteins and lipids, to the destination compartments, with an accumulation of cargo in the cytoplasm as a result. In addition, CCVs are crucial for the delivery of hydrolases to the lysosomes, thus impaired delivery of those hydrolyases could result in decreased cellular degradation capacity, which would further contribute to the formation of aggregates in cells.

Further work is required to characterize the nature of the observed protein/lipid aggregates, for example by staining for specific lipids and proteins. Lewy bodies are chiefly composed of α-synuclein, as well as other proteins such as tau and ubiquitin. Immunohistochemisry of these proteins in sections of the SN and striatum would greatly contribute to understand the nature of those aggregates. In addition, characterization of the lipid contents of the aggregates could be further characterized by staining for specific lipid species, such as ceramide.

In addition to the typical Parkinsonian motor phenotypes, Auxilin mutation carriers also develop atypical neurological phenotypes, such as seizures and cognitive decline. These phenotypes were found to be recapitulated by R857G Auxilin mice (see Chapter 4). Given that Auxilin is expressed in neurons across all brain areas, it is conceivable that lesions in other brain areas may underlie these neurological phenotypes. More experiments are therefore required to address neuropathology in different brain areas in addition to the nigrostriatal pathway.

A.4 MATERIAL AND METHODS

A.4.1 Immunohistochemistry

Animals were sacrificed at 1 year of age. Mice were deeply anesthetized with an intraperitoneal injection of 50 μl of 10% ketamine and the thoracic cavity was opened to expose the heart. Blood was flushed out using 10 ml of 0.9% NaCl for 2 minutes. Brains were removed, the left hemisphere was fresh frozen and the right hemisphere was fixed in 4% PFA for 48 hours. After 2 days, brains were transferred to 30% sucrose solution for cryoprotection and sectioning was started once brains had sunk to the bottom. The brains were cut into 30 m coronal sections and stored in antifreeze solution (0.5 M phosphate buffer, 30% glycerol, 30% ethylene glycol) at -20°C until further processing.

Immunohistochemical staining was performed under constant shaking on free-floating sections in a 24-well plate. Brain sections were transferred to 24-well plate and washed from antifreeze solution with PBS twice for 10 min.

Sections that were stained against DAT were subjected to antigen retrieval prior to immunostaining. Section were placed into Citric buffer (10mM sodium citrate, 0.05% Tween, pH 6) for 30 min at 80°C and were rinsed again afterwards with PBS buffer.

All sections were then incubated in PBS containing 10% NDS, 1% BSA and 0.3% Triton for 30 minutes. Following blocking, sections were incubated primary antibodies indicated in Table A.1 in antibody solution (1% NDS, 1% BSA and 0.3% Triton in PBS) overnight at 4°C.

Target	Host	Dilution	Vendor	Catalog number
TH	Mouse	1/500	Pel-freeze Biologicals	P40101-150
DAT	Rabbit	1/500	Abcam	ab111468
VMAT2	Rabbit	1/500	ImmunoStar	20042

Table A.1: **Primary antibodies used for IHC**

The next day, sections were rinsed three times with PBS for 10 min and incubated with the AlexaFluor labeled secondary antibody (1:500, Invitrogen, Donkey host) in antibody solution for 1 hour. Sections stained for TH were also incubated in 20 μg/ml BODIPY$^{493/503}$ (Invitrogen) to stain neutral lipids. Afterwards, sections were washed three times with PBS for 10 min, mounted on glass slides and coverslipped using Prolong Gold Antifade mounting media (Invitrogen).

A.4.2 Confocal laser-scanning microscopy and Airyscan processing

Confocal laser-scanning microscopy and Airyscan processing was performed as described in Section 5.4.11.

A.4.3 Electron microscopy

Electron microscopy was performed as described in Section 5.4.12.

A.4.4 Statistics

Data were plotted and statistical tests were performed using Prism 8 (Graphpad). The statistical test results are displayed in table A.2. n represents the number of animals, number of sections or number of cells included in each experiment and is explicitely mentioned in the caption of the figures.

Figure	Variable	Statistical test	Test result	P-value
A.1	Genotype	Welch's t-test	t = 0.4804	0.6364
A.2 C	Genotype	Welch's t-test	t = 0.8784	0.4205
A.2 F	Genotype	Welch's t-test	t = 0.9952	0.3808
A.2 I	Genotype	Welch's t-test	t = 0.4975	0.6479
A.3 D	Genotype	Welch's t-test	t = 2.391	0.0203
A.3 E	Genotype	Welch's t-test	t = 4.308	<0.0001
A.3 F	Genotype	Welch's t-test	t = 4.355	<0.0001
A.4 C	Genotype	Welch's t-test	t = 0.03784	0.9699
A.4 D	Genotype	Welch's t-test	t = 5.266	<0.0001

Table A.2: **Statistical test results**

B APPENDIX 2: MANUSCRIPTS

The following papers were published, submitted or prepared during the course of this PhD.

Manzoni, C., Mamais, A., **Roosen, D. A.**, Dihanich, S., Soutar, M. P. M., Plun-Favreau, H., Bandopadhyay, R., Hardy, J., Tooze, S. A., Cookson, M. R., and Lewis, P. A. (2016). mTOR independent regulation of macroautophagy by Leucine Rich Repeat Kinase 2 via Beclin-1. In: *Scientific Reports* 6.35106

I contributed to the acquisition of data in primary astrocytes.

Roosen, D. A. and Cookson, M. R. (2016). LRRK2 at the interface of autophagosomes, endosomes and lysosomes". In: *Molecular Neurodegeneration* 11.73

I contributed to the conceptualization and writing of the manuscript.

Roosen, D.A. and Singleton, A. B. (2017). Leucine rich repeat kinase knockout (LRRK KO) mouse model: linking paghological hallmarks of inherited and sporadic Parkinson's disease". In: *Movement disorders* 33.1

I contributed to the conceptualization and writing of the manuscript.

Roosen, D.A., Blauwendraat, C., Cookson, M. R. and Lewis, P. A. (2019). DNAJC proteins and pathways to parkinsonism". In: *FEBS Journal*

I contributed to the conceptualization and writing of the manuscript.

Roosen, D.A., Landeck, N., Conti, M., Twedell, E., Smith, N., Kaganovich, A., Saez-Atienzar, S., Ghosh, S., du Hoffmann, J., Beilina, A., Ding, J., Bonet-Poncet, L., Sampieri, L., Gershlick, D., Williamson, C., Bleck, C., Liu, C., Li, Y., Bonifacino, J., Kaliq, Z., Lewis, P. A. and Cookson, M. R. (2019). Parkinsons disease-associated Auxilin mutations impair clathrin trafficking at Golgi and synapses and underlie neurological phenotypes in mice". Manuscript in preparation.

I contributed to the conceptualization, design, acquisition and interpretation of data and writing of the manuscript.

SCIENTIFIC REPORTS

OPEN

mTOR independent regulation of macroautophagy by Leucine Rich Repeat Kinase 2 via Beclin-1

Received: 16 May 2016
Accepted: 22 September 2016
Published: 12 October 2016

Claudia Manzoni[1,2], Adamantios Mamais[3], Dorien A. Roosen[2,3], Sybille Dihanich[2], Marc P. M. Soutar[2], Helene Plun-Favreau[2], Rina Bandopadhyay[4], John Hardy[2], Sharon A. Tooze[5], Mark R. Cookson[3] & Patrick A. Lewis[1,2]

Leucine rich repeat kinase 2 is a complex enzyme with both kinase and GTPase activities, closely linked to the pathogenesis of several human disorders including Parkinson's disease, Crohn's disease, leprosy and cancer. LRRK2 has been implicated in numerous cellular processes; however its physiological function remains unclear. Recent reports suggest that LRRK2 can act to regulate the cellular catabolic process of macroautophagy, although the precise mechanism whereby this occurs has not been identified. To investigate the signalling events through which LRRK2 acts to influence macroautophagy, the mammalian target of rapamycin (mTOR)/Unc-51-like kinase 1 (ULK1) and Beclin-1/phosphatidylinositol 3-kinase (PI3K) pathways were evaluated in astrocytic cell models in the presence and absence of LRRK2 kinase inhibitors. Chemical inhibition of LRRK2 kinase activity resulted in the stimulation of macroautophagy in a non-canonical fashion, independent of mTOR and ULK1, but dependent upon the activation of Beclin 1-containing class III PI3-kinase.

Leucine rich repeat kinase 2 is one of the key genetic factors contributing to the risk of developing Parkinson's disease (PD), an irreversible, progressive neurodegenerative movement disorder primarily associated with neuronal cell loss in the *Substantia nigra pars compacta*. Coding mutations in the *LRRK2* gene are the most frequent genetic cause of familial PD, with polymorphisms in *LRRK2* associated with an increased risk of idiopathic PD[1–4]. In addition to this, genome wide association (GWA) studies recently identified the *LRRK2* locus as being involved in the risk for PD[5], Crohn's disease[6] and multibacillary leprosy[7,8]. Mutations in LRRK2 have also been linked to cancer[9], and the *LRRK2* region was identified as being subject to frequent carcinogenic alterations[10]. The *LRRK2* gene is therefore related to the etiopathogenesis of at least four human diseases, making it the focus of increasing attention as a putative drug target.

The physiological function of LRRK2 is as yet unclear. It is a complex enzyme, with active kinase and GTPase domains that are thought to reciprocally regulate one another's activity[11,12]. As detailed in the following section, several studies have indicated a putative role for LRRK2 in the control of macroautophagy, a process used by the cell to maintain a healthy microenvironment by removing misfolded proteins and damaged organelles[13]. The molecular mechanism underlying this association remains to be fully understood. While LRRK2 over-expression was associated with a macroautophagy-dependent induction of toxicity coupled with neurite atrophy[14], LRRK2 knock down was shown to both reduce and potentiate the autophagic flux[15,16]. Moreover, the overexpression of full-length LRRK2, or its kinase domain, as well as inhibition of LRRK2 kinase activity induced alterations of the macroautophagy-lysosomal pathway[17–19]. Macroautophagy was shown to be altered in human fibroblasts carrying LRRK2 pathogenic mutations associated with PD[20,21], in neurons derived from those human fibroblasts[22] and in transgenic or LRRK2 knock-out mouse models[23]. Finally, pathogenic mutations in LRRK2 have been linked to deregulation of chaperone mediated autophagy (CMA)[24]. More generally, LRRK2 was associated with vesicle trafficking and synaptic functionality[25,26], and with endocytosis and trans-Golgi network homeostasis[27,28].

[1]School of Pharmacy, University of Reading, Whiteknights, Reading, RG6 6AP, United Kingdom. [2]Department of Molecular Neuroscience, UCL Institute of Neurology, Queen Square, London WC1N 3BG, United Kingdom. [3]Cell Biology and Gene Expression Section, Laboratory of Neurogenetics, NIA, NIH, Building 35, 35 Convent Drive, Bethesda, MD 20892-3707, USA. [4]Reta Lila Weston Institute of Neurological Studies, UCL Institute of Neurology, 1 Wakefield Street London WC1N 1PJ, United Kingdom. [5]Francis Crick Institute, London Research Institute, 44 Lincoln's Inn Fields London, WC2A 3LY, United Kingdom. Correspondence and requests for materials should be addressed to C.M. (email: c.manzoni@reading.ac.uk) or P.A.L. (email: p.a.lewis@reading.ac.uk)

A hypothetical function for LRRK2 in the regulation of macroautophagy, and in general in vesicle homeostasis, is compelling considering that the macroautophagy/lysosomal system has an increasingly appreciated link to the etiology of PD[29], while it has long been considered a central player in the pathogenesis of Crohn's, leprosy and cancer.

The data presented herein demonstrate that the kinase activity of LRRK2 acts as a negative regulator of macroautophagy in astrocyte cell models. Our results suggest that LRRK2 may act to control a non-canonical pathway alternative and parallel to that regulated by the mammalian target of rapamycin (mTOR) and Unc-51 Like Kinase 1 (ULK1), but dependent on the presence of an active Beclin-1 complex. These data have important implications for the study of the physiological and pathological functions of LRRK2, in particular for any pharmacological intervention based upon LRRK2 inhibition.

Results

Inhibition of LRRK2 kinase activity increases LC3-II levels. LRRK2 is expressed at high levels in astrocytes within the brain[30,31]. Human H4 neuroglioma cells, originally derived from an astrocytoma, were previously used as a model to study LRRK2 function in macroautophagy[18,30]. Based on a previous work by our group[18], we here replicate and expand our previous analysis confirming that treatment of H4 cells for 150 minutes (acute treatment) or 18 hours (chronic treatment) with LRRK2 kinase inhibitors, either LRRK2in1[32] or GSK2578215A[33] result in a concentration dependent increase of LC3-II (Fig. 1a,b); no concomitant toxicity was recorded for the LRRK2in1 while a decrease in cell survival was detected for GSK2578215A starting at 30 μM (Supplementary Fig. S1a,b)[34]. A major confounding factor when using chemical inhibitors of enzymes is the possibility of off target effects. Although the inhibitors used are structurally distinct, it is critical to demonstrate that the cellular phenotypes measured are specific to the protein of interest. To achieve this, and as already previously proposed by our group, endogenous LRRK2 protein levels in H4 cells were decreased (~50%) by stable expression of LRRK2 shRNA (Fig.1c,d). 150 minutes (Fig. 1e,f) or 18 hours (Supplementary Fig. S1c) inhibition of LRRK2 kinase activity by LRRK2in1 increased LC3-II in scrambled controls cells but not in LRRK2 knocked-down cells, strongly suggesting that this is a LRRK2 dependent phenomenon. Interestingly, in this model system we consistently see no increase in basal LC3-II when knockin-down LRRK2. Further investigations are needed, however we suggest this may happen either because the knock-down is never complete, or alternative splicing isoforms may originate. Moreover, it is worth noticing that, with the knock-down strategy, we remove the kinase as well as the GTPase activities and the protein-protein interaction domains of LRRK2. Therefore the chemical kinase inhibition and the protein knock-down approaches may not represent a perfect phenocopy of each other. Primary astrocytes from LRRK2 knock-out mice were prepared and assessed for response to LRRK2 inhibition. An elevated, basal level of LC3-II was detected in the knock-out cells that was not significantly increased following treatment with LRRK2in1 (Fig. 1g,h, see Supplementary Fig. S1e for astrocytes evaluation by GFAP staining).

LRRK2 dependent increase of LC3-II is not due to decreased autophagosome-lysosome fusion. We have previously suggested that the increased levels of LC3-II after LRRK2 kinase inhibition were consequence of an increase in autophagosome production rather than a decrease in degradation. We here corroborate this data by improving the experimental setting including Torin-1 control, evaluating two distinct time-points of treatment, assessing the drug Chloroquine alongside with Bafilomycin (BafA1) and performing co-localization analysis of LAMP1 and p62. As first, H4 cells were co-treated with LRRK2 kinase inhibitor and BafA1 or Chloroquine. Results showed an additive effect of LRRK2in1 over BafA1 (or Chloroquine) treatment alone (Fig. 2a,b, Supplementary Fig. S2a) that appeared at 150 minutes and became significant at 18 hours (Fig. 2c–e), similarly to that observed with Torin-1, an mTOR inhibitor. This confirmed, as previously reported[18], that the LC3-II increase following inhibition of LRRK2 kinase activity, is different from the effect of BafA1, thus suggesting an increase in macroautophagy flux[34]. Since BafA1, which inhibits autophagosome-lysosome fusion, has an additional, distinct action in preventing lysosomal acidification[35], the pH of cellular vesicles was assessed in H4 cells treated for 150 minutes or 18 hours with LRRK2in1 or Torin-1, in the presence or absence of BafA1. Using neutral red accumulation no disruption of vesicle acidification was detected either with LRRK2in1 or Torin-1 (Supplementary Fig. S2b), further confirming that the inhibition of LRRK2 kinase activity does not affect lysosomal function. p62 is a cargo protein used to target substrates for degradation through autophagy. We evaluated the co-localization between p62 and LAMP1 (a lysosomal marker) to assess the fusion between lysosomes and autophagosomes[34,36] (Supplementary Fig. S3) showing that, whereas BafA1 was able to reduce the co-localization between p62 and LAMP1 as consequence of inhibition of autophagosome-lysosome fusion, cells treated with Torin-1 or LRRK2in1 were characterized by a higher proportion of co-localized vesicles suggesting that no impairment in autophagy degradation was occurring under such treatments.

Inhibition of LRRK2 kinase activity induces macroautophagy independently of mTOR/ULK1. In our previous work[18] we did not record any alteration of P70S6K and S6 phosphorylation when macroautophagy was induced by LRRK2 kinase inhibition. This suggested that, in this specific case, induction of macroautophagy may not follow the canonical mTOR pathway. With a new set of tailored experiments we here properly assess that previous suggestion and corroborate the idea that inhibition of LRRK2 kinase activity induces macroautophagy independently of mTOR/ULK1. In canonical macroautophagy, ULK1 is the key downstream effector of mTOR and AMP-activated protein kinase (AMPK) for phagophore generation[37]. Inactivation of mTOR (i.e. following Torin-1 treatment) results in de-phosphorylation of ULK1, and subsequent macroautophagy induction. Canonical macroautophagy induced by Torin-1 treatment and involving mTOR inhibition (as indicated by reduction in the phosphorylation level of p70S6 kinase at Thr389) was strongly associated with decreased mTOR-dependent phosphorylation of ULK1 at Ser758 (Fig. 3a). 150 minutes of LRRK2-in1 treatment was sufficient to increase the levels of the macroautophagy marker LC3-II, however no reduction of ULK1

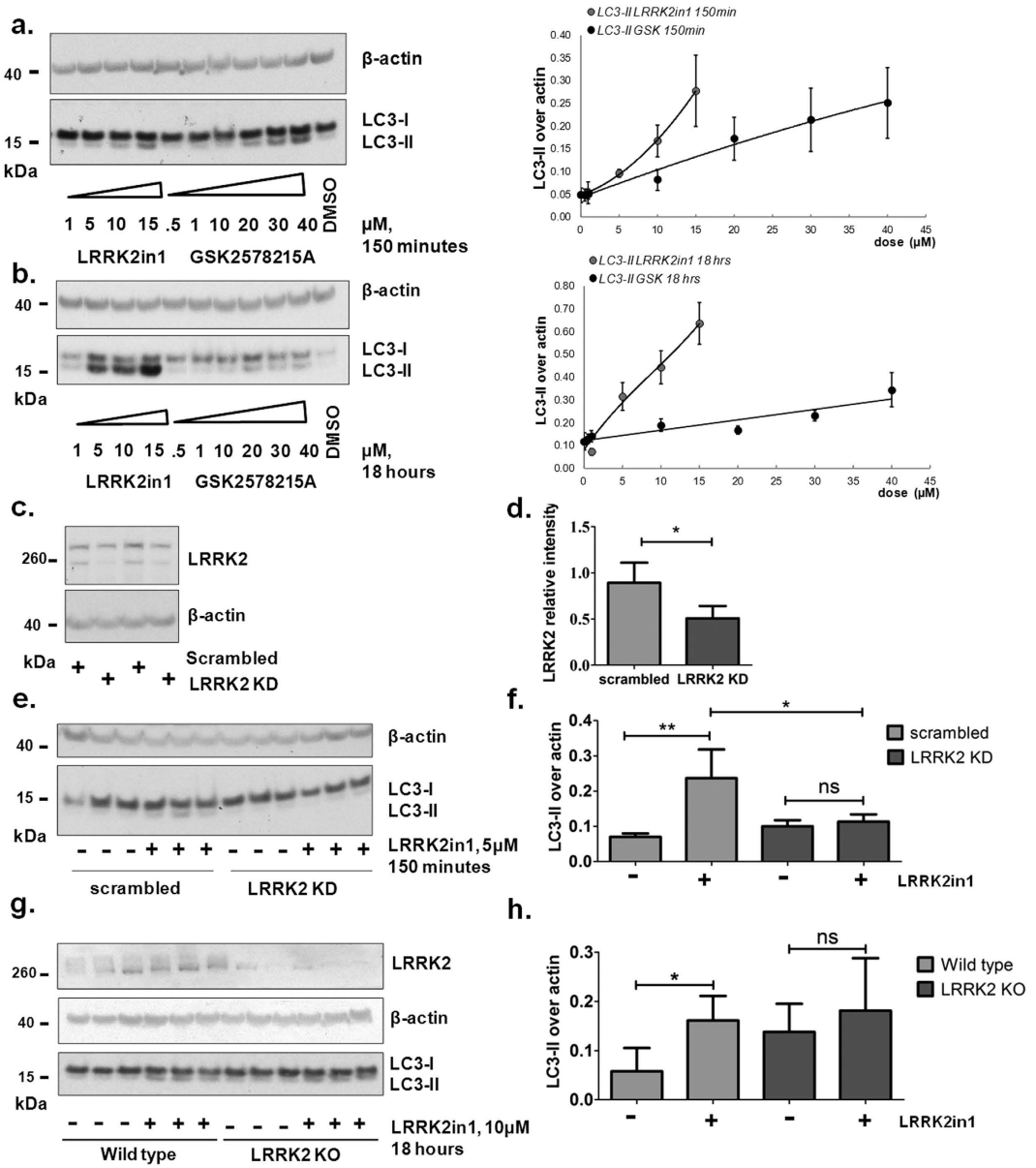

Figure 1. Inhibition of LRRK2 kinase leads to a dose response and time dependent increase in LC3-II. 150 minutes (**a**) or 18 hours (**b**) LRRK2in1 and GSK2578215A dose-response. The gels shown are representative of 3 independent experiments, LC3-II was quantified against β-actin, quantification was done for each single experiment; after normalization against the control in DMSO, data were pooled together in the dose-response curve (mean and SEM). (**c**) H4 cells with stable LRRK2 knock-down (~50% LRRK2 knock-down for KD#644167.03b transfection) as quantified in (**d**); LRRK2 was quantified (sum of the upper and lower bands) against β-actin, statistical analysis was performed by unpaired student t-test (mean and SD, p value = 0.0236). (**e**) 150 minutes LRRK2in1 treatment in scramble controls and in LRRK2 knock-down cells; the image shown (reporting 3 samples for each condition) is representative of 3 independent experiments and is quantified in (**f**); LC3-II was quantified against β-actin; statistical analysis was performed by 1way Anova followed by Tukey post-hoc test (mean and SD, $^{**}p < 0.01$; $^{*}p < 0.05$). (**g**) primary astrocytes from wild-type and LRRK2 knock-out mice treated with LRRK2in1 for 18 hours, the image shown is representative of 3 independent cell preparations, each replicated with 3 samples. (**h**) LC3-II was quantified against β-actin for each single experiment; after normalization against the internal control in DMSO, data were pulled together and statistical analysis was performed by 1way Anova followed by Tukey post-hoc test. (mean and SD, $^{*}p < 0.05$).

phosphorylation on Ser758, nor alteration of mTOR activity was observed, as indicated by phosphorylation levels of p70S6K at Thr389 (Fig. 3a).

In order to assess whether ULK1 is required for LRRK2-induced macroautophagy, ULK1 protein levels were stably reduced by 70% in H4 cells transfected with ULK1 shRNA. 150 minute treatment of LRRK2in1 led to a

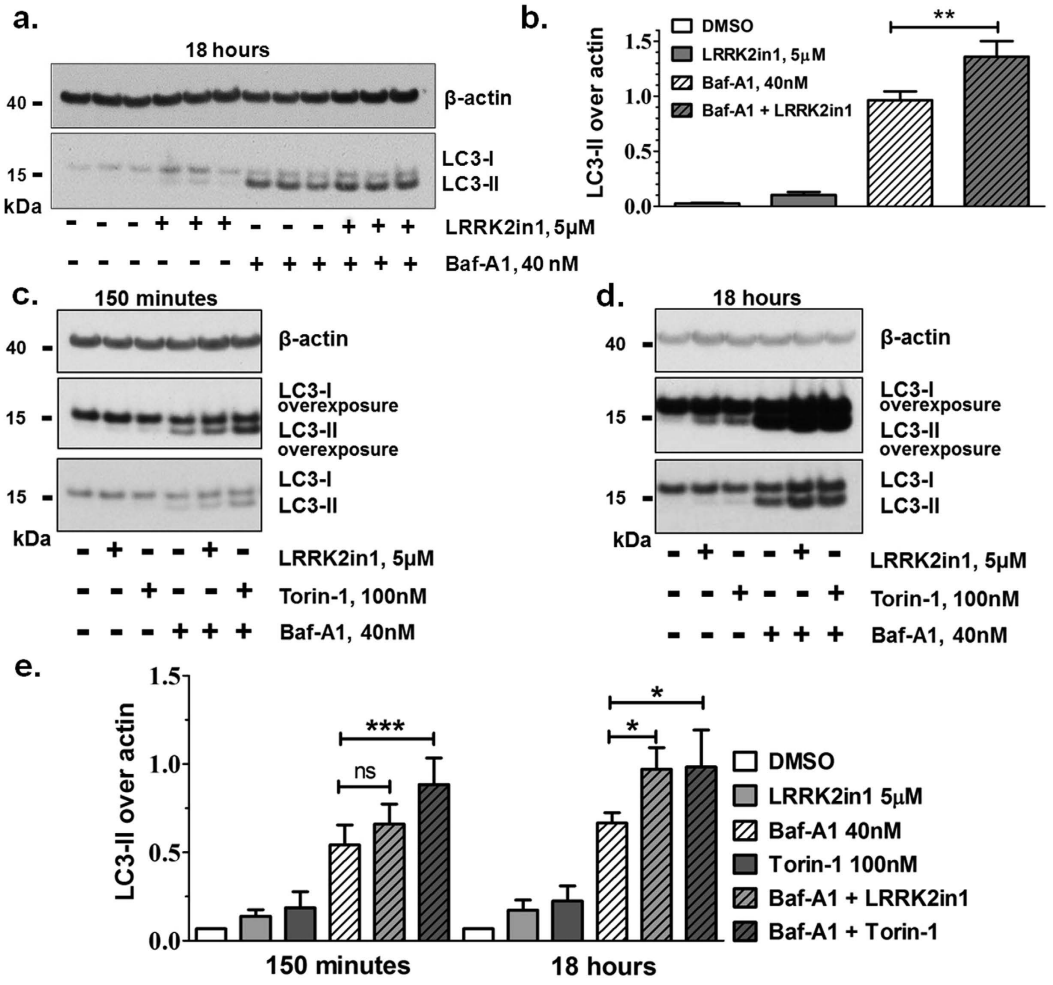

Figure 2. Increase in LC3-II after inhibition of LRRK2 kinase is due to an induction of the macroautophagy flux. (**a**) 18 hours treatment with LRRK2in1 in the presence and absence of BafA1 to block the autophagy flux. The gel shown is representative of 3 independent experiments, each performed in triplicate and it is quantified in (**b**). (**b**) LC3-II is quantified against β-actin; statistical analysis was performed by 1way Anova followed by Tukey post-hoc test (mean and SD, $^{**}p < 0.01$). 150 minutes (**c**) and 18 hours (**d**) treatment with LRRK2in1 or Torin-1 (to induce macroautophagy) in the presence and absence of BafA1. The gels shown are representative of at least 4 independent experiments summarized in (**e**). (**e**) LC3-II is quantified against β-actin for 5 replicates (150 minutes) and 4 replicates (18 hours); quantification was done for each single experiment; after normalization against the internal control in DMSO, data were pulled together and statistical analysis was performed by 1way Anova followed by Tukey post-hoc test (mean and SD, $^{***}p < 0.001$, $^{*}p < 0.05$).

comparable increase of LC3-II production in stable ULK1 knock-down as compared to scrambled control cells. These data indicate that ULK1 is dispensable for macroautophagy induced by LRRK2 kinase activity inhibition (Fig. 3b,c).

Co-treatment with LRRK2in1 and Torin-1 resulted in a stronger increase of LC3-II levels, as compared to single treatments with either LRRK2in1 or Torin-1 (Fig. 3d,e). This data supports an additive effect of the combined inhibition of LRRK2 and mTOR over the macroautophagy flux, further suggesting that these kinases act in parallel pathways to control macroautophagy induction and that the regulation of autophagy by LRRK2 is independent of mTOR/ULK1. Similar results were obtained when m-TOR was alternatively inhibited by aminoacid starvation (Supplementary Fig. S4a,b) or following Rapamycin treatment (Supplementary Fig. S4c), further demonstrating that LRRK2 control over autophagy is independent of mTOR.

Activation of macroautophagy after inhibition of LRRK2 kinase requires PI3P/Beclin-1. In addition to the ULK-kinase complex, canonical macroautophagy induction requires the class III PI3-kinase complex containing Beclin-1[38]. WIPI-2 is directly recruited to the nascent autophagosome by the presence of PI3P in the autophagosome membrane, following the activity of the Beclin-1 complex. We have previously shown that LRRK2in1 increases the number of WIPI2 positive punctae in cells[18]. To confirm that this effect can be reproduced, we repeated the prior experiment using a different quantification algorithm (Supplementary Fig. S5). This result suggests that, in contrast to mTOR inhibition and ULK1 activation, PI3P and WIPI-2 may be required for macroautophagy induced by LRRK2 inhibition. To further test this hypothesis, we performed a new and tailored

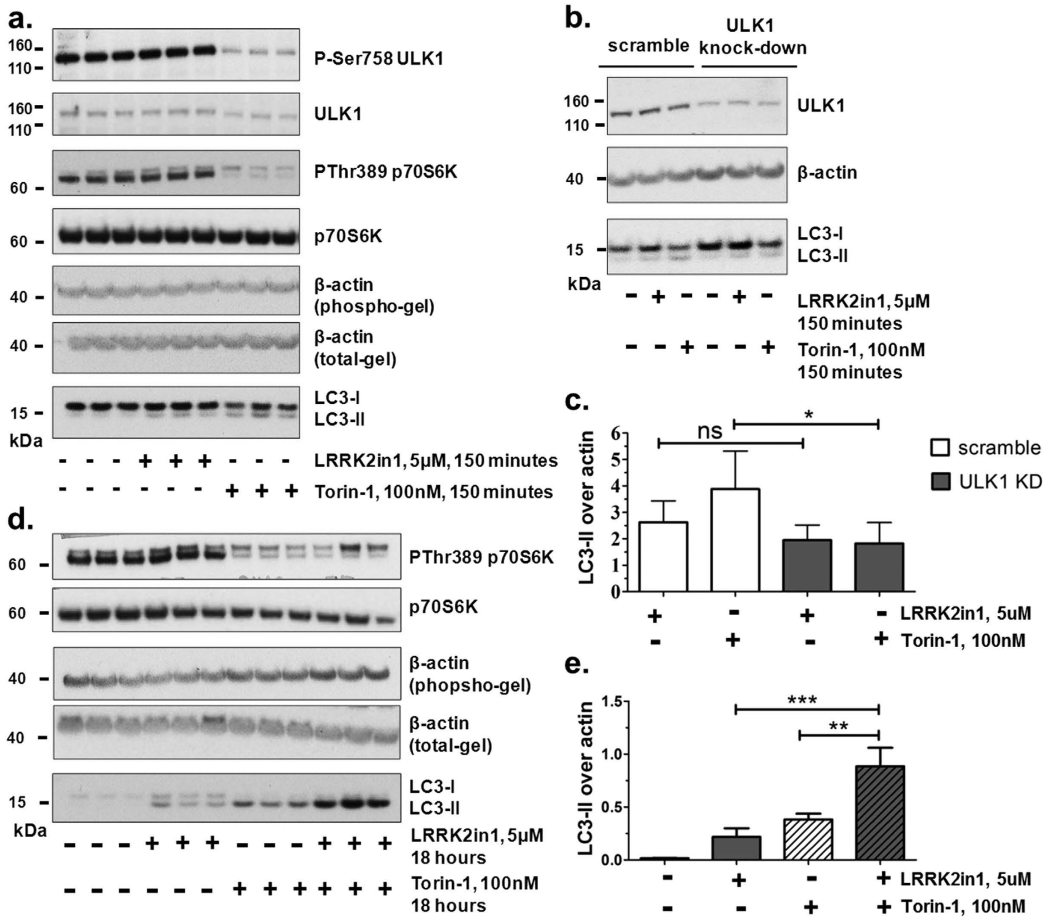

Figure 3. Increased macroautophagy following inhibition of LRRK2 kinase is mTOR independent. (**a**) 150 minutes treatment with LRRK2in1 or Torin-1 (to induce macroautophagy through mTOR). Phosphorylation of P70S6K and ULK1 were used as readout for mTOR inhibition. (**b**) 150 minutes treatment with LRRK2in1 or Torin-1 in scramble controls and in H4 cells with stable ULK1 knock-down (~70% ULK1 knock-down). The gel shown is representative of 4 independent experiments that are quantified in (**c**). (**c**) Quantification was done for each single experiment and LC3-II was normalized against β-actin. After normalization against the control in DMSO, data were pulled together and statistical analysis was performed by 1way Anova followed by Tukey post-hoc test (mean and SD, $*p < 0.05$). (**d**) 18 hours treatment with LRRK2in1 in the presence and absence of Torin-1. Phosphorylation on P70S6K was used as control for mTOR inhibition. The gel shown is representative of 3 independent experiments each performed in triplicate and quantified in (**e**). (**e**) LC3-II was quantified against β-actin; statistical analysis was performed by 1way Anova followed by Tukey post-hoc test (mean and SD, $**p < 0.01$, $***p < 0.001$).

set of experiments. LC3-II levels after LRRK2in1 treatment were assessed in H4 cells treated with wortmannin (or VPS34in1) to inhibit PI3K (or specifically VPS34) and consequently the production of PI3P. Co-treatment with wortmannin (Fig. 4a,b) or VPS34in1 (Fig. 4c,d) and either LRRK2in1 or Torin-1 blocked LRRK2-induced macroautophagy and mTOR-induced macroautophagy respectively further confirming that PI3P is required for autophagosome production under LRRK2 inhibition.

Finally, in order to assess whether Beclin-1 is required for LRRK2-induced macroautophagy, Beclin-1 protein levels were stably reduced in H4 cells transfected with Beclin-1 shRNA(s). Knock-down of Beclin-1 increased the basal level of LC3-II and this was not further increased after 150 minutes treatment with LRRK2-in 1, in contrast to scrambled shRNA controls which showed an enhancement of LC3-II compared to basal levels (Fig. 4e,f). This data further suggested that the macroautophagy pathway controlled by Beclin-1, but not ULK1, is required for the negative regulation by LRRK2 kinase.

Discussion

Despite its key role in the etiology of a number of human diseases, there is as yet no consensus regarding the physiological function of LRRK2; leading to the suggestion that LRRK2 may have contrasting roles depending on the cell type and condition under investigation[39]. A number of reports have implicated LRRK2 in the regulation of macroautophagy, in endocytosis and metabolism, however the precise molecular function of LRRK2 in these processes is still not defined. The data reported here demonstrate that, at least one of the functions supported

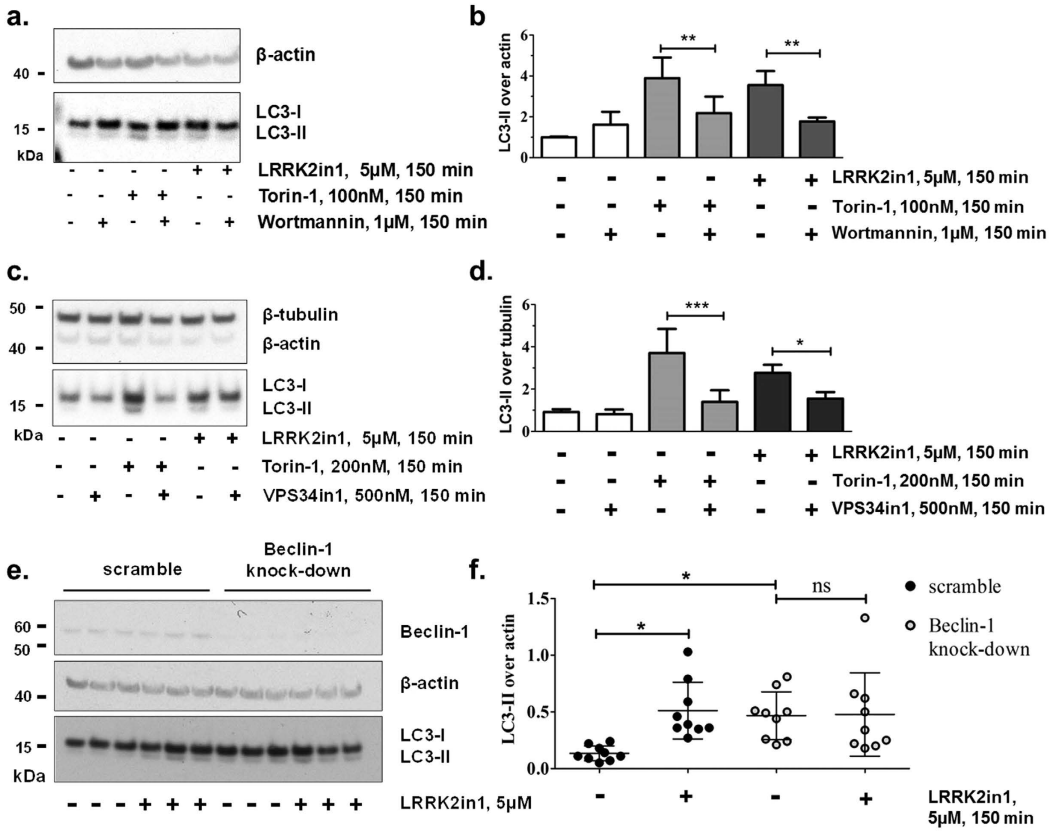

Figure 4. Increase in macroautophagy after inhibition of LRRK2 kinase and Beclin-1. (**a**) 150 minutes treatment with LRRK2in1 or Torin-1 (to induce macroautophagy) in the presence and absence of wortmannin. The gel shown is representative of 3 independent experiments as quantified in (**b**). (**b**) LC3-II was quantified against β-actin; quantification was done for each single experiment; after normalization against the control in DMSO, data were pulled together and statistical analysis was performed by 1way Anova followed by Tukey post-hoc test (mean and SD, ***$p < 0.001$, **$p < 0.01$). (**c**) 150 minutes treatment with LRRK2in1 or Torin-1 (to induce macroautophagy) in the presence and absence of VPS34in1. The gel shown is representative of 4 independent experiments as quantified in (**d**). (**d**) LC3-II was quantified against β-actin; quantification was done for each single experiment; after normalization against the control in DMSO, data were pulled together and statistical analysis was performed by 1way Anova followed by Tukey post-hoc test (mean and SD, ***$p < 0.001$, **$p < 0.01$). (**e**) 150 minutes treatment with LRRK2in1 in H4 cells stably expressing scrambled shRNA controls or shRNA for Beclin-1. The gel shown is representative of 3 independent experiments, each performed in triplicate and it is quantified in (**f**). (**f**) LC3-II was normalized against β-actin and statistical analysis was performed by Anova followed by Tukey post-hoc test (mean and SD, *$p < 0.05$).

by the endogenous LRRK2 kinase activity in a H4 glioma cell line and in primary astrocytes is involved in the non-canonical control of macroautophagy, working parallel to the mTOR/ULK1 pathway and dependent on PI3P and Beclin-1 activity.

The complex events regulating macroautophagy are yet to be fully characterised[40]. Two of the key regulatory systems have, however, been identified: the mTOR/ULK1 and the Beclin-1 pathways. While ULK1 is phosphorylated under basal conditions to repress macroautophagy, ULK1 phosphorylation is lost when macroautophagy flux is induced, via the orchestrated inhibition of mTOR in concert with as yet unidentified phosphatases[41,42]. Beclin-1 works in two distinct complexes, both necessary for the production of PI3P that is required first for the formation and later for the maturation of the nascent autophagosome. Non-canonical pathways have been described which do not require proteins crucial for canonical autophagy such as ULK1, Beclin-1 and LC3[43–45]. As an example, the phenotype of the double knock-out for both ULK1 and ULK2 is embryonic lethal, but mice embryonic fibroblasts on this background are able to activate a residual autophagy pathway that is, by definition, independent of ULK1/2 proteins[46]. Moreover, the knock-down of both ULK1 and ULK2 in a B-cell line (DT40) did not alter autophagy[47], thus confirming that an ULK1/2 alternative route does exist and suggesting different cell types have different ways to control and sustain macroautophagy. Finally, small molecules enhancers of rapamycin (SMERs) have been isolated to induce mTOR-independent autophagy[48].

In the current study, pharmacological inhibition of LRRK2 kinase activity resulted in an increase of LC3 processing consistent with induction of macroautophagy. Inhibition of mTOR using Torin-1 causes a complete loss of ULK1 phosphorylation on Ser758 and this loss of phosphorylation on ULK1 is required for translocation of the

ULK1/2 complex to the pre-autophagosomal structure[37]. In contrast, the lack of alteration in ULK1 phosphorylation following LRRK2 kinase inhibition, suggests the possible activation of a non-canonical pathway independent of ULK1. Autophagosomes produced due to loss of LRRK2 kinase activity were positive for WIPI-2 thus suggesting the activity of Beclin-1 and the generation of PI3P was conserved. Indeed, the inhibition of PI3P production by wortmannin or VPS34in1 was able to inhibit the induction of LRRK2-regulated macroautophagy. Finally, Beclin-1 knock-down cells were not responsive to LRRK2in1 treatment, thus confirming that Beclin-1/PI3P are involved either upstream or downstream of the induction of macroautophagy via LRRK2 inhibition. A possible link between Beclin-1 and LRRK2 is intriguing given the existing literature. The G2019S-LRRK2 mutant (which shows increased kinase activity), is able to bind to and phosphorylate Bcl-2 resulting in dysregulation of mitophagy[49]. Beclin-1 contains Bcl-2 binding sites that are important for its macroautophagy regulatory activities[50]. Beclin-1 has been found to be phosphorylated and regulated by the stress responsive kinases MAPKAPK2 and 3[51]; LRRK2 has been suggested to bind and phosphorylate MAP2K3 (MKK3) upstream of MAPKAPK2/3 in the p38-MAPK pathway[52]. It is also of note that the Beclin complex has a complex role in the regulation of macroautophagy, dependent upon the binding partners Beclin-1 is associated with[53–55]. In the presence of ATG14L or UVRAG, Beclin-1 acts as a positive regulator of macroautophagy – consistent with the data presented herein from H4 cells. In contrast, when bound to RUBICON Beclin-1 acts as a repressor of autophagy. Clarifying how LRRK2 relates to these distinct Beclin complexes will provide further insight into the precise mechanisms whereby LRRK2 can impact on autophagy, and may provide an explanation for the divergence in experimental data across the research literature. Strikingly, regulation of macroautophagy by LRRK2 is echoed by studies on Death Associated Protein kinase 1 (DAPK1), another member of the ROCO protein family to which LRRK2 belongs, and that has been proposed to be involved in the control of macroautophagy by both direct and indirect phosphorylation of Beclin-1[56,57]. Members of the ROCO family share a high homology in their GTPase and COR domains, while the kinase domains of LRRK2 and DAPK1 belong to different families. There is accumulating evidence, however, that the kinase and the GTPase activities present in LRRK2 are able to regulate one another[58]. These observations suggest that an understanding of both the kinase and GTPase activities of LRRK2 may be required to fully illuminate LRRK2's role in the regulation of macroautophagy. Within the current study we make use of chemical inhibition of LRRK2 kinase activity to infer how the endogenous protein regulates macroautophagy by physiological signaling in cells. However, we cannot currently determine if the effects here are solely due to kinase activity or are partially mediated through, for example, the GTPase function of LRRK2. Further experiments addressing the GTPase activity of LRRK2, either through genetic manipulations or small molecules that target this region of the protein, are therefore important in the future.The close genetic ties between LRRK2 and PD have resulted in extensive efforts to understand LRRK2 in the context of this disorder. The recent discovery of significant links between LRRK2 and a range of other, apparently unrelated, human disorders has further emphasised the importance of this protein to human health. A major challenge for LRRK2 research is, therefore, to reconcile the involvement of LRRK2 in the pathological pathways underlying these disparate disorders. Several complementary strands of evidence suggest that one key physiological function of LRRK2 is with regard to the control of macroautophagy and vesicle dynamics, raising the possibility that this may be the common theme behind the different disorders in the pathogenesis of which LRRK2 has been implicated. Another major problem in the study of LRRK2 patho-physiology is represented by the fact that it has been associated with a multiple array of cellular functions[59], and has many protein interactors[60], suggesting that LRRK2 acts as a hub protein able to work with a wide range of partners. This has led to the suggestion that LRRK2 may have different roles in different cell types and its function may be different depending on the situation/stimuli. The data presented in this study provides new insight into the dissection of the mechanism of LRRK2 function, information that will be critical for understanding the connection between LRRK2 and disease pathogenesis, to provide the basis for therapeutic intervention directed at LRRK2s activities and to consider the side effects and safety issues of chronic LRRK2 kinase inhibition in a human context.

Materials and Methods

Reagents. The LRRK2in1 compound and the VPS34in1 were purchased from the Division of Signal Transduction Therapy, School of Life Sciences, and University of Dundee, UK. The GSK2578215A compound was purchased from Tocris. Bafilomycin A1 (B1793-2UG), Chloroquine (C6628) and Wortmannin (W3144-250UL) were purchased from Sigma-Aldrich. Torin-1 (CAY10997) was purchased from Cayman Chemicals.

Antibodies used were as follows: LC3 antibody (NB100-2220, Novus Biologicals); LRRK2 antibodies (MJFF#2, 3514-1/ab133474, Epitomics); total S6 antibody (2317, Cell Signalling); phospho Ser235/236 S6 antibody (2211S, Cell Signalling); total P70S6K antibody (sc-8418, Santa Cruz); phospho Thr389 P70S6K (sc-11759, Santa Cruz); total ULK1 antibody (8054 and 4773, Cell Signalling); phospho Ser757 ULK1 antibody (6888, Cell Signalling); Beclin-1 antibody (3738, Cell Signalling); β-actin antibody (A1978, Sigma Aldrich); β-tubulin (T6199, Sigma Aldrich).

H4 cell culture and treatment. H4 cells (ATCC number HTB-148) were grown in DMEM containing 10% FCS. After 24 hours from plating, when at 80% confluence, H4 cells were treated with LRRK2 inhibitors LRRK2in1 or GSK2578215A, with BafA1 or Torin-1 or wortmannin at the concentrations and for the time reported in each experiment. For each experiment, DMSO vehicle controls were added. After washing in Dulbecco's phosphate buffered saline (DPBS) cells were collected in a lysis buffer containing: 0.5% Triton X-100, 2 mM ethylen di-ammonium tetra acetic acid (EDTA), 150 mM NaCl, 0.5% sodium deoxycholate, 0.1% sodium dodecyl sulphate (SDS), protease inhibitors (cOmplete, protease inhibitor cocktail, Roche) and phosphatase inhibitors (Halt phosphatase inhibitor cocktail, Pierce) in 50 mM TRIS-HCl pH 7.5.

Primary astrocytes culture. Primary astrocyte cultures were prepared from P3-4 mouse forebrain following a protocol adapted from Schildge *et al.*[61]. Briefly, brains were isolated in cold HBSS (Sigma-Aldrich). The forebrains were dissected and meninges removed. Forebrains were dissociated before incubation in papain (Worthington) at 37 °C for 30 min. The samples were triturated by pipetting and subsequently plated in DMEM supplemented with 10% FCS and 1% penicillin/streptomycin. At 14 divisions, microglia were dissociated by agitation for 1 hr at room temperature and astrocytes were re-plated following brief trypsinization to expand the culture. Astrocytes were aged to 45/47 divisions, plated in 6 well plates (1×10^6 cells/well), and at 80% confluency the cells were treated with LRRK2in1 or DMSO (control) as reported in figures. Following treatment, the cells were washed in DPBS, collected by scraping and cell pellets were frozen until Western blot analysis.

Western blotting. Cell lysates were frozen immediately upon collection or kept at 4 °C for 30 minutes; following thawing, they were clarified by centrifugation at 13000 rpm for 5 minutes at 4 °C, protein concentration was assessed by BCA assay (BCA Protein Assay Kit, Pierce) and 10–15 μg aliquots were added of NuPAGE sample buffer containing 2-mercaptoethanol (Invitrogen), denatured for 10 minutes at 70 °C and analysed using NuPAGE, Novex precasted Bis-Tris 4–12% (Invitrogen), in MES running buffer (Invitrogen). After electrophoresis, gels were blotted onto 0.45 μm cut-off, PVDF through conventional blotting. Membranes were blocked and processed with peroxidase-conjugated antibodies for enhanced chemiluminescence (ECL) detection. Films were acquired as images in jpg format using an EPSON Perfection 4870 photo scanner and processed by the ImageJ software (http://rsbweb.nih.gov/ij/).

Statistics. All the results have been repeated in at least 3 independent experiments (details are given in each figure legend). In the case of Western blot analysis for phospho-proteins, samples were divided in half and run in two parallel gels; one was processed for the phospho-antibody and one for the total-antibody (to avoid membrane stripping and re-probing). The total and the phospho bands were normalized against the respective β-actin loading control; then, the ratio of (normalized)phospho over (normalized)total protein was calculated. Statistical analyses were performed by the use of the Prism software (GraphPad) as described in each figure legend.

Generation of stable knock-down. H4 cells were transfected with 2 to 10 μg LRRK2 shRNA, ULK1 shRNA, Beclin-1 shRNA or scramble Open Biosystems GIPZ shRNAmir (V3LHS-644167, V2LHS-33057, V3LHS-349512 and -349514, Thermo Fisher Scientific) using PEI (Sigma-Aldrich) transfection reagent according to the manufacturer's instructions. ShRNA vectors contain a puromycin resistance gene. Cells were treated with 2 μg/ml puromycin supplemented DMEM 48 hrs after transfection and kept under selection for expansion. Puromycin selection was removed 24 hours before the experiment to avoid interference of the antibiotic with the treatment.

References

1. Hernandez, D. G., Reed, X. & Singleton, A. B. Genetics in Parkinson disease: Mendelian versus non-Mendelian inheritance. *J Neurochem*, doi: 10.1111/jnc.13593 (2016).
2. Paisan-Ruiz, C. *et al.* Cloning of the gene containing mutations that cause PARK8-linked Parkinson's disease. *Neuron* **44,** 595–600, doi: 10.1016/j.neuron.2004.10.023 (2004).
3. Singleton, A. B., Farrer, M. J. & Bonifati, V. The genetics of Parkinson's disease: progress and therapeutic implications. *Mov Disord* **28,** 14–23, doi: 10.1002/mds.25249 (2013).
4. Zimprich, A. *et al.* Mutations in LRRK2 cause autosomal-dominant parkinsonism with pleomorphic pathology. *Neuron* **44,** 601–607, doi: 10.1016/j.neuron.2004.11.005 (2004).
5. Nalls, M. A. *et al.* Large-scale meta-analysis of genome-wide association data identifies six new risk loci for Parkinson's disease. *Nat Genet* **46,** 989–993, doi: 10.1038/ng.3043 (2014).
6. Jostins, L. *et al.* Host-microbe interactions have shaped the genetic architecture of inflammatory bowel disease. *Nature* **491,** 119–124, doi: 10.1038/nature11582 (2012).
7. Fava, V. M. *et al.* A Missense LRRK2 Variant Is a Risk Factor for Excessive Inflammatory Responses in Leprosy. *Plos Negl Trop Dis* **10,** e0004412, doi: 10.1371/journal.pntd.0004412 (2016).
8. Zhang, F. R. *et al.* Genomewide association study of leprosy. *N Engl J Med* **361,** 2609–2618, doi: 10.1056/NEJMoa0903753 (2009).
9. Inzelberg, R. *et al.* The LRRK2 G2019S mutation is associated with Parkinson disease and concomitant non-skin cancers. *Neurology* **78,** 781–786, doi: 10.1212/WNL.0b013e318249f673 (2012).
10. Agalliu, I. *et al.* Higher frequency of certain cancers in LRRK2 G2019S mutation carriers with Parkinson disease: a pooled analysis. *JAMA Neurol* **72,** 58–65, doi: 10.1001/jamaneurol.2014.1973 (2015).
11. Biosa, A. *et al.* GTPase activity regulates kinase activity and cellular phenotypes of Parkinson's disease-associated LRRK2. *Hum Mol Genet* **22,** 1140–1156, doi: 10.1093/hmg/dds522 (2013).
12. Webber, P. J. *et al.* Autophosphorylation in the leucine-rich repeat kinase 2 (LRRK2) GTPase domain modifies kinase and GTP-binding activities. *J Mol Biol* **412,** 94–110, doi: 10.1016/j.jmb.2011.07.033 (2011).
13. Wirth, M., Joachim, J. & Tooze, S. A. Autophagosome formation–the role of ULK1 and Beclin1-PI3KC3 complexes in setting the stage. *Semin Cancer Biol* **23,** 301–309, doi: 10.1016/j.semcancer.2013.05.007 (2013).
14. Plowey, E. D., Cherra, S. J. 3rd., Liu, Y. J. & Chu, C. T. Role of autophagy in G2019S-LRRK2-associated neurite shortening in differentiated SH-SY5Y cells. *J Neurochem* **105,** 1048–1056, doi: 10.1111/j.1471-4159.2008.05217.x (2008).
15. Alegre-Abarrategui, J. *et al.* LRRK2 regulates autophagic activity and localizes to specific membrane microdomains in a novel human genomic reporter cellular model. *Hum Mol Genet* **18,** 4022–4034, doi: 10.1093/hmg/ddp346 (2009).
16. Schapansky, J., Nardozzi, J. D., Felizia, F. & LaVoie, M. J. Membrane recruitment of endogenous LRRK2 precedes its potent regulation of autophagy. *Hum Mol Genet* **23,** 4201–4214, doi: 10.1093/hmg/ddu138 (2014).
17. Gomez-Suaga, P. *et al.* Leucine-rich repeat kinase 2 regulates autophagy through a calcium-dependent pathway involving NAADP. *Hum Mol Genet* **21,** 511–525, doi: 10.1093/hmg/ddr481 (2012).
18. Manzoni, C. *et al.* Inhibition of LRRK2 kinase activity stimulates macroautophagy. *Biochim Biophys Acta* **1833,** 2900–2910, doi: 10.1016/j.bbamcr.2013.07.020 (2013).
19. Saez-Atienzar, S. *et al.* The LRRK2 inhibitor GSK2578215A induces protective autophagy in SH-SY5Y cells: involvement of Drp-1-mediated mitochondrial fission and mitochondrial-derived ROS signaling. *Cell Death Dis* **5,** e1368, doi: 10.1038/cddis.2014.320 (2014).

20. Bravo-San Pedro, J. M. *et al.* The LRRK2 G2019S mutant exacerbates basal autophagy through activation of the MEK/ERK pathway. *Cell Mol Life Sci* **70,** 121–136, doi: 10.1007/s00018-012-1061-y (2013).
21. Manzoni, C. *et al.* Pathogenic Parkinson's disease mutations across the functional domains of LRRK2 alter the autophagic/lysosomal response to starvation. *Biochem Biophys Res Commun* **441,** 862–866, doi: 10.1016/j.bbrc.2013.10.159 (2013).
22. Sanchez-Danes, A. *et al.* Disease-specific phenotypes in dopamine neurons from human iPS-based models of genetic and sporadic Parkinson's disease. *EMBO Mol Med* **4,** 380–395, doi: 10.1002/emmm.201200215 (2012).
23. Tong, Y. *et al.* Loss of leucine-rich repeat kinase 2 causes age-dependent bi-phasic alterations of the autophagy pathway. *Mol Neurodegener* **7,** 2, doi: 10.1186/1750-1326-7-2 (2012).
24. Orenstein, S. J. *et al.* Interplay of LRRK2 with chaperone-mediated autophagy. *Nat Neurosci* **16,** 394–406, doi: 10.1038/nn.3350 (2013).
25. Arranz, A. M. *et al.* LRRK2 functions in synaptic vesicle endocytosis through a kinase-dependent mechanism. *J Cell Sci* **128,** 541–552, doi: 10.1242/jcs.158196 (2015).
26. Belluzzi, E. *et al.* LRRK2 phosphorylates pre-synaptic N-ethylmaleimide sensitive fusion (NSF) protein enhancing its ATPase activity and SNARE complex disassembling rate. *Mol Neurodegener* **11,** 1, doi: 10.1186/s13024-015-0066-z (2016).
27. Chia, R. *et al.* Phosphorylation of LRRK2 by casein kinase 1alpha regulates trans-Golgi clustering via differential interaction with ARHGEF7. *Nat Commun* **5,** 5827, doi: 10.1038/ncomms6827 (2014).
28. Matta, S. *et al.* LRRK2 controls an EndoA phosphorylation cycle in synaptic endocytosis. *Neuron* **75,** 1008–1021, doi: 10.1016/j.neuron.2012.08.022 (2012).
29. Xilouri, M., Brekk, O. R. & Stefanis, L. Autophagy and Alpha-Synuclein: Relevance to Parkinson's Disease and Related Synucleopathies. *Mov Disord* **31,** 178–192, doi: 10.1002/mds.26477 (2016).
30. Henry, A. G. *et al.* Pathogenic LRRK2 mutations, through increased kinase activity, produce enlarged lysosomes with reduced degradative capacity and increase ATP13A2 expression. *Hum Mol Genet* **24,** 6013–6028, doi: 10.1093/hmg/ddv314 (2015).
31. Moehle, M. S. *et al.* LRRK2 inhibition attenuates microglial inflammatory responses. *J Neurosci* **32,** 1602–1611, doi: 10.1523/JNEUROSCI.5601-11.2012 (2012).
32. Deng, X. *et al.* Characterization of a selective inhibitor of the Parkinson's disease kinase LRRK2. *Nat Chem Biol* **7,** 203–205, doi: 10.1038/nchembio.538 (2011).
33. Reith, A. D. *et al.* GSK2578215A; a potent and highly selective 2-arylmethyloxy-5-substitutent-N-arylbenzamide LRRK2 kinase inhibitor. *Bioorg Med Chem Lett* **22,** 5625–5629, doi: 10.1016/j.bmcl.2012.06.104 (2012).
34. Klionsky, D. J. *et al.* Guidelines for the use and interpretation of assays for monitoring autophagy (3rd edition). *Autophagy* **12,** 1–222, doi: 10.1080/15548627.2015.1100356 (2016).
35. Mauvezin, C., Nagy, P., Juhasz, G. & Neufeld, T. P. Autophagosome-lysosome fusion is independent of V-ATPase-mediated acidification. *Nat Commun* **6,** 7007, doi: 10.1038/ncomms8007 (2015).
36. Tooze, S. A. *et al.* Assessing mammalian autophagy. *Methods Mol Biol* **1270,** 155–165, doi: 10.1007/978-1-4939-2309-0_12 (2015).
37. Papinski, D. & Kraft, C. Regulation of Autophagy By Signaling Through the Atg1/ULK1 Complex. *J Mol Biol*, doi: 10.1016/j.jmb.2016.03.030 (2016).
38. Johnson, C. W., Melia, T. J. & Yamamoto, A. Modulating macroautophagy: a neuronal perspective. *Future Med Chem* **4,** 1715–1731, doi: 10.4155/fmc.12.112 (2012).
39. Lewis, P. A. & Manzoni, C. LRRK2 and human disease: a complicated question or a question of complexes? *Sci Signal* **5**, pe2, doi: 10.1126/scisignal.2002680 (2012).
40. Ktistakis, N. T. & Tooze, S. A. Digesting the Expanding Mechanisms of Autophagy. *Trends Cell Biol*, doi: 10.1016/j.tcb.2016.03.006 (2016).
41. Alers, S., Loffler, A. S., Wesselborg, S. & Stork, B. Role of AMPK-mTOR-Ulk1/2 in the regulation of autophagy: cross talk, shortcuts, and feedbacks. *Mol Cell Biol* **32,** 2–11, doi: 10.1128/MCB.06159-11 (2012).
42. McAlpine, F., Williamson, L. E., Tooze, S. A. & Chan, E. Y. Regulation of nutrient-sensitive autophagy by uncoordinated 51-like kinases 1 and 2. *Autophagy* **9,** 361–373, doi: 10.4161/auto.23066 (2013).
43. Codogno, P., Mehrpour, M. & Proikas-Cezanne, T. Canonical and non-canonical autophagy: variations on a common theme of self-eating? *Nat Rev Mol Cell Biol* **13,** 7–12, doi: 10.1038/nrm3249 (2012).
44. Mauthe, M. *et al.* Resveratrol-mediated autophagy requires WIPI-1-regulated LC3 lipidation in the absence of induced phagophore formation. *Autophagy* **7,** 1448–1461 (2011).
45. Wang, J. *et al.* A non-canonical MEK/ERK signaling pathway regulates autophagy via regulating Beclin 1. *J Biol Chem* **284,** 21412–21424, doi: 10.1074/jbc.M109.026013 (2009).
46. Cheong, H., Lindsten, T., Wu, J., Lu, C. & Thompson, C. B. Ammonia-induced autophagy is independent of ULK1/ULK2 kinases. *Proc Natl Acad Sci USA* **108,** 11121–11126, doi: 10.1073/pnas.1107969108 (2011).
47. Alers, S. *et al.* Atg13 and FIP200 act independently of Ulk1 and Ulk2 in autophagy induction. *Autophagy* **7,** 1423–1433 (2011).
48. Sarkar, S. *et al.* Small molecules enhance autophagy and reduce toxicity in Huntington's disease models. *Nat Chem Biol* **3,** 331–338, doi: 10.1038/nchembio883 (2007).
49. Su, Y. C., Guo, X. & Qi, X. Threonine 56 phosphorylation of Bcl-2 is required for LRRK2 G2019S-induced mitochondrial depolarization and autophagy. *Biochim Biophys Acta* **1852,** 12–21, doi: 10.1016/j.bbadis.2014.11.009 (2015).
50. Decuypere, J. P., Parys, J. B. & Bultynck, G. Regulation of the autophagic bcl-2/beclin 1 interaction. *Cells* **1,** 284–312, doi: 10.3390/cells1030284 (2012).
51. Wei, Y. *et al.* The stress-responsive kinases MAPKAPK2/MAPKAPK3 activate starvation-induced autophagy through Beclin 1 phosphorylation. *Elife* **4,** doi: 10.7554/eLife.05289 (2015).
52. Gloeckner, C. J., Schumacher, A., Boldt, K. & Ueffing, M. The Parkinson disease-associated protein kinase LRRK2 exhibits MAPKKK activity and phosphorylates MKK3/6 and MKK4/7, *in vitro*. *J Neurochem* **109,** 959–968, doi: 10.1111/j.1471-4159.2009.06024.x (2009).
53. Funderburk, S. F., Wang, Q. J. & Yue, Z. The Beclin 1-VPS34 complex–at the crossroads of autophagy and beyond. *Trends Cell Biol* **20,** 355–362, doi: 10.1016/j.tcb.2010.03.002 (2010).
54. Matsunaga, K. *et al.* Two Beclin 1-binding proteins, Atg14L and Rubicon, reciprocally regulate autophagy at different stages. *Nat Cell Biol* **11,** 385–396, doi: 10.1038/ncb1846 (2009).
55. Zhong, Y. *et al.* Distinct regulation of autophagic activity by Atg14L and Rubicon associated with Beclin 1-phosphatidylinositol-3-kinase complex. *Nat Cell Biol* **11,** 468–476, doi: 10.1038/ncb1854 (2009).
56. Zalckvar, E., Berissi, H., Eisenstein, M. & Kimchi, A. Phosphorylation of Beclin 1 by DAP-kinase promotes autophagy by weakening its interactions with Bcl-2 and Bcl-XL. *Autophagy* **5,** 720–722 (2009).
57. Zalckvar, E. *et al.* DAP-kinase-mediated phosphorylation on the BH3 domain of beclin 1 promotes dissociation of beclin 1 from Bcl-XL and induction of autophagy. *EMBO Rep* **10,** 285–292, doi: 10.1038/embor.2008.246 (2009).
58. Liu, Z., Mobley, J. A., DeLucas, L. J., Kahn, R. A. & West, A. B. LRRK2 autophosphorylation enhances its GTPase activity. *FASEB J* **30,** 336–347, doi: 10.1096/fj.15-277095 (2016).
59. Wallings, R., Manzoni, C. & Bandopadhyay, R. Cellular processes associated with LRRK2 function and dysfunction. *FEBS J* **282,** 2806–2826, doi: 10.1111/febs.13305 (2015).
60. Manzoni, C., Denny, P., Lovering, R. C. & Lewis, P. A. Computational analysis of the LRRK2 interactome. *PeerJ* **3,** e778, doi: 10.7717/peerj.778 (2015).
61. Schildge, S., Bohrer, C., Beck, K. & Schachtrup, C. Isolation and culture of mouse cortical astrocytes. *J Vis Exp*, doi: 10.3791/50079 (2013).

Acknowledgements

The authors would like to acknowledge generous research support from the Michael J. Fox Foundation, Parkinson's UK and the Rosetrees Trust. PAL is a Parkinson's UK research fellow (grant F1002). This work was supported in part by the Wellcome Trust/MRC Joint Call in Neurodegeneration award (WT089698) to the UK Parkinson's Disease Consortium (UKPDC) whose members are from the UCL Institute of Neurology, the University of Sheffield and the MRC Protein Phosphorylation Unit at the University of Dundee, by a MRC New Investigator Research Grant (MR/L010933/1) to PAL, and by MRC programme grant MR/N026004/1 to JH, HPF and PAL. This research was supported in part by the Intramural Research Program of the NIH, National Institute on Aging. SAT was supported by the Francis Crick Institute which receives its core funding from Cancer Research UK (FC001187), the UK Medical Research Council (FC001187), and the Wellcome Trust (FC001187). We thank Dr. Claudio Galbiati and Dr. Miriam Manzoni at the Università degli Studi di Bergamo (IT) for the development of the image quantification script for Supplementary Figure S5. We thank the UCL Cancer Institute CAGE Facility, which provided the Open Biosystems GIPZ shRNAmir. The CAGE Facility is supported by the Welton Foundation, BRC and in part by the Cancer Research UK – UCL Centre.

Author Contributions

P.A.L. directed the research. P.A.L. and C.M. designed the experiments. C.M. performed most of the experiments. M.S. supervised the generation of knock-down cells. A.M. and D.R. prepared and were involved in the experiments with primary astrocytes. S.D. helped in the setup of experimental procedures. S.A.T., J.H., R.B., H.P.-F. and M.R.C. supported the work with guidance, advice and reagents. C.M. and P.A.L. wrote the manuscript.

Additional Information

Supplementary information accompanies this paper at http://www.nature.com/srep

Competing financial interests: The authors declare no competing financial interests.

How to cite this article: Manzoni, C. *et al.* mTOR independent regulation of macroautophagy by Leucine Rich Repeat Kinase 2 via Beclin-1. *Sci. Rep.* **6**, 35106; doi: 10.1038/srep35106 (2016).

Roosen and Cookson *Molecular Neurodegeneration* (2016) 11:73
DOI 10.1186/s13024-016-0140-1

Molecular Neurodegeneration

REVIEW Open Access

LRRK2 at the interface of autophagosomes, endosomes and lysosomes

Dorien A. Roosen[1,2] and Mark R. Cookson[1*]

Abstract

Over the past 20 years, substantial progress has been made in identifying the underlying genetics of Parkinson's disease (PD). Of the known genes, LRRK2 is a major genetic contributor to PD. However, the exact function of LRRK2 remains to be elucidated. In this review, we discuss how familial forms of PD have led us to hypothesize that alterations in endomembrane trafficking play a role in the pathobiology of PD. We will discuss the major observations that have been made to elucidate the role of LRRK2 in particular, including LRRK2 animal models and high-throughput proteomics approaches. Taken together, these studies strongly support a role of LRRK2 in vesicular dynamics. We also propose that targeting these pathways may not only be beneficial for developing therapeutics for LRRK2-driven PD, but also for other familial and sporadic cases.

Keywords: GTPases, Membrane proteins, Parkinson's disease, Protein kinases, Vesicular trafficking

Background

Understanding the etiology of a disease is often an important step for developing treatments. With many of the common neurodegenerative diseases, it is clear that single gene mutations account for some proportion of all cases while the rest are 'sporadic' in nature. This leads to the concept that genetic variants, acting within the context of the aging central nervous system and stochastic factors, leads to overall risk of disease. Thus, the etiology of neurodegeneration is at least partially tractable.

Parkinson's disease (PD) falls within this rubric, in that about 10% of cases have a clear family history while the remainder are scattered throughout the population. The nature of inheritance is variable, with both dominant and recessive genes being found that have age-dependent penetrance. Furthermore, within the sporadic PD population, genome-wide association studies (GWAS) have nominated multiple genomic regions as harboring variants that contribute to overall risk of disease throughout lifetime. PD genetics is therefore rarely pure and never simple but contributes to pathogenesis and, by extension, might be leveraged for therapeutic benefit.

Here, we will focus on one specific gene for PD that is relevant for both inherited and sporadic disease that has been the subject of recent attention as a potential drug target. We will focus specifically on the underlying biology that has been uncovered in recent years to discuss the concept of pathway risk in parkinsonism.

LRRK2 is in a pleomorphic risk locus for PD

In 2002, inherited PD in a large Japanese kindred was linked to the *PARK8* locus on chromosome 12 [1]. The same locus was found in independently ascertained families from different countries [2–4] and the underlying genetic cause, a mutation in the *LRRK2* gene, was discovered 2 years later [3, 5] an a series of *LRRK2* mutations nominated in additional families [6–10]. To date, five mutations in *LRRK2* have been shown unambiguously to segregate with familial PD and two additional variants have been nominated as risk factors (reviewed in [11, 12]). All of these *LRRK2* mutations show age-dependent incomplete penetrance, meaning that some *LRRK2* mutation carriers do not show clinical phenotypes during their lifetime [13].

Independently of mutations, GWAS approaches have also identified *LRRK2* to be a risk factor for sporadic PD [14]. The precise mechanism by which variations around the *LRRK2* gene region contribute to disease risk are not fully resolved, but given that the polymorphisms

* Correspondence: cookson@mail.nih.gov
[1]Cell Biology and Gene Expression Section, Laboratory of Neurogenetics, National Institute on Aging, National Institutes of Health, Bldg. 35, 35 Convent Drive, Bethesda, MD 20892-3707, USA
Full list of author information is available at the end of the article

associated with sporadic PD are in the promoter region of LRRK2, a reasonable hypothesis is that these variants do not change protein structure or function but instead alter expression levels of the gene, although this remains to be formally demonstrated for LRRK2. The chromosomal region containing *LRRK2* is therefore an example of a pleomorphic risk locus, i.e. a genomic region that harbors variants that increase disease risk but by different mechanisms [15]. Additionally, *LRRK2*-driven PD is clinically indistinguishable from idiopathic PD [16]. Collectively, these observations suggest that *LRRK2* plays a general role in the etiological mechanisms of both inherited and sporadic PD.

LRRK2 structure and enzymatic domains

LRRK2 encodes a large (2527 amino acid) multi-domain protein termed leucine rich repeat kinase 2 (LRRK2). The central portion of LRRK2 contains a Ras of Complex (Roc) GTPase and a C-terminus of Roc (COR) domain, followed immediately by a kinase domain. The ROC-COR bidomain and kinase region together constitute the catalytic core of LRRK2, which therefore encompasses two enzymatic activities. Several protein interaction domains surround this catalytic core, including N-terminal armadillo (Arm), ankyrin (Ank) and leucine rich repeat (LRR) domains and a C-terminal WD40 domain (Fig. 1). Interestingly, all the segregating mutations associated with PD are located within the enzymatic core of LRRK2 (Fig. 1) and mutated proteins have altered biochemical activity in vitro [17]. There are subtle differences between mutations, as the kinase domain mutations including G2019S and I2020T directly increase kinase activity [13] whereas those in the ROC-COR domains, the best studied of which are R1441C/G and Y1699C, decrease GTPase activity [18–21]. However, it is thought that the physical proximity of two enzyme activities encoded in the same protein structure implies that they regulate each other and lead to a co-ordinated output in cellular signaling [22, 23]. Therefore, even if mutations have differing effects on the proximal biochemical activity of LRRK2, they are likely to have a consistent effect on signaling in the cell. By extension, it is likely that evolution has selected for the multiple enzymatic and protein interaction domains of LRRK2 to be on a single polypeptide because they work together to generate one or more cellular outputs.

Despite being a large protein, several early studies showed that LRRK2 can form homodimers that localize to membrane compartments of the cell [24–26]. It is likely that dimer formation is part of the complex auto-regulatory function of LRRK2, relevant for the kinase and GTPase activities discussed above. Recently, a 3D structural model of full length LRRK2 has been described, showing that the LRRK2 homodimer adopts a compact architecture, highly suggestive of intramolecular regulation of the enzymatic activities [27]. In this model, the protein-protein interaction domains either serve to stabilize the dimer internally or are surface available for interactions with external binding partners (Fig. 1).

These biochemical and structural observations suggest, first, that LRRK2 is a co-ordinated signaling molecule that has linked enzyme activities and potentially multiple protein interaction partners and, second, that mutations associated with PD can modify these activities.

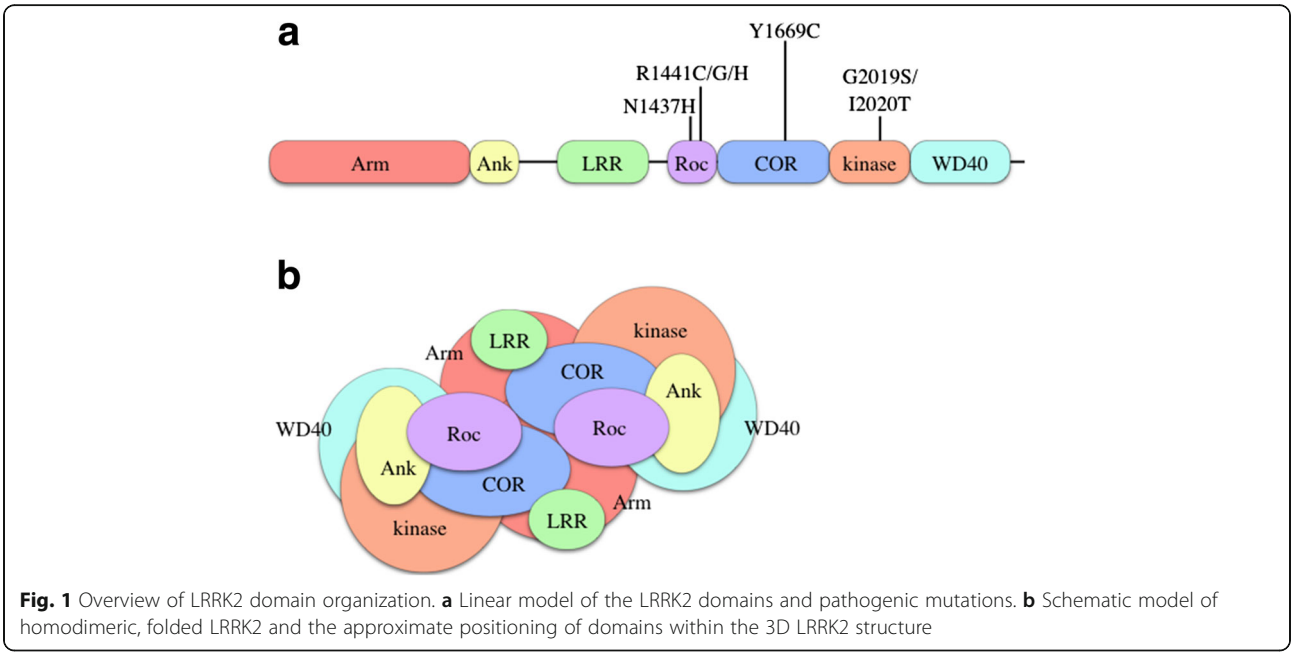

Fig. 1 Overview of LRRK2 domain organization. **a** Linear model of the LRRK2 domains and pathogenic mutations. **b** Schematic model of homodimeric, folded LRRK2 and the approximate positioning of domains within the 3D LRRK2 structure

Genetic clues for altered vesicular dynamics in PD

The next important question, is what effects LRRK2 has within cells and, therefore, within the organism. If we make the assumption that LRRK2 has some higher-level relationship with other genetic forms of PD, we might ascertain some candidates for LRRK2's cellular role.

The first gene cloned for inherited PD was *SNCA*, which encodes a small vesicular protein abundantly expressed in the brain, α – synuclein. As for LRRK2, the genetic region surrounding *SNCA* is a pleomorphic risk locus, containing point mutations, gene multiplications and risk variants for sporadic PD. Furthermore, aggregation of insoluble α-synuclein is one of the main pathological hallmarks of PD, in the form of Lewy bodies and Lewy neurites in multiple brain regions. Because of this accumulation of protein, impaired degradation pathways have been hypothesized to be one of the underlying disease mechanisms of PD [28]. Because neurons require substantial maintenance and recycling of vesicles and their associated proteins at synapses, a particularly attractive idea is that PD might result from a failure of degradative pathways for vesicular proteins. The majority of α-synuclein is degraded through the lysosome, perhaps by a specialized process called chaperone-mediated autophagy (CMA) [29]. It is known that CMA activity diminishes with age [30] and that the protein stability of α-synuclein increases with age as well as mutations [31]. With the assumption that multiplication mutations in *SNCA* increase protein levels, a possible explanation for the age-dependent penetrance of these mutations is that the protein levels are a critical driver of toxic events in the brain.

Since the initial cloning of *SNCA*, there have been multiple PD-related genes identified that additionally converge on the related autophagy-lysosome system and vesicle trafficking pathways (summarized in Table 1, extensively reviewed in [28, 32]). We will therefore summarize some of the key characteristics and players in these intracellular events before turning to the evidence that addresses the role(s) of LRRK2 in vesicle uptake and recycling.

The endosomal and autophagosomal pathways

Two major pathways for cellular homeostasis are endocytosis and autophagy (2). During endocytosis, extracellular components are engulfed at the plasma membrane and transported and sorted via early and late endosomes [33]. The eventual destinations of endocytosed materials are varied, including rapid recycling at the post-synaptic region of neurons [34]. However, a subset of endosomes matures for subsequent fusion events with other intracellular membranous vesicles. This is a highly regulated process influenced by several cellular signaling pathways, with key involvement of the members of the Rab family of membrane-associated small GTPases [35]. Early endosomes are enriched in the signaling lipid PI(3)P, generated by the VPS34 complex. Conversion of PI(3)P to PI(3,5)P2 by the kinase PIKFyve is important for endosome maturation [36], where Rab5-positive early endosomes mature to Rab7-positive late endosomes through a transient Rab5/Rab7-postive structure [37]. Rab9 and Rab7L1 are involved in the recycling of endosomal vesicles to the trans Golgi network (TGN) via several protein complexes called the retromer [38]. Outside of endosomes, other Rabs are critical for different membrane trafficking and fusion events. Rab8 and Rab10 mediate the transport of vesicles from the TGN to the plasma membrane, whereas Rab32 and Rab38 are

Table 1 PD-associated genes with a role in endomembrane trafficking. AD autosomal dominant, AR autosomal recessive

Gene	Inheritance	Role in endomembrane trafficking	References
Parkin	AR	Ubiquitination of damaged mitochondria for degradation by mitophagy	[86, 87]
PINK1	AR	Phosphorylation of mitochondria for parkin activation and mitophagy	[87–89]
DJ-1	AR	Mitophagy, mitochondrial dynamics	[87, 90, 91]
Fbxo7	AR	Mitophagy, interacts with parkin	[92]
α-synuclein	AD/risk factor	Substrate of CMA, pathogenic α-synuclein inhibits CMA and induces macroautophagy	[14, 28, 29, 93]
LRRK2	AD/risk factor	Autophagy, endomembrane trafficking	[14, 28]
Vps35	AD	Component of the retromer complex	[94, 95]
ATP13A2	AR	Lysosomal P5-type ATPase	[96]
DNAJC6	AR	Co-chaperone in clathrin-mediated trafficking	[97, 98]
SYNJ1	AR	Lipid phosphatase in clathrin mediated trafficking	[99]
GAK	Risk factor	Co-chaperone in clathrin-mediated trafficking, LRRK2 interactor	[14, 73]
Rab7L1	Risk factor	Small GTPase regulating endomembrane trafficking, LRRK2 interactor	[14, 73]
GBA	Risk factor	Lysosomal protease	[14, 100]
TMEM230	AD	Transmembrane protein of recycling/secretory vesicles	[101]

involved in the transport of specialized endomembrane compartments called melanosomes to the plasma membrane [39] (Fig. 2). Thus, the endosomal pathway consists of a series of discrete membrane organelles that rely on Rabs and other signaling molecules for efficient regulation.

Autophagy is derived from Greek root words for 'self-eating'. This highly regulated process maintains cellular homeostasis through lysosomal degradation of cellular components. There are three major types of autophagy: chaperone-mediated autophagy (CMA), microautophagy and macroautophagy. During CMA, substrates are selectively but directly delivered to the lysosomes by Hsc-70 and a specific lysosomal membrane receptor, LAMP2A [30]. In microautophagy, cellular targets are directly translocated to the lysosomes but in a relatively nonselective manner that involves invagination and scission of the lysosomal membrane [40].

Macroautophagy, often referred to as simply 'autophagy' due to it being relatively better studied than the other two processes, involves sequestration of substrates into a specialized organelle, the autophagosome [41]. The underlying process can be broken down into 3 steps: phagophore formation, elongation of the phagophore to encircle the cargo and finally fusion of the autophagosome with lysosomes, membrane bound organelles that are enriched for proteolytic enzymes to enable degradation of their cargo (Fig. 2).

Like the endosomal system, autophagy is highly regulated by several cellular signaling pathways. In the canonical pathway, activation of the Ulk1 complex through mTOR signaling is necessary for autophagy autophagy induction. Next, the vacuolar sorting protein 34 (VPS34) complex is relocated to the phagophore for the generation of phosphatidylinositol 3 phosphate (PI(3)P). The local enrichment of PI(3)P recruits proteins associated with the initiation of autophagy, including WIPI2 [42]. Non-canonical, PI3K-independent induction of autophagy has recently been reported as well [43]. WIPI2 next functions to recruit and conjugate Atg (autophagic genes) proteins to mediate the elongation of the phagophore. In this step, the cytosolic LC3-I is cleaved and lipidated to form LC3-II on the autophagosomal membrane. This conversion of LC3-I to LC3-II is necessary for phagophore elongation to form an enclosed vesicle and is widely used as a marker for the presence of active autophagy in cells and tissues. Finally, the autophagosome fuses with lysosomes forming autolysosomes [42].

There are also specialized forms of autophagy for degradation of selective cargoes. Several organelles can be degraded after fusion with autophagosomes, for example depolarized mitochondria are cleared by mitophagy [44, 45]. In most of these cases, there are adaptor proteins that bridge the cargo to the developing autophagic membrane [46], including the general adaptor p62/sequestosome that is also often used to identify the presence of autophagy in tissues [47].

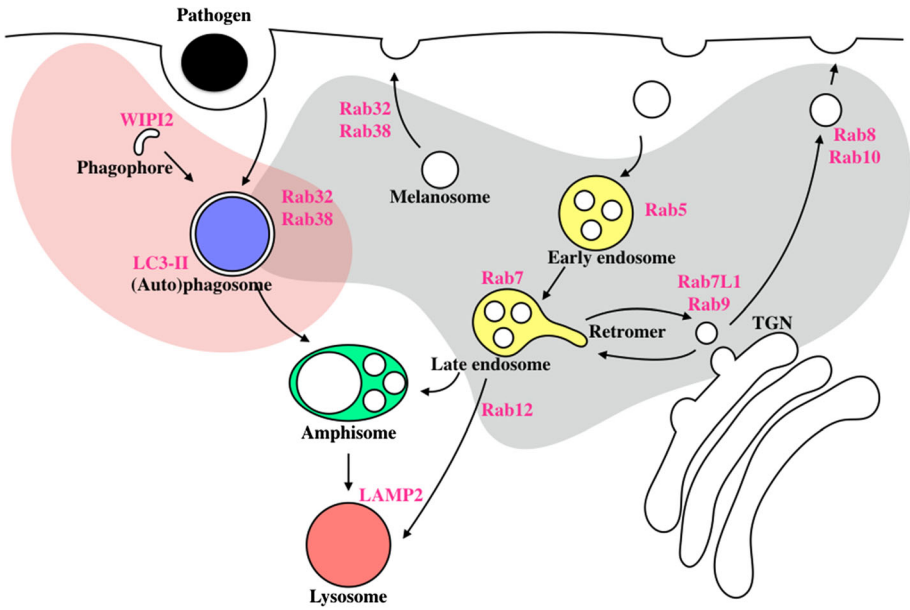

Fig. 2 Cartoon of endosomal trafficking and macroautophagy. WIPI2 is involved in the initiation of autophagy at the phagophore. LC3-II is involved for the elongation of the autophagosomal membrane. Phagosomes are formed upon the phagocytosis of extracellular pathogens. Rab proteins, including Rab5, Rab7, Rab9, Rab7L1, Rab8, Rab10, Rab12, Rab32 and Rab38 are key regulators of endomembrane trafficking. Autophagosomes and endosomes can fuse to form amphisomes. Amphisomes on their turn fuse with lysosomes for degradation of the autophagic/endocytic cargo. *Grey* shade indicates the involvement of LRRK2 in endomembrane trafficking through physical interactors and/or kinase substrates. *Pink* shade highlights parts of endomembrane trafficking where LRRK2 is implied having a regulatory role

Although the above discussion outlines endosomal and autophagy as discrete pathways, in practice there is extensive cross talk between these vesicular events. For example, a subset of endosomes will fuse either directly with lysosomes in a Rab12-dependent manner or indirectly after first fusing with autophagosomes, to generate multivesicular bodies (MVBs) or amphisomes. Even more impressively, while lysosomes might be described as a waste disposal, in fact they are an important signaling platform, for example by controlling transcriptional responses to cellular metabolic state [48]. Therefore, there are likely to be signaling events that co-ordinate the overall balance between degradation and recycling of membranes and proteins in the cell.

A physiological role for LRRK2 at vesicular membranes

The first indications for a role of LRRK2 in vesicular dynamics came from subcellular localization studies, showing localization of LRRK2 with endosomes, lysosomes and MVBs in rodent brain [49] and with punctate, vesicular structures in human brain [49, 50]. Studies in cells overexpressing low levels of tagged LRRK2 showed specific localization of LRRK2 to MVBs and autophagic vacuoles [51]. Collectively, these observations suggest that LRRK2 may have a regulatory role in the autophagic and endosomal pathways.

LRRK2 KO models: clues for a physiological role of LRRK2 in autophagy and lysosomal function

Important evidence for a physiological role of LRRK2 in regulating autophagy came from knockout animals. Specifically, there is an accumulation of lipofuscin granules, aggregated α-synuclein and increased levels of the autophagosomal marker LC3-II in LRRK2 knockout kidneys [52]. These effects are age-dependent, in that there are bi-phasic alterations in autophagy, with an initial increase of p62 and LC3-II at 7 months and a decrease at 20 months. No changes in LC3-II were observed in an independent study of kidneys of 14 month-old LRRK2 KO mice [53].

However, no apparent signs of neurodegeneration have been observed in LRRK2 KO rodents. The 6-fold higher expression levels of LRRK2 in kidney compared to brain and the absence of its homologue LRRK1 may explain this severe kidney phenotype [52, 54]. Knockout of dLrrk, the single *Drosophila* homologue of LRRK1/2, has been shown to cause alterations in lysosomal positioning [55]. Along the same lines, knockout of the single *C elegans* homologue, Lrk-1 m causes defects in synaptic vesicle protein positioning in neurons [56].

Several studies in cells have indicated a role for LRRK2 in the regulation of autophagy. Under conditions that stimulate autophagy but prevent fusion to lysosomes, knockdown of LRRK2 led to a decreased accumulation of autophagosomes [57]. LRRK2 kinase inhibition has also been shown to increase levels of the lipdated autophagosome marker LC3-II and the adaptor protein p62 [58, 59]. Recent findings have shown that this kinase-dependent regulation of LC3 lipidation is mediated through Beclin-1 signaling but independent of mTOR/ULK1 signaling, suggesting non-canonincal regulation of autophagy [60].

There is a potential discrepancy between LC3-II levels, which generally increase with LRRK2 knockout or kinase inhibition [58, 59], and accumulation of autophagosomes, which decrease under similar conditions [57]. Iit is important to note that at steady state these two measures can be difficult to interpret in terms of overall flux through the autophagy pathway. For example, both induction of autophagy and inhibition of autophagosome clearance results in the accumulation of lipidated LC3-II. In H-4 cells, a combined treatment with a LRRK2 kinase inhibitor and bafilomycin, to block lysosomal acidification, results in an additive increase in LC3-II [58]. This suggests that LRRK2 inhibition does not block flux through the overall autophagy pathway but rather increases formation of autophagosomes. By extension, these considerations suggest that LRRK2 normally functions to block autophagosome formation.

However, even these data are complicated by the observation that, in microglial cells, knockdown of LRRK2 can decrease LC3-II formation after lysosomal inhibition [57], in contrast to increases in mice [52] and H4 cells [58, 59]. It is possible therefore that there are cell-type specific signaling events that can modulate the direction of effect of LRRK2 on autophagy markers, indicating that autophagy regulation may be a downstream consequence of LRRK2 deficiency rather than a primary event.

In addition, higher levels of lysosomal markers and the lysosomal protease cathepsin D are seen in LRRK2 knockout mouse kidneys compared to their wild type counterparts irrespective of age [54]. Similar phenotypic changes, including lipofuscin accumulation and increase in lysosomal markers have been observed in LRRK2 KO rats [61, 62]. Therefore, while influencing autophagosome formation, LRRK2 may also play a role in lysosomal maturation and/or trafficking. How these two events are related is not immediately clear and, given then age-dependence of some changes [52, 54], it remains possible that alterations in one part of the autophagy-lysosome system are compensated for by alterations in other degradative processes.

Pathogenic mutations in LRRK2 KO affect vesicular events in vitro and in vivo

The above data show that the normal function of LRRK2 appears to be related to vesicular trafficking. Several

observations in different systems further suggest that LRRK2 mutations across multiple domains of the protein also alter vesicular dynamics.

Fibroblasts derived from PD patients carrying mutations across several enzymatic domains of LRRK2 (G2019S, Y1669C, R1441C) show a diminished autophagic response to starvation, measured by LC-3 conversion, compared to control fibroblasts [63]. Cells overexpressing R1441C LRRK2 show an increase in MVBs and autophagic vacuoles [51]. Overexpression of G2019S in cells also results in an increase in autophagic vacuoles and decreased neuronal process length. Knockdown of the conserved autophagy genes LC3 and Atg7 as well as inhibition of ERK signaling reversed this effect [64]. Overexpression of wild type LRRK2 in cells has also been reported to result in an increase of autophagosomes [65].

iPSC derived dopaminergic neurons from G2019S mutation carriers show an increase of autophagic vacuoles and an accumulation of aggregated α-synuclein [66, 67]. In these cells, there were no changes in *SNCA* transcription, suggesting an impaired degradation of α-synuclein [67]. G2019S LRRK2 iPSC showed a decrease in neurite length compared to control iPSC and induction of autophagy further exacerbated this phenotype [66]. An independent study of G2019S iPSC derived dopaminergic neurons and isogenic controls also showed neurite shortening in an ERK-dependent way [67]. Notably, G2019S LRRK2-mediated effects on autophagy in cells have also been reported to be mediated through ERK signaling [68]. Finally, in vivo, mice carrying the G2019S mutation show an accumulation of autophagic vacuoles in the cerebral cortex, as do R1441C LRRK2 transgenic mice [69].

The collective data available therefore suggests that mutant forms of LRRK2 decrease LC3 lipidation and result in the accumulation of autophagic vacuoules. The observations with LC3 are consistent with the data from knockout and inhibition models that LRRK2 normal function is to block autophagosome formation and that dominant mutations enhance this activity. However, the subsequent accumulation of autophagic vesicles suggests that there are additional effects of mutations in LRRK2 on the overall function of the autophagy-lysosomal pathway. One possible explanation for this apparent discrepancy comes from the observec concurrent increase in autophagic vacuoles and accumulation of α-synuclein in cells with G2019S LRRK2 [66, 67]. Because α-synuclein is degraded by the lysosome [70], the available data could suggest that G2019S mutant of LRRK2 simultaneously block autophagosome formation and lysosomal function, which contrasts perhaps with the accumulation of lysosomal enzymes in LRRK2 knockout animals [52, 54].

Candidate mechanisms for LRRK2 effects on vesicular trafficking

There are several potential mechanisms by which LRRK2 may affect vesicular trafficking. Indirect mechanism, such as those where LRRK2 has direct effects on metabolic or cellular signaling pathways that then indirectly affect autophagy, may explain some of the observed correlated changes noted above. However, here we will focus on regulation of vesicular trafficking events that are potentially mediated by direct protein-protein interactions. The rationale for this limitation on discussion of mechanisms is that as LRRK2 has multiple protein interaction domains, these are likely important effectors of its function in cells.

Unbiased proteomics approaches have provided important insights into the functional roles of LRRK2. Rab5 was first found to interact with LRRK2 using a yeast-two-hybrid screening approach [71]. Conversely, LRRK2 was identified as an interaction partner in a yeast-two-hybrid screen for Rab32 [72]. High-throughput protein-protein interaction arrays have shown that LRRK2 physically interacts with Rab7L1 (also known as Rab29) [73]. In the latter case, we have found that Rab7L1/Rab29 is important for recruiting LRRK2 to the TGN, along with the clathrin-uncoating protein cyclin-G associated kinase (GAK) and the co-chaperone BAG5. This protein complex may be conserved as similar proteins are important for the recruitment of Lrk-1 to the golgi apparatus in *C elegans* [74], Importantly, Rab7L1 and GAK are nominated to be risk factors for sporadic PD [14]. Clearance of Golgi-derived vesicles by the LRRK2 complex including Rab7L1 is enhanced by mutations across all enzymatic domains of LRRK2 whereas hypothesis testing LRRK2 mutations, including those that are kinase dead or cannot bind GDP/GTP, were ineffective in TGN vesicle clearance [73]. This suggests that enzymatic activities of LRRK2 are required to promote TGN clustering and clearance and that pathogenic mutations result in a gain-of-function that enhance this phenotype [73].

In addition, LRRK2 was shown to interact with a number of other Rab GTPases, including Rab32 and Rab38 [72]. Recently, phosphoproteomic screens were performed in an effort to identify *bona fide* LRRK2 kinase substrates [75]. Two screens were performed using cells from mice engineered to have either the kinase hyperactive G2019S or kinase inhibitor resistant A2016T LRRK2, in combination with treatment of distinct LRRK2 kinase inhibitors. Overlap of these screens resulted in the identification of a single LRRK2 kinase substrate, Rab10. Further analysis in HEK293FT cells indicated that Rab10 as well as Rab8 and Rab12 are direct physiological LRRK2 substrates [75].

Although publication of independent confirmation of these findings is still awaited, they suggest that one of the key functions of LRRK2, kinase activity, is important in control of Rabs and, hence vesicular trafficking events. Furthermore, in cells (but not in vitro), mutations in several different regions of LRRK2 consistently result in increased Rab phosphorylation, supporting the contention that different LRRK2 domains work together to produce functional output [75]. Along the same lines, all pathogenic mutations in LRRK2 increase Rab7L1-dependent retention at the TGN [73]. However, the precise mechanism(s) by which LRRK2 domains interact in cells remain to be determined.

Collectively, these data place LRRK2 at the scene of the crime for vesicle sorting. A recent computational analysis of the LRRK2 interactome further supports a potential role for LRRK2 in vesicular dynamics such as endocytosis and autophagy [76]. However, the range of Rabs identified suggests multiple roles for LRRK2 at different intracellular membranes. It is also of interest that LRRK2 has a different set of Rabs that appear to be direct substrates from those that were nominated as stronger binding partners, perhaps suggesting that depending on the Rab, LRRK2 may have different modes of action. Further confirmation of the binding and phosphorylation events are needed before we can be certain of the precise role that LRRK2 plays in Rab biology and vice-versa. Nonetheless, because Rab proteins are important in vesicular dynamics, these results suggest that the mechanism by which LRRK2 affects intracellular membranes is mediated via Rab interactions.

There are several pieces of evidence to suggest that, in different tissues and systems, the physiological interaction with Rabs is important for mediating the effects of mutations in LRRK2 on membrane trafficking. As well as causing changes in autophagy, pathogenic LRRK2 mutations have also been shown to lead to alterations in synaptic vesicle trafficking in neurons. Rab5 has a particularly strong role in synaptic vesicle endocytosis. Overexpression of WT LRRK2 impaired synaptic vesicle endocytosis and this effect was further enhanced by overexpression of G2019S LRRK2, whereas-expression of Rab5 rescued this phenotype [77].

Further supporting the idea that LRRK2 and Rabs cooperate to modulate vesicular trafficking, Rab7L1 KO mice have the same lysosomal pathology in the kidneys as LRRK2 KO mice and the combined deficiency of both proteins also results in a similar phenotype suggesting a genetic interaction with consistent direction between these two proteins [78]. Whether this is true for other Rabs that are direct substrates of LRRK2 is not known, and future studies are required to further substantiate the relationship between LRRK2, Rabs and regulation of the autophagy-lysosome system.

Studies in *C. elegans* neurons suggest that suggests that the LRRK2 nematode ortholog acts downstream of Rab7L1 ortholog in endo-lysosomal trafficking. Furthermore, cellular work showed that LRRK2 interacts with AP-3 as a downstream effector, essential for trafficking of lysosomal membrane proteins from the Golgi to the lysosomes [78]. The *Drosophila* homolog of LRRK2 (dLrrk) colocalizes with endosomes and lysosomes and interacts late endosomal protein Rab7. dLrrk loss-of-function mutants have abnormalities in the endosome and dLrrk can negatively regulate Rab7-dependent perinuclear localization of lysosome [55]. In contrast, a mutation in dLrrk corresponding to the G2019S mutation in LRRK2 promotes Rab7-dependent perinuclear positioning of lysosomes [55]. Accumulation of autophagosomes and presence of enlarged lysosomes and endosomes were also observed in *dLrrk* loss-of-function mutants [79]. This phenotype was rescued by overexpression of Rab9, which promotes recycling of endosomes to the TGN via the retromer, again possibly due to a direct interaction [79]. As noted above, dLrrk is paralog of LRRK1/LRRK2 [80] and therefore may interact with a slightly different or broader set of Rabs than LRRK2. Nonetheless, these collective data strongly suggest that the effects of LRRK2 across several species depend on Rab GTPases in different tissues and cells, not just in neurons.

Fibroblasts of PD patients carrying the G2019S mutation showed decreased Rab7 activity. Overexpression of G2019S as well as R1441C LRRK2 cause a decrease of Rab7 activity in cells [81]. Moreover, expression of mutant LRRK2 caused a delay in early to late endosomal trafficking, as evidenced by a decreased Rab5 to Rab7 transitioning [81]. A dramatic delay of trafficking out of late endosomes was observed in cells overexpressing G2019S and R1441C LRRK2. These late endosomes showed a marked increase in Rab7-positive tubules [81].

However, in addition to Rab proteins, LRRK2 may also mechanistically alter membrane dynamics via other important interacting proteins. LRRK2 has been shown to interact and colocalize with Sec16, a key protein involved in ER-Golgi transport [82]. The R1441C LRRK2 mutation impaired this interaction and mouse primary fibroblasts from R1441C transgenic mice showed impaired ER to Golgi trafficking [82].

LRRK2 and its *Drosophila* homologue dLRRK were shown to phosphorylate the synaptic vesicle endocytosis protein endophilin-A in vitro [83, 84]. In *Drosophila*, increased endophilinA phosphorylation by G2019S dLrrk resulted impaired synaptic endocytosis [83]. Moreover, dLRRK-dependent phosphorylation of endophilinA was recently shown to stimulate autophagy in at Drosophila synapses, highlighting cross-talk between endosomal and autophagosomal signaling networks [85].

Collectively, these data show that LRRK2 can interact with multiple vesicle-associated proteins. One of the most important remaining questions for LRRK2 biology is how binding to Rabs or other proteins influences the observed alterations in autophagy and lysosomal markers seen in cells and animal models, or whether other mechanisms are at play. A particular complexity of vesicular trafficking is that events are often inter-related as, for example, multiple Rabs co-operate to influence overall protein and vesicle sorting [35]. Thus, overall flux through a pathway may depend on interactions between multiple partners some of which may anatogonize each other. Further complicating interpretation, presumably most tissues and cells have compensatory mechanisms that will at least partially recover function in vesicle sorting. It will therefore be important to examine multiple steps of vesicular sorting to see which are consistently and directly affected by LRRK2 deficiency and mutations to determine which events are direct and which are consequential.

Conclusions

A substantial amount of evidence shows that LRRK2 plays an important role in vesicular trafficking. LRRK2 KO models and studies using LRRK2 kinase inhibitors have highlighted a regulatory role for LRRK2 in autophagy. Proteomics approaches have greatly helped to identify physical interactors as well as *bona fide* kinase substrates of LRRK2. Importantly, given the high interconnectivity of endosomal, lysosomal and autophagosomal pathways, dysfunctions in one system may well trigger alterations in another.

However, how altered vesicular trafficking can ultimately lead to neurodegeneration is not well understood in the context of LRRK2 mutations. Understanding such pathobiological roles of LRRK2 is critical for the development of therapeutic strategies. If LRRK2 mutations result in a gain of biochemical function, targeting the kinase and/or GTPase activity of LRRK2 could be helpful to modulate disease progression. More broadly, if it is true that multiple PD-related genes converge on vesicular trafficking pathways, regulatory and partially redundant mechanisms for autophagy might be targetable for therapeutics.

Abbreviations

AD: Autosomal dominant; Ank: Ankyrin; AR: Autosomal recessive; Arm: Armadillo, Atg, Autophagic genes; CMA: Chaperone-mediated autophagy; COR: C-terminus of Roc; LRR: Leucine rich repeat; LRRK1/2: Leucine rich repeat kinase 1/2; MVB: Multivesicular body; PD: Parkinson's disease; PI(3)P: Phosphatidylinositol 3-phosphate; PI(3,5)P2: Phosphatidylinositol 3,5-biphosphate; Roc: Ras of complex; TGN: Trans-golgi network; Vps: Vacuolar sorting protein

Acknowledgements

Not applicable.

Funding

This research was supported by the Intramural Research Program of the NIH, National Institute on Aging.

Availability of data and materials

Not applicable.

Authors' contributions

DR and MRC wrote the manuscript. Both authors read and approved the final manuscript.

Competing interests

The authors declare that they have no competing interests.

Consent for publication

Not applicable.

Ethics approval and consent to participate

Not applicable.

Author details

[1]Cell Biology and Gene Expression Section, Laboratory of Neurogenetics, National Institute on Aging, National Institutes of Health, Bldg. 35, 35 Convent Drive, Bethesda, MD 20892-3707, USA. [2]School of Pharmacy, University of Reading, Whiteknights, Reading RG6 6AP, UK.

Received: 26 October 2016 Accepted: 3 December 2016
Published online: 07 December 2016

References

1. Funayama M, Hasegawa K, Kowa H, Saito M, Tsuji S, Obata F. A new locus for Parkinson's disease (PARK8) maps to chromosome 12p11.2-q13.1. Ann Neurol. 2002;51:296–301.
2. Zimprich A, Müller-Myhsok B, Farrer M, Leitner P, Sharma M, Hulihan M, et al. The PARK8 locus in autosomal dominant parkinsonism: confirmation of linkage and further delineation of the disease-containing interval. Am J Hum Genet. 2004;74:11–9.
3. Khan NL, Jain S, Lynch JM, Pavese N, Abou-Sleiman P, Holton JL, et al. Mutations in the gene LRRK2 encoding dardarin (PARK8) cause familial Parkinson's disease: clinical, pathological, olfactory and functional imaging and genetic data. Brain. 2005;128:2786–96.
4. Wszolek ZK, Pfeiffer RF, Tsuboi Y, Uitti RJ, McComb RD, Stoessl AJ, et al. Autosomal dominant parkinsonism associated with variable synuclein and tau pathology. Neurology. 2004;62:1619–22.
5. Zimprich A, Biskup S, Leitner P, Lichtner P, Farrer M, Lincoln S, et al. Mutations in LRRK2 cause autosomal-dominant parkinsonism with pleomorphic pathology. Neuron. 2004;44:601–7.
6. Mata IF, Kachergus JM, Taylor JP, Lincoln S, Aasly J, Lynch T, et al. Lrrk2 pathogenic substitutions in Parkinson's disease. Neurogenetics. 2005;6:171–7.
7. Zabetian CP, Samii A, Mosley AD, Roberts JW, Leis BC, Yearout D, et al. A clinic-based study of the LRRK2 gene in Parkinson disease yields new mutations. Neurology. 2005;65:741–4.
8. Di Fonzo A, Rohe C, Ferreira J, Chien H, Vacca L, Stocchi F, et al. A frequent gene mutation associated with autosomal dominant Parkinson's disease. Lancet. 2005;365:412–5.
9. Gilks WP, Abou-Sleiman PM, Gandhi S, Jain S, Singleton A, Lees AJ, et al. A common LRRK2 mutation in idiopathic Parkinson's disease. Lancet. 2005;365:415–6.
10. Funayama M, Hasegawa K, Ohta E, Kawashima N, Komiyama M, Kowa H, et al. An LRRK2 mutation as a cause for the parkinsonism in the original PARK8 family. Ann Neurol. 2005;57:918–21.
11. Paisán-Ruiz C, Lewis PA, Singleton AB. LRRK2: cause, risk, and mechanism. J Park Dis. 2013;3:85–103.
12. Dächsel JC, Farrer MJ. LRRK2 and Parkinson disease. Arch Neurol. 2010;67:542–7.
13. Cookson MR. LRRK2 pathways leading to neurodegeneration. Curr Neurol Neurosci Rep. 2015;15:564.
14. Nalls MA, Pankratz N, Lill CM, Do CB, Hernandez DG, Saad M, et al. Large-scale meta-analysis of genome-wide association data identifies six new risk loci for Parkinson's disease. Nat Genet (Nature Publishing Group). 2014;46:989–93.
15. Singleton A, Hardy J. A generalizable hypothesis for the genetic architecture of disease: pleomorphic risk loci. Hum Mol Genet. 2011;20:R158–62.
16. Hardy J, Cai H, Cookson MR, Gwinn-Hardy K, Singleton A. Genetics of Parkinson's disease and parkinsonism. Ann Neurol. 2006;60:389–98.

17. Rudenko IN, Cookson MR. Heterogeneity of leucine-rich repeat kinase 2 mutations: genetics, mechanisms and therapeutic implications. Neurotherapeutics. 2014;11:738–50.
18. Lewis PA, Greggio E, Beilina A, Jain S, Baker A, Cookson MR. The R1441C mutation of LRRK2 disrupts GTP hydrolysis. Biochem Biophys Res Commun. 2007;357:668–71.
19. Daniëls V, Vancraenenbroeck R, Law BMH, Greggio E, Lobbestael E, Gao F, et al. Insight into the mode of action of the LRRK2 Y1699C pathogenic mutant. J Neurochem. 2011;116:304–15.
20. Liao J, Wu C-X, Burlak C, Zhang S, Sahm H, Wang M, et al. Parkinson disease-associated mutation R1441H in LRRK2 prolongs the "active state" of its GTPase domain. Proc Natl Acad Sci U S A. 2014;111:4055–60.
21. Guo L, Gandhi PN, Wang W, Petersen RB, Wilson-Delfosse AL, Chen SG. The Parkinson's disease-associated protein, leucine-rich repeat kinase 2 (LRRK2), is an authentic GTPase that stimulates kinase activity. Exp Cell Res. 2007;313:3658–70.
22. Rosenbusch KE, Kortholt A. Activation mechanism of LRRK2 and its cellular functions in Parkinson's disease. Park Dis. 2016;2016:7351985.
23. Mata IF, Wedemeyer WJ, Farrer MJ, Taylor JP, Gallo KA. LRRK2 in Parkinson's disease: protein domains and functional insights. Trends Neurosci. 2006;29:286–93.
24. Gloeckner CJ, Kinkl N, Schumacher A, Braun RJ, O'Neill E, Meitinger T, et al. The Parkinson disease causing LRRK2 mutation I2020T is associated with increased kinase activity. Hum Mol Genet. 2006;15:223–32.
25. Greggio E, Zambrano I, Kaganovich A, Beilina A, Taymans JM, Daniels V, et al. The Parkinson disease-associated leucine-rich repeat kinase 2 (LRRK2) is a dimer that undergoes intramolecular autophosphorylation. J Biol Chem. 2008;283:16906–14.
26. Zdenek B, Smith KA, Lavoie MJ. Membrane localization of LRRK2 is associated with increased formation of the highly active LRRK2 dimer and changes in its phosphorylation. Biochemistry (Mosc). 2010;49:5511–23.
27. Guaitoli G, Raimondi F, Gilsbach BK, Gómez-Llorente Y, Deyaert E, Renzi F, et al. Structural model of the dimeric Parkinson's protein LRRK2 reveals a compact architecture involving distant interdomain contacts. Proc Natl Acad Sci (National Academy of Sciences). 2016;113:E4357–66.
28. Beilina A, Cookson MR. Genes associated with Parkinson's disease: regulation of autophagy and beyond. J. Neurochem. 2015;n/a – n/a.
29. Cuervo AM, Stefanis L, Fredenburg R, Lansbury PT, Sulzer D. Impaired Degradation of Mutant α -Synuclein by Chaperone-Mediated Autophagy. Science. 2004;305(5688):1292–5.
30. Cuervo AM, Wong E. Chaperone-mediated autophagy: roles in disease and aging. Cell Res (Nature Publishing Group). 2014;24:92–104.
31. Li W. Stabilization of -synuclein protein with aging and familial Parkinson's disease-linked A53T mutation. J Neurosci. 2004;24:7400–9.
32. Kumaran R, Cookson MR. Pathways to parkinsonism redux: convergent pathobiological mechanisms in genetics of Parkinson's disease. Hum Mol Genet. 2015;9:1–37.
33. Jovic M, Sharma M, Rahajeng J, Caplan S. The early endosome: a busy sorting station for proteins at the crossroads. Histol Histopathol. 2010;25:99–112.
34. Sudhof TC. The synaptic vesicle cycle. Annu Rev Neurosci. 2004;27:509–47.
35. Stenmark H. Rab GTPases as coordinators of vesicle traffic. Nat Rev Mol Cell Biol. 2009;10:513–25.
36. Marat AL, Haucke V. Phosphatidylinositol 3 -phosphates — at the interface between cell signalling and membrane traffic. EMBO J. 2016;35:561–79.
37. Vanlandingham PA, Ceresa BP. Rab7 Regulates Late Endocytic Trafficking Downstream of Multivesicular Body Biogenesis and Cargo Sequestration *. J Biol Chem. 2009;284:12110–24.
38. Huotari J, Helenius A. Endosome maturation. EMBO J (Nature Publishing Group). 2011;30:3481–500.
39. Zhen Y, Stenmark H. Cellular functions of Rab GTPases at a glance. J Cell Sci. 2015;128:3171–6.
40. Wen-wen L, Jian L, Jin-ku B. Microautophagy: lesser-known self-eating. J Cell Mol Life Sci. 2012;69:1125–36.
41. Feng Y, He D, Yao Z, Klionsky DJ. The machinery of macroautophagy. Cell Res. 2014;24:24–41.
42. Behrends C, Sowa ME, Gygi SP, Harper JW. Network organization of the human autophagy system. Nature (Nature Publishing Group). 2010;466:68–76.
43. Vicinanza M, Korolchuk V, Ashkenzai A, Puri C, Menzies F, Clarke J, et al. PI(5)P regulates autophagosome biogenesis. Mol Cell Biol. 2015;57.
44. Okamoto K. Organellophagy: eliminating cellular building blocks via selective autophagy. J Cell Biol. 2014;205:435–45.
45. Youle RJ, Narendra DP. Mechanisms of mitophagy. Nat Rev Mol Cell Biol. 2011;12:9–14.
46. Xu Z, Yang L, Xu S, Zhang Z, Cao Y. The receptor proteins: pivotal roles in selective autophagy. Acta Biochim Biophys Sin. 2015;47:571–80.
47. Bitto A, Lerner CA, Nacarelli T, Crowe E, Torres C, Sell C. P62/SQSTM1 at the interface of aging, autophagy, and disease. Age Dordr Neth. 2014;36:9626.
48. Lim C-Y, Zoncu R. The lysosome as a command-and-control center for cellular metabolism. J Cell Biol. 2016;214:653–64.
49. Biskup S, Moore DJ, Celsi F, Higashi S, West AB, Andrabi SA, et al. Localization of LRRK2 to membranous and vesicular structures in mammalian brain. Ann Neurol. 2006;60:557–69.
50. Higashi S, Biskup S, West AB, Trinkaus D, Dawson VL, Faull RLM, et al. Localization of Parkinson's disease-associated LRRK2 in normal and pathological human brain. Brain Res. 2007;1155:208–19.
51. Alegre-Abarrategui J, Christian H, Lufino MMP, Mutihac R, Venda LL, Ansorge O, et al. LRRK2 regulates autophagic activity and localizes to specific membrane microdomains in a novel human genomic reporter cellular model. Hum Mol Genet. 2009;18:4022–34.
52. Tong Y, Yamaguchi H, Giaime E, Boyle S, Kopan R, Kelleher RJ, et al. Loss of leucine-rich repeat kinase 2 causes impairment of protein degradation pathways, accumulation of alpha-synuclein, and apoptotic cell death in aged mice. Proc Natl Acad Sci U S A. 2010;107:9879–84.
53. Herzig MC, Kolly C, Persohn E, Theil D, Schweizer T, Hafner T, et al. LRRK2 protein levels are determined by kinase function and are crucial for kidney and lung homeostasis in mice. Hum Mol Genet. 2011;20:4209–23.
54. Tong Y, Giaime E, Yamaguchi H, Ichimura T, Liu Y, Si H, et al. Loss of leucine-rich repeat kinase 2 causes age-dependent bi-phasic alterations of the autophagy pathway. Mol Neurodegener. 2012;7:2.
55. Dodson MW, Zhang T, Jiang C, Chen S, Guo M. Roles of the Drosophila LRRK2 homolog in Rab7-dependent lysosomal positioning. Hum Mol Genet. 2012;21:1350–63.
56. Sakaguchi-Nakashima A, Meir JY, Jin Y, Matsumoto K, Hisamoto N. LRK-1, a C. elegans PARK8-related kinase, regulates axonal-dendritic polarity of SV proteins. Curr Biol. 2007;17:592–8.
57. Schapansky J, Nardozzi JD, Felizia F, LaVoie MJ. Membrane recruitment of endogenous LRRK2 precedes its potent regulation of autophagy. Hum Mol Genet. 2014;23:4201–14.
58. Manzoni C, Mamais A, Dihanich S, Abeti R, Soutar MPM, Plun-Favreau H, et al. Inhibition of LRRK2 kinase activity stimulates macroautophagy. Biochim Biophys Acta (The Authors). 1833;2013:2900–10.
59. Saez-Atienzar S, Bonet-Ponce L, Blesa JR, Romero FJ, Murphy MP, Jordan J, et al. The LRRK2 inhibitor GSK2578215A induces protective autophagy in SH-SY5Y cells: involvement of Drp-1-mediated mitochondrial fission and mitochondrial-derived ROS signaling. Cell Death Dis. 2014;5:e1368.
60. Manzoni C, Mamais A, Roosen DA, Dihanich S, Soutar MPM, Plun-Favreau H, et al. mTOR independent regulation of macroautophagy by Leucine Rich Repeat Kinase 2 via Beclin-1. Sci Rep. 2016;6:35106.
61. Baptista MAS, Dave KD, Frasier MA, Sherer TB, Greeley M, Beck MJ, et al. Loss of leucine-rich repeat kinase 2 (LRRK2) in rats leads to progressive abnormal phenotypes in peripheral organs. PLoS One. 2013;8:e80705.
62. Ness D, Ren Z, Gardai S, Sharpnack D, Johnson VJ, Brennan RJ, et al. Leucine-rich repeat kinase 2 (LRRK2)-deficient rats exhibit renal tubule injury and perturbations in metabolic and immunological homeostasis. PLoS One. 2013;8:e66164.
63. Manzoni C, Mamais A, Dihanich S, McGoldrick P, Devine MJ, Zerle J, et al. Pathogenic Parkinson's disease mutations across the functional domains of LRRK2 alter the autophagic/lysosomal response to starvation. Biochem Biophys Res Commun (Elsevier Inc). 2013;441:862–6.
64. Plowey ED, Cherra SJ, Liu YJ, Chu CT. Role of autophagy in G2019S-LRRK2-associated neurite shortening in differentiated SH-SY5Y cells. J Neurochem. 2008;105:1048–56.
65. Gómez-Suaga P, Luzón-Toro B, Churamani D, Zhang L, Bloor-Young D, Patel S, et al. Leucine-rich repeat kinase 2 regulates autophagy through a calcium-dependent pathway involving NAADP. Hum Mol Genet. 2012;21:511–25.
66. Sánchez-Danés A, Richaud-Patin Y, Carballo-Carbajal I, Jiménez-Delgado S, Caig C, Mora S, et al. Disease-specific phenotypes in dopamine neurons from human iPS-based models of genetic and sporadic Parkinson's disease. EMBO Mol Med. 2012;4:380–95.
67. Reinhardt P, Schmid B, Burbulla LF, Schöndorf DC, Wagner L, Glatza M, et al. Genetic correction of a LRRK2 mutation in human iPSCs links parkinsonian neurodegeneration to ERK-dependent changes in gene expression. Cell Stem Cell. 2013;12:354–67.

68. Bravo-San Pedro JM, Niso-Santano M, Gómez-Sánchez R, Pizarro-Estrella E, Aiastui-Pujana A, Gorostidi A, et al. The LRRK2 G2019S mutant exacerbates basal autophagy through activation of the MEK/ERK pathway. Cell Mol Life Sci. 2013;70:121–36.
69. Ramonet D, Daher JPL, Lin BM, Stafa K, Kim J, Banerjee R, et al. Dopaminergic neuronal loss, reduced neurite complexity and autophagic abnormalities in transgenic mice expressing G2019S mutant LRRK2. PLoS One. 2011;6:e18568.
70. Paxinou E, Chen Q, Weisse M, Giasson BI, Norris EH, Rueter SM, et al. Induction of alpha-synuclein aggregation by intracellular nitrative insult. J Neurosci Off J Soc Neurosci. 2001;21:8053–61.
71. Heo HY, Kim K-S, Seol W. Coordinate regulation of neurite outgrowth by LRRK2 and its interactor, Rab5. Exp Neurobiol. 2010;19:97.
72. Waschbüsch D, Michels H, Strassheim S, Ossendorf E, Kessler D, Gloeckner CJ, et al. LRRK2 transport is regulated by its novel interacting partner Rab32. PLoS One. 2014;9:e111632.
73. Beilina A, Rudenko IN, Kaganovich A, Civiero L, Chau H, Kalia SK, et al. Unbiased screen for interactors of leucine-rich repeat kinase 2 supports a common pathway for sporadic and familial Parkinson disease. Proc Natl Acad Sci U S A. 2014;111:2626–31.
74. Fukuzono T, Pastuhov SI, Fukushima O, Li C, Hattori A, Iemura S-I, et al. Chaperone complex BAG2-HSC70 regulates localization of Caenorhabditis elegans leucine-rich repeat kinase LRK-1 to the Golgi. Genes Cells Devoted Mol Cell Mech. 2016;21:311–24.
75. Steger M, Tonelli F, Ito G, Davies P, Trost M, Vetter M, et al. Phosphoproteomics reveals that Parkinson's disease kinase LRRK2 regulates a subset of Rab GTPases. eLife. eLife Sciences Publications, Ltd; 2016;5. doi:10.7554/eLife.12813.
76. Manzoni C, Denny P, Lovering RC, Lewis PA. Computational analysis of the LRRK2 interactome. PeerJ. 2015;3:e778.
77. Shin N, Jeong H, Kwon J, Heo HY, Kwon JJ, Yun HJ, et al. LRRK2 regulates synaptic vesicle endocytosis. Exp Cell Res. 2008;314:2055–65.
78. Kuwahara T, Inoue K, D'Agati VD, Fujimoto T, Eguchi T, Saha S, et al. LRRK2 and RAB7L1 coordinately regulate axonal morphology and lysosome integrity in diverse cellular contexts. Sci Rep (Nature Publishing Group). 2016;6:29945.
79. Dodson MW, Leung LK, Lone M, Lizzio MA, Guo M. Novel ethyl methanesulfonate (EMS)-induced null alleles of the Drosophila homolog of LRRK2 reveal a crucial role in endolysosomal functions and autophagy in vivo. Dis Model Mech. 2014;7:1351–63.
80. Marín I. Ancient origin of the Parkinson disease gene LRRK2. J Mol Evol. 2008;67:41–50.
81. Gómez-Suaga P, Rivero-Ríos P, Fdez E, Blanca Ramírez M, Ferrer I, Aiastui A, et al. LRRK2 delays degradative receptor trafficking by impeding late endosomal budding through decreasing Rab7 activity. Hum Mol Genet. 2014;23:6779–96.
82. Cho HJ, Yu J, Xie C, Rudrabhatla P, Chen X, Wu J, et al. Leucine-rich repeat kinase 2 regulates Sec16A at ER exit sites to allow ER-Golgi export. EMBO J. 2014;33:2314–31.
83. Matta S, Van Kolen K, da Cunha R, van den Bogaart G, Mandemakers W, Miskiewicz K, et al. LRRK2 controls an EndoA phosphorylation cycle in synaptic endocytosis. Neuron. 2012;75:1008–21.
84. Arranz AM, Delbroek L, Van Kolen K, Guimarães MR, Mandemakers W, Daneels G, et al. LRRK2 functions in synaptic vesicle endocytosis through a kinase-dependent mechanism. J. Cell Sci. 2014;128:541–52.
85. Soukup S-F, Kuenen S, Vanhauwaert R, Manetsberger J, Hernández-Díaz S, Swerts J, et al. A LRRK2-Dependent EndophilinA Phosphoswitch Is Critical for Macroautophagy at Presynaptic Terminals. Neuron. 2016;92:6982–7.
86. Okatsu K, Koyano F, Kimura M, Kosako H, Saeki Y, Tanaka K, et al. Phosphorylated ubiquitin chain is the genuine Parkin receptor. J Cell Biol. 2015;209:111–28.
87. Cookson MR. Parkinsonism Due to Mutations in PINK1, Parkin, and DJ-1 and Oxidative Stress and Mitochondrial Pathways. Cold Spring Harb. Perspect. Med. 2012;2:1–11.
88. Kane LA, Lazarou M, Fogel AI, Li Y, Yamano K, Sarraf SA, et al. PINK1 phosphorylates ubiquitin to activate parkin E3 ubiquitin ligase activity. J Cell Biol. 2014;205:143–53.
89. Koyano F, Okatsu K, Kosako H, Tamura Y, Go E, Kimura M, et al. Ubiquitin is phosphorylated by PINK1 to activate parkin. Nature (Nature Publishing Group). 2014;510:162–6.
90. Thomas KJ, McCoy MK, Blackinton J, Beilina A, van der Brug M, Sandebring A, et al. DJ-1 acts in parallel to the PINK1/parkin pathway to control mitochondrial function and autophagy. Hum Mol Genet. 2011;20:40–50.
91. Wang X, Petrie TG, Liu Y, Liu J, Fujioka H, Zhu X. Parkinson's disease-associated DJ-1 mutations impair mitochondrial dynamics and cause mitochondrial dysfunction. J Neurochem. 2012;121:830–9.
92. Burchell VS, Nelson DE, Sanchez-Martinez A, Delgado-Camprubi M, Ivatt RM, Pogson JH, et al. The Parkinson's disease-linked proteins Fbxo7 and Parkin interact to mediate mitophagy. Nat Neurosci. 2013;16:1257–65.
93. Xilouri M, Vogiatzi T, Vekrellis K, Park D, Stefanis L. Abberant α-synuclein confers toxicity to neurons in part through inhibition of chaperone-mediated autophagy. PLoS One. 2009;4:16–20.
94. Zimprich A, Benet-Pagès A, Struhal W, Graf E, Eck SH, Offman MN, et al. A mutation in VPS35, encoding a subunit of the retromer complex, causes late-onset parkinson disease. Am J Hum Genet. 2011;89:168–75.
95. Vilariño-Güell C, Wider C, Ross OA, Dachsel JC, Kachergus JM, Lincoln SJ, et al. VPS35 mutations in parkinson disease. Am J Hum Genet. 2011;89:162–7.
96. Ramirez A, Heimbach A, Gründemann J, Stiller B, Hampshire D, Cid LP, et al. Hereditary parkinsonism with dementia is caused by mutations in ATP13A2, encoding a lysosomal type 5 P-type ATPase. Genetics. 2006;38:1184–91.
97. Elsayed LEO, Drouet V, Usenko T, Mohammed IN, Hamed AAA, Elseed MA, et al. A novel nonsense mutation in *DNAJC 6* expands the phenotype of autosomal-recessive juvenile-onset Parkinson's disease. Ann Neurol. 2016;79:335–7.
98. Olgiati S, Quadri M, Fang M, Rood JPMA, Saute JA, Chien HF, et al. DNAJC6 mutations associated with early-onset Parkinson's disease. Ann Neurol. 2016;79:244–56.
99. Krebs CE, Karkheiran S, Powell JC, Cao M, Makarov V, Darvish H, et al. The sac1 domain of SYNJ1 identified mutated in a family with early-onset progressive parkinsonism with generalized seizures. Hum Mutat. 2013;34:1200–7.
100. Sidransky E, Nalls MA, Ph D, Aasly JO, Annesi G, Barbosa ER, et al. Multi-center analysis of glucocerebrosidase mutations in Parkinson disease. N Engl J Med. 2010;361:1651–61.
101. Deng H-X, Shi Y, Yang Y, Ahmeti KB, Miller N, Huang C, et al. Identification of TMEM230 mutations in familial Parkinson's disease. Nat Genet. Nature Publishing Group; 2016;advance on:733–9.